Université catholique de Louvain,
Ecole polytechnique de Louvain,
Institute of Information and Communication Technologies,
Electronics and Applied Mathematics,
Mathematical Engineering department,
Center for Systems Engineering and Applied Mechanics

Behavioral and modeling studies of eye and head coordination

Pierre M. Daye

Thesis submitted in partial fulfillment
of the requirements for the degree of
Docteur en Sciences de l'Ingénieur

Jury members:

Prof. **P. Van Dooren**, Chair (Université catholique de Louvain, Belgium)
Prof. **G. Barnes**, (University of Manchester, Manchester, UK)
Dr. **L.M. Optican**, (National Institutes of Health, Bethesda, USA)
Prof. **G. Blohm**, (Queen's University, Kingston, Canada)
Prof. **V. Wertz**, Supervisor (Université catholique de Louvain, Belgium)
Prof. **P. Lefèvre**, Supervisor (Université catholique de Louvain, Belgium)

October 26, 2010

Remerciements

Il serait complètement injuste d'attribuer la réalisation du travail que vous tenez entre vos mains à ma seule personne. Les quelques mots qui suivent sont pour vous, collègues, amis et membres de ma famille qui durant ces (trop) longues années avez su (dû) me supporter...

En premier lieu, je tiens à saluer l'investissement du Pr. Philippe Lefèvre et du Pr. Vincent Wertz, mes promoteurs de thèse. Au travers de nombreux échanges, ils ont essayé de me former à analyser une situation, en extraire les faits importants et communiquer ceux-ci à la communauté scientifique de manière adéquate. Ensuite, il y a leur côté humain... Les soupers informels organisés par Philippe, Marie-Madeleine et leurs enfants ont toujours été des moments agréables dans une ambiance détendue. Ils ont aussi su m'apporter un support discret, parfaitement dosé dans les moments délicats de ma vie personnelle. Pour cela et bien d'autres choses, je tiens à les remercier chaleureusement.

Ensuite, je tiens à remercier le Pr. Gunnar Blohm pour l'aide qu'il m'a fournie durant ma thèse. Les connaissances, les capacités d'analyse et le perfectionnisme de Gunnar m'ont permis d'augmenter la qualité de ce travail de manière significative.

Mes remerciements les plus sincères vont aussi au Dr. Lance M. Optican. Les discussions (au bureau ou durant un repas avec son épouse, Donna) que nous avons eues

Acknowledgments

It would be extremely unfair to award the accomplishment of the work you hold in your hands to my sole person. The few next words are for you, colleagues, friends and family members whom during all those (many) years knew (had to know) how to support me...

First, I want to hail the devotion of Pr. Philippe Lefèvre and Pr. Vincent Wertz, my thesis supervisors. Through a lot of discussions, they tried to train me to analyze a situation, extract from it the important features and communicate those ones to the scientific community adequately. Then, there is their human side... The informal dinners organized by Philippe, Marie-Madeleine and their children have always been pleasant moments in a relaxed atmosphere. They also knew how to give me a discreet stand, perfectly proportioned during the tough moments of my personal life. For this and a lot of other reasons, I want to thank them warmly.

Then, I want to thank Pr. Gunnar Blohm for the help he gave me during my PhD. The knowledge, the analysis skills and the perfectionism of Gunnar allowed me to increase significantly the quality of this work.

My most sincere acknowledgments also go to Dr. Lance M. Optican. The discussions (in the lab or during a dinner with his wife, Donna) we had during my short-term stays

durant mes séjours au LSR resteront dans mon esprit parmi les meilleurs moments de ma thèse.

Je voudrais remercier particulièrement les autres membres de mon jury: le Pr. Paul Van Dooren et le Pr. Graham Barnes. A travers vos remarques constructives et vos suggestions, vous avez contribué à l'amélioration de ce manuscrit.

Merci aussi à vous tous, locataires du bâtiment Euler. Je crois que peu d'endroits fournissent un environement de travail aussi agréable que l'Euler. Mais tout cela ne serait rien sans le groupe de gens sympathiques que vous êtes. Comme j'ai trop peur d'oublier quelqu'un (cela m'est arrivé une fois... Pas deux!), je préfère vous remercier tous pour nos discussions, nos nombreuses tranches de fou-rires et parfois nos coups de gueule.

Merci aussi à vous, mes amis Brainois de toujours. Depuis de nombreuses années nous avons eu la chance de tisser des liens que ni la distance ni le temps ne pourront détruire.

A toi, qui apprends juste à parler et m'appelles "parrain". Sans t'en rendre compte, tu m'apportais un peu d'air dans des moments difficiles.

Merci, Gaëlle, pour la patience dont tu as dû faire preuve durant ces années. Ta gentillesse et ta présence ont facilité la réussite de ce travail.

Merci à vous, maman et papa pour votre soutien indéfectible tout au long de ces années. Papa, tu seras toujours pour moi un modèle de réussite et de générosité. Maman, ton optimisme et ta foi en la vie jusqu'à la dernière seconde restent pour moi une source d'inspiration de tous les instants.

at the LSR will stay in my mind among the best memories of my PhD.

I would like to thank especially the others members of my PhD jury: Pr. Paul Van Dooren and Pr. Graham Barnes. Through your constructive comments and your suggestions, you contributed to the improvement of this manuscript.

Thank you also to all of you, tenants of the Euler building. I believe that few places give a working environment as nice as the Euler building. But all this would be nothing without the bunch of friendly people that you are. As I am too afraid to forgot somebody (it happened once... Not twice!), I prefer to thank you all for our discussions, our numerous fits of the giggles and sometimes our rants.

I also thank you, my forever friends from Braine-l'Alleud. For many years we have been fortunate to build relationships that neither time nor distance can destroy.

To you, who just learned how to talk and called me "parrain". Without realizing it, you brought me a little air in difficult times.

Thank you, Gaëlle, for the patience you had during all those years. Your kindness and your presence has facilitated the success of this work.

Thank you, Mom and Dad for your unwavering support throughout all these years. Dad, you will always be for me a model of success and generosity. Mom, your optimism and your faith in life until the very last second is for me a constant source of inspiration.

Vous qui avez consacré votre vie à notre réussite, ce travail est le vôtre.
You whom have devoted your life to our success, this work is yours.

Pierre

Contents

Part I

General introduction

1

In everyday life...

Moving eyes and head to orient the visual axis accordingly with a center of interest is a routine movement for foveate animals. From reading a book to driving a car or playing tennis, we constantly have to change our line of sight in relation with the current activity. At first the brain must analyze the visual environment to extract the main features linked to the needs of the task. Once the information is extracted and the goal computed, the central nervous system has to control and coordinate adequately the movements of several body parts (eye, head, trunk, etc.) to achieve accurately the task: modify the orientation of the visual axis. This first chapter gives an overview of the challenges that must be tackled to keep an accurate and stable vision during a gaze reorientation.

Since the early 1900s (Dodge, 1903), we know that eye movements can be divided into several categories depending on the visual task: making a rapid shift from one point to another is different than tracking a plane into the sky. Those two types of movements are fundamentally distinct both for motor control and visual perception. However, they share a common visual goal: keep the center of interest on the most accurate part of the retina: the fovea.

The light-sensitive part of the eye, the retina is divided into two systems based on their sensitivities to light intensity. The first system (the photopic system) is more efficient in bright light while the second one (the scotopic system) has a high sensitivity to light intensity in dim light. Those two systems are different both in their function and in their anatomy; the scotopic system is mainly composed of rod cells while the cone cells compose the photopic system.

The cone cells are concentrated close to the center of the retina in an area called the fovea that has a diameter of approximately 1 [mm]. They are responsible for the high accuracy of the vision at the center of the gaze[1], the perception of the objects' color but are less responsive when the light intensity

[1] Few studies have looked at the distribution of the cone and the rod cells in primates. In the rhesus monkey, Wikler et al. (1990) have shown that the retina has on average $(6.1 \pm 0.75) * 10^7$ rod cells and $(3.1 \pm 0.13) * 10^6$ cone cells. If the density of cones is high in the fovea (peak density around 141000 $[cells/mm^2]$), it decreases quickly toward the retinal periphery (by a factor 100). The density of rods on the fovea is close to zero, increases quickly up to a maximum of 184000 $[cells/mm^2]$. Then it decreases toward the periphery with a factor of ~ 9.

decreases. The rod cells are the most numerous photoreceptors of the retina, they are not sensitive to color but are highly sensitive to light intensity. That is the reason why stars in the sky are visible when you do not stare at them but disappear if you do.

Just as the perception of the visual environment (the sensor part) takes time[2], the computation of the motor commands (the programming part) and the eye/head movements generated (the motor output) are not instantaneous. The stream of information passes through several cortical areas[3] to analyze the visual surroundings and then to compute the goal(s) required by the task. The elapsed time needed by the cortical computations constitutes a second incompressible delay[4].

At the output level, the extraocular/neck muscles are not reacting immediately to the commands sent by the motoneurons[5]. The inertia and the mass of the eye are small and hence are generally ignored compared to the extraocular muscles strength[6]. In parallel, the head has a much higher mass. Thus the subsequent head inertia[7] significantly increases the settling time of a head response to neck muscles' contraction. Therefore, the head mechanical properties and the time course of the neck/extraocular muscles' contraction are such that a motor command does not instantly generate a head/eye movement.

Remarkably, despite the small visual angle of the fovea ($\sim$1 [deg]) and the sum of all the previous delays (sensors, task goal(s) computation and motor responses), foveate mammals can equally well track moving targets with velocities as high as 80 [deg/s] with the head either fixed (Meyer et al., 1985) or free to move (Dubrovski and Cullen, 2002). It has been demonstrated that a pure delay in the sensor/motor part of a controlled system can lead to instabilities (Smith, 1959) if it is not appropriately accounted for. From those observations, it is easily understandable that the visual system needs a proper control policy to track moving objects to avoid blurring vision.

Decades before researchers started to study the implications of the internal delays of the ocular sensorimotor apparatus, Dodge (1903) already reported important properties of the tracking system. Among other things, he observed that the ratio between gaze velocity and target velocity (called pursuit gain) remained generally inferior to one. Because of this suboptimal gain, the gaze stays behind the tracked target. Therefore, rapid position shifts of the visual

[2] 30 to 100 [ms] between flash presentation and cone cells peak discharge (Baylor et al., 1974; Schnapf et al., 1990).

[3] See sections 3.3 and 4.7 for a description of the main visual cortical areas.

[4] There is a latency of 55 to 95 [ms] between visual stimulations and recorded activity at the output of the visual cortical areas (FEF, MT and MST. See chapter 2 for a description of those areas) (Schmolesky et al., 1998).

[5] A delay of approximately 2.5 [ms] exists between a stimulation of the extraocular muscle fibers and the beginning of the muscles' contraction (Lennerstrand, 1979).

[6] Eye rotational inertia = 6.12 10^{-5} [kg/(deg/sec^2)]] (Robinson, 1981). For an eye acceleration of 50000 [deg/s^2], the amplitude of the inertial force corresponds to $\sim$3% of the other forces' amplitude (Robinson, 1981).

[7] Head linear inertia = 0.02-0.04 [kg m^2] depending of the axis of rotation (Winters, 1988).

axis, called "saccades", are executed to negate the increasing error between the position of the moving target and the gaze position.

From the first observations of Dodge (1903) (and several studies that followed this one), authors have shown that the visual system uses two main mechanisms to reorient the line of sight depending on the task. The **pursuit system** cancels any velocity mismatch between a moving target and the eye. The **saccadic system** compensates for the angular deviation between the fovea and the center of interest. A dedicated chapter of this introduction will explain the main characteristics of both pursuit and saccades.

A third orienting movement arises from the need to coordinate the movement of two eyes for animals with frontal binocular vision: the **vergence**. Because the eyes are separated by several centimeters, a similar orientation of both eyes with respect to the head would not place the object of interest on both foveas at the same time. Thus, to make a saccade from one target to another, the variation of the eyes' orientation must incorporate two components. The first displacement corresponds to the relative jump of the target between two positions. The second one is a separate angular correction linked to the distance between the centers of rotation of the eyes. The current thesis does not account for the vergence system. All the analyses were carried out assuming a cyclopean eye. Therefore, this type of eye movement will not be discussed further.

It must be stressed that the preceding paragraphs describe eye movements in head-restrained conditions. With the head fixed, young human subjects can rotate their eyes up to ± 55 [deg] horizontally (Guitton and Volle, 1987) and ± 45 [deg] vertically (Huaman and Sharpe, 1993). The range of accessible eye positions is called the ocular motor range (OMR). To reach targets located outside the OMR, subjects have to move both eye and head to reorient accurately their visual axis, or gaze, toward the target. The gaze corresponds to the vector sum of the head position with respect to an inertial reference frame (head-in-space) to the eye position with respect to a head-fixed reference frame (eye-in-head). It represents the eye position with respect to a spatially-fixed reference frame (eye-in-space). Practically, with the head free to move, subjects start to combine eye movements and head movements even when the eccentricity of the target is smaller than the boundaries of the OMR[8]. An important feature of head-unrestrained movements is that an equivalent gaze displacement can be executed through an infinite number of combinations of eye movements and head movements, as long as the sum of their displacements remains constant. With the head free to move, the contribution of the eye and the head to the displacement of the gaze varies between subjects of identical species. Even the same subject can be instructed to move more or less their head during an experiment. Fuller (1992) studied the propensity of human subjects to use head movement during gaze saccade. He showed, that with the same experimental conditions, some subjects (called "head movers") tended to use the head more than others (called "head non-movers").

[8] Stahl (1999) defined the eye-only range (EOR) as the eccentricity of the eye movement for which no head movement is triggered ($\pm$ 17 [deg] in humans) during a reorientation of the visual axis.

While moving the head can, as described, increase the range of accessible targets; everyday activities also induce involuntary head-in-space movements (e.g. walking creates vertical movements of the head). Those head displacements can alter a stable vision if they are not accounted for. Many systems work concurrently to stabilize vision. For humans, the most important of them is the **vestibulo-ocular reflex (VOR)**. When the head is passively[9] rotated, the eyes in the orbit are counter-rotated by the VOR to keep the gaze stable with a latency[10] for humans of approximately 10 [ms]. To achieve such a short response time, the VOR uses head-in-space velocity sensors located inside the inner ear that are connected to the eye muscles through a three-neurons arc. A detailed description of the VOR and its interactions with the active gaze movements will be given in a chapter of this introduction.

Finally, a target does not need to be visible to reach it (we can scratch our back without seeing the itching spot). Without a visual input, authors have shown the ability of the subjects to build a spatial representation of their environment using extra-retinal information (Blohm et al., 2003b,a, 2005b; Blouin et al., 1995, 1998). With the head fixed, Blohm et al. (2003b,a, 2005b) showed that subjects can redirect their eyes to the remembered position of a target flashed during an ongoing pursuit movement. They showed that the accuracy of the eye saccade was a function of the latency between the presentation of the flash and the onset the eye movement: the longer the latency, the better the accuracy. The internal representation and the update of the visual surroundings according to our own movements is called "spatial constancy".

Issues addressed in the thesis

This thesis contains six parts that address different questions linked to the control of gaze and the coordination of eye and head movements. Two methodologies were used throughout the thesis to help answering those questions. A first one (parts II and III) uses behavioral experiments to generalize previously reported observations with the head restrained to head-free situations. The second approach (parts IV and V) proposes novel mathematical models of the head-unrestrained control of movements. The models were developed either to find a consensus about fundamental questions of eye-head coordination or to stress the importance of taking into account the delays of the sensory part in the control. No direct link exists between the behavioral and the modeling studies. The major aim of the thesis being the understanding of primary unsolved issues in eye-head coordination. Nevertheless, the circuitries presented in parts IV and V could be augmented by including cortical mechanisms to simulate the behavior reported in parts II and III.

[9] Passive head rotations are not related to a gaze movement.

[10] Elapsed time between the onset of a head movement and the onset of an eye movement.

Part I: general introduction

The present part of the thesis proposes a summary of the current knowledge of head-unrestrained saccades, head-unrestrained pursuit and VOR behavior and neurophysiology. This part contains information provided to the naive reader to help him/her understand the major questions addressed and the assumptions made throughout this thesis. The introduction will also remind different aspects of head-unrestrained studies to the reader with general oculomotricity knowledge. The description of each movement (saccades, pursuit and VOR) is divided into three sections. In a first step, a typical movement is described. Then the major behavioral characteristics of the movement are presented. Finally, the main neural areas involved in the control of the corresponding movement are explained. At the end of each section, a box will present a short summary of the section.

Part II: head-unrestrained spatial constancy

As explained in the previous section, the central nervous system can update its internal representation of the surrounding space to account for self-generated eye movements in a head-restrained condition (Blohm et al., 2003b,a, 2005b). With the release of the head, the central nervous system must integrate ongoing eye and head movements to update correctly the visual environment. No evidence in the literature allows to predict if active head movements will be taken into account during the updating process when subjects actively track a moving target. However, it has been shown that saccades compensate for active head rotations (Medendorp et al., 2002a; Herter and Guitton, 1998) and active head translations (Medendorp et al., 2002b) while maintaining fixation. This question is of particular interest because it is an intermediate step to understand how human beings build and update their internal representation of the surrounding space when several limbs are moving. It also reflects their capacity to modify an initial motor plan to integrate self-generated movements; hence ensuring an accurate displacement. As previously stated, an infinite number of combinations of eye and head displacements can give a similar gaze movement. Even if there is an update of the visual environment when the head is free to move, the sensitivity of the process to a change of eye (or head) contribution is of great interest. If the updating process is insensitive to a variation of eye (head) contribution, this would mean that both eye and head displacements are taken equally into account despite their different dynamics. Finally, with the head free to move, the central nervous system has to account for the VOR. Several studies have looked at the VOR modulation during head-unrestrained gaze movements. Evaluating the interactions between the VOR and the updating process is a step further to understand better how the VOR interacts with vision during everyday life activities.

Part III: head-unrestrained tracking

When an object is moving slowly, subjects can track it with combined eye-head movements. Several studies have looked at the coordination of eye and head

when a subject pursued a target moving horizontally[11] (one-dimensional target movement). Interestingly, there is no previous study of the head-free tracking behavior when the target moves in two dimensions (horizontal and vertical displacement). Because differences have been reported between one-dimensional and two-dimensional pursuit movements with the head fixed[12], analyses of two-dimensional head-free tracking is of particular interest. The generalization of head-restrained observations to the head-unrestrained condition is not straightforward. As for the preceding paragraph, the relative contribution of the head (or the eye) to the gaze tracking can differ between subjects and change the general behavior. Additionally, because the eye and the head have different dynamics, there is no evidence that they could respond identically to different target parameters (orientation, velocity, etc.). Therefore, characterizing the performances during the initiation and the maintenance of pursuit in head-unrestrained condition for two-dimensional targets could fill an important gap in the current state of the literature.

Part IV: model of head-unrestrained gaze saccades

As stated in the previous paragraphs, a similar gaze displacement can be made through an infinite number of eye and head movements, as long as their sum remains the same. It is of particular interest to understand how the brain coordinates the movements of the eyes and the head to achieve a desired gaze saccade. A good way to test theoretical assumptions is to use a modeling approach. With a mathematical model close to the physiology, experiments could be tested and behavioral predictions could be made. Two trends of thoughts currently exist to model the eye-head coordination during gaze saccades. Both theoretical concepts have pitfalls that could not be solved easily. As a result, no consensus has been found yet concerning a control structure that mimics the eye-head behavior during gaze shift. Thus, a model that solves the drawbacks of the two current theoretical solutions is of particular interest for the scientific community.

Part V: model of the VOR

To keep the vision stable, the VOR compensates for head perturbations. The compensation efficiency depends on several factors. Among those parameters, a critical one is the level of accuracy of the evaluation of the perturbing movements. The first part of this introduction demonstrated the importance of a proper control policy to account for the internal delays of the sensory part of the visual system. As for the eye, the sensors that measure head velocity have internal delays that must be integrated to evaluate correctly the head movements. An accurate evaluation of the head movements is critical to ensure the stability of the controlled head trajectory. Therefore, a VOR model that includes the sensors' time delay and estimates the current head perturbation is a major asset to test the interactions between the VOR and active head movements during reorientations of the gaze.

[11] See section 4.6 for a review of head-unrestrained tracking behavior.

[12] E.g., horizontal and vertical pursuit in head-restrained condition have different performances (Rottach et al., 1996; Leung and Kettner, 1997; Kettner et al., 1996).

Part VI: concluding remarks and perspectives

The concluding part will first summarize the findings and the contributions of the thesis. Then, I will give some general comments about head-unrestrained studies. Finally, I will present some open questions that arise from the different studies of the thesis. To help answer those questions, I will propose either behavioral experiments or improvements of the models.

2

Oculomotricity studies: VOR, saccade and pursuit from one milestone paper to another

This chapter starts with a presentation of the anatomy of the eye and the head. Then a review of the literature will describe our current understanding of eye and/or head movements during a reorientation of the gaze. Afterwards, an overview of our current understanding of the neural areas involved in eye movement control will be presented. Through this chapter, unsolved questions and assumptions linked to this thesis will be mentioned. It must be stressed that this chapter does not claim to include a global history/description of eye movements. It will provide to the reader enough information to help him/her to evaluate the different assumptions used in the document.

1 Anatomy

This section presents the main anatomical features of the eye and the head that are necessary for understanding the remaining of the text.

1.1 The eye

1.1.1 The light pathway

Figure I-1 shows a schematic diagram of the eye. The light enters the eye through a transparent surface called the cornea (item 3 in Fig. I-1). Then it goes through the anterior chamber (item 2 in Fig. I-1), the pupil (item 1 in Fig. I-1), the lens (item 5 in Fig. I-1) and hits the light-sensitive part of the eye, the retina (item 17 in Fig. I-1).

To regulate the amount of light that hits the retina, the iris sphincter muscle (also called pupillary sphincter, not shown in Fig. I-1) opens or closes the iris (item 4 in Fig. I-1) which increases or decreases the radius of the pupil allowing more or less light to enter the posterior compartment of the eye.

When the light hits the retina, cone cells and rod cells discharge and send pre-processed information to the primary visual cortical areas[13] through the optical nerve (item 13 in Fig. I-1).

[13] For a review on the computations done by the retina, see (Gollisch and Meister, 2010).

As previously mentioned, the most accurate part of the retina, the fovea (item 15 in Fig. I-1), contains a high concentration of cone cells. The fovea is located in the macula (item 14 in Fig. I-1), a pigmented yellow spot located close to the center of the retina that still contains a high proportion of cone cells.

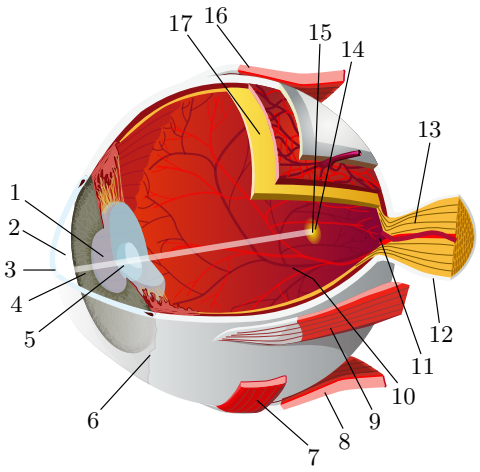

Fig. I-1: **Eye diagram**
(adapted from Wikipedia)

1. Pupil
2. Anterior chamber
3. Cornea
4. Iris
5. Lens
6. Conjunctiva
7. Inferior oblique muscle
8. Inferior rectus muscle
9. Medial rectus muscle
10. Retinal arteries and veins
11. Optic disc
12. Dura mater
13. Optical nerve
14. Macula
15. Fovea
16. Superior rectus muscle
17. Retina

1.1.2 The eye muscles

Each eyeball is held in the orbital cavity by several muscles, ligaments and fascial expansions that surround the eyeball. There are six extraocular muscles organized in three antagonist pairs (four of those muscles are represented in Fig. I-1):

1. The *superior rectus* and the *inferior rectus*.
2. The *medial rectus* (nasal side) and the *lateral rectus*.
3. The *superior oblique* and the *inferior oblique*.

There is also the *levator palpebrae* which is the muscle used for the elevation of the superior eyelid.

Because of their connection to the eyeball, these muscles have several functions. Depending on the initial eye orientation, the extraocular muscles can have a different action on the next rotation. The summary of these actions is shown in the table I-1.

Finally, the eyes have a small inertia (Eye rotational inertia = $6.12\ 10^{-5}$ $[\mathsf{kg}/(\mathsf{deg}/\mathsf{sec}^2)]$] (Robinson, 1981)) that is traditionally assumed negligible in

Muscle	Primary function	Secondary function	Tertiary function
Levator palpebrae superioris	Elevation of the superior eyelid		
Superior rectus	Elevation	Intorsion	Adduction
Inferior rectus	Depression	Extorsion	Adduction
Lateral rectus	Abduction		
Medial rectus	Adduction		
Superior oblique	Intorsion	Depression	Abduction
Inferior oblique	Extorsion	Elevation	Abduction

Table I-1: Functions of the different eye muscles

models of the saccadic system. This assumption is easily validated because the amplitude of the inertial force linked to an acceleration of 50000 [deg/s^2] corresponds to ∼3% of the amplitude of the other forces (Robinson, 1981). As several other modeling studies (Robinson, 1973; Lefèvre et al., 1998; Quaia et al., 1999), this manuscript will use a linear model of the eye with two time constants: 5 and 150 [ms]. This model must be seen as a highly simplified mathematical representation of the eye mechanical properties (Quaia et al., 2009a,b).

1.2 The head

1.2.1 The semicircular canals (SCC)

As described in a previous section, the retina is the sensory part of the eyes that provides visual information for the control of eyes' position. To control head movement, the central nervous system also needs sensors to accurately and rapidly measured 3-D rotational and linear head accelerations with respect to an inertial reference frame. This is the function of the labyrinth located in the inner ear. Because of its sensitivity to head accelerations, the labyrinth is also a part of the system detecting self-motion. Figure I-2 represents schematically the labyrinth anatomy.

The labyrinth has three canals: the horizontal canal (item 8 in Fig. I-2), the posterior canal (item 7 in Fig. I-2) and the superior canal (item 5 in Fig. I-2). Because of their geometries (see Fig. I-2), the three canals are called the "semicircular canals" (SCC). The canals are geometrically arranged to form an approximately orthogonal reference frame. The horizontal canal is roughly aligned with the axis of rotation of horizontal head rotations. Each canal has a specialized part called the cupula located in an enlarged zone called the ampulla (items 3, 4 and 9 in Fig. I-2). A cupula contains the sensory part of the labyrinth: the hair cells that transform mechanical stress into neural signals. The canals are filled with a viscous liquid called the endolymph. With a head rotation, the endolymph in the canals remains stationary with respect to an inertial reference frame and induces a strain in the cupula. This strain is transmitted to hair cells, which change their discharge rate. The disposition of the

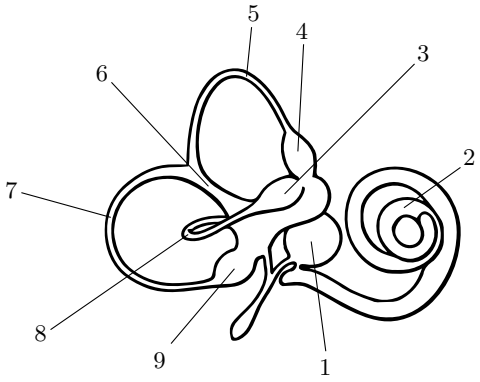

Fig. I-2: **Schematic representation of the labyrinth**

1. saccule
2. cochlea
3. horizontal canal ampulla
4. superior canal ampulla
5. superior canal
6. common canal
7. posterior canal
8. horizontal canal
9. posterior canal ampulla

canals permits them to be sensitive to head rotational acceleration. However, it has been shown that the discharge at the output of SCC is proportional to the head velocity (Goldberg and Fernandez, 1971; Fernandez and Goldberg, 1971). This observation points to a first integration (from head acceleration to head velocity) made by the semicircular canals. The labyrinth contains a second type of sensor in the saccule that reacts to linear 3-D accelerations of the head: the otolith. The discharge of the otolith is proportional to the acceleration (Fernndez and Goldberg, 1976a,b). There is no "primary integration" as in the semicircular canals. Both otolith and semicircular canal discharges must be combined to provide an estimate of the rotational and angular head velocities with respect to an inertial reference frame (Angelaki and Cullen, 2008). A two-stages integration scheme is necessary to combine the linear acceleration information from the otolith with the rotational velocity measurement from the semicircular canals. In a modeling study, Green and Angelaki (2004) proposed a neural network that could solve this issue. The interaction between the otolith and the semicircular canals is not taken into account in this manuscript. We assume that the discharge of the semicircular canals is proportional to the head rotational velocity.

1.2.2 Rotations of the head

The skull is held on the cervical spine by several muscles. Figure I-3 represents the principal ones involved during a head rotation. Table I-2 describes the main effect on head rotations when one of those muscles is innervated. As it can be observed, some are innervated during a specific rotation (e.g. Rectus capitis posterior major/minor, Obliquus capitis superior, etc.) while others can have antagonist actions depending on the muscle's fibers activated (e.g. Sternocleidomastoideus). Additionally, it can be seen from table I-2 that even primary rotations involve a combined action of several muscles.

If the center of rotation of the eyes can be approximated as stationary with respect to a head-fixed reference frame, this is not the case for the center of rotation of the head. The most striking example concerns the rotations around

the pitch axis[14]. The head can extend around the cervical spine vertebra c_1[15] for a movement inside a $[0^o \dots 25^o]$ range. For bigger amplitudes, the spine starts to extend (cervical spine vertebrae from c_1 to c_7) to allow movements in a range of $[25^o \dots 30^o]$. A similar mechanism applies for negative pitch rotations[16]. In a small range of movements, the head can rotate around c_1 to reach rotation angles of $[0^o \cdots -10^o ... -15^o]$. If the rotation is bigger, the spine starts to bend to reach amplitudes between $-10^o ... -15^o$ and $-35^o ... -45^o$.

Action	**Muscles**
Flexion	Sternocleidomastoideus (anterior fibers)
	Longus capitis
	Rectus capitis anterior
Extension	Semispinalis capitis
	Splenus
	Rectus capitis posterior major
	Rectus capitis posteror minor
	Obliquus capitis superior
	Longissimus capitis
	Trapezius (upper fibers)
	Sternocleidomastoideus (posterior fibers)
Lateral Flexion (Abduction) Reduction (Adduction) Rotation	Sternocleidomastoideus
	Obliquus capitis inferior
	Obliquus capitis superior
	Rectus capitis lateralis
	Longissimus capitis
	Splenius
	Semispinalis capitis
	Trapezius (upper fibers)

Table I-2: Muscles involved during head-neck rotations

Therefore, a rotation of the head must be ideally modeled by a piecewise equation: a first part would represent rotations of the skull around c_1. A second part would model the bending of the cervical spine. The head control mechanisms involved in this thesis are sufficiently general that they do not need such a level of details. Thus several assumptions concerning the head movements were made to focus on the main messages of the studies. As an example, the set of muscles that must be activated to generate a head rotation were pooled into a single multi-axis push-pull muscle. However, the overall system has to be described to understand the consequences of the simplifications used during the modeling or the analysis of combined eye-head movements.

Contrary to the eye, the head has a much higher inertia (Head linear inertia = 0.02-0.04 $[\mathsf{kg\,m^2}]$ depending of the axis of rotation (Winters, 1988)). This

[14] Vertical rotations of the head.
[15] Also called "atlas"
[16] Vertical downward rotations.

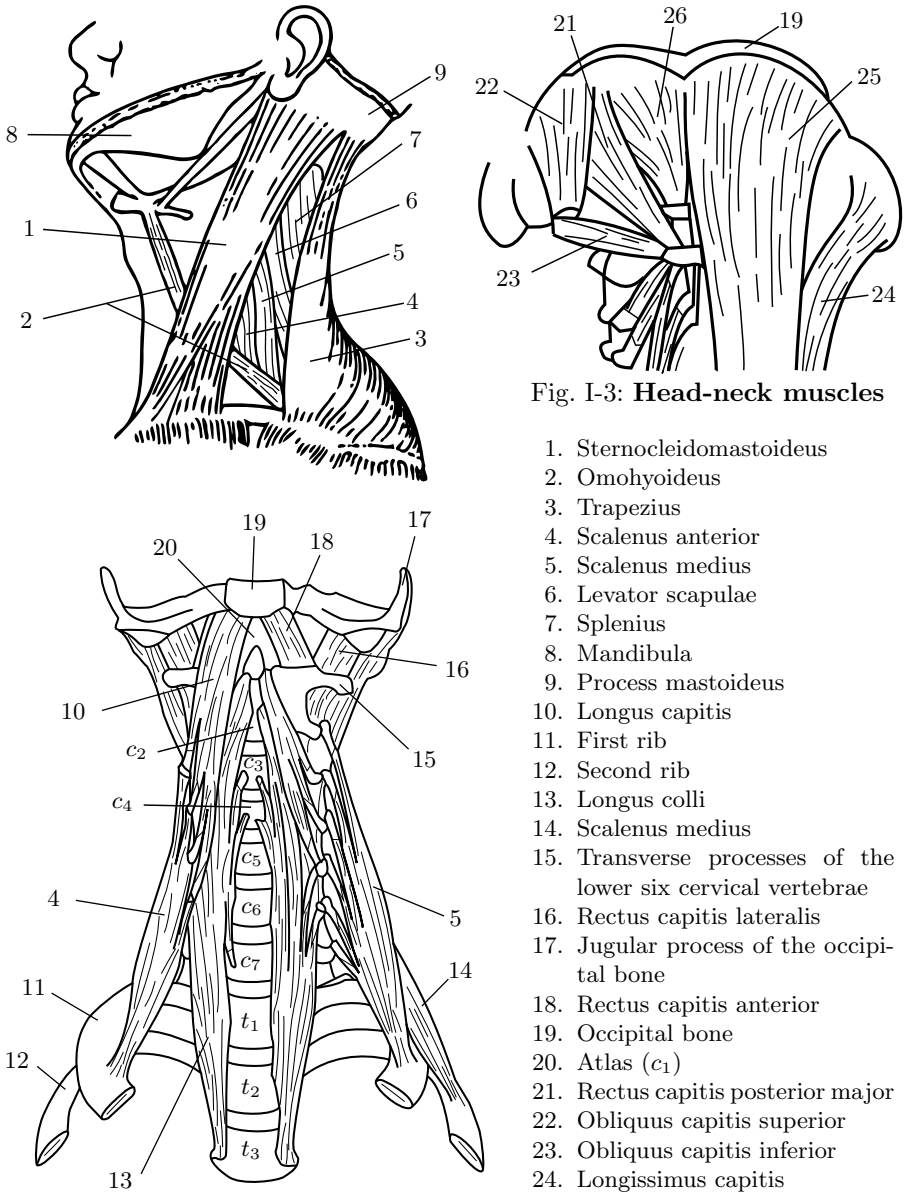

Fig. I-3: **Head-neck muscles**

1. Sternocleidomastoideus
2. Omohyoideus
3. Trapezius
4. Scalenus anterior
5. Scalenus medius
6. Levator scapulae
7. Splenius
8. Mandibula
9. Process mastoideus
10. Longus capitis
11. First rib
12. Second rib
13. Longus colli
14. Scalenus medius
15. Transverse processes of the lower six cervical vertebrae
16. Rectus capitis lateralis
17. Jugular process of the occipital bone
18. Rectus capitis anterior
19. Occipital bone
20. Atlas (c_1)
21. Rectus capitis posterior major
22. Obliquus capitis superior
23. Obliquus capitis inferior
24. Longissimus capitis
25. Semispinalis capitis
26. Rectus capitis posteror minor

inertia increases significantly the settling time of a head response to neck muscle contraction. The analyses and the models built in this manuscript will assume that the head mechanical properties can be mathematically represented by a linear transfer function with a double time constant of 300 [ms].

Anatomy: section summary

Eye	
Sensor:	Retina (most accurate part: fovea)
Muscles:	Three pairs of antagonist muscles
Modeled muscles:	Single push-pull universal muscle for all rotations
Inertia:	Low
Head-Neck	
Sensor:	Labyrinth
Modeled sensor:	Provides the actual head rotational velocity
Muscles:	Several muscles with different actions function of the muscle fibers innervated
Modeled muscles:	Single push-pull universal muscle for all rotations
Inertia:	Large

2 Dodge (1903): first behavioral characterization of eye movements

Dodge (1903) proposed a classification of the eye movements in 1903 that remains valid today! Prior to his study, researchers used direct observation of the movements of their subjects' eyes or compared two photographic plates to study steady state configurations linked to the eye displacements. To analyze the time course of eye movements, Dodge designed an acquisition apparatus that could record horizontal eye movements. Subjects looked at a target while a bright light indirectly illuminated one of their eyes. The light reflected by the subject's eye hit a photosensitive plate. The whole iris was reflected by the eye surface except for the pupil that left a black line on the plate. By imposing a constant velocity to the falling plate, Dodge could record transient horizontal eye movements. Using his recording device, Dodge (1903) described five different types of eye movements (numbered I to V).

The next sections will describe Dodge's findings and explain the current understanding of the three first types of movements he described in head-restrained condition. Finally, a brief neurophysiological description of the central nervous system areas involved in the control of each type of eye movement will be given.

3 Type I: The saccadic system

Dodge (1903) first described a type of eye movement known now as saccade: *"Those movements of the eye in which the point of regard wanders over any relatively fixed section of the field of vision are doubtless the most numerous... [and] naturally constitute the first type"*.

3.1 Typical head-unrestrained saccade

Figure I-4 shows a typical trial of a head-unrestrained saccade. A gaze saccade can be divided into two steps: the gaze displacement and the stabilization process.

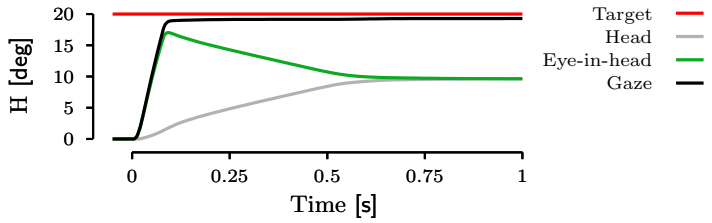

Fig. I-4: **Typical horizontal head-unrestrained gaze saccade.** This figure shows the time course of the head (gray line), the eye-in-head (green line) and the gaze (black line) position when a target (red line) was presented at 20 [deg] to the right. Gaze, head and eye-in-head started aligned. The time origin corresponds to the onset of the gaze saccade. This example has been generated by the model presented in part IV.

During the displacement of the gaze, the eye quickly drives the gaze onto the target while the head starts its movement more slowly than the eye. As soon as the gaze is on the target, any remaining head movement is compensated for by the vestibulo-ocular reflex (VOR) through a counter-rotation of the eye in the orbit to keep the gaze stable. Therefore, the head continues its movement without affecting the gaze position.

If the time course of the saccade is well defined, there are several key problems linked to the control and the coordination of eyes and head when the gaze must be quickly redirected from one position to another. Thus, it is critical to review the key characteristics of saccades to model and study correctly their behavior in head-free condition. First, behavioral studies are used to present the characteristics of head-unrestrained saccades. Then the main cortical areas involved in the generation of saccades between a visual input and the programming of a saccadic goal are presented. Finally, two key areas, the superior colliculus and the cerebellum, are described more extensively because of their central role during head-unrestrained saccades.

3.2 Behavioral characteristics of saccades

Dodge (1903) was the first to describe qualitatively several key features of head-restrained saccades. He showed that the duration of a saccadic eye movement is linked to the amplitude of the saccade. He also observed that saccades undershoot target position when a target with a big eccentricity is presented. Furthermore, he reported that centripetal (from an eccentric initial position toward the primary orbital position) and centrifugal (from the primary orbital position toward an eccentric position) saccades have different kinematics. Finally, he demonstrated that vision is blurred during a saccadic movement.

From the original observations made in (Dodge, 1903), authors have extended our understanding of the saccadic behavior. Becker and Fuchs (1969) studied the accuracy of large eye-only saccades. They showed that subjects used two saccades to fixate a target with an eccentricity equal to 40 [deg]. A first saccade does 90% of the needed displacement and a second one corrects the remaining error to accurately foveate the target. The same analysis in head-unrestrained situation appears to be more controversial. Guitton and Volle (1987) showed that head-free gaze shifts are very accurate (see dotted-dashed line in Fig. 5 of (Guitton and Volle, 1987)) pointing toward a difference in accuracy between head-restrained and head-unrestrained saccades. A year later, Pélisson et al. (1988) showed that the accuracy of gaze shifts are equivalent in both conditions for gaze saccades up to 40 [deg]. Finally, Freedman and Sparks (1997) showed that head-unrestrained gaze saccades undershot the target by approximately 10% in monkeys. Their results confirmed the analyses of Becker and Fuchs (1969) and pointed toward a systematic undershoot of the target by the gaze in both head-fixed and head-free conditions.

It is widely accepted now that head-fixed saccades between stationary targets are relatively stereotyped. Bahill et al. (1975) defined the main sequence relationships to characterize the kinematics of saccades. This relationship linked the amplitude of a head-fixed saccade to either the duration or the peak velocity of the saccade. The main sequence expresses that for an increasing amplitude of the eye-only saccade, there is a saturation of the peak velocity of the eye movement[17]. Being fairly uniform within individuals of a species, the main sequence is widely used to detect and analyze pathologies in patients (e.g. spinocerebellar degeneration induces slow saccades but regular pursuit (Zee et al., 1976)).

Later, Pélisson and Prablanc (1988) quantified the qualitative observation made by Dodge (1903) about the sensitivity of head-fixed saccade kinematics on the initial position of the eye in the orbit. If the eye does not start centered in the orbit, saccades toward the primary position (centripetal saccades) are faster than if the eye is initially centered in the orbit and moves toward an eccentric position (centrifugal saccades) (Pélisson and Prablanc, 1988). Freedman and Sparks (1997) studied the effect of the initial position in the orbit during head-unrestrained saccades. As for the head-fixed situation, they showed that the mean eye velocity is bigger when the target is centripetal than when the eye is centered in the orbit (Fig. 16B in (Freedman and Sparks, 1997)). The effect on gaze (eye-in-space) velocity is less obvious.

[17] Around 500 [deg/s] for human (Bahill et al., 1975)

As pointed out by Dodge (1903), a “gray-out” due to the fast image motion on the retina will appear during each saccade if vision is not ”suppressed“ during the eye rotations. Because saccades are the most numerous eye movements, those blurred images would result in constant visual instabilities without any compensation. Two mechanisms have been described to explain how the vision is blurred during saccades. Campbell and Wurtz (1978) demonstrated the principle of image masking: the blurred images that could result from saccadic movements are partially masked by stationary scenes at saccades' onset and offset. Comparing the contrast sensitivity when a saccade was executed to an equivalent movement of the target on the retina while the eyes remained fixed, Diamond et al. (2000) showed that extraretinal information is also used during saccadic suppression.

With the head free to move, authors have observed that the eye and the head trajectories are usually strongly coupled during head-unrestrained gaze saccades (e.g. (Guitton et al., 1990; Bizzi et al., 1971; Guitton et al., 1984)). However, several observations also demonstrated a certain level of independence between the gaze and the head movements. Authors showed that the head and the gaze trajectories can have different orientations (Goossens and Van Opstal, 1997) or can be temporally unsynchronized (Freedman and Sparks, 1997). Finally, Guitton and Volle (1987); Freedman and Sparks (1997) showed that the charateristics of head movements vary as a function of the gaze saccade amplitude. Some authors have tried to express equivalent main sequences in head-unrestrained conditions (Freedman and Sparks, 1997; Zangemeister et al., 1981). (Freedman and Sparks, 1997) showed that gaze saccades peak velocity increases linearly up to $\sim$600 [deg/s] for gaze amplitude smaller than $\sim$20 [deg]. Then the peak velocity decreases to reach a plateau of $\sim$400 [deg/s] for saccade amplitudes larger than 40 [deg]. The peak velocity of the head movement during head-free saccades increases linearly with the amplitude of the gaze shifts in the range of observed saccades (up to 55 [deg]). A major issue in building an equivalent relationship to the head-fixed main sequence for head-unrestrained conditions comes from idiosyncrasies in the head movement behavior. Therefore, a saccade in head-unrestrained conditions is not stereotyped as in head-restrained conditions. As an example, Fuller (1992) studied the propensity of human subject to make large volitional head movements. He defined two classes of persons depending on the gain of the head movement[18]. With the same experimental conditions, ”head movers“ tended to make larger head-movement (higher gain) than ”head non-movers“. Additionally, we can make voluntarily a larger or a faster head movement whereas it is not possible to modulate the amplitude or the velocity of eye movements to reach a target[19]. From those observations, it appears clearly that it is difficult to control the repeatability of a head-unrestrained movement to collect enough data and then, to report a coherent behavior in head-unrestrained condition.

[18] Ratio of head movement amplitude to gaze saccade amplitude.

[19] There is a difference between deciding to look at a specific region of the visual space and deciding to do a saccade of a particular orientation, amplitude and/or velocity.

Finally, using perturbations of the head movement during an ongoing gaze shift, several behavioral experiments indicate the ability of the gaze control system to reject perturbations that can occur during a saccade (Guitton et al., 1984; Laurutis and Robinson, 1986; Guitton and Volle, 1987; Choi and Guitton, 2006, 2009). Even when a brake abruptly stops an ongoing head movement, the gaze ends close to the position of the unperturbed gaze saccade. The ability to correct for such large perturbations of gaze trajectory strongly suggests a feedback of gaze position.

3.3 Neurophysiology

Several areas of the central nervous system are involved to control and coordinate the eye and head trajectory during a gaze shift. First the target information must be extracted from the projection of the environment on the retina. Then, the desired displacement must be planned. Finally, the commands sent to the extraocular and the neck muscles must be correctly computed to achieve accurately the movement. This section does not have the pretension to exhaustively present all the neural areas involved during the programing and the execution of saccades. It will present the main pathways reported to be active during saccades. In the first sections, the areas involved during head-restrained saccades will be described. The last section will present the neural circuitry for the control of head movements.

3.3.1 From the retina to the cerebellum and the superior colliculus

The information from the retinal ganglion cells (R in Fig. I-5) project to the primary visual cortex (V1: (Hendrickson et al., 1978), V2: (Fries, 1981; Bullier and Kennedy, 1983)) through the lateral geniculate nucleus (LGN, 3 in Fig. I-5) (Perry et al., 1984).

Then, primary computations are realized from V1 to V4 in the primary visual cortex (PVC, 5 in Fig. I-5). A lot of studies have been conducted to describe the activity of the primary visual areas (V1: horizontal disparity-sensitive cells (Cumming, 2002), V2: depth perception (Hubel and Wiesel, 1970), V3/V3a: global motion processing (Braddick et al., 2001; Koyama et al., 2005), V4: color specific cells (Zeki, 1978), attentional modulation (Moran and Desimone, 1985)). However, it appears that there is no border between functions as discrete as the anatomical differences. The functional organization is more gradual. Therefore, the primary visual areas must be seen more as a large set that transforms the retinal image into something behaviorally relevant. The activity of areas V3 and V4 projects to the lateral intraparietal area (LIP, 4 in Fig. I-5) (Blatt et al., 1990).

LIP is known to be an important neural structure during saccadic eye movements (Shibutani et al., 1984). Particularly, some LIP cells (intended cells) have an activity correlated with the planned movement during the latency of a saccade toward a remembered target location (Gnadt and Andersen, 1988). LIP projects to the frontal eye field (FEF, 2 in Fig. I-5) and the superior colliculus (SC, 7 in Fig. I-5).

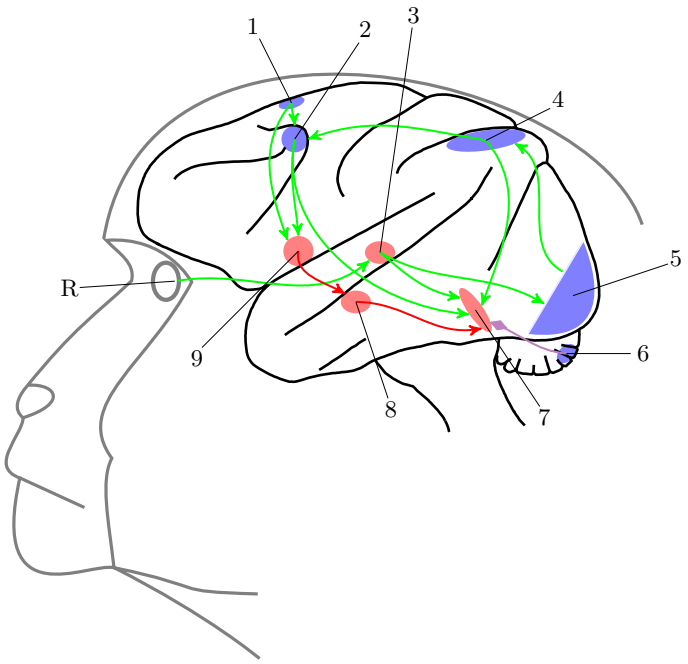

Fig. I-5: **Main cortical saccadic pathways to the superior colliculus.** Excitatory connections are represented in green, inhibitory connections in red. Facilitations are represented in purple with a diamond tip. Blue structures are on the cortex surface, red structures are hidden by the cortex. For clarity, the FEF ⇒ VERM excitatory connection is not represented. See text for more details. **1** SEF: supplementary eye field, **2** FEF: frontal eye field, **3** LGN: lateral geniculate nucleus, **4** LIP: lateral intraparietal area, **5** PVC: primary visual cortex (V1 ⇒ V4), **6** VERM: cerebellar vermis, **7** SC: superior colliculus, **8** SNr: substantia nigra pars reticulata, **9** CN: caudate nucleus, **R**: retina

FEF is a roughly retinotopically organized neural structure of the prefrontal cortex[20] (Bruce et al., 1985). It is involved in "whether, when and to where" a saccade must be triggered (Bruce and Goldberg, 1985; Bruce et al., 1985; Schall, 2002). Stimulations of FEF neurons evoke saccades with fixed amplitude and orientation without an effect of eye position (fixed-vector saccades) (Bruce et al., 1985). When FEF is stimulated in head-unrestrained conditions, Tu and Keating (2000) reported that the evoked gaze shifts were qualitatively similar to natural gaze saccades. Another important input to FEF in the control of saccadic eye movements is the supplementary eye field (SEF, 1 in Fig. I-5). Micro-stimulations of SEF also induce saccades (Schlag and Schlag-Rey, 1985, 1987). However, a significant proportion of generated saccadic eye movements from SEF stimulations are goal-directed (34%), the remaining proportion being either fixed-vector saccades (43%) or of undetermined type (33%) (Schlag

[20] Shorter saccades represented ventrally, larger saccades medially.

and Schlag-Rey, 1987). The study of Schlag and Schlag-Rey (1987) has been conducted in head-fixed monkeys. Martinez-Trujillo et al. (2003b) stimulated SEF in the head-unrestrained monkeys. They observed that all the evoked saccades were composed of a combined eye-head displacement. Martinez-Trujillo et al. (2003b) also compared the kinematics of the stimulated saccades to the kinematics of visually triggered saccades. They did not observe any difference. The same year, Martinez-Trujillo et al. (2003a) demonstrated that freeing the head changes the convergence of the stimulated gaze saccades[21]. FEF projects directly to SC and indirectly through the caudate nucleus (CN, 9 in Fig. I-5) and to the substantia nigra pars reticulata (SNr, 8 in Fig. I-5) of the basal ganglia.

CN and SNr are both included in a neural structure called "the basal ganglia". Authors have shown that apart from its involvement in the control of saccades, the basal ganglia also plays a significant role in attention, working memory, decision making, expectation, etc. Here we will cite the major contributions of the basal ganglia in the saccadic control. A general review of the different functions of the basal ganglia in the central nervous system is made by Hikosaka et al. (2000). In a simplified description, the basal ganglia can be seen as a central inhibitory area of the central nervous system (Hikosaka et al., 2000).

CN is one of the three input nuclei of the basal ganglia[22]. It receives inputs from both the FEF and the SEF (Parthasarathy et al., 1992; Shook et al., 1991). Electrophysiology studies have shown that CN inhibits monosynaptically SNr (Hikosaka et al., 1989a; Yoshida and Precht, 1971). CN neurons' activity related to saccades can be divided into three categories. A first type of neurons modulated their discharge during memory-guided saccades[23]. A second population changes their activity during visual saccades[24]. The activity of the third one changes during the preparation of saccades (Hikosaka et al., 1989a,b).

SNr is one of the two major outputs of the basal ganglia[25]. Hikosaka and Wurtz (1983, 1985) showed with electrophysiological recordings and chemical injections in SNr or SC that SNr cells tonically inhibit SC neurons related to saccadic movements[26].

Up to now, the neural computations extracted the target information from the visual environment and computed the goal of a saccadic movement. The

[21] Stimulated saccades with the head free were more goal-directed than saccades with the head free to move.

[22] The others are the putamen (PUT) and the nucleus accumbens (NAcc). Pooled together, CN, PUT and NAcc are called the striatum (STR) and constitute the input stage of the basal ganglia

[23] In this task, a target is briefly presented while the monkey fixates a second target. After a variable delay, the monkey receives a cue to initiate a saccade toward the remembered position of the flash.

[24] As soon as the subject sees the target, he/she must reorient his/her visual axis toward the target.

[25] The second one is the internal segment of the globus pallidus: GPi

[26] SNr cells stop to discharge before visual or memory-guided saccades. Therefore, they stop inhibiting SC cells and a saccade is initiated (Hikosaka and Wurtz, 1983).

next two sections (3.3.2 and 3.3.3) will describe two key subcortical areas for the execution and the control of gaze saccades.

3.3.2 The superior colliculus

The superior colliculus (SC) is a layered neural structure of the midbrain. SC is composed by seven layers grouped in three main parts: the superficial layers (laminae I, II and III), the intermediate layers (laminae IV and V) and the deep layers (laminae VI and VII). The superficial and the intermediate layers receive inputs from the LGN (Apter, 1945), from SNr (Jayaraman et al., 1977; Hikosaka and Wurtz, 1983), from the deep cerebellar nuclei (dCN) (Niemi-Junkola and Westby, 2000; Gonzalo-Ruiz and Leichnetz, 1987; Gayer and Faull, 1988), from FEF (Stanton et al., 1988) and from LIP (Blatt et al., 1990). Those inputs convey information from several modalities: auditory, visual, somatosensory, etc. The different activities are combined inside the intermediate and the superior layers (Wallace et al., 1998; Wickelgren, 1971) and sent to the deep layers (Mooney et al., 1988).

SC activity and head-restrained movements

SC relationship to eye movements is known since the original study of Adaműk[27] in 1872. From this initial study, a lot of experiments have permitted to understand better how SC activity was correlated with visual inputs (superficial layers) or motor commands (deep layers). In 1945, Apter (1945) stimulated the retina of cats while simultaneously recording in SC. She established the first collicular map[28] by linking the maximum recorded activity with the position of the electrode on SC's superficial layers. Later, Goldberg and Wurtz (1972a,b) established the receptive field of the cells in the superficial layers of SC and showed how the amplitude of the collicular neurons' discharge was modulated by attention[29].

In parallel to studies about the sensory layers of SC, authors looked at the properties of the motor layers. Wurtz and Goldberg (1971) showed that neurons in SC deep layers discharge prior to an eye saccade. Using electrical stimulation, Robinson (1972) found a similar mapping of SC motor layers as the one observed in the superficial layers by Apter (1945). Robinson (1972) called this map "the motor map" of SC because stimulations at a specific area of this map evoke fixed-vector saccades. Figure I-6 presents the motor collicular map as described by Robinson (1972). From this map, one can determine the amplitude of an electrically evoked saccade by looking at the location of the stimulation. Red lines in Fig. I-6 correspond to the vertical amplitude of the stimulated movement while black lines correspond to the horizontal saccadic component.

---

[27] The original paper of Adaműk: *Uber angeborene und erworbene Association von F. C. Donders.* has been published in German in 1872. A summary of Adaműk's results is provided in the introduction of (Robinson, 1972).

[28] See Fig. 2 and Fig. 3 of (Apter, 1945)

[29] The activity of a cell is enhanced when a saccade is triggered toward its receptive field (Goldberg and Wurtz, 1972b)

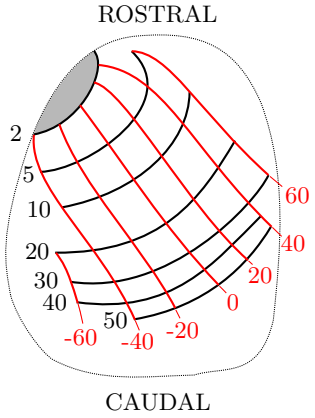

Fig. I-6: **Left SC motor map**

This figure shows the motor map of the deep layers of the superior colliculus (SC) as described by Robinson (1972). The map linked the amplitude of a stimulated saccade with the location of the stimulation. Red lines correspond to vertical component of the induced saccade while black lines correspond to its horizontal amplitude. The rostral gray area corresponds to the "fixation zone" initially described by Munoz and Wurtz (1993).

As it can be seen in Fig. I-6, a "hole" remained in the original SC map proposed by Robinson (1972). What is happening when a stimulation is applied in the extreme rostral part of SC (gray area in Fig. I-6)? Munoz and Wurtz (1993) recorded the neural activity of the intermediate layers in this area and reported that neurons discharged when subjects fixated a stationary target or pursued a moving target and paused when they made a saccade. Following those observations, they called the neurons in this area of the SC motor map "fixation neurons". Later, Munoz and Wurtz (1995a,b) continued to characterize the activity of neurons in the SC maps. They described two types of neurons in SC intermediate layers. The burst neurons discharge just before saccades' onset and cease to fire with saccades' offset while the buildup neurons gradually increase their discharge long before the saccade and stop discharging at the end of the movement. Munoz and Wurtz (1995b) also showed that the center of activity of burst neurons remained stationary during a saccade while the center of activity of the buildup neurons moved and formed a continuum with the fixation neurons where they thought saccades ended. Using functional imaging, Moschovakis et al. (2001) showed later that the activity of the superficial and intermediate layers of the superior colliculus do not move during a saccade. Recently, Hafed et al. (2009) recorded neurons in the "fixation zone" with discharges correlated with microsaccades[30] as the one observed by (Munoz and Wurtz, 1995a,b) more caudally. Their results showed that SC map is continuous from the caudal part to the rostral part.

SC activity and head-unrestrained movements

Electrophysiological studies in head-unrestrained conditions are harder to conduct than the same studies with the head fixed. One of the biggest challenges is to keep the probe used to stimulate or record brain areas fixed on the isolated neuron during several trials to observe a global behavior.

Four major studies have initially stimulated collicular neurons in head-free conditions: two with cats (Guitton et al., 1980; Roucoux et al., 1980) and two with monkeys (Freedman et al., 1996; Stryker and Schiller, 1975). Stryker and

[30] Microsaccades are saccades with an amplitude smaller than 12 min arc

Schiller (1975) showed that a stimulation of SC invoked a combined eye-head movement. They showed that the characteristics of the evoked head movements were not as stereotyped as the eye movements evoked by SC stimulations in head-fixed condition. They concluded that the superior colliculus could not be the center for the generation of head movements in species with a large oculomotor range.

In a pair of companion papers, Guitton et al. (1980) and Roucoux et al. (1980) showed that the characteristics of evoked saccades in head-fixed and in head-free conditions are similar. They also showed that when stimulation is applied in the very caudal part of cats' SC, saccades both in head-restrained and in head-unrestrained conditions are goal-directed oppositely to the fixed-vector saccades in more rostral stimulations. The null effect of a release of the head on the properties of the stimulated saccades is a strong argument for a gaze command delivered by the superior colliculus.

Freedman et al. (1996) extended the observations of Guitton et al. (1980); Roucoux et al. (1980) by looking at the effect of the stimulation parameters on the evoked gaze shifts. They showed that gaze shift amplitude is a saturated function of the stimulation duration: the amplitude of the combined eye head movement increases with the duration of the stimulation until it reaches a plateau. Further augmentations of the stimulation duration generate a second saccade of the same amplitude.

Outputs of the superior colliculus

SC neurons project to different neuron populations in the brainstem and in the spinal cord. Two projections from SC to the brainstem area have been shown: one to the paramedian pontine reticular formation (PPRF) (Scudder et al., 1996) and the second to the nucleus raphe interpositus (RIP) (Langer and Kaneko, 1984; Fuchs et al., 1985; Scudder et al., 1996).

In parallel, Anderson et al. (1971) showed that a stimulation of SC deep layers induced excitatory potentials on the neck motoneurons in the cat spinal cord. They showed that the recorded potential is probably disynaptic and corresponds to a tectoreticulospinal[31] pathway rather than a tectospinal[32] pathway.

3.3.3 The cerebellum

The cerebellum is located under the posterior cerebral cortex (item 6 in Fig. I-5 is a part of the cerebellum). A large part of the cerebral cortex surrounds the cerebellar cortex. Despite the external visual impression, there is no direct connection between the cerebellum and the posterior cerebral cortex. The cerebellum is attached to the rest of the central nervous system through the brainstem by three pairs of tracks: the inferior (item 8 in Fig. I-7), the middle (item 9 in Fig. I-7) and the superior (item 10 in Fig. I-7) cerebellar peduncles. As shown in Fig. I-7, it has two hemispheres (item 2 in Fig. I-7) and a central common part called the vermis (item 11 in Fig. I-7).

[31] Projection from the colliculus to the spinal cord through the reticular formation in the brainstem.

[32] Direct projection from the colliculus to the spinal cord.

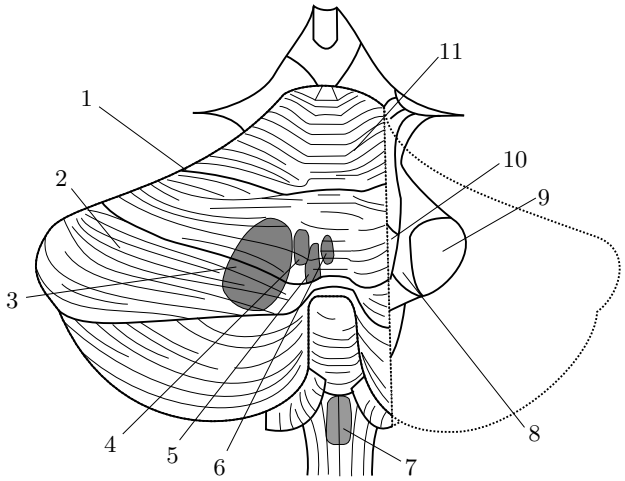

Fig. I-7: **Cerebellum, inferior olivary and deep nuclei** This figure represents a dorsal view of the cerebellum with the deep cerebellar nuclei (dCN) highlighted. **1.** Primary fissure **2.** Hemisphere **3.** Dendate nucleus **4.** Emboliform nucleus **5.** Globose nucleus **6.** Fastigial nucleus **7.** Inferior olivary nucleus **8.** Inferior cerebellar peduncle **9.** Middle cerebellar peduncle **10.** Superior cerebellar peduncle **11.** Vermis. Adapted from R.M. Berne, M.N. Levy, Physiology, Mosby-Year Book Inc., 1993.

Cerebellar neural network

Despite its small size (10% of the total volume of the cerebrum), the cerebellum contains approximately half the number of the central nervous system neurons (Kandel et al., 2000). The neural network in the cerebellum has a remarkably stereotyped architecture represented schematically in Fig. I-8. The mossy (item 3 in Fig. I-8) and the climbing (item 1 in Fig. I-8) fibers are the two inputs of the cerebellar neural circuit. Five types of cells composed the primary network in the cerebellum's cortex: the Purkinje cells (item 8 in Fig. I-8), the granule cells (item 4 in Fig. I-8), the Golgi cells (item 6 in Fig. I-8), the stellate cells (item 9 in Fig. I-8) and the basket cells (item 7 in Fig. I-8). Those cells are grouped in three layers: the molecular layer, the Purkinje cells layer and the granular layer.

The granule cells are connected with the mossy fibers (excitatory input) and the Golgi cells (inhibitory input) in an agglomerate called glomerulus (item 2 in Fig. I-8) at the level of the granular layer. The mossy fibers convey information from the reticular formation in the brainstem, from the spinal cord, from the cerebral cortex and from the vestibular nerve. The axons of the granule cells travel to the superficial layer and constitute the parallel fibers (item 10 in Fig. I-8). The parallel fibers excite a large number of Purkinje cells in the superficial

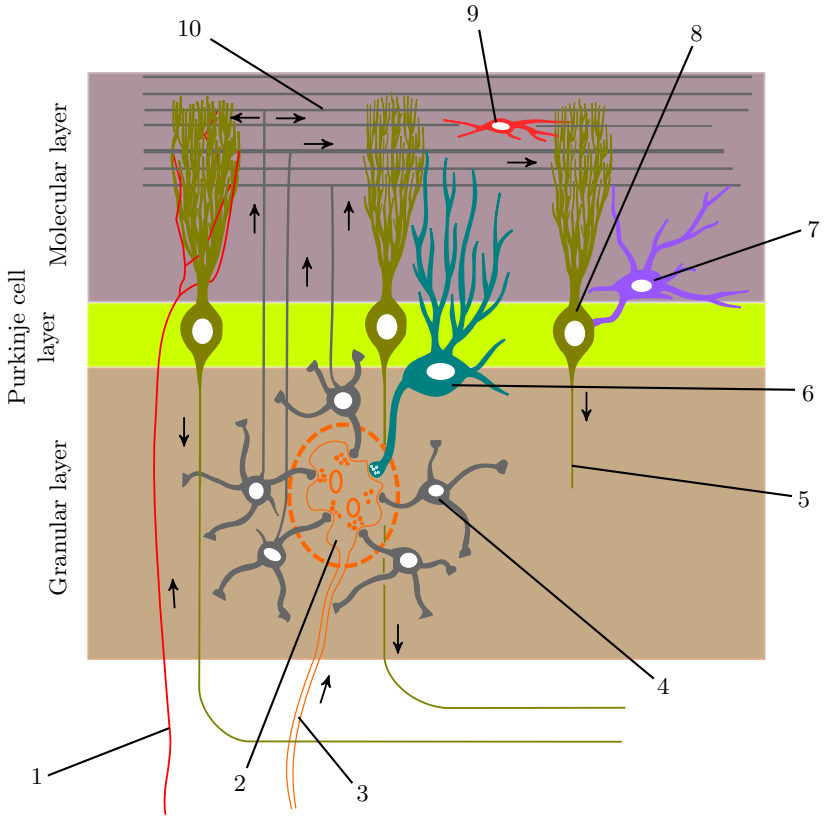

Fig. I-8: **Cerebellum cortex neural networks** This diagram shows the general neural network of the cerebellar cortex. **1.** Climbing fibers **2.** Glomerulus **3.** Mossy fibers **4.** Granule cell **5.** Purkinje cell axon **6.** Golgi cell **7.** Basket cell **8.** Purkinje cell **9.** Stellate cell **10.** Parallel fibers

layer. In addition to the connection with the parallel fibers, each Purkinje cell receives a connection from a single climbing fiber. The climbing fibers come from the inferior olivary nuclei and transmit cerebral, visual and somatosensory information. Finally, the basket cells inhibit the body of Purkinje cells while the stellate cells inhibit the dendritic arbor of the Purkinje cells.

The axons of the Purkinje cells constitute the output of the cerebellar circuitry: they inhibit the deep cerebellar nuclei (the dendate nucleus, the emboliform nucleus, the globose nucleus and the fastigial nucleus). The output of dCN projects to the motor system (in our case to the brainstem and the spinal cord).

Cerebellum and saccades

Since the early 1900's, Holmes (1917) already showed the importance of the cerebellum for the control of movements. He specifically pointed out an effect of cerebellar lesions on eye movements. However, if the neural architecture of

the superior colliculus provides a precise link between the collicular activity and the resulting gaze displacement (see section 3.3.2), it is much more complicated to find a clear relationship linking the position of one of the neurons (or a population of neurons) in the cerebellar cortex to a resulting eye movement. The first attempt to create a mapping of the surface activity of the cerebellum linked to either an auditory, a tactile or a visual stimulation was made by Snider and Stowell (1944). The authors recorded the electrical activity on the surface of the cerebellar cortex and reported the different areas that discharged during one of the stimulations. Snider and Stowell (1944) reported that visual stimulation evoked electrical activity on the vermis. Later, Ron and Robinson (1973) tried to build a motor map similar to the collicular map by electrically stimulating the cortical surface of the cerebellum. They were able to generate saccades and smooth eye movements when they stimulated lobules V-VII in the vermis (see Fig. 8 in (Ron and Robinson, 1973)) or the crus I and II of the hemispheres (see Fig. 9 in (Ron and Robinson, 1973)). However, even if a large variety of the possible eye movements was electrically evoked, no map as clear as the collicular one resulted from the stimulations.

Later, Noda and Suzuki made considerable advances in understanding the relationship that links the cerebellum and eye movements (Noda and Suzuki, 1979a,b). They classified the Purkinje cells in the monkey flocculus based on the cells' activity with respect to saccades. Either the cells stop discharging (pause cells), or they discharge for all directions (burst cells), or they burst for a particular direction and pause for the opposite one (burst-pause cells) (Noda and Suzuki, 1979b). They also showed a similar correlation between the activity of the afferents of Purkinje cells and saccades (Noda and Suzuki, 1979a)[33]. Looking at one of the output nuclei of the flocculus and the vermis, Fuchs et al. (1993) recorded the activity of neurons in the fastigial nucleus of monkeys and showed a correlation between the recorded fastigial neurons activity and saccade amplitude or duration. However, Fuchs et al. (1993) pointed out that the discharge of the fastigial neurons was variable even for similar saccadic movements in the preferred direction of the neurons.

In parallel to the recording experiments, authors created cerebellar lesions in monkeys (Barash et al., 1999; Robinson et al., 1993; Optican and Robinson, 1980; Ritchie, 1976) and studied patients with cerebellar lesions (Waespe and Baumgartner, 1992; Zee et al., 1976) to show how a perturbation on the cerebellum modifies saccade trajectory. Zee et al. (1976) showed that patients with spinocerebellar ataxia, a genetic progressive degeneration of the cerebellum, can make accurate saccades albeit extremely slow. The same year, Ritchie (1976) bilaterally removed both the oculomotor part of the vermis and some parts of the cerebellar hemisphere. Following the lesions, Ritchie (1976) recorded saccades that were either hypermetric[34] or hypometric[35] but more importantly for this thesis, he showed that the saccadic behavior was similar if the head was

[33] It is important to stress that Noda and Suzuki (1979a,b) showed the implication of the flocculus cells in eye movement but did not map the cells location with the evoked eye movement as in (Ron and Robinson, 1973).

[34] Saccade overshoot the target

[35] Saccade undershoot the target

free to move or not. This result implies a role for the cerebellum in the control of the gaze, not in a separate control of the eye. Later, Vilis and Hore (1981) confirmed the dysmetric behavior of saccades using a reversible inactivation of the cerebellar nuclei[36]. Using pharmacological lesions of the fastigial nucleus, Robinson et al. (1993) could create lesions less diffused than (Ritchie, 1976; Vilis and Hore, 1981). The authors reported that saccades were hypermetric in the direction of the unilateral lesion and hypometric in the opposite direction. They also reported more variability at the endpoint of saccades with a fastigial lesion compared to a healthy situation.

In parallel to the studies on cerebellar activity during normal saccades, authors showed the importance of the cerebellum in the adaptation of the eye movements with respect to a perturbation. McLaughlin (1967) was the first to propose a protocol that demonstrated the adaptive mechanism of the saccadic system. As mentioned in the general introduction, vision is impaired during a saccade. Thus a position step of the target during the execution of a saccade is only perceived by the subject when the movement is finished. The unexpected error at saccade's offset is compensated for by a corrective saccade toward the modified target position. If the same protocol is repeated several times (around 200 times for humans and 1000 times for monkeys), subjects can make a movement directly toward the final position of the target while ignoring the initial position of the target (which is the actual visual input of the saccadic system). Optican and Robinson (1980) were the first to study the effect of large cerebellar lesions[37] on the adaptive mechanism of the saccades. They showed that cerebellar-lesioned monkeys were not able to adapt the amplitude of the saccade to reach accurately the target in a single adapted movement. Later, Barash et al. (1999) showed the same behavior but restricted the extent of the cerebellar lesion to the oculomotor vermis. As postulated sooner by Optican et al. (1985), Barash et al. (1999) demonstrated that the rapid adaptation mechanism of the cerebellum is present amongst other things to overcome the extraocular muscles weakness linked to the fatigue of repetitive eye movements.

As a summary, authors have shown that lesions of the cerebellum do not impair the ability to execute a saccade. However, they alter the accuracy, the consistency, the velocity and the adaptive mechanism of saccadic movements.

Cerebellum and head-unrestrained saccades

The studies of the cerebellar involvement during head-unrestrained saccadic movements appeared later than the studies in the head-restrained condition (except for (Ritchie, 1976)). Shimizu et al. (1981b,a) looked at the eye-head coordination in patients with cerebellar ataxia. They showed that patients generated gaze saccades that were, as in head-restrained condition, dysmetric. Additionally, he pointed out that the amplitude of the head movements for those patients was bigger than for normal subjects.

Looking at the importance of the output nuclei of the cerebellum on the coordination of eye and head movements during head-unrestrained gaze saccades,

[36] Vilis and Hore (1981) also showed that the amplitude of the dysmetria was proportional to the position of the eye in the orbit.

[37] Vermis, paravermis and fastigial nuclei were removed in two monkeys.

Pélisson et al. (1998) inactivated the rostral part of the fastigial nucleus (rFN) in cats. They observed that the saccades were hypermetric when they were directed toward the side of the lesion (ipsilesioned saccades). On the contrary, saccades were hypometric when directed toward the opposite side of the lesion (contralesioned saccades). Additionally, Pélisson et al. (1998) showed that the amplitude of the dysmetria was proportional to the amplitude of the gaze shift. Finally, the same authors showed that changes in the head trajectory were correlated with a change in saccade trajectory. The same year, Goffart et al. (1998a,b); Goffart and Pélisson (1998) studied the effect of an inactivation of the caudal fastigial nucleus (cFN) in the cat on head-unrestrained gaze saccades. Goffart et al. (1998a) recorded hypermetric ipsilesional saccades. However, contrary to the observations of Pélisson et al. (1998) with rFN lesions, the amplitude of the dysmetria remained fixed with respect to the saccade amplitude. Ipsilesional head-unrestrained gaze saccades appeared to be goal-directed when cFN is lesioned (see Fig. 6 in (Goffart et al., 1998a)). If a difference occurred between the lesions in cFN and in rFN for the ipsilesional gaze saccades, Goffart et al. (1998a) reported that the effects of the lesion on the contralesional saccadic movements were similar to the observations made by Pélisson et al. (1998)[38]. Goffart et al. (1998b) showed that the observed dysmetria of the gaze saccades when the cFN was lesioned is equally distributed on both the head and the eye components of the gaze movement: a change of the gaze amplitude by a certain factor corresponds to an equivalent change of both eye and head displacements by the same factor. Goffart et al. (1998b) also pointed out a small decrease of the maximum velocity of the eye and the head components when the cFN is lesioned. Finally, Goffart and Pélisson (1998) showed that even when the cFN was lesioned a perturbation on gaze before the execution of a saccade toward a remembered target was taken into account to correct the amplitude of the movement[39].

Recently, Quinet and Goffart (2005, 2007) reproduced in the monkey the experiments made by Goffart et al. (1998a,b) in the cat. They showed the same behavior as the one reported in the cat with a main difference: in the monkey, the eye movement is almost totally responsible for the dysmetria, the head seems to be less influenced by a cFN lesion. Quinet and Goffart (2007) also showed that vertical saccades were deviated toward the side of the lesion as previously observed in head-restrained conditions by Robinson et al. (1993). Finally, Quinet and Goffart (2009) electrically stimulated the cFN to study the evoked gaze movements. As for Ron and Robinson (1973), the authors did not find a topographical organization of the neurons in the cFN. They also showed that the stimulation induced eye movements but did not easily evoke head displacement.

[38] Hypermetric saccades with an amplitude of the dysmetria proportional to the amplitude of the gaze saccade.

[39] The amplitude of the dysmetria remains equal with or without a perturbation.

3.3.4 Brainstem areas involved in eye movements

As shown in the two previous sections, the SC and the cerebellum sent commands to the eye through the brainstem. A first region of the brainstem, the paramedian pontine reticular formation (PPRF) in the pons, is associated since the 1960's with horizontal saccades and quick phases of the nystagmus (Cohen and Feldman, 1968). The activity of the second, the rostral mesencephalic reticular formation (rMRF), is related to vertical saccades and torsional eye movements (King and Fuchs, 1979). For clarity, the circuitry involved in the generation of horizontal eye movements will be first described. Then a second paragraph will present the main differences between the horizontal and the vertical "channels".

The brainstem neural circuitry for conjugate horizontal eye movements

In the late 1960's, trying to understand how saccades are generated by the central nervous system, Cohen and Feldman (1968) recorded neural activity in the PPRF associated with horizontal saccades and quick phases of the nystagmus. Later, Sparks and Travis (1971) and Luschei and Fuchs (1972) extended the results of Cohen and Feldman (1968) and characterized PPRF neurons as a function of their activity with respect to saccadic eye movements. They found three major types of neurons: the first one discharges vigorously ("burst neurons") with a saccade, the second category has a background activity during fixation but stops discharging during the saccade ("pausing neurons") and the last population has an activity correlated with the eye position in the orbit ("tonic neurons"). Luschei and Fuchs (1972) also showed that the saccade duration was proportional to the duration of the burst and the pause duration. Later, Keller (1974) showed that the amplitude of the activity of the burst neurons is related to the direction of the saccadic movements ("directional neurons") while pause neurons stop discharging for all the saccades, independently of the saccade orientation ("omnipause neurons", OPNs). In the same study, Keller showed that the frequency of discharge of the burst neurons is proportional to the eye velocity during the saccade. All those experiments pointed toward a projection of the PPRF neurons to the extraocular muscles responsible for horizontal eye movements.

Up to the late 1980's, researchers have studied the connectivity of the neurons in the brainstem. A summary of the results can be represented by the connectivity diagram of Fig. I-9. Figure I-9 represents the different connections between the populations of neurons involved during horizontal eye movements. Mechanically, to generate a saccadic eye movement to the left (red arrows in Fig. I-9), the medial rectus of the right eye (MR_R in Fig. I-9) and the lateral rectus of the left eye (LR_L in Fig. I-9) must be contracted while the lateral rectus of the right eye (LR_R in Fig. I-9) and the medial rectus of the left eye (MR_L in Fig. I-9) must be extended.

The abducens nucleus (ABD in Fig. I-9, also called VI nucleus) contains motoneurons (MN in Fig. I-9) that are directly connected to the ipsilateral[40]

[40] Neuron and muscle on the same side.

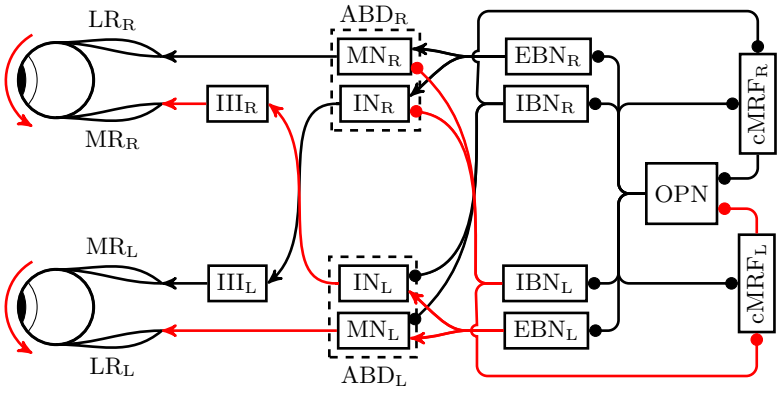

Fig. I-9: **Brainstem connections diagram for horizontal eye movements** This figure represents the connections between populations of neurons in the brainstem. Subscript "L" corresponds to the neurons on the left side while subscript "R" corresponds of neurons on the right side. Arrow tips correspond to excitatory connections. Filled circle tips correspond to inhibitory connections. EBN: excitatory burst neurons, IBN: inhibitory burst neurons, OPN: omnipause neurons, cMRF: central mesencephalic reticular formation, ABD: abducens nucleus, MN: motoneurons, IN: interneurons, III: third nucleus.

lateral rectus (LR in Fig. I-9). ABD also contains interneurons (IN in Fig. I-9) that are connected to the contralateral[41] medial rectus (MR in Fig. I-9) through the third nucleus (III in Fig. I-9). Hikosaka et al. (1978) showed that the burst neurons previously described in (Cohen and Feldman, 1968; Sparks and Travis, 1971; Luschei and Fuchs, 1972; Keller, 1974, 1977) contained two separate populations of neurons. The first one inhibits the contralateral ABD: the inhibitory burst neurons (IBNs in Fig. I-9). The second population, the excitatory burst neurons (EBNs in Fig. I-9), projects to the ipsilateral ABD (Grantyn et al., 1980). EBNs and IBNs receive excitatory projections from the cerebellum (Noda et al., 1990) and the superior colliculus (Raybourn and Keller, 1977). Additionally, both EBNs and IBNs populations are inhibited by the OPNs (Langer and Kaneko, 1983; Nakao et al., 1980; Keller, 1977).

During fixation, no discharge goes out of either EBNs or IBNs because of the OPNs's inhibition, and the eyes remained stationary. Therefore, OPNs must be deactivated to trigger a saccade. King et al. (1980); Langer and Kaneko (1984); Fuchs et al. (1985) studied the afferent connection to the OPNs. They showed that both SC and cerebellum inhibit the OPNs. Thus a collicular and/or a cerebellar discharge can theoretically trigger a saccadic movement. However, the trigger is necessary but not sufficient to execute a saccade. As shown by Keller (1977), the OPNs do not discharge during the whole saccade. An ongoing saccadic movement is stopped if they are stimulated. Therefore a "latch" must keep the OPNs activity low during the saccade. Ramat et al. (2007) proposed that the central mesencephalic reticular formation (cMRF in Fig. I-9) plays

[41] Neuron and muscle on the opposite side.

this role. The cMRF receives inhibitory projections from the OPNs (Scudder et al., 1996; Cromer and Waitzman, 2006; Graf and Ugolini, 2006; Horn, 2006) and from the ipsilateral IBNs (Fuchs et al., 1985). Additionally, the cMRF inhibits the OPNs (Langer and Kaneko, 1984). Therefore, as soon as the OPNs' activity is inhibited, the contralateral cMRF starts to discharge and sustains their activity low. At the end of the saccade, the contralateral IBNs discharge to slow down the eye movement (Quaia et al., 1999; Lefèvre et al., 1998). They also inhibit the cMRF which stops discharging. Then OPNs are reactivated, they inhibit IBNs and EBNs populations and the saccade ends.

The brainstem neural circuitry for conjugate vertical eye movements

After the studies of the brainstem structures involved in the control of horizontal saccadic movements, authors studied the specialized areas of the brainstem involved during vertical saccades. Researchers made parallels between the neural areas involved during horizontal and vertical saccades. Büttner et al. (1977); King and Fuchs (1979) recorded neurons in the rostral interstitial nuclei of the medial longitudinal fasciculus (riMLF) and in the interstitial nucleus of Cajal (INC) that bursted with vertical saccadic movements. This second population of burst neurons shares a lot of properties with the burst neurons related to horizontal saccadic movements. They are directionally selective. The duration of the burst is related to the duration of the saccade. The firing frequency is proportional to the velocity of the eye and the number of spikes is proportional to the amplitude of the vertical component (Moschovakis et al., 1991a,b; Vilis et al., 1989; Delgado-Garca et al., 1988). As for the neurons in the PPRF, the vertical burst neurons receive inputs projections from the superior colliculus (Nakao et al., 1990) and from the cerebellum (Asanuma et al., 1983; Noda et al., 1990) and they are inhibited by the OPNs (Nakao et al., 1988; Ohgaki et al., 1989; Langer and Kaneko, 1983). In the early 2000's, Horn et al. (2003) showed that the same division between inhibitory and excitatory burst neurons can be made for the vertical burst neurons. They showed that the inhibitory neurons are mostly located in the INC while the excitatory neurons are mainly located in the riMLF.

However, a major difference between the horizontal and the vertical channel appears when one compares the projections from the burst neurons to the motoneurons and the eye muscles. Vilis et al. (1989) showed that the neural areas involved in the generation of vertical eye saccades also discharges during torsional eye movements. Laterally, a stimulation of the riMLF neurons induced a torsional eye movement. From the point of view of the subject, Vilis et al. (1989) showed that a stimulation of the right riMLF evoked a clockwise torsion of the eyes. On the opposite, a stimulation of the left riMLF induced a counterclockwise torsional rotation. Those results pointed toward a projection of the burst neurons in the riMLF and the INC to both the superior oblique, the inferior oblique, the superior rectus and the inferior rectus extraocular muscles. Later, Suzuki et al. (1995) confirmed the results of (Vilis et al., 1989). They compared the deficits after unilateral and bilateral lesions of riMLF in the monkey. Suzuki et al. (1995) showed that unilateral lesions create a large torsional deficit but almost no vertical change while bilateral lesions removed

all torsional and vertical movements. Because the current thesis does not study torsional eye movements, no more details on the neural architecture of the torsional component will be given. However, it was necessary to point out that the final commands sent to the horizontal and vertical channels are not strictly identical, even if the models developed in this thesis consider them as similar.

The brainstem studies in head-unrestrained conditions

During the study of OPNs' discharge associated with head-fixed saccades, Keller (1977) did some recordings with the head free to move. He showed that the stimulation of the omnipause neurons region stops saccades during head-unrestrained movements but not the head movement[42]. As soon as the OPNs stimulation was over, the saccade restarted and reached its target (Keller, 1977). Seven years later, Whittington et al. (1984) were the first to study exclusively the behavior of brainstem burst neurons in head-unrestrained conditions. They showed that the burst neurons can be divided into two pools according to their discharge with respect to head-unrestrained gaze shifts. A first group had a discharge correlated with the gaze amplitude ("gaze bursters"). The discharge of the second population was related to the amplitude of the saccadic eye movement ("saccade bursters"). Later, Cullen et al. (1993) recorded the activity of the inhibitory burst neurons during head-unrestrained gaze shifts and during vestibular stimulation. They did not find a single "saccade-related" neuron. The neuronal discharge was better correlated with the gaze displacement and almost no correlation was found with the eye saccadic part of the gaze displacement. Cullen and Guitton (1997a,b,c) continued the study of IBNs discharge in head-restrained (Cullen and Guitton, 1997a) and head-unrestrained condition (Cullen and Guitton, 1997b,c). They confirmed that the firing rate of the IBNs was better correlated with the gaze displacement than with the eye displacement (Cullen and Guitton, 1997b). They showed that a model based on the firing pattern of IBNs in head-restrained condition cannot be used to predict the discharge in head-unrestrained condition (Cullen and Guitton, 1997b). Finally, Cullen and Guitton (1997c) showed that the IBNs discharge was better correlated with the dynamics of the gaze saccade than with the gaze motor error[43]. To study the action of PPRF during head-unrestrained gaze saccades, Gandhi et al. (2008) stimulated this area with the head either fixed or free to move. They showed that the gaze (in head-unrestrained condition) or the eye (in head-restrained condition) amplitude was linearly correlated with the duration of the stimulation. Confirming the observations of (Cullen and Guitton, 1997b,c), Gandhi et al. (2008) showed that PPRF stimulation did not reproduce gaze (or eye) movements similar to the visually-guided ones. A stimulation generated an increase of the velocity of either the gaze (in head-unrestrained condition) or the eye (in head-restrained condition) up to a saturated value. The bell-shaped saccadic velocity profile was never generated from a stimulation of the PPRF. Finally, the contribution of the head during the gaze movement was variable depending on the stimulated site.

[42] This observation was confirmed 30 years later by Gandhi and Sparks (2007).
[43] Difference between the target position and the gaze displacement.

In parallel to the studies on IBNs' discharge during head-unrestrained gaze shifts, Paré and Guitton (1998) studied the OPNs' activity during head-unrestrained saccades in the cat. They showed that the time during which the OPNs ceased to fire was proportional to the duration of the gaze saccade, not to the duration of the eye saccadic part. They also observed qualitatively a decrease in the head velocity when the OPNs were stimulated during a head-unrestrained gaze shift. Ten years later, Gandhi and Sparks (2007) confirmed the change in head velocity linked to OPNs stimulation. The velocity of the head decreased at the onset of the OPNs stimulation and the head accelerated when the stimulation ended. In another set of experiments, Paré and Guitton (1998) used a brake on the head during the gaze shift and recorded the activity of the OPNs. They showed that during a long brake of the head, the OPNs are reactivated. 20 [ms] after the release of the brake, the OPNs paused again until the gaze reached its destination.

Looking at the discharge of the motoneurons in the abducens nuclei, Cullen et al. (2000) showed that the neuronal discharge during head-unrestrained gaze saccades was correlated with the amplitude of the eye saccadic movement, not with the gaze movement. This raised an important question. As previously mentioned, authors have shown that the IBNs' discharge is proportional to the gaze movement, not to the eye movement (Cullen and Guitton, 1997b,c). Therefore, a transformation is necessary to pass from the gaze signals represented by the discharge of the burst neurons to the motor commands of the extraocular muscles that rotate the eye. Currently, no solution is found to explain how this transformation is done.

Additionally, several findings showed that the SC spatially encodes the gaze displacement in the superficial layer (see section 3.3.2) and a filtered version of the gaze motor error in the deep layers (Choi and Guitton, 2006, 2009). Again, as shown by Cullen and Guitton (1997c), the activity of the IBNs is related to the gaze dynamics. Therefore, a spatial to temporal transformation of the collicular activity is needed. Several suggestions have been made to explain this transformation. Lefèvre and Galiana (1992) proposed a unidimensional neural network of the superior colliculus that performed the spatial to temporal transformation intrinsically. As previously mentioned, this assumption was initially validated by experimental results of (Munoz and Wurtz, 1995a) but later Moschovakis et al. (2001) showed that it was not the case. Recently, Pathmanathan et al. (2006b,a) proposed that neurons in the contralateral mesencephalic reticular formation (cMRF) participate in the spatial to temporal conversion of the collicular discharge. They recorded two types of neurons in the cMRF during head-unrestrained saccades. One class bursts before the onset of the gaze shift (pre-saccadic neurons). A second class starts to burst after the onset of the gaze saccade (post-saccadic neurons). Pathmanathan et al. (2006b,a) showed that the activity of the pre-saccadic neurons was well correlated with the gaze saccades parameters and that the activity of the post-saccadic neurons was better correlated with the head movement. They argued that because cMRF neurons project to burst neurons and receive inputs from the colliculus, their activity could be used to do the spatial to temporal transformation[44].

[44] Even if they do not propose a clear mechanism...

Following the different observations made by authors during the last 30 years, it appears that the diagram proposed in Fig. I-9 must be seen as a highly simplified version of the actual brainstem neural circuitry. However, the purpose of the current thesis is to understand better the behavior of the eye-head system. A model that includes too many details would drive the reader away from the central questions that this work tries to answer. Therefore, it is important to adjust carefully the level of details of a mathematical representation of a system according to the questions raised by the study.

3.3.5 The head pathways: from "head brainstem areas" to the spinal cord

Activation and coordination of the neck muscles is a challenging process for the brain. As previously mentioned, the head-neck mechanical system is composed of seven cervical bones and the skull (see Fig. I-3) and moved by more than 20 muscles. The skull can rotate around the first cervical vertebra around one axis and each cervical vertebra can rotate around three axes. Thus, the head-neck mechanical system has roughly 19 degrees of freedom. In parallel, a muscle can only pull (it cannot push). Therefore, if a single action is linked to a single muscle[45], there are more muscles to orient the head-neck mechanical system than its number of degree of freedom: the system is overcomplete (Pellionisz, 1988). This means that several patterns of neck muscles activated can theoretically lead to a similar head-neck posture.

The current section will present the head-neck sub-cortical pathways. The majority of the studies cited in this section used the cat as experimental animals. It must be noted that, even if cats are quadrupedal animals, they have a lot of common anatomical head-neck properties with monkeys and humans (Richmond et al., 1988). Those shared anatomical features allow a direct comparison between the experimental results in the cat and the actual network controlling head-neck movements of human beings.

The general structure of the subcortical neural circuitry involved in head movements is presented in Fig. I-10. Structures involved in horizontal head movements are represented in black while structures involved in vertical head movements are represented in red. Anderson et al. (1971) was the first to stimulate the superior colliculus while recording activity in the spinal cord. They found that SC stimulation generated excitatory potentials in the contralateral neck motoneurons. The range of recorded latencies between stimulations and evoked potentials was comprised of monosynaptic and polysynaptic connections, suggesting the existence of two pathways. A first one projects directly from SC to the spinal cord (tectospinal pathway, from SC to the spinal cord in Fig. I-10) and a second one that goes through intermediate areas. Because Anderson et al. (1971) recorded polysynaptic connections between SC and the spinal cord, authors started to look at the structures between the two that

[45] This is a simplification, some neck muscles have different actions depending on the muscles fibers innervated.

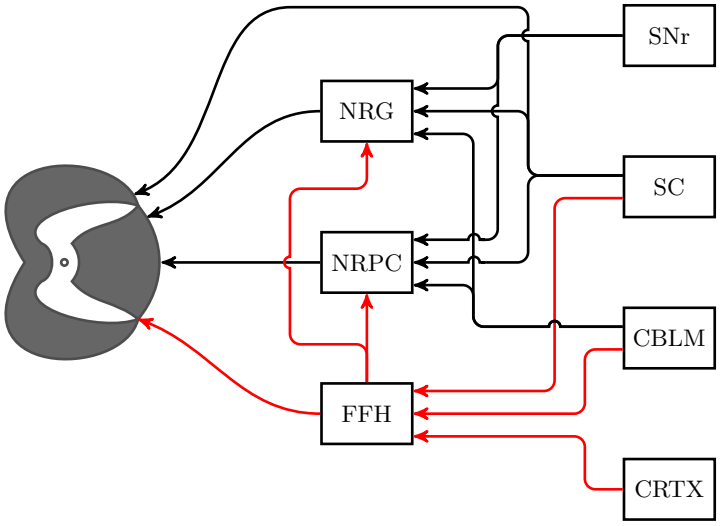

Fig. I-10: **Head subcortical network circuitry** The figure represents the connectivity between populations of neurons in the brainstem that are discharging during head-movements. Left shape represents a cross-section of the cervical spinal cord. SNr: substancia nigra pars reticulata. SC: superior colliculus. CBLM: cerebellum. CRTX: cortex. NRG: nucleus reticularis gigantocellularis. NRPC: nucleus reticularis pontis caudalis. FFH: Forel's field of H. Red lines correspond to the connections for vertical head rotations. Black lines represent the connections for horizontal head rotations.

were discharging accordingly to a head movement. Peterson et al. (1974) stimulated the upper cervical cord while recording in the medial reticular formation. Potentials were antidromically evoked in two areas: the nucleus reticularis gigantocellularis (NRG in Fig. I-10) and the nucleus reticularis pontis caudalis (NRPC in Fig. I-10). They also stimulated the pericrusiate cortex and the superior colliculus and found orthodromically evoked potentials in the same regions. Following his study, the neurons that project from the medial reticular formation to the spinal cord were labeled reticulospinal neurons (RSN, pathway from SC to NRG and NRPC and then to the spinal cord in Fig. I-10). A year after, Peterson et al. (1975) stimulated NRG and NRPC and found that the two reticular areas were also projecting further than the upper cervical cord (activity was recorded in the lumbar and the thoracic spinal cord), suggesting their implications in the control of body orientation.

From this point, authors tried to draw parallels between the brainstem structures involved during saccadic movements and the structures that discharge during head movements. As for the IBNs and EBNs described in section I-9, Peterson et al. (1978) found that neurons in the dorsal part of the NRG send inhibitory projections to neck motoneurons. They also found that both the caudal part of NRG and NRPC send excitatory connections to the neck motoneurons that innervate muscles responsible for horizontal head movements. Later, Grantyn et al. (1992) characterize the neurons in NRG and found

two classes of neurons. A first one sends collaterals to the abducens nuclei and the second class projects directly to the neck motoneurons. Using modern labeling techniques, Sasaki and Iwamoto (1999) showed that NRG projects to the cervical spinal cord at the level of the second and the third cervical vertebra. Motoneurons at this level activate muscles responsible for horizontal head rotations. Twenty years before, Fukushima et al. (1978) stimulated the interstitial nucleus of Cajal (INC) and recorded excitatory activity in the neck motoneurons that discharged during vertical head rotations. Therefore, a division between the areas involved during horizontal and vertical head rotations is present for head rotations as for eye rotations.

Because of the strong involvement of both NRG and NRPC in horizontal head movements, several studies focused on the inputs of those areas. Looking at the afferents of the deep nuclei of the cerebellum, Eccles et al. (1975) showed that some NRG and NRPC neurons received projections from both fastigial nuclei in the cat. Twenty years later, Robinson et al. (1994) used labeling methods and confirmed projections from the fastigial nuclei to NRG and NRPC in the monkey. Robinson et al. (1994) proposed that the fastigial nuclei are involved in the control of the head trajectory. Manetto and Lidsky (1987) reported a modulation of both NRG and NRPC activity by a discharge from the substantia nigra pars reticulata (SNr). Investigating more precisely the cortical input to the reticular formations involved in the control of head movements, Alstermark et al. (1985) stimulated the pyramidal tract (Pyr). This tract conveys activity from the cerebral cortex. The authors recorded disynaptic evoked potentials (excitatory and inhibitory) in the neck motoneurons when they stimulated the Pyr. Following this study, Iwamoto et al. (1988) studied the inputs of RSN and confirmed that the disynaptic connection passed through NRPC and NRG[46]. They showed that the collicular activity sent to NRG was facilitated by a discharge from Pyr. The relay position of NRG and NRPC between cortical inputs from Pyr and the spinal cord was confirmed later (Alstermark et al., 1992a,b). Alstermark et al. (1992a) showed that after a lesion of NRG and NRPC, no more activity was recorded in the neck motoneurons. Alstermark et al. (1992b) also confirmed that Pyr activity facilitated the discharge sent to the spinal cord from the superior colliculus through the NRG and showed that the activity sent from Pyr to the spinal cord through NRPC was facilitated by a collicular projection.

Authors also have looked at the brain areas that project to the spinal cord. In two companion papers, Guitton and Mandl (1978a,b) studied the interactions between the frontal eye field (FEF) and eye and head movements. Using stimulations, Guitton and Mandl (1978a) showed that FEF stimulation generates activity in the neck muscles that **precedes** the eye displacement by approximately 25-30 [ms]. In the companion paper, Guitton and Mandl (1978b) recorded cells (26%) that discharge before the onset and during neck muscles activity. The activity of those cells was not correlated with the eye movement. The same cells responded to neck muscles stimulation with a latency to the peak response between 15 and 30 [ms] (Guitton and Mandl, 1978b). Because

[46] The connections from the cortex (CRTX) to NRG and NRPC are not represented in Fig. I-10

FEF stimulations generate neck muscles' activity and FEF is sensitive to neck muscles' stimulation, this area of the frontal cortex could influence head trajectory/goal control. He et al. (1993) found neurons in the dorsal and the ventral premotor areas (PMd and PMv) that project to the cervical spine. He et al. (1995) also found neurons in the supplementary motor area (SMA) and in the cingulate motor area (CMA) that project to the superior cervical regions. SMA, PMd and PMv activity is usually related to the motor control of limbs. Dum and Strick (1996) studied more precisely the terminations of SMA and CMA neurons in the spinal cord. They found projections at c_2-c_4 vertebrae levels, where the motoneurons involved in the control of head movements are located.

In parallel with the studies on the areas involved during horizontal head rotations, Isa et al. (1988b,a) used labeling methods and found projections from the Forel's field of H (FFH) to the specialized neck motoneurons for vertical head rotations in the cat. Isa et al. (1988b) found excitatory projections in the spinal cord at the levels of c_1-c_3 and projections to NRG and NRPC. As for the two classes observed by Grantyn et al. (1992) for the bursters in NRG, Isa et al. (1988a) divided FFH neurons into two subtypes. Type I neurons send collaterals to the third nuclei while type II neurons do not send collaterals to the third nuclei. Isa et al. (1988a) postulated that the FFH type I neurons are involved in the coordination of eye and head movements while type II neurons are involved in the independent control of eye and head. Later, Alstermark et al. (1992c) found that FFH receives inputs from the intermediate layers of the superior colliculus. The same year, Isa et al. (1992) used labeling methods and found projections from FFH to the spinal cord at the level of the first and the second cervical vertebrae.

In the preceding paragraphs, authors stimulated a region of the central nervous system and recorded activity in another one or used labeling methods to find the areas involved in the activation of neck muscles and the pathways that linked them. In parallel, researchers recorded activity during head movements or induced lesions in those areas and looked at the implications for the generated head movements. Isa and Sasaki (1988) showed that unilateral lesions of NRG and NRPC removed horizontal head movement toward the side of the lesion without affecting the contralateral movements. Isa and Naito (1994) recorded neurons in FFH during head movements of cats. They found that 95% of the recorded cells had an upward preferred direction. The activity of the recorded neurons always preceded the initiation of the head vertical rotation. Isa and Naito (1994) also stimulated FFH area. The authors demonstrated that unilateral stimulations induced oblique upward rotations of the head with a torsional component while a bilateral stimulation generated pure upward rotations. Finally, Isa and Naito (1994) showed that the activity of FFH neurons is correlated with the maximum vertical velocity of the head. Isa and Naito (1995) recorded the activity in NRG and NRPC during head-unrestrained gaze saccades. They demonstrated that NRG and NRPC neurons' firing rate was related to the amplitude and the velocity of the horizontal head component of the gaze shift (like the previously described link between firing rate of EBNs and the maximum velocity of the horizontal component of the gaze saccade, see section I-9). Using a two-dimensional paradigm, Sasaki et al. (1999) showed

that unilateral lesions of NRPC and NRG do not impair vertical head rotations but drastically modify the horizontal behavior. Sasaki et al. (1999) showed that oblique head trajectories toward the ipsilesioned side were first made by zig-zag trajectories. After a recovery period of approximately ten days, head oblique movements were again coordinated, the velocity of the vertical component being adjusted with respect to the impaired horizontal velocity (Sasaki et al., 1999). Finally, Isa et al. (1992) showed that lesions in FFH severely impaired the vertical rotation of the head.

As for the pathways in the brainstem presented in section 3.3.4, the specialized subcortical areas for head movements have a lot of particularities that were not addressed in the present thesis. Because this work focuses on the control of gaze, the pathways for the control of the head were highly simplified compared to the real circuitry. However, as for the descriptions of the preceding neural circuitries, it is important to know the actual network to evaluate correctly the consequences of the assumptions that we used through the document.

Neck muscles' synergy

Thomson et al. (1994, 1996) have studied the influence of the neck posture on the activation of 16 neck muscles in cats during active and passive head rotations. They demonstrated that the neck muscles can be divided into two pools: the activity of the first one was not influenced by the head-neck posture while the activity of the second pool of muscles changed as a function of the neck orientation. They proposed a control scheme for head rotations based on two parallel pathways. The general orientation commands are sent to a defined set of neck muscles regardless of the neck posture while a second set of commands are sent to the other pool of muscles to control specifically the orientation of the cervical vertebrae (Thomson et al., 1994). This proposed organization in two pools simplified the general problem of control of the head-neck muscles.

The suggestion made by Thomson et al. (1994, 1996) has neurophysiologic support. Iwamoto and Sasaki (1990) demonstrated that a single NRPC or NRG neuron projects to several neck motoneurons in the spinal cord. Shinoda et al. (1996) investigated the same behavior but at the level of the superior colliculus. They found that collicular cells project to motoneurons of the neck related to different muscles. They demonstrated a direct connection between superior colliculus cells and the neurons in the spinal cord. Interestingly, Shinoda et al. (1996) showed that the projection to the spinal cord is not a direct projection to the motoneurons. Instead the reticulospinal, tectospinal and tectoreticulospinal neurons project to interneurons that then project to several motoneurons corresponding to different neck muscles. Following their observations of multiple connectivity at the level of the motoneurons, Iwamoto and Sasaki (1990) and Shinoda et al. (1996) proposed that muscles' synergy already occurs in NRG and NRPC or even at the collicular level. These synergies at a higher level than the motoneurons could explain the observation of Thomson et al. (1994, 1996).

The neck muscle synergy presented in this section is of particular interest for our analysis. A model that studies the control of the head trajectory could generate spatial commands (upward, downward, leftward, rightward head rotations) instead of commands related directly to the neck muscles' activity. A

second class of models could address the problem of neck muscles' synergy. This model would transform commands expressed in a spatial reference frame into muscles' commands. Therefore, a model that simulates the control of the gaze trajectory could totally ignore the pattern of neck muscles that must be activated to execute a specific head rotation. This is the approach used in the current thesis.

3.4 Saccades and models

From behavioral experiments and electrophysiological recordings, researchers started to build mathematical model of the saccadic system. Those models are used to test assumptions about the functions of neural areas during saccades. They can also be useful to demonstrate the feasibility of a control structure.

A milestone in the modeling of head-restrained saccadic control is the model by Robinson (1975). The innovation of this model, used in most of the following saccade models, is the insertion of an internal, or local, feedback loop that controls eye position using a motor error signal built from an efference copy of the eye position (motor error is defined as the difference between eye position and target position). However, that early model was based on the very small amount of physiological data available at the time. Subsequent experiments have led to the need to extend or alter the details of the original model of Robinson (1975), although its key idea, the local feedback loop, remains. One of the most important alterations was to change the feedback from an efference copy of position to an efference copy of velocity. This required the inclusion of a resettable or bootstrap integrator in the local feedback loop (Jürgens et al., 1981).

With more and more information available, models' complexity increased to simulate many different saccadic behaviors and to incorporate important neuronal structures that were reported to be involved in saccadic control. As models became more complex, new hypotheses concerning the mechanisms involved in eye control were proposed. In a distributed model of head-restrained saccades, Lefèvre et al. (1998); Quaia et al. (1999) used the interaction between two pathways (one through the cerebellum and one through the superior colliculus) to simulate the behavior of eye saccades.

With the appearance of head-unrestrained behavioral recordings (Bizzi et al., 1971), authors proposed models of eye-head coordination during saccades. Extending the principle introduced in (Robinson, 1975) to head-unrestrained movements, Guitton and Galianna proposed a model including feedback control of gaze position. In their model, a common command is sent to the eye and the head (Guitton et al., 1990; Galiana and Guitton, 1992; Lefèvre and Galiana, 1992); this motor command is a function of the gaze motor error. The principle behind the common motor command theory comes from the observed tight coupling between eye and head displacements, especially in head-unrestrained cat (Guitton et al., 1990). The core neuronal area of the model of (Guitton et al., 1990; Galiana and Guitton, 1992; Lefèvre and Galiana, 1992) is SC. They proposed that SC is the central controller of the gaze trajectory and that it is included in the feedback loop.

As pointed out in section 3.2, even though strong coupling between eye and head has been observed, there are numerous situations in which they can have an uncoupled behavior. Based on those observations, Freedman (2001, 2008) proposed a new architecture for the control of head-unrestrained saccadic movements based on an a priori decomposition of the desired gaze displacement into its eye and head components. Those components are then sent to two separate controllers, one for the head and one for the eye movement. The only interaction between the two separate pathways is an inhibitory signal sent from the head controller to the saccade generator. This inhibition modulates the maximum eye velocity in proportion to the head velocity, although a reason for this is not made clear. In the Freedman model, the eye displacement is controlled using feedback of eye motor error as in (Robinson, 1975), but no feedback is included for the control of head trajectory.

Saccades: section summary

- Quick reorientation of the visual axis from one position to an other.
- Main goal: cancel any position difference between the target and the fovea.
- Fastest gaze movement (peak velocity ∼600 [deg/s]).
- Head and gaze trajectories can have similar or dissociated trajectories.
- Two levels of neural control:
  - Cortical level: analysis and selection of visual targets (Not modeled in the present manuscript).
  - Sub-cortical level: control of eye and head trajectories (Core of the model presented in part IV).
- Perturbations of the head trajectory do not influence final gaze position.

4 Type II and type III: The pursuit system and the vestibulo-ocular reflex

Dodge (1903) defined two types of movements following his description of the saccadic system. As it will be shown, if those movements can be dissociated using specific paradigms in head-restrained conditions, it is impossible to separate them when a subject is tracking a moving target with the head free to move.

The second type of movement is described by Dodge (1903) as *"... those eye movements in which the line of regard follows an object moving across the field of vision"*. Dodge (1903) defined those movements as pursuit movements.

He also reported a third type of eye movement and described it as *"... those movements of the eyes by which the constant fixation of an unmoved object of interest is maintained during rotation of the head"*. Those movements are known now to be generated by the vestibulo-ocular reflex (VOR) and are not characterized as a particular type of eye movements. It must be noted that two types of VOR exist: linear VOR and angular VOR. Because in this thesis we only account for the rotations of the head, the eye-in-head and the gaze, the

text will not present the linear VOR characteristics; it will focus on the angular VOR response.

4.1 Typical head-restrained pursuit movement

Figure I-11 showed a typical pursuit movement in head-restrained condition of a 20 year old woman. The upper row of Fig. I-11 represents the change of gaze (thin black line) and target (red line) position as a function of time. The lower row represents the time-course of gaze and target velocity. Thick black lines represent saccades. The subject initially looked at a stationary target 20 [deg] on her left. After 350 [ms], the target started to move toward the right of the screen at a constant velocity of 15 [deg/s]. During the first 100 [ms] of target movement, a position error[47] occurred and increased because the subject did not react instantaneously to the change of target velocity. Then a saccade was triggered to cancel the accumulated position error. After the corrective saccade, the subject pursued the target with a velocity gain[48] close to unity. From there, she followed the target until the end of the trial.

Because the initiation of the pursuit movement takes some time, generating a pure pursuit movement is not a simple task[49]. To that goal, Rashbass (1961) designed a protocol in which the target does a position step and a velocity step. By adjusting adequately the amplitude of the position step and the velocity of the target, he recorded pursuit movements in human subjects during which subjects did not trigger saccades during the initiation of the pursuit.

A typical example of a 25 year old male subject pursuing a Rashbass target is presented in Fig. I-12. The same conventions as in Fig. I-11 are used. During the first 200 [ms], the subject looked at a stationary target located 20 [deg] on his right. Then the target made a 3 [deg] step to the right and started to move toward the left side of the screen at a constant velocity of -15 [deg/s]. Because of the position step, the position error decreased during the initiation of the pursuit movement. Therefore, when the subject reached the velocity of the target, no position error remained. As a result, there was no need to trigger a saccade.

4.2 Typical response of the vestibulo-ocular reflex (VOR)

To quantify the behavior of the vestibulo-ocular reflex more precisely than the initial observations of Dodge (1903), researchers compared the effect of a head rotation on the compensatory eye movements. Because head movements are not as stereotyped as eye movements, it could be difficult to impose accurately similar head trajectories. To force specific head movements, subjects sit on a rotating chair with their head fixed with respect to the chair. Thus a rotation of the chair induced a similar rotation of the head.

[47] Difference between the target position and the gaze position.

[48] Ratio between the eye/gaze velocity and the target velocity.

[49] In his study, Dodge (1903) already observed that when subjects tried to track a moving target, there was a combination of pursuit and saccades.

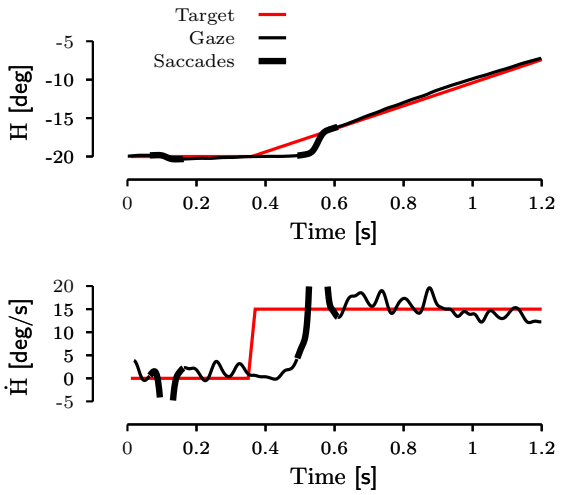

Fig. I-11: **Typical horizontal head-restrained pursuit.** This figure represents a typical pursuit trial for a target that moved at 15 [deg/s]. Upper row represents the time-course of gaze (thin black line) and target (red line) position. Lower row represents the evolution of gaze and target velocity as a function of time (same color convention). Thick black lines represent saccades. Initially, the subject looked at a fixed target located 20 [deg] on her left. After 350 [ms], the target made a step in velocity and moved at a constant velocity of 15 [deg/s]. After a latency of 100 [ms], the subject triggered a first saccade toward the target to cancel the accumulating position error. At saccade offset, the subject tracked the target with a unitary gain. See text for more details. Special thanks to Sebastien Coppe for providing the data.

Figure I-13 represents a typical VOR test. Upper row Fig. I-13 represents the opposite target velocity (red line), the eye velocity (green line) and an exponential piecewise fit on the compensatory phases (dashed black lines). The lower row in Fig. I-13 represents the evolution of the VOR gain (defined as the ratio of the eye velocity to the chair velocity) when the chair is rotating.

Two situations are presented in Fig. I-13. In the first one, represented by dark boxes in Fig. I-13, the subject sat in the dark on the rotating chair with the head fixed with respect to the chair. After 5 [s], the chair made a velocity step of 50 [deg/s]. In reaction to the chair rotation, the subject counter-rotated the eye in the orbit to stabilize the gaze. As shown by Fig. I-13, the initial compensatory eye movement in the dark is not perfect (gain of the VOR = 0.5). Because the semicircular canals are stimulated with a constant velocity, the VOR response decayed exponentially. As soon as the chair rotation ended, a post-rotatory movement, opposite to the compensatory movement occurred. This post-rotatory phase is linked to the opposite stimulation of the semicircular canals when the chair rotation stopped.

In the second situation, the same protocol is used (with the chair moving in the opposite direction) but the subject sat on the chair with the light on.

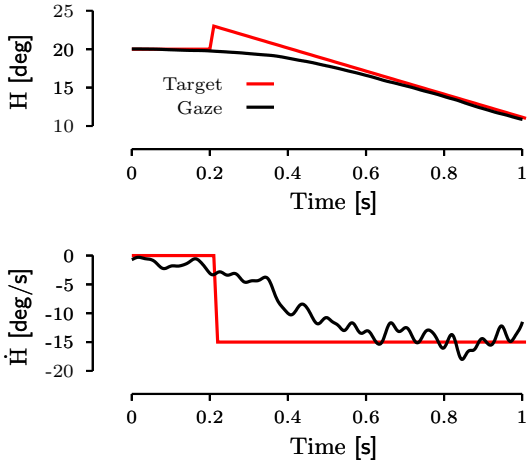

Fig. I-12: **Typical horizontal head-restrained pursuit with a rashbass protocol.** This figure represents a typical pursuit trial when a subject tracked a target that had a step-ramp trajectory. The upper plot row represents gaze and target position. The lower plot row represents gaze and target velocity. Same color convention as in Fig. I-11. Subject initially fixated the target situated at 20 [deg] on his right. After 200 [ms], the target made simultaneously a position step (3 [deg] to the right) and a velocity step (-15 [deg/s]). The subject started to pursue the target and did not trigger a saccade to cancel the initial error of position. See text for more details. Special thanks to Caroline Ego for providing the data.

As it can be seen, the compensatory eye movement is better (gain of the VOR = 0.8) with light and almost no post-rotatory rotation occurred (max velocity amplitude = 2 [deg/s]).

4.3 Behavioral characteristics of pursuit

Traditionally, the pursuit system is seen as the control mechanism of eye movements that cancels a difference between velocity of a slowly moving target and eye velocity, called retinal slip (RS). A pursuit movement can be divided into two parts: the initiation and the maintenance of pursuit. The following paragraphs will give a description of the two subparts and will stress the importance of expectation/prediction of target movements for the control of eye movements during pursuit.

Initiation of the pursuit

In his original study, Dodge (1903) mentioned that *"the movement of the object must already be apprehended before the pursuit can begin"*, pointing to the need of a retinal slip different from zero to initiate the pursuit. This observation was confirmed later by Westheimer (1954). In his study, Westheimer (1954)

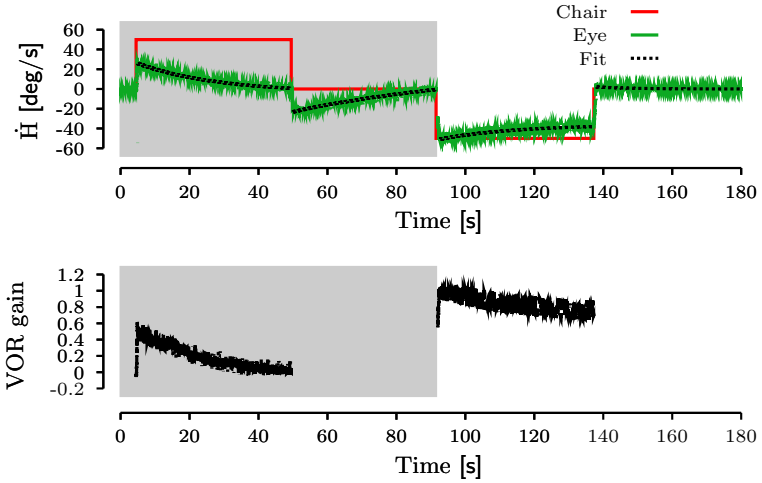

Fig. I-13: **Typical VOR response to velocity steps.** This figure represents the typical response of a subject to a step in velocity of the chair in the dark (gray boxes) followed by a step in the opposite direction in the light. Upper row represents the opposite chair velocity (red line), the eye-in-head velocity (green line) and an exponential piecewise fit on the compensatory phases (dashed black lines). The lower row represents the evolution of the VOR gain when the chair is rotating. See text for more details. Special thanks to Dr. David Zee for providing the data.

compared the pursuit of a moving target with a constant velocity, an unpredictable movement, a sinusoidal movement and target with a constant velocity with occlusion of the target. Figure I-11 showed the major observation made by Westheimer (1954) when he studied the pursuit of a constant velocity moving target: initiation of the movement after 150 [ms] - 250 [ms] with a saccade and then pursuit with a fixed gain. Westheimer (1954) argued that a moving stimulus on the retina is needed to initiate the pursuit. Twenty years later, Steinbach (1976) showed that human subjects can initiate a pursuit movement with the perception of a movement[50] and not uniquely with a target moving on the retina. Finally, Braun et al. (2006) showed that a pursuit movement can be initiated even in the absence of a moving stimulus. The authors used a visual illusion known as the motion after effect[51] (MAE) to generate a pursuit movement while subjects were looking at a stationary sinusoidal grating. Thus, it appears that the perception (illusory or not) of a target movement is sufficient to initiate a smooth pursuit movement.

[50] E.g., subject were able to track an invisible hub of a rolling wheel if two lights were fixed oppositely on the wheel's rim.

[51] The motion after effect is one of the oldest known visual illusion. Adams (1834) reported that after staring at a waterfall for a certain amount of time, when he looked at a stationary rock, he had the impression that the rock was moving upward; in the opposite direction of the falling water.

Anticipation during pursuit

Westheimer (1954) also pointed out the importance of prediction during pursuit because of the internal delays present in the visual system. He compared the behavior of a subject pursuing an unpredictable moving target and a subject pursuing a target with a sinusoidal velocity. The initiation of the movement was similar (pursuit with constant velocity intermingled with saccades to correct the position error) in both the random and the sinusoidal conditions. However, after several cycles, there was no more velocity or position error between the target and the eye when the subject tracked the sinusoidal target. Because of the internal delays present in the visual system, the experiment made by Westheimer (1954) stressed the importance of prediction during pursuit.

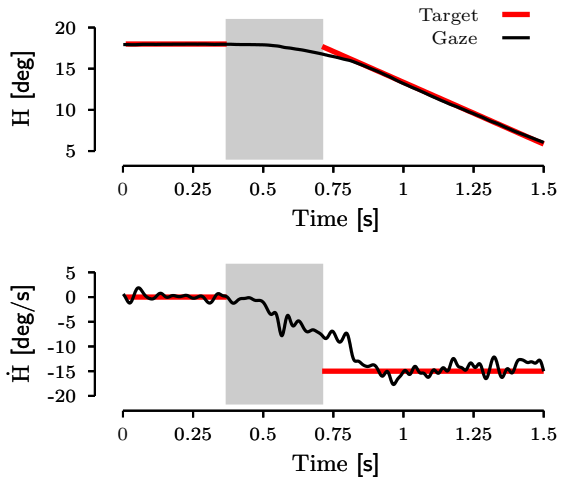

Fig. I-14: **Typical anticipation of pursuit.** This figure represents a typical pursuit trial with an anticipatory smooth movement of a 60 years old man. Upper row represents the time-course of gaze (black line) and target (red line) position. Lower row represents the evolution of gaze and target velocity as a function of time (same color convention). Gray rectangles represent the time during which no target was presented on the screen (gap period). Initially, the subject looked at a fixed target located 18 [deg] on his right. After 370 [ms], the target disappeared for a duration of 340 [ms]. Then the target made a velocity step of -15 [deg/s] to the left. The subject started his smooth movement approximately 130 [ms] after the onset of the gap. At target reappearance, the subject already moved at 8 [deg/s] and he made a displacement of 1.2 [deg]. Therefore, he was leading the target. Special thanks to Sebastien Coppe for providing the data.

If a predictive mechanism is implicated after several cycles of a periodic target, a similar kind of "prediction" can occur at the initiation of a movement if the same trajectory of the target is repeated many times. This behavior is called "anticipatory". A typical example of anticipation during pursuit is shown

in Fig. I-14. Kowler and Steinman (1979a,b) demonstrated that the anticipative eye displacements are conditioned by the *expectation* of the moving stimulus. If a subject knows in advance the direction, the onset timing and the amplitude of the target velocity, Kowler and Steinman (1979a,b) showed that he/she will start a pursuit movement before the onset of either a ramp or a step target motion. A decade later, Boman and Hotson (1988) confirmed the observations of (Kowler and Steinman, 1979a,b). They demonstrated that a visual stimulus was not required to generate anticipatory smooth eye movements. On the contrary, they showed that a gap period of 200 [ms] up to 800 [ms] enhances the anticipatory behavior: the longer the gap, the shorter the reaction time and the bigger the velocity amplitude of the anticipation. Boman and Hotson (1988) showed that a similar anticipation can be found at the end of the movement. Subjects decreased their eye velocity prior to the end of the target movement. Later, Barnes et al. (1995) compared the open-loop and the closed-loop behavior of human subjects who pursued a periodical target that was illuminated only during a small duration when the target passed through the center of the screen. Barnes et al. (1995) showed that the anticipatory movements as reported by Kowler and Steinman (1979a,b) have the same trajectory in either the open- or the closed-loop condition. The authors also showed that the retinal information provides a supplementary signal used to calibrate the eye velocity to the target velocity.

Maintaining the pursuit movement

As pointed out by Westheimer (1954), prediction also appeared to be an important factor of the pursuit movements. A decade after the study of Westheimer (1954), Stark et al. (1962) formalized the importance of prediction by showing that pursuit of a periodical target could only be done accurately by getting rid of the inherent internal delays of the visual system. A year after, Dallos and Jones (1963) were the first to compute the pursuit gain in open-loop[52] conditions from the bode plot of tracking behavior in normal conditions for a target with either random or sinusoidal velocity.

More evidence was given by researchers to provide information about the predictive behavior during the maintaining of pursuit. Since Westheimer (1954) observed that the pursuit movement is not altered if the target is flashed during its displacement (as a stroboscope), authors looked at the effect of occlusions during an ongoing pursuit. Following this observation, Becker and Fuchs (1985) were the first to quantify the effect of occlusions on the pursuit behavior of a constant velocity target. They showed that the pursuit velocity decreases exponentially to a baseline velocity during the occlusion. They showed that if the target velocity was predictable, the relative residual velocity is independent of the velocity of the target. On the contrary, if the target velocity was randomized, the baseline velocity decreases with an increase of the target velocity. More than a decade later, Kettner et al. (1996) studied the pursuit behavior when monkeys tracked a two-dimensional periodic target[53]. They showed that

[52] It supposed that the system does not have a visual input to correct its trajectory through a feedback.

[53] The target was composed by a two-dimensional sum-of-sines.

the gain of the vertical component of tracking was smaller than the gain of the horizontal component. The study of Kettner et al. (1996) is a supplementary evidence that the pursuit system used prediction because the eye movement lagged behind the target with a mean delay smaller than the one of the pursuit system. A year later, Leung and Kettner (1997) randomly changed the trajectory of a predictive target. The latency of the response to the change of target trajectory was larger than the phase lag of the pursuit. This is an evidence of the strong role of the prediction during pursuit of a target.

Like for the initiation of pursuit, it was originally believed that a retinal slip larger than zero was necessary to maintain a pursuit movement (Robinson, 1965; Rashbass, 1961; Dallos and Jones, 1963). However, authors showed that other inputs play a role in maintaining pursuit. Pola and Wyatt (1980) used feedback to stabilize electronically the target position on the fovea during a pursuit movement[54]. The authors called this stimulus "velocity-only" input because no position error was present during the tracking period. The same stimulus is also called open-loop behavior because the pursuit system does not receive any velocity mismatch information from the visual input[55]. Pola and Wyatt (1980) showed that subjects could maintain a pursuit movement with a velocity-only protocol. Morris and Lisberger (1987) used the same approach (stabilized image on the retina) and compared two conditions. In the first one, the authors forced a fixed retinal position error while in the second they imposed a velocity error. As Pola and Wyatt (1980), Morris and Lisberger (1987) showed that monkeys could maintain a pursuit movement with no retinal velocity error. The authors also showed that forcing either a position or a velocity error during an ongoing pursuit movement induced an acceleration of the eye in the direction of the error. On the contrary, if a position error was imposed during a fixation, monkeys only generated saccades while if a velocity error was imposed during a fixation, they generated a pursuit movement. Because no visual input is present during an occlusion, the experiment of Becker and Fuchs (1985) is supplementary evidence that RS is not the sole input of the pursuit system.

Finally, to compare the behavior during saccades and the main sequence described by Bahill et al. (1975) with the pursuit behavior, Meyer et al. (1985) studied the behavioral limits of the pursuit system. The authors showed that, as for saturation of the peak velocity with an increasing saccadic amplitude, the pursuit velocity saturates for target velocity faster than 90 [deg/s]. Below this limit, the mean pursuit gain was equal to 0.86 (Meyer et al., 1985).

As a summary, all the described studies pointed toward other inputs to the pursuit system than the retinal slip or the retinal position error: e.g. extra-retinal information from the eye commands at the output of the burst neurons in the brainstem (see section 3.3.4).

[54] With the stabilization technique, it is the eye that makes the target moving, not an external signal generator. Therefore the target is always located at the same place on the fovea.

[55] As opposed to the normal condition, or closed-loop condition, in which the target and the eye are not linked by a feedback.

4.4 Behavioral characteristics of VOR response

Dodge (1903) studied less intensively the third type of eye movements. However, he qualitatively reported that *"the compensatory eye movements were accurate for moderate velocities and head displacements"*. To quantify more precisely the behavior of the VOR with respect to passive head rotations, experimenters generally extracted two parameters: the gain and the phase of the VOR. The VOR gain is traditionally computed as the ratio between eye and head velocity. The phase allowed the experimenter to test if the eye movement lags or leads the movement of the chair. Ideally, the gain of the VOR must be equal to one[56] (1) and the phase of the vestibular compensation must be equal to 180[57] [deg]. If those two conditions are met, any head movement is perfectly compensated for by an opposite rotation of the eye-in-the orbit. Therefore the gaze remains stable during the whole experiment.

4.4.1 VOR in the dark

In a dark room, subjects sit on a rotating chair with their head fixed with respect to the chair. When the chair is rotating sinusoidally without any visual target, a nystagmus is evoked. A nystagmus eye movement is composed of two phases: a fast one and a slow one. In a first phase (slow phase), the eye in the orbit smoothly rotates in the opposite direction to the chair. When the eye passes a position threshold, a quick eye movement in the direction of the chair resets the eye in the orbital position toward a central location in the oculomotor range. Fast and slow phases follow each other when the chair is rotating and the subjects sit in the dark. With this method, the VOR behavior can be quantified without any visual interaction.

The behavior of the VOR response has been quantified around the three axes of rotation: the yaw[58] (horizontal VOR), the pitch[59] (vertical VOR) and the roll[60] axis (torsional VOR). When the frequency of the rotating chair is low, VOR gains are small[61] because the semicircular canals' discharge is weak and noisy (see section 1.2.1 for a description of the semicircular canals). Additionally, compensatory eye movements lead the chair rotations for low frequencies. With an increase of the frequency to 1 [Hz], the gains also increase and remain stable until 2 [Hz][62]. The horizontal VOR gain decreases between 2 and 8 [Hz]

[56] This reflects that the velocity of the eye is equal in amplitude to the velocity of the head.

[57] The eyes must be in anti-phase with the head movements

[58] Rotation around an axis perpendicular to the earth surface. Generate horizontal eye movements.

[59] Rotation around an axis parallel to the earth surface passing through the two ears. Generate vertical eye movements.

[60] Rotation around the nasooccipital axis. Generate vertical torsional movements.

[61] $\sim$0.5 for horizontal VOR, $\sim$0.5 for vertical VOR and $\sim$0.2 for torsional VOR at 0.05 [Hz] (Bockisch et al., 2005; Schmid-Priscoveanu et al., 2000; Barnes and Forbat, 1979)

[62] $\sim$0.9 for horizontal VOR, $\sim$0.7 for vertical VOR and $\sim$0.3 for torsional VOR at 1 [Hz] (Bockisch et al., 2005; Schmid-Priscoveanu et al., 2000; Barnes and Forbat, 1979)

(Tabak and Collewijn, 1994). Finally, between 8 and 20 [Hz], the gain increases to approximately 1.4 (Tabak and Collewijn, 1994). For higher frequencies, the movement lags behind the target by roughly 2.5 [deg] at 2 [Hz] but the lag reaches 45 [deg] at 20 [Hz] (Tabak and Collewijn, 1994).

Figure I-15 represents a Bode plot (gain and phase as a function of the chair oscillation frequency) of the horizontal, the vertical and the torsional VOR responses to chair rotations for frequencies up to 1.25 [Hz].

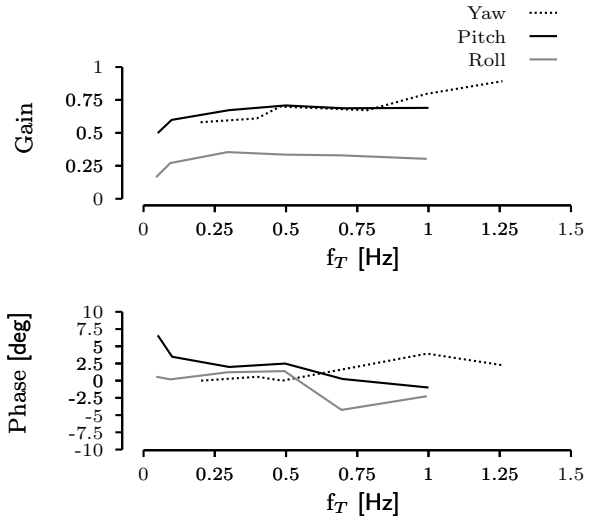

Fig. I-15: **Evolution of the VOR gain as a function of the chair oscillation frequency.** This figure represents the evolution of the VOR gain in the dark with a chair rotating around the three main axis of rotation. A positive (negative) phase corresponds to a lead (lag) of the signal with respect to the chair rotation. For low frequencies, the gain of the VOR is small and it increases with an increase of the chair oscillation frequency to reach a plateau value. As it can be observed in Fig. I-15, the horizontal and vertical gains are similar while the gain for the torsional VOR is smaller. For low frequencies, the compensatory eye movements are either synchronized (horizontal and torsional), or they lead (vertical) the chair movements. With an increase of the frequency, the vertical and torsional VOR begin to lag behind the chair movements. Finally, the horizontal VOR slightly leads the chair rotations. Data for the yaw adapted from (Barnes and Forbat, 1979). Data for the pitch adapted from (Bockisch et al., 2005). Data for the roll adapted from (Schmid-Priscoveanu et al., 2000).

4.4.2 VOR enhancement

The results obtained when testing the VOR in the absence of a visual stimulus cannot easily be compared with everyday life situations. Therefore, researchers tested the VOR in more realistic conditions. Several factors have proven to be

important modifiers for VOR behavior. Three effects will be described in the following paragraphs: the effect of a visible target, the mental set and the effect of the distance to the target.

Visual enhancement

Authors looked at the changes of the VOR properties linked to the fixation of a visible earth-fixed target while the chair is rotating. A good response to oscillations in a large range of frequencies is a critical factor for a stable vision. Inaccurate VOR responses can give the illusion of movement of a fixed target called oscillopsia (Maas et al., 1989).

Several authors have shown that the VOR response is enhanced when the subject is asked to look at a visible target while the chair is rotating. As an example, Johnston and Sharpe (1994) reported that the mean horizontal VOR gain increases from 0.9 to 0.95 when subjects looked at an earth-fixed target. To understand why this enhancement occurs, Han et al. (2005) used target flashed at different frequencies (to provide or not retinal slip information to the subject) while subjects were on the vestibular chair. Those authors showed that the VOR behavior when subjects looked at an earth-fixed target is the sum of three components: the VOR in the dark (75%) and both RS and the predictability of the stimulus (25%). Those observations reflect the implication of the pursuit system when looking at an earth-fixed target on a rotating chair.

Minor et al. (1999) showed that the visual enhancement is not only linked to the presence of a target: an increase of the VOR gain appears when the light in the experimental room is switched on. This reflects that a global motion on the retina enhances the VOR response.

The mental set

If a visual target enhances the response of the VOR, Barr et al. (1976) showed that the mental set of the subjects also modulates the VOR response. Barr et al. (1976) asked subjects to look at an earth-fixed target while the chair was rotating and reported a VOR gain close to one (as expected, see the preceding paragraph). Then, the target disappeared and the authors instructed the subjects to look at the imaginary position of the target. The authors observed a VOR gain close to 0.95. An identical procedure during which subjects were instructed to look at a chair-fixed target gave a gain close to zero when the target was visible and a gain around 0.35 when the subject had to imagine the target (Barr et al., 1976). Finally, Barr et al. (1976) showed that when subjects did mental arithmetic during a VOR test in the dark, the VOR gain was close to 0.65.

The study of Barr et al. (1976) restricted the frequency of the chair movement between 0.1 and 0.9 [Hz]. Paige et al. (1998) demonstrated that if imaginary targets can enhance or attenuate the response of the VOR, the effect is almost gone with a chair rotation frequency of 4 [Hz].

Target distance

Viirre et al. (1986) were the first to demonstrate the influence of target distance on the gain of the VOR. Because of the distance between the two eyes in

human beings and non-human primates with frontal binocular vision and the offset between the center of rotation of the head and the eyes, the amplitude of the compensatory eye rotation to a head rotation is a function of the distance between the target and the subject. With near targets, the rotations of the eyes must be larger than the rotation of the head to ensure a proper fixation. This corresponds to a VOR gain bigger than one[63]. Additionally, Viirre et al. (1986) showed that when the target is close to the subject, a chair rotation induces a different rotation for the left and the right eye pointing toward dissimilar VOR gains for each eye.

Those findings were later confirmed by Medendorp et al. (2000). The authors showed that the gain but not the phase of the VOR varies as a function of the vergence angle. The importance of the vergence angle was also reported by Han et al. (2005). They reported that the vergence angle affects the VOR gain only during binocular viewing.

It is worth noting that if there is an effect of the distance to the target for horizontal and vertical VOR, torsional compensatory movements remain unchanged with a variation of the distance to the target (Migliaccio et al., 2006).

4.5 VOR and active head movements: need for a gain modulation

As mentioned in the previous sections, the VOR purpose is to stabilize vision by compensating for any perturbation of the head by a counter-rotation of the eye in the orbit. However, in some situations a compensatory movement could be counterproductive. The typical inefficient case is a situation in which both gaze and head are moving in the same direction. In this situation, a fully working VOR will systematically drive the eye-in-head in the opposite direction of the head, away from the target. To prevent those inefficient situations, authors have shown that the central nervous system uses two strategies: VOR cancellation and VOR suppression. Even if the mechanisms used are different in both situations (see following paragraphs), their purpose is similar: modulating the gain of the VOR during active head movements to avoid undesirable compensation.

4.5.1 VOR cancellation during head-unrestrained pursuit

During a head-unrestrained pursuit movement, gaze and head are generally moving in the same direction. Therefore, as mentioned in the preceding paragraph, a fully operational VOR would drive the eye in the opposite direction than the direction of the gaze goal, hence being inefficient. Because the gaze (eye-in-space) is the sum of head-in-space and eye-in-head displacements, during head-unrestrained tracking, two extreme theoretical situations can occur. In the first one, the pursuit system does not send a command to the eye and the gain of the VOR is set to zero while in the second one a signal opposite to the pursuit signal is sent to the eye to negate the effect of the VOR and keep the eye stable in the orbit.

[63] Around 1.65 for a target at 16 [cm] (Viirre et al., 1986)

To test the validity of those two assumptions, Lanman et al. (1978) compared the behavior of labyrinthine-lesioned and healthy monkeys during head-unrestrained pursuit after a brake suddenly stops the head movements. Because of the time constant linked to the initiation of pursuit, if a change in gaze trajectory is observed after the onset of the brake, this would mean that the pursuit system is activated. On the contrary, if no modification of the trajectory is observed, the pursuit system was always active, and negated the VOR. Lanman et al. (1978) observed no modification of the trajectory after the onset of the head brake for healthy monkeys. Interestingly, they showed a temporary plateau of gaze position for labyrinthine-deficient monkeys when the brake was applied. The duration of the plateau was compatible to the initiation of a pursuit movement. This experiment demonstrates clearly that the pursuit system is active during head-unrestrained tracking and negates the VOR signal. The addition of an external signal in the opposite direction of the VOR signal to cancel the VOR during pursuit is called "**VOR cancellation**". To test if the pursuit system is the source of the cancellation signal used to negate the VOR, Barnes et al. (1978) compared the dynamic characteristics of the pursuit and the VOR cancellation. The authors showed that the responses in the two situations were very similar, demonstrating the key importance of the pursuit signal in the modulation of the VOR during head-unrestrained pursuit[64]. The same year, Lau et al. (1978) proposed a model in which linear summation of the vestibular and the pursuit signals are used to cancel the VOR. A decade later, Leigh et al. (1989) demonstrated the limitation of the linear model of Lau et al. (1978). Because there are no torsional pursuit movements, he showed that the modulation of the torsional VOR can only be explained by a parametric change of the VOR gain. Therefore, the results of Leigh et al. (1989) suggest that a second VOR modulation mechanism is used during head-unrestrained tracking in addition to the main cancellation mechanism.

4.5.2 VOR suppression during head-unrestrained saccades

Following the studies on VOR cancellation during head-unrestrained pursuit, authors looked at the modulation of the VOR component during gaze saccades. As for the pursuit movements, a fully working VOR would be counterproductive if gaze and head are moving in the same direction during a head-free saccade.

Tomlinson and Bahra (1986) slowed the saccades of monkeys using Diazepam (commercialized under the name "Valium"). With slower saccadic movements, Tomlinson and Bahra (1986) had enough time to perturb the head during the gaze shift. They showed that a perturbation on the head is transmitted to the gaze, reflecting a VOR gain smaller than unity. Laurutis and Robinson (1986) tested if the VOR was present during gaze saccades in humans. The authors accelerated or decelerated head movements during very large saccades in humans[65]. Laurutis and Robinson (1986) reported that the

[64] Those results were reproduced later by Koenig et al. (1986) and confirmed the initial observation of Barnes et al. (1978).

[65] They used very large saccades (∼120 [deg]) to increase the duration of the movements. Therefore, they had enough time to perturb the head movement during the gaze saccades.

amplitude of the head perturbation was reflected on the gaze, again pointing toward an absent VOR during large gaze saccades.

Another evidence for the absence of the VOR during saccadic movements came from a comparison between behavioral studies on the VOR and on head-unrestrained gaze saccades. Pulaski et al. (1981) studied the limits of the compensatory eye movements and showed that the VOR saturated around 350 [deg/s]. On the other side, Laurutis and Robinson (1986) reported gaze saccades with peak velocity up to ∼800 [deg/s]. Therefore, it appears that the gaze shift, being the sum of eye and head movement, could not attain those high velocities with a VOR cancellation mechanism as described in the preceding section. To use the cancellation mechanism, the VOR signal should not saturate for those velocities. From those behavioral studies, it appears clearly that the gain of the VOR is modulated during gaze saccades. This mechanism is called "**VOR suppression**".

To quantify more accurately the modulation of the VOR gain during VOR suppression, Lefèvre et al. (1992) compared the behavior of saccades in head-unrestrained and head-restrained condition. They showed that the gain increases before the end of the gaze saccade and that the restoring time (∼40 [ms]) was insensitive to the amplitude of the saccade. Lefèvre et al. (1992) showed that the VOR was fully operational as soon as the gaze is on the target. Twelve years later, Cullen et al. (2004) perturbed the head movements at different instants after gaze saccade onset. With this technique, they computed the percentage of VOR attenuation as a function of the elapsed time in the saccade. Cullen et al. (2004) showed that the decrease of the gain is maximal at the onset of the saccades and then the gain progressively increases before the end of the saccade, confirming the findings of Lefèvre et al. (1992).

4.6 Head-unrestrained pursuit: behavior

The preceding sections explained why it is difficult to dissociate VOR, head and eye movements during head-unrestrained tracking of a moving object. More precisely, since the experiments of Lanman et al. (1978) and Barnes et al. (1978), it is known that the eye-in-head movements during head-free tracking are the sum of the VOR and the pursuit commands. As it was also shown in section 4.5.1, the VOR gain is not similar in all subjects and can change during the same task depending on several factors. Only the output of the combination of the pursuit command and the VOR, the eye movement, is measurable during head-unrestrained behavioral studies. A modulation of the VOR gain during the stationary phase of a head-free tracking can be compensated for by an appropriate pursuit command sent to the eye. Thus, no transient linked to the VOR modulation would be observed in the eye movement. Therefore, as the gaze is the sum of head and eye displacement, it is impossible to isolate during natural head-unrestrained pursuit the contribution to the gaze movement made by each of its component (VOR, eye and head). This, added to the general difficulty to record head-unrestrained movements, is probably the reason why there are less studies dedicated to head-unrestrained pursuit.

In the end of the 1970's, Gresty and Leech (1977) looked specifically at the coordination of eye and head movements during the tracking of periodical and

random target trajectories. The authors reported that subjects had difficulties to pursue the target with combined eye-head movements when the frequency of the oscillating target increased. With the target frequency higher than 0.8-1 [Hz], subjects used less head movements and favored an eye-only pursuit strategy (see Fig. 2 of (Gresty and Leech, 1977)). However, the gain and the phase of the gaze remained fairly constant on the tested range of frequencies[66]. In contrast, when Gresty and Leech (1977) compared the head-restrained and head-unrestrained behavior during the pursuit of an unpredictable moving target, they showed that the pursuit was facilitated when the head was free to move. A year later, Lanman et al. (1978) compared the tracking behavior between the head-fixed and head-free conditions. The authors did not find a difference between the eye-only pursuit behavior and the head-unrestrained gaze tracking behavior. Additionally, Lanman et al. (1978) reported that monkeys used different strategies to control the head displacement while pursuing a periodical target with the head free to move. Either the head lagged behind the target with a delay up to 200 [ms] or the head anticipated the target movements[67]. During the head-unrestrained tracking of a periodical target, Lanman et al. (1978) reported that head movements accounted for approximately 75% of the gaze displacements while the eye-in-head remained relatively stationary at the center of the orbit.

In the end of the 1980's, Barnes and Lawson (1989) used a protocol composed by the sum of four sinusoids at different frequencies to study the coordination of eye and head movements during head-unrestrained pursuit. They also compared the head-free and head-fixed behavior. As Lanman et al. (1978), Barnes and Lawson (1989) showed that head movements account for 70% to 100% of the gaze displacement during head-unrestrained tracking. Additionally, the head displacement appeared to be less sensitive to a variation of the frequency of the target, the opposite being true for the eye velocity. Barnes and Lawson (1989) also reported that the behavior of the gaze in head-unrestrained condition is similar to the behavior of the eye in head-restrained condition. In a last experiment, Barnes and Lawson (1989) used feedback on the rotations of the vestibular chair to negate the head movements naturally generated by the subjects during head-free tracking. The authors reported that the behavior with the compensation of the head movement was similar to the behavior when the head was either free to move or not[68].

To my knowledge, only two studies looked at the initiation of head-unrestrained tracking (Dubrovski and Cullen, 2002; Wellenius and Cullen, 2000). Both studies used step-ramp target motion to look at eye-head coordination and to study the parameters that modify the initiation of head-unrestrained pursuit. Wellenius and Cullen (2000) compared pursuit initiation between head-fixed and head-free conditions. The authors reported an effect

[66] This observation points toward a central control of the gaze instead of a separate control of the eye and the head during head-unrestrained tracking.

[67] This can be seen as an evidence that the head trajectory can be controlled independently of the gaze trajectory.

[68] This observation points toward a central control for the gaze.

of the eye-in-head position[69] on the latency of the pursuit initiation for both conditions. Wellenius and Cullen (2000) also showed that the head movement always lags behind the gaze at the initiation of an unpredictable step-ramp target motion. Two years later, Dubrovski and Cullen (2002) compared both the initiation and the maintenance of the pursuit between head-restrained and head-unrestrained condition. The authors reported that the gain of the tracking movement is significantly bigger when the head was free to move compared to a head-fixed situation. Dubrovski and Cullen (2002) also used a stabilized target on the fovea to study the open-loop behavior of head-free tracking movements. No significant difference was found when the open-loop behavior of tracking movements in head-restrained and in head-unrestrained situations were compared. As a conclusion, Dubrovski and Cullen (2002) suggested that eye and head movements are controlled to satisfy the general purpose of the task: tracking accurately a moving target with gaze.

4.7 Neurophysiology of the pursuit system

Like for the control of saccades presented in section 3.3, an important number of cortical and subcortical areas are involved during the preparation and the execution of a pursuit movement.

4.7.1 From the retina to middle temporal (MT) and medial superior temporal (MST) areas

The pathways from the retina to the output of the primary visual areas are similar to the previously described saccadic pathways (see section 3.3). Briefly, retina ganglion cells project to the lateral geniculate nucleus (LGN, item 3 in Fig. I-16). Then the magnocellular layer of LGN projects to the primary visual cortex (PVC, item 6 in Fig. I-16). From there the pathways involved during pursuit movements diverge from the pathways for saccadic movements presented in 3.3.1. The middle temporal area (MT) receives direct projections from the primary visual cortex. Then MT projects to its neighboring area: the medial superior temporal area (MST). It has been shown that both MT and MST are key players in the visual processing of target motion. The following paragraphs will summarize their functions during the tracking of a moving target.

4.7.2 Medial temporal (MT) and medial superior temporal (MST) areas: processing of target motion

Located in the posterior bank of the superior temporal sulcus, the middle temporal (MT) and the medial superior temporal (MST) areas are neighbors. At first, a lot of studies focused on the role and processing of MT neurons. Gattass and Gross (1981) recorded activity of MT neurons while stimulating visually the contralateral retina. The authors showed that MT neurons receptive fields are

[69] Not the initial position of either the gaze or the head!

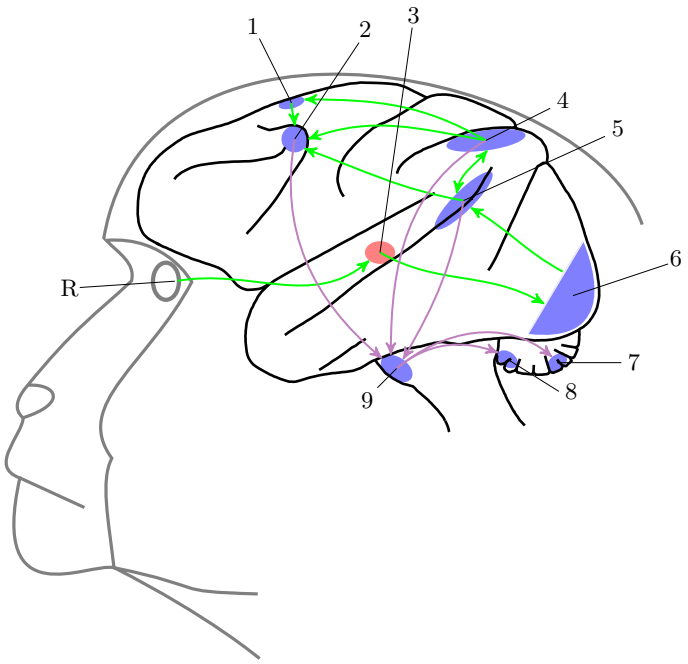

Fig. I-16: **Main pursuit pathways to the cerebellum.** Corticocortical connections are represented in green while corticopontal and subcortical connections are represented in purple. Blue structures are on the cortex surface. Red structures are hidden by the cortex. See text for more details. **1** SEF: supplementary eye field, **2** FEF: frontal eye field, **3** LGN: lateral geniculate nucleus, **4** LIP/VIP: lateral/ventral intraparietal area, **5** MT/MST: middle temporal (MT) and medial superior temporal (MST) areas, **6** PVC: primary visual cortex (V1 ⇒ V4), **7** VERM: cerebellar vermis, **8** VPF: ventral paraflocculus, **9** PON: Visuomotor nuclei in the pontine nuclei, **R**: retina

visuotopically organized[70]. More precisely, Gattass and Gross (1981) demonstrated that the whole contralateral visual field is mapped by MT neuron receptive fields. Later, Maunsell and van Essen (1983b) showed that MT neurons are directionally selective for moving objects and that the population response is uniform (all moving directions are equally represented in MT). Additionally, Maunsell and van Essen (1983b) showed that the amplitude of the discharge varies with the speed of the moving target. Because of its strong response to moving stimuli, Maunsell and van Essen (1983a) looked at the connectivity of MT to study its function in visual processing. They showed that MT receives projections from V1, V2, V3 and from an anatomically distinct neighbor area. They named this new area the medial superior temporal area (MST). Maunsell and van Essen (1983a) showed that MT projects to MST and to the pontine

[70] Each part of the visual field corresponds to a defined zone of MT.

nuclei[71,72] (PON). Because the recorded activity in MT has some common features with the activity of V1, Albright (1984) compared systematically both areas. He confirmed the findings of Maunsell and van Essen (1983b) (directionally selectivity of MT neurons) and showed that the average discharge of V1 neurons for moving stimuli is weaker than the discharge of MT neurons. The same year, Albright et al. (1984) showed that neurons in MT have a columnar organization: neurons with an identical preferred axis of motion are clustered in a column[73].

After the discovery of MT and MST and their functions in motion processing, researchers looked at their activity during pursuit movement. Newsome et al. (1985) showed that a lesion of MT impaired the pursuit initiation and the accuracy of saccades triggered during an ongoing pursuit movement (catch-up saccades). However, once pursuit initiated, there was no difference between lesioned and healthy situations. The authors concluded that MT must be involved in the initiation of motion processing. To refine the understanding of MT and MST neuron behavior during pursuit movements, Komatsu and Wurtz (1988) recorded neurons in both areas while monkeys pursued a spot of light in a dark room. They showed that MST was not visuotopically organized like MT. However, Komatsu and Wurtz (1988) found neurons in MT and in MST that increased their discharge rate during a pursuit movement (pursuit cells). In the companion paper of (Komatsu and Wurtz, 1988), Newsome et al. (1988) studied the difference between pursuit neurons located in MT or in MST. The authors stabilized the target on the retina or blinked the target during the pursuit. They showed that the discharge of MT neurons strongly decreases during blinking/stabilization while the activity of MST neurons remains unchanged. From those observations, it appears that pursuit cells in MST do not receive only visual information[74]. Therefore, Newsome et al. (1988) proposed that MT cells receive visual inputs while MST pursuit neurons receive both visual and extraretinal[75] inputs. To characterize further the difference between MT and MST, Dürsteler and Wurtz (1988) reproduced in MST the lesion study in MT of Newsome et al. (1985). They showed two deficits following MST lesions. The first one is similar to the one observed by Newsome et al. (1985) in MT: impairment of pursuit initiation and inaccuracy of catch-up saccades in the contralesioned side. Additionally, Dürsteler and Wurtz (1988) showed that the gain of the pursuit decreases when the movement is directed toward the lesioned side, even if the target is in the ipsilesioned side, where no deficit of the first type is present. Finally, Dürsteler and Wurtz (1988) showed that MST must be involved in the processing of the retinal slip, because the sensitivity to RS

[71] As it will be shown later, the pontine nuclei play a key role during pursuit eye movements.

[72] In the conclusion of the study, Maunsell and van Essen (1983a) already proposed a functional organization of the visual areas that is close to the one represented in Fig. I-16.

[73] MT is not the only structure with a columnar organization. E.g., Hubel and Wiesel (1969) demonstrated a columnar organization in the striate cortex (V1) of monkeys.

[74] Otherwise, those cells would stop to discharge during target blink/stabilization.

[75] To maintain pursuit inputs during target blink/stabilization.

decreased after the lesion. The implications of MT and MST neurons in pursuit was further demonstrated by Komatsu and Wurtz (1989). The authors stimulated the MT and MST during ongoing pursuit movements. They showed that the stimulations evoked an acceleration of the maintained pursuit toward the stimulated side. This change of velocity induced a retinal slip that was not corrected by the pursuit system. Therefore, Komatsu and Wurtz (1989) proposed that the stimulated areas were functionally located before the motion feedback and altered the visual input of the pursuit controller. Eight years later, Groh et al. (1997) defined more accurately the effect of MT stimulations on pursuit movements. Using MT stimulation, the authors could modify the trajectory of the pursuit movement in a predictable way. Groh et al. (1997) showed that the output eye motion is an average of the velocity visually evoked and the velocity generated by stimulation at a defined site of MT.

Again, it must be pointed out that all the preceding studies were carried out while monkeys had their head fixed. To my knowledge, the only exception is the study of Thier and Erickson (1992). In this study, the authors used the cancellation of the VOR to show that MST has vestibular inputs. Thier and Erickson (1992) showed that the sensitivity to motion of MST neurons was similar in both eye-only movements and VOR cancellation. Those results pointed toward a reconstruction of target velocity with respect to a space-fixed reference at the level of MST.

4.7.3 Downstream MT and MST: LIP, VIP, FEF, SEF, PON during pursuit

In their study of MT connectivity, Maunsell and van Essen (1983a) reported projections to a part of the intraparietal sulcus. They named this area the ventral intraparietal area (VIP). This projection from MT to VIP was later confirmed by Colby et al. (1993). The authors recorded VIP neurons' activity. They reported that their activity was tuned, as MT neurons, by both speed and direction of a moving object. Additionally, no activity was recorded when monkeys did saccades, pointing toward their implication in the motion process and not in the position process. Recently, Schlack et al. (2003) observed neurons in VIP that were sensitive to smooth pursuit eye movements ($\sim$50% of the recorded neurons). The authors showed that the velocity tuning of those neurons is more important for high velocity targets. Using target blinks, Schlack et al. (2003) also demonstrated that the neural activity of VIP pursuit neurons is related to extraretinal signals and not to visual stimulation. In their conclusion, Schlack et al. (2003) suggested that VIP is involved in the coordination and the control of eye and head movements in the "near extra-personal space".

A second structure of the intraparietal sulcus received projections from MT and MST: the lateral intraparietal area (LIP) (Blatt et al., 1990). As reported in section 3.3.1, LIP is a structure initially reported as involved during saccadic movements. However, the connectivity of LIP with areas known to discharge during pursuit raised the question of its implication in pursuit. To test this assumption, Bremmer et al. (1997) recorded activity in LIP and found neurons in the dorsoposterior region that responded during pursuit movements but were

not modulated by retinal slip. As for saccades, Bremmer et al. (1997) showed that the activity of pursuit-related LIP neurons was modulated by the eye position in the orbit. The LIP neurons project to the PON and to FEF/SEF (Blatt et al., 1990).

In their original study on FEF involvement during saccadic movements, Bruce et al. (1985) reported that a stimulation of a small area in FEF evoked smooth eye movements that were directionally selective. The involvement of FEF during pursuit was later confirmed by several authors using microstimulations (Gottlieb et al., 1993; Tanaka and Lisberger, 2002; Tian and Lynch, 1996b) or lesions (Keating, 1991). Keating (1991) lesioned the FEF and reported that movement initiation and maintenance were degraded during visually guided pursuit. Using microstimulations, Gottlieb et al. (1993) showed that the acceleration and velocity of pursuit initiation were a function of the current intensity and that the velocity of the evoked movement quickly saturated. Using stabilization of the target on the retina, the authors reported that the eye velocity increased proportionally with stimulation duration, with a more important saturation threshold. From this observation, Gottlieb et al. (1993) proposed that FEF was located inside the feedback loop of the pursuit control[76]. Tian and Lynch (1996b) used stimulation to map more precisely FEF. They defined two areas: one that generates only saccadic movements (FEF_{sacc}) and another one that evokes exclusively smooth eye movements (FEF_{sem}). In a second study, Tian and Lynch (1996a) showed that FEF receives inputs from MT, MST, LIP and SEF. Tanaka and Lisberger (2002) used stimulation to study the influence of FEF_{sem} during pursuit movements. They showed that FEF_{sem} stimulation also influenced the pursuit gain during the maintenance part of the movement. Tanaka and Lisberger (2002) reported two effects from the stimulation. The first one is a directional effect: stimulation evoked eye movement in a direction independent of the current eye velocity. The second effect is a global modification of the pursuit gain.

Using VOR cancellation, Fukushima et al. (2000) reported that the activity of the majority of the pursuit-related cells in FEF_{sem} ($\sim$66%) were correlated with gaze movements and not eye movements. The authors also showed that those cells continue to discharge even during target blinks.

A second structure of the frontal cortex initially assigned to saccades appeared also to be involved during pursuit: SEF. Heinen (1995) recorded the activity of SEF neurons during smooth pursuit. The neural activity was modulated by the direction of the movement, as for FEF_{sem}. Heinen (1995) also reported that the peak of activity is correlated with pursuit initiation. Using microstimulations, Tian and Lynch (1996b) confirmed the findings of Heinen (1995) and found two areas, as for FEF, inside SEF: one is related to saccadic eye movements and the second is related to smooth eye movements. More recently, Missal and Heinen (2001) studied the effect of SEF stimulation on pursuit eye movements. The authors showed that the stimulations modified the initiation of the pursuit but not the maintenance. Missal and Heinen (2001) reported that the facilitation of pursuit movement by stimulation is not a function

[76] Oppositely to the observed behavior in MT/MST (Komatsu and Wurtz, 1989), see section 4.7.2

of the movement direction or the target velocity but is tuned by eye velocity. Finally, SEF stimulation affects pursuit initiation if and only if it is applied before pursuit initiation (Missal and Heinen, 2001).

MT, MST, LIP and FEF_{sem} where all reported to project heavily to the pontine nuclei (Blatt et al., 1990; Maunsell and van Essen, 1983a; Huerta et al., 1986). Therefore, authors started to look at the neural activity in the PON because it was a known relay between the previously described cortical structures and the cerebellum. The dorsolateral pontine nuclei (DLPN) contains neurons sensitive to target motion and/or to smooth eye movements (Suzuki and Keller, 1984; Mustari et al., 1988; Thier et al., 1988). Suzuki and Keller (1984) were the first to record neural activity in DLPN of monkeys during visual pursuit. They found a majority of cells that reacted to the motion of visual stimuli and were tuned to the orientation and the velocity of the stimulus. Suzuki and Keller (1984) reported that a movement of the visual field was necessary to evoke a discharge of DLPN neurons. Four years later, Thier et al. (1988) and Mustari et al. (1988) confirmed the results[77] of Suzuki and Keller (1984). Both studies defined three categories of DLPN neurons[78]. The first one (visual-only DLPN neurons) discharges only for movement of a visible target in a preferred direction. A second class of neurons (visual-tracking neurons) discharges during smooth eye movements but not during visual stimulation. The last category discharges in both situations. DLPN neurons do not discharge during saccades (Mustari et al., 1988). Using lesions, May et al. (1988) demonstrated the importance of DLPN in pursuit movements. When monkeys were lesioned, the pursuit toward the side of the lesion was impaired during both initiation and maintenance of the movement (May et al., 1988).

4.7.4 Cerebellum and pursuit movements

A lot of studies have shown an implication of the cerebellum during pursuit movements. Westheimer and Blair (1973) were the first to demonstrate the inability of cerebellectomized monkeys to make smooth pursuit movements. The same year, in their attempt to map eye movements on the cerebellar cortex, Ron and Robinson (1973) reported that electrical stimulation of either the flocculus or the vermis evoked smooth pursuit eye movements.

Following the observations of Ron and Robinson (1973), Lisberger and Fuchs (1978) recorded the activity of Purkinje cells (P-cells) in the flocculus during smooth eye movements, VOR in the dark and VOR cancellation. The authors demonstrated that floccular P-cells activity is modulated by eye velocity. They also recorded neurons that were discharging during both smooth pursuit and VOR cancellation. The activity of those floccular P-cells appeared to be correlated with the vector sum of eye and head velocity, pointing toward a gaze velocity modulation of floccular P-cells activity (Lisberger and Fuchs, 1978).

[77] In two different journals, one study was published in March and the second in August.

[78] They did not use the same name for the categories. Therefore, the name of the first published study (Thier et al., 1988) will be used in the text.

Later, Stone and Lisberger (1990) showed that floccular P-cells are directionally selective: they increase their background activity during movements in the ON-direction and decrease it during movement in the OFF-direction. Using stabilization of the target on the fovea, Stone and Lisberger (1990) also demonstrated that the sustained response of floccular P-cells is driven by extraretinal signals. From their observations, the flocculus appears to play two roles during pursuit: visual activity is conveyed by P-cells to drive the pursuit during movement initiation while an eye-velocity corollary discharge is used in a positive feedback to maintain pursuit (Stone and Lisberger, 1990).

A second part of the cerebellum was reported to be involved during pursuit movements: the vermis. Suzuki et al. (1981) recorded two types of P-cells in the vermis: the first population modulated its discharge with the eye velocity during smooth pursuit. The activity of the second population of neurons was correlated with the retinal slip. Later, Suzuki and Keller (1988a) recorded P-cells in the vermis with an activity modulated by both eye and/or head velocity. In the companion paper of (Suzuki and Keller, 1988a), Suzuki and Keller (1988b) reported P-cells with an activity modulated by eye and head velocity and also by the retinal slip. From those observations, the authors postulated the probable existence of two pools of P-cells in the vermis. A first population modulates its discharge with respect to gaze velocity (sum of eye and head velocity) and a second one with respect to the target velocity (sum of eye, head and retinal slip) (Suzuki and Keller, 1988a,b). The presence of those signals in the cerebellum is of major importance for the cerebellum to control gaze velocity during head-unrestrained pursuit.

As for the previously presented neural areas, authors also induced lesions to test the behavioral effect of a population removal on pursuit behavior. Using more precise lesions than the original study of Westheimer and Blair (1973), Zee et al. (1981) showed that contrary to the incapacity to generate pursuit movements when the whole cerebellum is ablated, removal of the flocculus and the paraflocculus impaired pursuit and VOR cancellation but monkeys still generate smooth movements. Those results were confirmed later by others (Rambold et al., 2002).

To confirm the involvement of the vermis during pursuit, Takagi et al. (2000) studied the impact of vermal ablations on smooth eye movements. They reported a large change during the open-loop part of the movement (pursuit initiation) and a small modulation of the mean pursuit gain between healthy and lesioned monkeys. Takagi et al. (2000) used a protocol similar to saccadic adaptation (see section 3.3.3) for pursuit adaption to test pursuit initiation. They changed the velocity of the target during the open-loop part of the movement, at the initiation of pursuit. Healthy monkeys adapted their eye velocity to match the increased target velocity while lesioned monkeys lack pursuit adaptation (Takagi et al., 2000).

4.8 Pursuit and models

As for saccades, authors also built models of the pursuit movements. As presented in the previous chapters, a model of the pursuit movement must include

several factors that are less critical in a model of gaze shifts (e.g., initiation, anticipation, prediction, etc).

The first model of the pursuit system was built to evaluate the importance of the delays in the sensory system. Dallos and Jones (1963) proposed a very simple model of the "fixation system". This model does not have a physiological meaning but was built to demonstrate the importance of including the delays in the control of the eye movement during pursuit. Following this highly simplified model, Bahill and McDonald (1983) published a model that includes an adaptive mechanism to compensate for the inherent delays of the pursuit system. Their model, albeit not close to physiology, could simulate the previously reported zero-latency tracking of an oscillating target.

Three years later, Robinson et al. (1986) proposed a model of the pursuit system based on the same architecture than the saccadic model of (Robinson, 1975). The pursuit model includes three feedback loops. The outer feedback loop computed a velocity error (difference between the target velocity and the eye velocity) that drives the eye based on the visual inputs of the target on the retina. Two other feedback loops (a positive one and a negative one) ensure that the model could reproduce adequately the ringing settling to a steady state[79] while including an acceleration saturation.

If the model of Robinson et al. (1986) could simulate the pursuit behavior when the target has a constant velocity, it does not include a prediction term that would allow it to simulate pursuit of periodic target. In a complete study of the prediction mechanisms in human smooth pursuit, Barnes and Asselman (1991) proposed a model that includes a predictive component and could also simulate, to a certain extent, head-unrestrained pursuit. The predictive component of this model is based on a buffer that stores target motion. Therefore, the larger the buffer, the higher the performance of the model. Unfortunately, it is not easy to link the buffer mechanism with the behavior of a neural structure involved in pursuit.

Later, Krauzlis and Lisberger (1994) published a model based on three parallel pathways that can simulate pursuit behavior when tracking targets with constant velocity. Compared to the model of Robinson et al. (1986), Krauzlis and Lisberger (1994) uses exclusively the motion of the target on the retina (and its derivative, the acceleration of the target) and not on internal signals to drive the eye movement. The first pathway uses the velocity of the target on the retina, the second one uses the acceleration of the target on the retina. The third pathway (motion transient pathway) discharges during a short period of time (20 [ms]) to add a pulse linked to image velocity after a step of target velocity. Again, none of the different transfer functions present in the model corresponds to a defined neural area.

The first model that mimics more closely the neural circuitry known to be involved during pursuit has been proposed by Kettner et al. (1997). The authors focused their pursuit model on the predictive behavior of the pursuit. They built a distributed mathematical representation of the cerebellum that learns

[79] During the initiation of a pursuit movement, there is an oscillation of the eye movement around the desired target velocity (Robinson et al., 1986). This overshoot is damped and the amplitude of the oscillations decreased to a stable steady state.

the predictive component of the target movement. The proposed architecture simulates the predictive behavior of monkeys during two-dimensional tracking reported by Kettner et al. (1996) and the perturbation responses showed by Leung and Kettner (1997).

4.9 Neurophysiology of VOR

Section 1.2.1 describes anatomically the angular sensors of head movements: the semi-circular canals (SCC). In this section, the neural circuitry from the output of the semi-circular canals to the generation of horizontal compensatory eye movements is described.

4.9.1 Neural pathway for compensatory eye rotations

Because of the short response time of the VOR to head perturbations, researchers studied the neural circuitry involved in the compensatory eye movements. Szentagothai (1950) stimulated independently each canal and recorded simultaneously extraocular muscles' activity. He built a correspondence table between each stimulated canal and the activated extraocular muscles (see table I-3 for a summary of the results). In the following section, the neural circuitry

Stimulated canal	**Extraocular muscle activated**
Horizontal	ipsilateral medial rectus contralateral lateral rectus
Superior	ipsilateral superior rectus contralateral inferior oblique
Inferior	ipsilateral superior oblique contralateral inferior rectus

Table I-3: Muscles activated by canal stimulation

involved in the generation of horizontal compensatory eye movements is presented. Similar (but not identical) pathways exist for the generation of vertical and torsional VOR compensatory movements.

Several authors have shown the influence of the otolith[80] on rotational-VOR. Rotations around the axes that generate a change of the otoliths orientation with respect to gravity (pitch and roll axis) have a higher VOR gain with otolith stimulation than without (Bockisch et al., 2005; Schmid-Priscoveanu et al., 2000; Bartl et al., 2005). However, the otolith-SCC interactions is not addressed in this thesis. Thus the labyrinthine apparatus is seen as a combined sensor during the studies.

[80] The otoliths are the linear sensors of head acceleration. See section 1.2.1.

Horizontal compensatory pathways

Several studies have looked at the neural architecture of the VOR pathways. In the early 1930's, Lorente de No (1933) used independent caloric stimulation of the canals while recording activity in the extraocular muscles of the rabbit. He tried to isolate the VOR reflex arc from external inputs using lesions of the brainstem. Lorente de No (1933) showed the importance of the eye motoneurons (the abducens nuclei and the third nuclei), the vestibular nuclei and the nerves that interconnect them. In his study, Szentagothai (1950) confirmed the observations made by Lorente de No (1933) and showed that a lesion of the medial longitudinal fasciculus (MLF, fiber tracts that convey among other things the vestibular information between the vestibular nuclei and the eye motoneurons) impaired the VOR while a section of the brainstem does not change the reflex behavior. This removed the possibility that the burst neurons described in a preceding section (see 3.3.4) are involved in the direct pathways of the VOR.

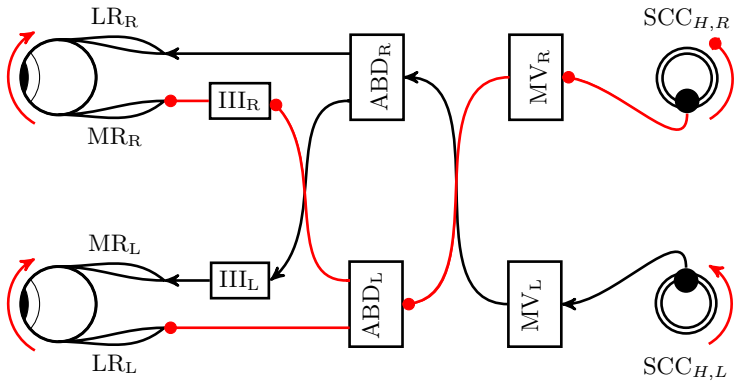

Fig. I-17: **Vestibulo-ocular direct pathways** This figure represents the connections between populations of neurons involved in the direct pathway of the VOR. Subscripts "L" correspond to the neurons on the left side while subscripts "R" correspond of neurons on the right side. Arrow tips correspond to excitatory connections. Filled circle tips correspond to inhibitory connections. SCC $_H$: horizontal semicircular canals, MV: medial vestibular nucleus, ABD: abducens nucleus, III: third nucleus.

Figure I-17 represents a simplified circuitry that links the horizontal canals to the lateral and medial recti. When the head is passively rotated counterclockwise, the left horizontal semicircular canal (SCC$_{H,L}$ in Fig. I-17) excites the ipsilateral medial vestibular nucleus (MV$_L$ in Fig. I-17). MV$_L$ projects to the contralateral abducens nucleus (ABD$_R$ in Fig. I-17) (Highstein, 1973b) and to the contralateral third nucleus (III$_L$ in Fig. I-17) (Highstein, 1973a). The pro-

jections from ABD_R excite both the right lateral rectus (LR_R in Fig. I-17) and the left medial rectus (MR_L in Fig. I-17) through the third nucleus.

In parallel with the excitatory pathway, the right horizontal semicircular canal ($SCC_{H,R}$ in Fig. I-17) decreases its discharge rate to the right medial vestibular nucleus (MV_R in Fig. I-17) (Ito et al., 1976). MV_R inhibits the contralateral abducens nucleus (ABD_L in Fig. I-17). Then ABD_L activity decreases and both the right medial rectus (MR_R in Fig. I-17) and the left lateral rectus (LR_L in Fig. I-17) relax their pulling strengths.

The combined action of both the contraction of LR_R and MR_L muscles with the relaxation of LR_L and MR_R muscles creates a clockwise rotation of the eye-in-the orbit in response to the counterclockwise rotation of the head. Therefore, the gaze remains stable. As mentioned in the section linked to VOR behavior (section 4.4), the VOR gain is not constant, it is modulated. Consequently, researchers looked at the structures that project to the direct pathway and that are able to modify the discharge characteristics. As previously reported, the cerebellum appears as a key player for the modulation of the vestibulo-ocular reflex.

Cerebellum and VOR

To define the neural implication of the cerebellum during VOR, Ito et al. (1973b) concurrently stimulated the cerebellar flocculus and the semicircular canals of rabbits. The authors showed that floccular stimulation modulates the muscular activity linked to vestibular stimulation. In a parallel study, Ito et al. (1973a) showed that the flocculus inhibits the output of VN. The cerebellum also sends an inhibitory projection to the III nucleus (Highstein, 1973a) and to ABD (Highstein, 1973b). To test the hypothesis that the cerebellum is an important structure for the VOR, Ito et al. (1977) studied the influence of a stimulation applied to the inferior olivary or to the optic tract to the vestibulo-ocular reflex. In healthy rabbit, an olivary stimulation induced a depression of the discharge sent by the semicircular canals. However, when the flocculus was ablated, an electrical stimulation did not modify the discharge of the vestibular nuclei. The pattern of cerebellar inhibitions to the different stages of the VOR direct pathway is entirely compatible with the previously reported observations of the VOR modulation and adaptation by the flocculus (see section 4.5).

In parallel with the electrophysiological studies, authors tested the effect of a lesion on the VOR. Using spectacles that reversed left and right direction[81] on cats, Robinson (1976) showed that cats are able to adapt their VOR gain to minimize the retinal slip and ensure a quasi-stable vision. Robinson (1976) reported two-scales of adaptation: a fast one that was quickly forgotten when the spectacles were removed and a long-term one that lasted longer after the prisms' removal. When the flocculus, paraflocculus and some parts of the vermis were removed, Robinson (1976) reported no more long- or short-term adaptation. Later, Zee et al. (1981) reported that a cerebellectomy did not drastically change the VOR in the dark (increases in the mean gain) but modified the can-

[81] When the cat was rotated to the right (left), the visual field moved to the right (left).

cellation mechanism when pursuing a head-fixed target. Those studies pointed toward a regulation and not a control of the VOR by the cerebellum.

4.9.2 Active and passive head movements, which one and how to compensate?

As described in section 4.5, the VOR must be modulated to account for situations in which its action could be counterproductive. How this modulation is done at a neuronal level has been a matter of debate for several years. Initially, authors thought that the activity at the output of the semicircular canals was modulated by efferent signals. To test this hypothesis, Cullen and Minor (2002) recorded the activity of SCC afferents during active and passive head movements. They showed that the SCC activity during active movements are well predicted by a model built on passive discharge recordings, pointing toward no modulation of the SCC output by efferent signals. The same year, Roy and Cullen (2002) showed that the on-line modulation of the neurons in the vestibular nuclei is related to the task goal (neurons discharged during gaze stabilization and paused during gaze redirection). Additionally, they showed that the neck proprioceptive inputs have no effect on the neuronal activity modulation.

Looking for the origin of the activity modulation in the vestibular nuclei, Roy and Cullen (2004) did a series of experiments involving active and passive head movements while recording activity of vestibular neurons. With those experiments, they tested the validity of four different assumptions: direct inhibition of the canal output by a head command, inhibition of the vestibular nuclei by a head command, neck proprioceptive input to the vestibular neurons gated by the head command or a matching template between the expected head movement from a head command and the neck proprioceptive output. The experiments of Roy and Cullen (2004) allowed the authors to isolate the input of each hypothesis and to demonstrate that the discharge of vestibular neurons is modulated when the neck proprioceptive inputs matched the expected consequences of a head motor command. In the discussion of the studies, Roy and Cullen (2004) suggested the cerebellum as a candidate for the "matching operator". This suggestion is well supported by the anatomy literature (see preceding section).

4.10 VOR and models

The simplest VOR models are included in gaze saccade models. They traditionally used a modulation of the VOR gain through a gating mechanism (Laurutis and Robinson, 1986; Guitton et al., 1990; Lefèvre and Galiana, 1992; Galiana and Guitton, 1992) that switches off the VOR at the onset of the gaze shift and reactivates it at the end. Goossens and Van Opstal (1997) included a slight modification by modulating the VOR gain with respect to the gaze motor error[82].

[82] Difference between the target position and the gaze position.

To help clinicians diagnose vestibular deficiencies, Schmid et al. (1971) built a model of the VOR in the dark based on human behavioral recordings[83]. The authors also included a very simple model of the fast phase of the nystagmus to center the eye in the orbit when the position was larger than a threshold. They compared the frequency response of their model to the behavior of young human subjects. As it can be easily understood, Schmid et al. (1971) did not try to link their model to the activity of a neural area involved in the VOR. Thirteen years later, Galiana and Outerbridge (1984) published a bilateral model of the VOR in the dark. The circuitry of the model is based on the anatomy of the main neuronal connections present in the central VOR pathway[84]. The model can reproduce the activity of the different populations of neurons when a subject is rotated in the dark. However, as for Schmid et al. (1971), it can not simulate the cancellation or the suppression VOR modulation mechanisms. Finally, Green and Angelaki (2004) proposed a neural network based model that integrates the sensory information from both the otolith and the semicircular canals. Through the combination of the two sensors' output, the model of Green and Angelaki (2004) can simulate the VOR response for rotations around the three axes (yaw, pitch and roll) as well as the linear-VOR (translations of the whole body).

Finally, a class of model simulates the visual-vestibular interaction (Lau et al., 1978; Schmid et al., 1980; Barnes, 1993). Lau et al. (1978) published a VOR model with a linear interaction between the vestibular and the visual component. With this simple model, they simulated the behavior of the VOR in the dark, in the light, with a head-fixed target and with a target oscillation added to the chair oscillations. Unfortunately, the model of Lau et al. (1978) was built to reproduce all the experimental conditions for a single oscillation frequency of 0.05 [Hz]. Two years later, Schmid et al. (1980) updated the model of Lau et al. (1978) and integrated non-linear elements to represent better the behavior of the visual-vestibular interaction on a larger range of target velocity. A decade later, Barnes (1993) proposed a model that includes three loops to model the visual modulation during pursuit and the non-visual modulation of the VOR. In this model, a central control triggers either an enhancement or a decrease of the VOR response to model a volitional control of the VOR.

Pursuit and VOR: section summary

Pursuit

- Slow movement of the visual axis to track a moving target.
- Main goal: cancel any gaze-target velocity mismatch.
- Two levels of neural control:
  - Cortical level: analysis and selection of visual targets.
  - Sub-cortical level: control of eye and head trajectories.

[83] Schmid et al. (1971) fitted a transfer function with six poles and a null zero!

[84] Between the VIII nerve at the output of the semicircular canals and the inputs of the ocular motor nuclei (III and VI, see Fig. I-9).

Pursuit and VOR: section summary (cont.)

VOR

- Stabilization mechanism of the visual axis.
- Main goal: compensate for head perturbing movements through a counter-rotation of the eye in the orbit.
- Two mechanisms are used to avoid inefficient compensations:
  - Suppression: modulation of the output gain of the VOR.
  - Cancellation: addition of a signal opposite to the VOR to the VOR signal.

5 Neural control of eye movement: independent systems or global mechanism

5.1 Saccade-pursuit interactions

If initially researchers studied the pursuit and the saccadic system separately, a large amount of evidence started to demonstrate a connection between the different mechanisms that drive eye movements in everyday life. Section 4.3 gives evidence that oppositely to the first beliefs, imposing a position error (through stabilization of the target on the fovea) also modified the pursuit behavior (Pola and Wyatt, 1980; Morris and Lisberger, 1987). Therefore, a velocity error is not essential to maintain pursuit, even if a motion (or the illusion/perception of a motion (Steinbach, 1976; Braun et al., 2006)) is necessary to initiate smooth eye movements (Morris and Lisberger, 1987). Additionally, Blohm et al. (2005a) used a protocol in which a target was flashed while human subjects pursued another target. Through the analysis of the normal component of the ongoing pursuit trajectory, Blohm et al. (2005a) demonstrated that the pursuit movement was modulated by the position error of the flash[85].

In parallel to the studies that demonstrated a position error input to the pursuit system, several experiments showed that the saccadic system uses velocity error in addition to the position error to trigger and control saccade amplitude. For example, when a saccade is triggered during an ongoing pursuit movement to cancel a position error (catch-up saccades), the amplitude of the saccade must account for the displacement of the target during the latency period linked to programming and the execution of the saccade to ensure the movement accuracy.

The first evidence for an interaction between the pursuit and the saccadic systems during catch-up saccades came from studies with lesions. When areas that were initially thought to be pursuit-only were lesioned; authors found

[85] An additional smooth movement occurred perpendicularly to the ongoing target trajectory 85 [ms] after the flash presentation before the execution of a saccade toward the remembered position of the flash. The velocity of this movement was proportional to the amplitude of the position error

a modification of the catch-up saccades' amplitude, leading to inaccuracy of the compensatory movement. Lesions of MT (Newsome et al., 1985) or MST (Dürsteler and Wurtz, 1988) were reported to change the accuracy of catch-up saccades. Later, Groh et al. (1997) reported that the amplitude of the saccades was modified when MT was stimulated during saccades between stationary targets. Consequently, it is plausible that MT/MST gives velocity information to the saccadic system. As explained in section 4.7.3, FEF appears to be divided in a saccadic (FEF_{sacc}) and a smooth eye movement (FEF_{sem}) region (Tian and Lynch, 1996a). Those two regions were reported to be interconnected (Tian and Lynch, 1996b), allowing velocity and position information to be shared by both the saccadic and the pursuit systems. Additionally, FEF lesions affect the accuracy of catch-up saccades (Keating, 1991). Finally, May et al. (1988) reported that following lesions of the DLPN, saccades between fixed targets were accurate while catch-up saccades were hypometric, showing the effect of the velocity on saccadic movements.

de Brouwer et al. (2001, 2002b) were the first to quantify the importance of the retinal slip during the programing and the execution of head-restrained catch-up saccades. The authors showed that the amplitude of catch-up saccades can be explained by the sum of two terms. One term is correlated with the position error and the second term is proportional to target velocity[86]. de Brouwer et al. (2002b) proposed to separate the velocity input (from the pursuit system) and the position input (from the saccadic system) to correct the amplitude of the catch-up saccades. To correct the amplitude of a saccade, de Brouwer et al. (2002b) removed a term equal to the product between the duration of the saccade and the mean smooth pursuit velocity during the saccade[87]. With this procedure, the authors showed that the amplitude-corrected saccades were closer to the main sequence defined for saccades between stationary targets (de Brouwer et al., 2002b).

At a first glance, when one looks at a pursuit trial, it could seem that catch-up saccades are triggered "randomly". If the position error seems to be a key parameters to determine when a catch-up saccade will be triggered, saccades are also triggered with small position errors (less than 1 [deg], see Fig. 2A in (de Brouwer et al., 2002a)). de Brouwer et al. (2002a) proposed a rule to evaluate the instant when a catch-up saccade will be triggered. The authors demonstrated that the saccadic system predicts the time at which the eye trajectory will cross the target trajectory (called *eye crossing time* = ratio between the position error and the retinal slip). If the eye crossing time is comprised between 40 [ms] and 180 [ms], no saccade is triggered (smooth zone) (de Brouwer et al., 2002a). If the eye trajectory would cross the target too quickly (eye crossing time $<$ 40 [ms]) or not fast enough (eye crossing time $>$ 180 [ms]), the saccadic system triggers a saccade after approximately 125 [ms] (de Brouwer et al., 2002a).

[86] Built from an efference copy of the eye velocity and the retinal slip.
[87] Defined as the mean between the velocities at onset and offset of the saccade.

5.2 Spatial constancy

As mentioned in the general introduction (see chapter 1), human beings and non-human primates have a perception of their body position in their surrounding environment. The accuracy of this spatial perception is linked to their capacity to take into account self-motion in the planning of task-related movements. Therefore, to trigger a saccade to a remembered position of a target, there must be some internal memory that is updated according to the generated movements.

Initially, spatial constancy has been studied for saccadic eye movements in head-restrained condition. To test the visual input during saccades, Hallett and Lightstone (1976b) presented a target that stepped after a random time. At the initiation of the saccade, the protocol of Hallett and Lightstone (1976b) generated a second position step of the target which extinguished 300 [ms] later. Hallett and Lightstone (1976b) demonstrated that subjects can generate corrective saccades toward the remembered position of the target (the target was no more visible when the subject triggered the corrective saccade). In a second paper, Hallett and Lightstone (1976a) demonstrated that subjects were also able to redirect their visual axis to a second flashed target just before the execution of a first saccade. The protocol designed by Hallett and Lightstone (1976b,a) is now known as the double-step saccade paradigm. The results of Hallett and Lightstone (1976b,a) imply that subjects can build an internal representation of the second target spatial position and correct the initial retinal error (before the onset of the first saccade) with an efference copy of their own saccadic movement.

The update of the internal representation of the spatial environment has also been studied for intervening pursuit movements. McKenzie and Lisberger (1986) were the first to test how spatial constancy was modulated when a target was flashed during an ongoing pursuit movement. Flashed targets were used to cancel any self-movement velocity information and ensured that only the target position on the retina had to be updated. McKenzie and Lisberger (1986) reported that monkeys were unable to correct the target position and triggered saccades based on the retinal error. Those results were later challenged by Schlag et al. (1990). The authors varied the parameters of the protocol (pursuit target velocity, flash duration, etc.) and showed that the monkeys were able, at least partially, to update the retinal position of the flashed target. Later, Blohm et al. (2003b,a, 2005b) used a 2-D updated version of the protocol used in (McKenzie and Lisberger, 1986; Schlag et al., 1990). They showed that an ongoing pursuit movement is taken into account to compensate the retinal position error if the saccadic system is given sufficient time. It appears from the studies of Blohm et al. (2003b,a, 2005b) that the latency, not the number of saccades, is the key factor that determines saccade accuracy: the longer the latency, the better the update of target position.

All the preceding studies were carried out in head-restrained condition (McKenzie and Lisberger, 1986; Schlag et al., 1990; Blohm et al., 2003b,a, 2005b). The only exception is a study by Herter and Guitton (1998). In this head-unrestrained study, the authors flashed a target while subjects looked at the fixation target. Then the fixed target started to move, and as soon as it ex-

tinguished, subjects were asked to look at the remembered position of a flashed target. Herter and Guitton (1998) demonstrated that subjects could update the position of the flash with the head either fixed or free to move.

Global vision mechanism: section summary

- There are interactions between the saccadic and the pursuit system:
  - Saccades integrate the target velocity to correct their amplitude.
  - Pursuit velocity is modulated by the position error of the target on the fovea.
- With the head fixed, the central nervous system can account for self-generated movements during the programming of a saccadic movement.

References

Adams, R. (1834). An account of a peculiar optical phenomenon seen after having looked at a moving body, etc. *London and Edinb. Phil. Mag. J. Science*, 5:373–374.

Albright, T. D. (1984). Direction and orientation selectivity of neurons in visual area MT of the macaque. *J Neurophysiol*, 52(6):1106–1130.

Albright, T. D., Desimone, R., and Gross, C. G. (1984). Columnar organization of directionally selective cells in visual area mt of the macaque. *J Neurophysiol*, 51(1):16–31.

Alstermark, B., Pinter, M. J., and Sasaki, S. (1985). Pyramidal effects in dorsal neck motoneurones of the cat. *J Physiol*, 363:287–302.

Alstermark, B., Pinter, M. J., and Sasaki, S. (1992a). Descending pathways mediating disynaptic excitation of dorsal neck motoneurones in the cat: brain stem relay. *Neurosci Res*, 15(1-2):42–57.

Alstermark, B., Pinter, M. J., and Sasaki, S. (1992b). Descending pathways mediating disynaptic excitation of dorsal neck motoneurones in the cat: facilitatory interactions. *Neurosci Res*, 15(1-2):32–41.

Alstermark, B., Pinter, M. J., and Sasaki, S. (1992c). Tectal and tegmental excitation in dorsal neck motoneurones of the cat. *J Physiol*, 454:517–532.

Anderson, M. E., Yoshida, M., and Wilson, V. J. (1971). Influence of superior colliculus on cat neck motoneurons. *J Neurophysiol*, 34(5):898–907.

Angelaki, D. E. and Cullen, K. E. (2008). Vestibular system: the many facets of a multimodal sense. *Annu Rev Neurosci*, 31:125–150.

Apter, J. T. (1945). Projections of the retina on superior colliculus of cats. *J Neurophysiol*, 8(2):123–134.

Asanuma, C., Thach, W. T., and Jones, E. G. (1983). Brainstem and spinal projections of the deep cerebellar nuclei in the monkey, with observations on the brainstem projections of the dorsal column nuclei. *Brain Res*, 286(3):299–322.

Bahill, A., Clark, M., and Stark, L. (1975). The main sequence, a tool for studying human eye movement. *Mathematical biosciences*, 24:191–204.

Bahill, A. T. and McDonald, J. D. (1983). Model emulates human smooth pursuit system producing zero-latency target tracking. *Biol Cybern*, 48(3):213–222.

Barash, S., Melikyan, A., Sivakov, A., Zhang, M., Glickstein, M., and Thier, P. (1999). Saccadic dysmetria and adaptation after lesions of the cerebellar cortex. *J Neurosci*, 19(24):10931–10939.

Barnes, G., Goodbody, S., and Collins, S. (1995). Volitional control of anticipatory ocular pursuit responses under stabilised image conditions in humans. *Exp Brain Res*, 106(2):301–317.

Barnes, G. R. (1993). Visual-vestibular interaction in the control of head and eye movement: the role of visual feedback and predictive mechanisms. *Prog Neurobiol*, 41(4):435–472.

Barnes, G. R. and Asselman, P. T. (1991). The mechanism of prediction in human smooth pursuit eye movements. *J Physiol (Lond)*, 439:439–61.

Barnes, G. R., Benson, A. J., and Prior, A. R. (1978). Visual-vestibular interaction in the control of eye movement. *Aviat Space Environ Med*, 49(4):557–564.

Barnes, G. R. and Forbat, L. N. (1979). Cervical and vestibular afferent control of oculomotor response in man. *Acta Otolaryngol*, 88(1-2):79–87.

Barnes, G. R. and Lawson, J. F. (1989). Head-free pursuit in the human of a visual target moving in a pseudo-random manner. *J Physiol*, 410:137–155.

Barr, C. C., Schultheis, L. W., and Robinson, D. A. (1976). Voluntary, non-visual control of the human vestibulo-ocular reflex. *Acta Otolaryngol*, 81(5-6):365–375.

Bartl, K., Schneider, E., and Glasauer, S. (2005). Dependence of the torsional vestibulo-ocular reflex on the direction of gravity. *Ann N Y Acad Sci*, 1039:455–458.

Baylor, D. A., Hodgkin, A. L., and Lamb, T. D. (1974). The electrical response of turtle cones to flashes and steps of light. *J Physiol*, 242(3):685–727.

Becker, W. and Fuchs, A. F. (1969). Further properties of the human saccadic system: eye movements and correction saccades with and without visual fixation points. *Vision Res*, 9(10):1247–1258.

Becker, W. and Fuchs, A. F. (1985). Prediction in the oculomotor system: smooth pursuit during transient disappearance of a visual target. *Exp Brain Res*, 57(3):562–575.

Bizzi, E., Kalil, R., and Tagliasco, V. (1971). Eye-head coordination in monkeys : Evidence for centrally patterned organization. *Science*, 173:452–454.

Blatt, G. J., Andersen, R. A., and Stoner, G. R. (1990). Visual receptive field organization and cortico-cortical connections of the lateral intraparietal area (area lip) in the macaque. *J Comp Neurol*, 299(4):421–445.

Blohm, G., Missal, M., and Lefèvre, P. (2003a). Interaction between smooth anticipation and saccades during ocular orientation in darkness. *J Neurophysiol*, 89(3):1423–1433.

Blohm, G., Missal, M., and Lefèvre, P. (2003b). Smooth anticipatory eye movements alter the memorized position of flashed targets. *J Vis*, 3(11):761–770.

Blohm, G., Missal, M., and Lefèvre, P. (2005a). Direct evidence for a position input to the smooth pursuit system. *J Neurophysiol*, 94(1):712–721.

Blohm, G., Missal, M., and Lefèvre, P. (2005b). Processing of retinal and extraretinal signals for memory-guided saccades during smooth pursuit. *J Neurophysiol*, 93(3):1510–1522.

Blouin, J., Gauthier, G. M., van Donkelaar, P., and Vercher, J. L. (1995). Encoding the position of a flashed visual target after passive body rotations. *Neuroreport*, 6(8):1165–1168.

Blouin, J., Labrousse, L., Simoneau, M., Vercher, J. L., and Gauthier, G. M. (1998). Updating visual space during passive and voluntary head-in-space movements. *Exp Brain Res*, 122(1):93–100.

Bockisch, C. J., Straumann, D., and Haslwanter, T. (2005). Human 3-d avor with and without otolith stimulation. *Exp Brain Res*, 161(3):358–367.

Boman, D. K. and Hotson, J. R. (1988). Stimulus conditions that enhance anticipatory slow eye movements. *Vision Res*, 28(10):1157–1165.

Braddick, O. J., O'Brien, J. M., Wattam-Bell, J., Atkinson, J., Hartley, T., and Turner, R. (2001). Brain areas sensitive to coherent visual motion. *Perception*, 30(1):61–72.

Braun, D. I., Pracejus, L., and Gegenfurtner, K. R. (2006). Motion aftereffect elicits smooth pursuit eye movements. *J Vis*, 6(7):671–684.

Bremmer, F., Distler, C., and Hoffmann, K. P. (1997). Eye position effects in monkey cortex. ii. pursuit- and fixation-related activity in posterior parietal areas lip and 7a. *J Neurophysiol*, 77(2):962–977.

Bruce, C. J. and Goldberg, M. E. (1985). Primate frontal eye fields. i. single neurons discharging before saccades. *J Neurophysiol*, 53(3):603–635.

Bruce, C. J., Goldberg, M. E., Bushnell, M. C., and Stanton, G. B. (1985). Primate frontal eye fields. ii. physiological and anatomical correlates of electrically evoked eye movements. *J Neurophysiol*, 54(3):714–734.

Bullier, J. and Kennedy, H. (1983). Projection of the lateral geniculate nucleus onto cortical area v2 in the macaque monkey. *Exp Brain Res*, 53(1):168–172.

Büttner, U., Büttner-Ennever, J. A., and Henn, V. (1977). Vertical eye movement related unit activity in the rostral mesencephalic reticular formation of the alert monkey. *Brain Res*, 130(2):239–252.

Campbell, F. W. and Wurtz, R. H. (1978). Saccadic omission: why we do not see a grey-out during a saccadic eye movement. *Vision Res*, 18(10):1297–1303.

Choi, W. Y. and Guitton, D. (2006). Responses of collicular fixation neurons to gaze shift perturbations in head-unrestrained monkey reveal gaze feedback control. *Neuron*, 50(3):491–505.

Choi, W. Y. and Guitton, D. (2009). Firing patterns in superior colliculus of head-unrestrained monkey during normal and perturbed gaze saccades reveal short-latency feedback and a sluggish rostral shift in activity. *J Neurosci*, 29(22):7166–7180.

Cohen, B. and Feldman, M. (1968). Relationship of electrical activity in pontine reticular formation and lateral geniculate body to rapid eye movements. *J Neurophysiol*, 31(6):806–817.

Colby, C. L., Duhamel, J. R., and Goldberg, M. E. (1993). Ventral intraparietal area of the macaque: anatomic location and visual response properties. *J Neurophysiol*, 69(3):902–914.

Cromer, J. A. and Waitzman, D. M. (2006). Neurones associated with saccade metrics in the monkey central mesencephalic reticular formation. *J Physiol*, 570(Pt 3):507–523.
Cullen, K. E., Galiana, H. L., and Sylvestre, P. A. (2000). Comparing extraocular motoneuron discharges during head-restrained saccades and head-unrestrained gaze shifts. *J Neurophysiol*, 83(1):630–637.
Cullen, K. E. and Guitton, D. (1997a). Analysis of primate ibn spike trains using system identification techniques. i. relationship to eye movement dynamics during head-fixed saccades. *J Neurophysiol*, 78(6):3259–3282.
Cullen, K. E. and Guitton, D. (1997b). Analysis of primate ibn spike trains using system identification techniques. ii. relationship to gaze, eye, and head movement dynamics during head-free gaze shifts. *J Neurophysiol*, 78(6):3283–3306.
Cullen, K. E. and Guitton, D. (1997c). Analysis of primate ibn spike trains using system identification techniques. iii. relationship to motor error during head-fixed saccades and head-free gaze shifts. *J Neurophysiol*, 78(6):3307–3322.
Cullen, K. E., Guitton, D., Rey, C. G., and Jiang, W. (1993). Gaze-related activity of putative inhibitory burst neurons in the head-free cat. *J Neurophysiol*, 70(6):2678–2683.
Cullen, K. E., Huterer, M., Braidwood, D. A., and Sylvestre, P. A. (2004). Time course of vestibuloocular reflex suppression during gaze shifts. *J Neurophysiol*, 92(6):3408–3422.
Cullen, K. E. and Minor, L. B. (2002). Semicircular canal afferents similarly encode active and passive head-on-body rotations: implications for the role of vestibular efference. *J Neurosci*, 22(11):RC226.
Cumming, B. G. (2002). An unexpected specialization for horizontal disparity in primate primary visual cortex. *Nature*, 418(6898):633–636.
Dallos, P. and Jones, R. W. (1963). Learning behavior of the eye fixation control system. *IEEE Transactions on automatic control*, 8(3):218–227.
de Brouwer, S., Demet, Y., Blohm, G., Missal, M., and Lefèvre, P. (2002a). What triggers catch-up saccades during visual tracking ? *Journal of Neurophysiology*, 87:1646–1650.
de Brouwer, S., Missal, M., Barnes, G., and Lefèvre, P. (2002b). Quantative analysis of catch-up saccades during sustained pursuit. *Journal of Neurophysiology*, 87:1772–1780.
de Brouwer, S., Missal, M., and Lefèvre, P. (2001). Role of retinal slip in the prediction of target motion during smooth and saccadic pursuit. *J Neurophysiol*, 86(2):550–558.
Delgado-Garca, J. M., Vidal, P. P., Gmez, C., and Berthoz, A. (1988). Vertical eye movements related signals in antidromically identified medullary reticular formation neurons in the alert cat. *Exp Brain Res*, 70(3):585–589.
Diamond, M. R., Ross, J., and Morrone, M. C. (2000). Extraretinal control of saccadic suppression. *J Neurosci*, 20(9):3449–3455.
Dodge, R. (1903). Five types of eye movement in the horizontal meridian plane of the field of vision. *Am J. Physiol.*, 8:307–329.

Dubrovski, A. and Cullen, K. (2002). Gaze-, eye-, and head-movement dynamics during closed- and open-loop gaze pursuit. *Journal Of Neurophysiology*, 87:859–875.

Dum, R. P. and Strick, P. L. (1996). Spinal cord terminations of the medial wall motor areas in macaque monkeys. *J Neurosci*, 16(20):6513–6525.

Dürsteler, M. R. and Wurtz, R. H. (1988). Pursuit and optokinetic deficits following chemical lesions of cortical areas mt and mst. *J Neurophysiol*, 60(3):940–965.

Eccles, J. C., Nicoll, R. A., Schwarz, W. F., Tborikov, H., and Willey, T. J. (1975). Reticulospinal neurons with and without monosynaptic inputs from cerebellar nuclei. *J Neurophysiol*, 38(3):513–530.

Fernandez, C. and Goldberg, J. M. (1971). Physiology of peripheral neurons innervating semicircular canals of the squirrel monkey. ii. response to sinusoidal stimulation and dynamics of peripheral vestibular system. *J Neurophysiol*, 34(4):661–675.

Fernndez, C. and Goldberg, J. M. (1976a). Physiology of peripheral neurons innervating otolith organs of the squirrel monkey. i. response to static tilts and to long-duration centrifugal force. *J Neurophysiol*, 39(5):970–984.

Fernndez, C. and Goldberg, J. M. (1976b). Physiology of peripheral neurons innervating otolith organs of the squirrel monkey. ii. directional selectivity and force-response relations. *J Neurophysiol*, 39(5):985–995.

Freedman, E. G. (2001). Interactions between eye and head control signals can account for movement kinematics. *Biol Cybern*, 84(6):453–462.

Freedman, E. G. (2008). Coordination of the eyes and head during visual orienting. *Exp Brain Res*, 190(4):369–387.

Freedman, E. G. and Sparks, D. L. (1997). Eye-head coordination during head-unrestrained gaze shifts in rhesus monkeys. *J Neurophysiol*, 77(5):2328–2348.

Freedman, E. G., Stanford, T. R., and Sparks, D. L. (1996). Combined eye-head gaze shifts produced by electrical stimulation of the superior colliculus in rhesus monkeys. *J Neurophysiol*, 76(2):927–952.

Fries, W. (1981). The projection from the lateral geniculate nucleus to the prestriate cortex of the macaque monkey. *Proc R Soc Lond B Biol Sci*, 213(1190):73–86.

Fuchs, A. F., Kaneko, C. R., and Scudder, C. A. (1985). Brainstem control of saccadic eye movements. *Annu Rev Neurosci*, 8:307–337.

Fuchs, A. F., Robinson, F. R., and Straube, A. (1993). Role of the caudal fastigial nucleus in saccade generation. i. neuronal discharge pattern. *J Neurophysiol*, 70(5):1723–1740.

Fukushima, K., Sato, T., Fukushima, J., Shinmei, Y., and Kaneko, C. R. (2000). Activity of smooth pursuit-related neurons in the monkey periarcuate cortex during pursuit and passive whole-body rotation. *J Neurophysiol*, 83(1):563–587.

Fukushima, K., van der Hoeff-van Halen, R., and Peterson, B. W. (1978). Direct excitation of neck motoneurons by interstitiospinal fibers. *Exp Brain Res*, 33(3-4):565–581.

Fuller, J. H. (1992). Head movement propensity. *Exp Brain Res*, 92(1):152–164.

Galiana, H. and Guitton, D. (1992). Central organisation and modeling of eye-head coordination during orienting gaze shifts. *Annals of the New York Academy of Sciences*, 656:452–471.

Galiana, H. L. and Outerbridge, J. S. (1984). A bilateral model for central neural pathways in vestibuloocular reflex. *J Neurophysiol*, 51(2):210–241.

Gandhi, N. J., Barton, E. J., and Sparks, D. L. (2008). Coordination of eye and head components of movements evoked by stimulation of the paramedian pontine reticular formation. *Exp Brain Res*, 189(1):35–47.

Gandhi, N. J. and Sparks, D. L. (2007). Dissociation of eye and head components of gaze shifts by stimulation of the omnipause neuron region. *J Neurophysiol*, 98(1):360–373.

Gattass, R. and Gross, C. G. (1981). Visual topography of striate projection zone (mt) in posterior superior temporal sulcus of the macaque. *J Neurophysiol*, 46(3):621–638.

Gayer, N. S. and Faull, R. L. (1988). Connections of the paraflocculus of the cerebellum with the superior colliculus in the rat brain. *Brain Res*, 449(1-2):253–270.

Gnadt, J. W. and Andersen, R. A. (1988). Memory related motor planning activity in posterior parietal cortex of macaque. *Exp Brain Res*, 70(1):216–220.

Goffart, L., Guillaume, A., and Pélisson, D. (1998a). Compensation for gaze perturbation during inactivation of the caudal fastigial nucleus in the head-unrestrained cat. *J Neurophysiol*, 80(3):1552–1557.

Goffart, L. and Pélisson, D. (1998). Orienting gaze shifts during muscimol inactivation of caudal fastigial nucleus in the cat. 1. gaze dysmetria. *J Neurophysiol*, 79(4):1942–1958.

Goffart, L., Pélisson, D., and Guillaume, A. (1998b). Orienting gaze shifts during muscimol inactivation of caudal fastigial nucleus in the cat. ii. dynamics and eye-head coupling. *J Neurophysiol*, 79(4):1959–1976.

Goldberg, J. M. and Fernandez, C. (1971). Physiology of peripheral neurons innervating semicircular canals of the squirrel monkey. i. resting discharge and response to constant angular accelerations. *J Neurophysiol*, 34(4):635–660.

Goldberg, M. E. and Wurtz, R. H. (1972a). Activity of superior colliculus in behaving monkey. I. visual receptive fields of single neurons. *J Neurophysiol*, 35(4):542–559.

Goldberg, M. E. and Wurtz, R. H. (1972b). Activity of superior colliculus in behaving monkey. II. effect of attention on neuronal responses. *J Neurophysiol*, 35(4):560–574.

Gollisch, T. and Meister, M. (2010). Eye smarter than scientists believed: Neural computations in circuits of the retina. *Neuron*, 65(2):150–164.

Gonzalo-Ruiz, A. and Leichnetz, G. R. (1987). Collateralization of cerebellar efferent projections to the paraoculomotor region, superior colliculus, and medial pontine reticular formation in the rat: a fluorescent double-labeling study. *Exp Brain Res*, 68(2):365–378.

Goossens, H. and Van Opstal, A. (1997). Human eye-head coordination in two dimensions under different sensorimotor conditions. *Experimental Brain Research*, 114:542–560.

Gottlieb, J. P., Bruce, C. J., and MacAvoy, M. G. (1993). Smooth eye movements elicited by microstimulation in the primate frontal eye field. *J Neurophysiol*, 69(3):786–799.

Graf, W. M. and Ugolini, G. (2006). The central mesencephalic reticular formation: its role in space-time coordinated saccadic eye movements. *J Physiol*, 570(Pt 3):433–434.

Grantyn, A., Berthoz, A., Hardy, O., and Gourdon, A. (1992). Contribution of reticulospinal neurons to the dynamic control of head movements: presumed neck bursters. *The Head-Neck Sensory-Motor System*, pages 318–329.

Grantyn, R., Baker, R., and Grantyn, A. (1980). Morphological and physiological identification of excitatory pontine reticular neurons projecting to the cat abducens nucleus and spinal cord. *Brain Res*, 198(1):221–228.

Green, A. M. and Angelaki, D. E. (2004). An integrative neural network for detecting inertial motion and head orientation. *J Neurophysiol*, 92(2):905–925.

Gresty, M. and Leech, J. (1977). Coordination of the head and eyes in pursuit of predictable and random target motion. *Aviat Space Environ Med*, 48(8):741–744.

Groh, J. M., Born, R. T., and Newsome, W. T. (1997). How is a sensory map read out? effects of microstimulation in visual area mt on saccades and smooth pursuit eye movements. *J Neurosci*, 17(11):4312–4330.

Guitton, D., Crommelinck, M., and Roucoux, A. (1980). Stimulation of the superior colliculus in the alert cat. I. eye movements and neck emg activity evoked when the head is restrained. *Exp Brain Res*, 39(1):63–73.

Guitton, D., Douglas, R. M., and Volle, M. (1984). Eye-head coordination in cats. *J Neurophysiol*, 52(6):1030–1050.

Guitton, D. and Mandl, G. (1978a). Frontal 'oculomotor" area in alert cat. i. eye movements and neck activity evoked by stimulation. *Brain Res*, 149(2):295–312.

Guitton, D. and Mandl, G. (1978b). Frontal 'oculomotor' area in alert cat. ii. unit discharges associated with eye movements and neck muscle activity. *Brain Res*, 149(2):313–327.

Guitton, D., Munoz, D., and H.L., G. (1990). Gaze control in the cats: Studies and modeling of the coupling between orienting eye and head movements in different behavioral tasks. *J Neurophysiol*, 64(2):509–531.

Guitton, D. and Volle, M. (1987). Gaze control in humans: eye-head coordination during orienting movements to targets within and beyond the oculomotor range. *J Neurophysiol*, 58(3):427–459.

Hafed, Z. M., Goffart, L., and Krauzlis, R. J. (2009). A neural mechanism for microsaccade generation in the primate superior colliculus. *Science*, 323(5916):940–943.

Hallett, P. E. and Lightstone, A. D. (1976a). Saccadic eye movements to flashed targets. *Vision Res*, 16(1):107–114.

Hallett, P. E. and Lightstone, A. D. (1976b). Saccadic eye movements towards stimuli triggered by prior saccades. *Vision Res*, 16(1):99–106.

Han, Y. H., Kumar, A. N., Reschke, M. F., Somers, J. T., Dell'Osso, L. F., and Leigh, R. J. (2005). Vestibular and non-vestibular contributions to eye movements that compensate for head rotations during viewing of near targets. *Exp Brain Res*, 165(3):294–304.

He, S. Q., Dum, R. P., and Strick, P. L. (1993). Topographic organization of corticospinal projections from the frontal lobe: motor areas on the lateral surface of the hemisphere. *J Neurosci*, 13(3):952–980.

He, S. Q., Dum, R. P., and Strick, P. L. (1995). Topographic organization of corticospinal projections from the frontal lobe: motor areas on the medial surface of the hemisphere. *J Neurosci*, 15(5 Pt 1):3284–3306.

Heinen, S. J. (1995). Single neuron activity in the dorsomedial frontal cortex during smooth pursuit eye movements. *Exp Brain Res*, 104(2):357–361.

Hendrickson, A. E., Wilson, J. R., and Ogren, M. P. (1978). The neuroanatomical organization of pathways between the dorsal lateral geniculate nucleus and visual cortex in old world and new world primates. *J Comp Neurol*, 182(1):123–136.

Herter, T. M. and Guitton, D. (1998). Human head-free gaze saccades to targets flashed before gaze-pursuit are spatially accurate. *J Neurophysiol*, 80(5):2785–2789.

Highstein, S. M. (1973a). The organization of the vestibulo-oculomotor and trochlear reflex pathways in the rabbit. *Exp Brain Res*, 17(3):285–300.

Highstein, S. M. (1973b). Synaptic linkage in the vestibulo-ocular and cerebello-vestibular pathways to the vith nucleus in the rabbit. *Exp Brain Res*, 17(3):301–314.

Hikosaka, O., Igusa, Y., Nakao, S., and Shimazu, H. (1978). Direct inhibitory synaptic linkage of pontomedullary reticular burst neurons with abducens motoneurons in the cat. *Exp Brain Res*, 33(3-4):337–352.

Hikosaka, O., Sakamoto, M., and Usui, S. (1989a). Functional properties of monkey caudate neurons. i. activities related to saccadic eye movements. *J Neurophysiol*, 61(4):780–798.

Hikosaka, O., Sakamoto, M., and Usui, S. (1989b). Functional properties of monkey caudate neurons. ii. visual and auditory responses. *J Neurophysiol*, 61(4):799–813.

Hikosaka, O., Takikawa, Y., and Kawagoe, R. (2000). Role of the basal ganglia in the control of purposive saccadic eye movements. *Physiol Rev*, 80(3):953–978.

Hikosaka, O. and Wurtz, R. H. (1983). Visual and oculomotor functions of monkey substantia nigra pars reticulata. iv. relation of substantia nigra to superior colliculus. *J Neurophysiol*, 49(5):1285–1301.

Hikosaka, O. and Wurtz, R. H. (1985). Modification of saccadic eye movements by gaba-related substances. ii. effects of muscimol in monkey substantia nigra pars reticulata. *J Neurophysiol*, 53(1):292–308.

Holmes, G. (1917). The symptoms of acute cerebellar injuries due to gunshot injuries. *Brain*, 40(4):461–535.

Horn, A. K. E. (2006). The reticular formation. *Prog Brain Res*, 151:127–155.

Horn, A. K. E., Helmchen, C., and Wahle, P. (2003). Gabaergic neurons in the rostral mesencephalon of the macaque monkey that control vertical eye movements. *Ann N Y Acad Sci*, 1004:19–28.

Huaman, A. G. and Sharpe, J. A. (1993). Vertical saccades in senescence. *Invest Ophthalmol Vis Sci*, 34(8):2588–2595.

Hubel, D. H. and Wiesel, T. N. (1969). Anatomical demonstration of columns in the monkey striate cortex. *Nature*, 221(5182):747–750.

Hubel, D. H. and Wiesel, T. N. (1970). Stereoscopic vision in macaque monkey. cells sensitive to binocular depth in area 18 of the macaque monkey cortex. *Nature*, 225(5227):41–42.

Huerta, M. F., Krubitzer, L. A., and Kaas, J. H. (1986). Frontal eye field as defined by intracortical microstimulation in squirrel monkeys, owl monkeys, and macaque monkeys: I. subcortical connections. *J Comp Neurol*, 253(4):415–439.

Isa, T., Itouji, T., Nakao, S., and Sasaki, S. (1988a). Subtypes of neurones in forel's field h as defined by their axonal projection. *Neurosci Lett*, 90(1-2):95–99.

Isa, T., Itouji, T., and Sasaki, S. (1988b). Excitatory pathways from forel's field h to head elevator motoneurones in the cat. *Neurosci Lett*, 90(1-2):89–94.

Isa, T., Itouji, T., and Sasaki, S. (1992). *Control of vertical head movement via Forel's field H*, chapter 52, pages 331–317. Oxford University Press, USA.

Isa, T. and Naito, K. (1994). Activity of neurons in forel's field h during orienting head movements in alert head-free cats. *Exp Brain Res*, 100(2):187–199.

Isa, T. and Naito, K. (1995). Activity of neurons in the medial pontomedullary reticular formation during orienting movements in alert head-free cats. *J Neurophysiol*, 74(1):73–95.

Isa, T. and Sasaki, S. (1988). Effects of lesion of paramedian pontomedullary reticular formation by kainic acid injection on the visually triggered horizontal orienting movements in the cat. *Neurosci Lett*, 87(3):233–239.

Ito, M., Nisimaru, N., and Yamamoto, M. (1973a). The neural pathways relaying reflex inhibition from semicircular canals to extraocular muscles of rabbits. *Brain Res*, 55(1):189–193.

Ito, M., Nisimaru, N., and Yamamoto, M. (1973b). Specific neural connections for the cerebellar control of vestibulo-ocular reflexes. *Brain Res*, 60(1):238–243.

Ito, M., Nisimaru, N., and Yamamoto, M. (1976). Pathways for the vestibulo-ocular reflex excitation arising from semicircular canals of rabbits. *Exp Brain Res*, 24:257–271.

Ito, M., Nisimaru, N., and Yamamoto, M. (1977). Specific patterns of neuronal connexions involved in the control of the rabbit's vestibulo-ocular reflexes by the cerebellar flocculus. *J Physiol*, 265(3):833–854.

Iwamoto, Y. and Sasaki, S. (1990). Monosynaptic excitatory connexions of reticulospinal neurones in the nucleus reticularis pontis caudalis with dorsal neck motoneurones in the cat. *Exp Brain Res*, 80(2):277–289.

Iwamoto, Y., Sasaki, S., and Suzuki, I. (1988). Descending cortical and tectal control of dorsal neck motoneurons via reticulospinal neurons in the cat. *Prog Brain Res*, 76:97–108.

Jayaraman, A., Batton, R. R., and Carpenter, M. B. (1977). Nigrotectal projections in the monkey: an autoradiographic study. *Brain Res*, 135(1):147–152.

Johnston, J. L. and Sharpe, J. A. (1994). The initial vestibulo-ocular reflex and its visual enhancement and cancellation in humans. *Exp Brain Res*, 99(2):302–308.

Jürgens, R., Becker, W., and Kornhuber, H. H. (1981). Natural and drug-induced variations of velocity and duration of human saccadic eye movements: evidence for a control of the neural pulse generator by local feedback. *Biol Cybern*, 39(2):87–96.

Kandel, E. R., Schwartz, J. H., and Jessell, T. M. (2000). *Principles of Neural Science*. McGraw-Hill Medical, 4th edition.

Keating, E. G. (1991). Frontal eye field lesions impair predictive and visually-guided pursuit eye movements. *Exp Brain Res*, 86(2):311–323.

Keller, E. L. (1974). Participation of medial pontine reticular formation in eye movement generation in monkey. *J Neurophysiol*, 37(2):316–332.

Keller, E. L. (1977). *Control of saccadic eye movements by midline brain stem neurons.*, pages 327–336. Elsevier/North-Holland.

Kettner, R. E., Leung, H. C., and Peterson, B. W. (1996). Predictive smooth pursuit of complex two-dimensional trajectories in monkey: component interactions. *Exp Brain Res*, 108(2):221–235.

Kettner, R. E., Mahamud, S., Leung, H. C., Sitkoff, N., Houk, J. C., Peterson, B. W., and Barto, A. G. (1997). Prediction of complex two-dimensional trajectories by a cerebellar model of smooth pursuit eye movement. *J Neurophysiol*, 77(4):2115–2130.

King, W. M. and Fuchs, A. F. (1979). Reticular control of vertical saccadic eye movements by mesencephalic burst neurons. *J Neurophysiol*, 42(3):861–876.

King, W. M., Precht, W., and Dieringer, N. (1980). Afferent and efferent connections of cat omnipause neurons. *Exp Brain Res*, 38(4):395–403.

Koenig, E., Dichgans, J., and Dengler, W. (1986). Fixation suppression of the vestibulo-ocular reflex (vor) during sinusoidal stimulation in humans as related to the performance of the pursuit system. *Acta Otolaryngol*, 102(5-6):423–431.

Komatsu, H. and Wurtz, R. H. (1988). Relation of cortical areas mt and mst to pursuit eye movements. i. localization and visual properties of neurons. *J Neurophysiol*, 60(2):580–603.

Komatsu, H. and Wurtz, R. H. (1989). Modulation of pursuit eye movements by stimulation of cortical areas mt and mst. *J Neurophysiol*, 62(1):31–47.

Kowler, E. and Steinman, R. M. (1979a). The effect of expectations on slow oculomotor control. i. periodic target steps. *Vision Res*, 19(6):619–632.

Kowler, E. and Steinman, R. M. (1979b). The effect of expectations on slow oculomotor control. ii. single target displacements. *Vision Res*, 19(6):633–646.

Koyama, S., Sasaki, Y., Andersen, G. J., Tootell, R. B. H., Matsuura, M., and Watanabe, T. (2005). Separate processing of different global-motion structures in visual cortex is revealed by fmri. *Curr Biol*, 15(22):2027–2032.

Krauzlis, R. J. and Lisberger, S. G. (1994). A model of visually-guided smooth pursuit eye movements based on behavioral observations. *J Comput Neurosci*, 1(4):265–283.

Langer, T. P. and Kaneko, C. R. (1983). Efferent projections of the cat oculomotor reticular omnipause neuron region: an autoradiographic study. *J Comp Neurol*, 217(3):288–306.

Langer, T. P. and Kaneko, C. R. (1984). Brainstem afferents to the omnipause region in the cat: a horseradish peroxidase study. *J Comp Neurol*, 230(3):444–458.

Lanman, J., Bizzi, E., and allum, J. (1978). The coordination of eye and head movement during smooth pursuit. *Progress in Brain Research*, 153:39–53.

Lau, C. G., Honrubia, V., Jenkins, H. A., Baloh, R. W., and Yee, R. D. (1978). Linear model for visual-vestibular interaction. *Aviat Space Environ Med*, 49(7):880–885.

Laurutis, V. P. and Robinson, D. A. (1986). The vestibulo-ocular reflex during human saccadic eye movements. *J Physiol*, 373:209–233.

Lefèvre, P., Bottemanne, I., and Roucoux, A. (1992). Experimental study and modeling of vestibulo-ocular reflex modulation during large shifts of gaze in humans. *Exp Brain Res*, 91(3):496–508.

Lefèvre, P. and Galiana, H. L. (1992). Dynamic feedback to the superior colliculus in a neural network model of the gaze control system. *Neural Netw.*, 5(6):871–890.

Lefèvre, P., Quaia, C., and Optican, L. M. (1998). Distributed model of control of saccades by supperior colliculus and cerebellum. *Neural Networks*, 11:1175–1190.

Leigh, R. J., Maas, E. F., Grossman, G. E., and Robinson, D. A. (1989). Visual cancellation of the torsional vestibulo-ocular reflex in humans. *Exp Brain Res*, 75(2):221–226.

Lennerstrand, G. (1979). Contractile properties of extraocular muscle in siamese cat. *Acta Ophthalmol (Copenh)*, 57(6):1030–1038.

Leung, H. C. and Kettner, R. E. (1997). Predictive smooth pursuit of complex two-dimensional trajectories demonstrated by perturbation responses in monkeys. *Vision Res*, 37(10):1347–1354.

Lisberger, S. G. and Fuchs, A. F. (1978). Role of primate flocculus during rapid behavioral modification of vestibuloocular reflex. i. purkinje cell activity during visually guided horizontal smooth-pursuit eye movements and passive head rotation. *J Neurophysiol*, 41(3):733–763.

Lorente de No, R. (1933). Vestibulo-ocular reflex arc. *Arch Neurol Psychiatry*, 30:245–291.

Luschei, E. S. and Fuchs, A. F. (1972). Activity of brain stem neurons during eye movements of alert monkeys. *J Neurophysiol*, 35(4):445–461.

Maas, E. F., Huebner, W. P., Seidman, S. H., and Leigh, R. J. (1989). Behavior of human horizontal vestibulo-ocular reflex in response to high-acceleration stimuli. *Brain Res*, 499(1):153–156.

Manetto, C. and Lidsky, T. I. (1987). Influences of the basal ganglia on the medullary reticular formation. *Neurosci Lett*, 75(3):278–282.
Martinez-Trujillo, J. C., Klier, E. M., Wang, H., and Crawford, J. D. (2003a). Contribution of head movement to gaze command coding in monkey frontal cortex and superior colliculus. *J Neurophysiol*, 90(4):2770–2776.
Martinez-Trujillo, J. C., Wang, H., and Crawford, J. D. (2003b). Electrical stimulation of the supplementary eye fields in the head-free macaque evokes kinematically normal gaze shifts. *J Neurophysiol*, 89(6):2961–2974.
Maunsell, J. H. and van Essen, D. C. (1983a). The connections of the middle temporal visual area (mt) and their relationship to a cortical hierarchy in the macaque monkey. *J Neurosci*, 3(12):2563–2586.
Maunsell, J. H. and van Essen, D. C. (1983b). Functional properties of neurons in middle temporal visual area of the macaque monkey. i. selectivity for stimulus direction, speed, and orientation. *J Neurophysiol*, 49(5):1127–1147.
May, J. G., Keller, E. L., and Suzuki, D. A. (1988). Smooth-pursuit eye movement deficits with chemical lesions in the dorsolateral pontine nucleus of the monkey. *J Neurophysiol*, 59(3):952–977.
McKenzie, A. and Lisberger, S. G. (1986). Properties of signals that determine the amplitude and direction of saccadic eye movements in monkeys. *J Neurophysiol*, 56(1):196–207.
McLaughlin, S. (1967). Parametric adjustment in saccadic eye movements. *Perception & Psychophysics*, 2:359–362.
Medendorp, W., Vin Gisbergen, J., and Gielen, C. (2002a). Human gaze stabilization during active head translations. *Journal Of Neurophysiology*, 87:295–304.
Medendorp, W. P., Gisbergen, J. A. V., Pelt, S. V., and Gielen, C. C. (2000). Context compensation in the vestibuloocular reflex during active head rotations. *J Neurophysiol*, 84(6):2904–2917.
Medendorp, W. P., Smith, M. A., Tweed, D. B., and Crawford, J. D. (2002b). Rotational remapping in human spatial memory during eye and head motion. *J Neurosci*, 22(1):RC196.
Meyer, C. H., Lasker, A. G., and Robinson, D. A. (1985). The upper limit of human smooth pursuit velocity. *Vision Res*, 25(4):561–563.
Migliaccio, A. A., Santina, C. C. D., Carey, J. P., Minor, L. B., and Zee, D. S. (2006). The effect of binocular eye position and head rotation plane on the human torsional vestibuloocular reflex. *Vision Res*, 46(16):2475–2486.
Minor, L. B., Lasker, D. M., Backous, D. D., and Hullar, T. E. (1999). Horizontal vestibuloocular reflex evoked by high-acceleration rotations in the squirrel monkey. I. Normal responses. *J Neurophysiol*, 82(3):1254–1270.
Missal, M. and Heinen, S. J. (2001). Facilitation of smooth pursuit initiation by electrical stimulation in the supplementary eye fields. *J Neurophysiol*, 86(5):2413–2425.
Mooney, R. D., Nikoletseas, M. M., Hess, P. R., Allen, Z., Lewin, A. C., and Rhoades, R. W. (1988). The projection from the superficial to the deep layers of the superior colliculus: an intracellular horseradish peroxidase injection study in the hamster. *J Neurosci*, 8(4):1384–1399.

Moran, J. and Desimone, R. (1985). Selective attention gates visual processing in the extrastriate cortex. *Science*, 229(4715):782–784.
Morris, E. J. and Lisberger, S. G. (1987). Different responses to small visual errors during initiation and maintenance of smooth-pursuit eye movements in monkeys. *J Neurophysiol*, 58(6):1351–1369.
Moschovakis, A. K., Gregoriou, G. G., and Savaki, H. E. (2001). Functional imaging of the primate superior colliculus during saccades to visual targets. *Nat Neurosci*, 4(10):1026–1031.
Moschovakis, A. K., Scudder, C. A., and Highstein, S. M. (1991a). Structure of the primate oculomotor burst generator. i. medium-lead burst neurons with upward on-directions. *J Neurophysiol*, 65(2):203–217.
Moschovakis, A. K., Scudder, C. A., Highstein, S. M., and Warren, J. D. (1991b). Structure of the primate oculomotor burst generator. ii. medium-lead burst neurons with downward on-directions. *J Neurophysiol*, 65(2):218–229.
Munoz, D. P. and Wurtz, R. H. (1993). Fixation cells in monkey superior colliculus. i. characteristics of cell discharge. *J Neurophysiol*, 70(2):559–575.
Munoz, D. P. and Wurtz, R. H. (1995a). Saccade-related activity in monkey superior colliculus. i. characteristics of burst and buildup cells. *J Neurophysiol*, 73(6):2313–2333.
Munoz, D. P. and Wurtz, R. H. (1995b). Saccade-related activity in monkey superior colliculus. ii. spread of activity during saccades. *J Neurophysiol*, 73(6):2334–2348.
Mustari, M. J., Fuchs, A. F., and Wallman, J. (1988). Response properties of dorsolateral pontine units during smooth pursuit in the rhesus macaque. *J Neurophysiol*, 60(2):664–686.
Nakao, S., Curthoys, I. S., and Markham, C. H. (1980). Direct inhibitory projection of pause neurons to nystagmus-related pontomedullary reticular burst neurons in the cat. *Exp Brain Res*, 40(3):283–293.
Nakao, S., Shiraishi, Y., Li, W. B., and Oikawa, T. (1990). Mono- and disynaptic excitatory inputs from the superior colliculus to vertical saccade-related neurons in the cat forel's field h. *Exp Brain Res*, 82(1):222–226.
Nakao, S., Shiraishi, Y., Oda, H., and Inagaki, M. (1988). Direct inhibitory projection of pontine omnipause neurons to burst neurons in the forel's field h controlling vertical eye movement-related motoneurons in the cat. *Exp Brain Res*, 70(3):632–636.
Newsome, W. T., Wurtz, R. H., Drsteler, M. R., and Mikami, A. (1985). Deficits in visual motion processing following ibotenic acid lesions of the middle temporal visual area of the macaque monkey. *J Neurosci*, 5(3):825–840.
Newsome, W. T., Wurtz, R. H., and Komatsu, H. (1988). Relation of cortical areas mt and mst to pursuit eye movements. ii. differentiation of retinal from extraretinal inputs. *J Neurophysiol*, 60(2):604–620.
Niemi-Junkola, U. J. and Westby, G. W. (2000). Cerebellar output exerts spatially organized influence on neural responses in the rat superior colliculus. *Neuroscience*, 97(3):565–573.
Noda, H., Sugita, S., and Ikeda, Y. (1990). Afferent and efferent connections of the oculomotor region of the fastigial nucleus in the macaque monkey. *J Comp Neurol*, 302(2):330–348.

Noda, H. and Suzuki, D. A. (1979a). Processing of eye movement signals in the flocculus of the monkey. *J Physiol*, 294:349–364.
Noda, H. and Suzuki, D. A. (1979b). The role of the flocculus of the monkey in saccadic eye movements. *J Physiol*, 294:317–334.
Ohgaki, T., Markham, C. H., Schneider, J. S., and Curthoys, I. S. (1989). Anatomical evidence of the projection of pontine omnipause neurons to midbrain regions controlling vertical eye movements. *J Comp Neurol*, 289(4):610–625.
Optican, L. M. and Robinson, D. A. (1980). Cerebellar-dependent adaptive control of primate saccadic system. *J Neurophysiol*, 44(6):1058–1076.
Optican, L. M., Zee, D. S., and Chu, F. C. (1985). Adaptive response to ocular muscle weakness in human pursuit and saccadic eye movements. *J Neurophysiol*, 54(1):110–122.
Paige, G. D., Telford, L., Seidman, S. H., and Barnes, G. R. (1998). Human vestibuloocular reflex and its interactions with vision and fixation distance during linear and angular head movement. *J Neurophysiol*, 80(5):2391–2404.
Paré, M. and Guitton, D. (1998). Brain stem omnipause neurons and the control of combined eye-head gaze saccades in the alert cat. *J Neurophysiol*, 79(6):3060–3076.
Parthasarathy, H. B., Schall, J. D., and Graybiel, A. M. (1992). Distributed but convergent ordering of corticostriatal projections: analysis of the frontal eye field and the supplementary eye field in the macaque monkey. *J Neurosci*, 12(11):4468–4488.
Pathmanathan, J. S., Cromer, J. A., Cullen, K. E., and Waitzman, D. M. (2006a). Temporal characteristics of neurons in the central mesencephalic reticular formation of head unrestrained monkeys. *Exp Brain Res*, 168(4):471–492.
Pathmanathan, J. S., Presnell, R., Cromer, J. A., Cullen, K. E., and Waitzman, D. M. (2006b). Spatial characteristics of neurons in the central mesencephalic reticular formation (cmrf) of head-unrestrained monkeys. *Exp Brain Res*, 168(4):455–470.
Pélisson, D., Goffart, L., and Guillaume, A. (1998). Contribution of the rostral fastigial nucleus to the control of orienting gaze shifts in the head-unrestrained cat. *J Neurophysiol*, 80(3):1180–1196.
Pélisson, D. and Prablanc, C. (1988). Kinematics of centrifugal and centripetal saccadic eye movements in man. *Vision Res*, 28(1):87–94.
Pélisson, D., Prablanc, C., and Urquizar, C. (1988). Vestibuloocular reflex inhibition and gaze saccade control characteristics during eye-head orientation in humans. *J Neurophysiol*, 59(3):997–1013.
Pellionisz, A. (1988). Tensorial aspects of the multidimensional massively parallel sensorimotor function of neuronal networks. *Prog Brain Res*, 76:341–354.
Perry, V. H., Oehler, R., and Cowey, A. (1984). Retinal ganglion cells that project to the dorsal lateral geniculate nucleus in the macaque monkey. *Neuroscience*, 12(4):1101–1123.

Peterson, B. W., Anderson, M. E., and Filion, M. (1974). Responses of pontomedullary reticular neurons to cortical, tectal and cutaneous stimuli. *Exp Brain Res*, 21(1):19–44.

Peterson, B. W., Maunz, R. A., Pitts, N. G., and Mackel, R. G. (1975). Patterns of projection and braching of reticulospinal neurons. *Exp Brain Res*, 23(4):333–351.

Peterson, B. W., Pitts, N. G., Fukushima, K., and Mackel, R. (1978). Reticulospinal excitation and inhibition of neck motoneurons. *Exp Brain Res*, 32(4):471–489.

Pola, J. and Wyatt, H. J. (1980). Target position and velocity: the stimuli for smooth pursuit eye movements. *Vision Res*, 20(6):523–534.

Pulaski, P. D., Zee, D. S., and Robinson, D. A. (1981). The behavior of the vestibulo-ocular reflex at high velocities of head rotation. *Brain Res*, 222(1):159–165.

Quaia, C., Lefèvre, P., and Optican, L. (1999). Model of the control of saccades by superior colliculus and cerebellum. *Journal of Neurophysiology*, 82:999–1018.

Quaia, C., Ying, H. S., Nichols, A. M., and Optican, L. M. (2009a). The viscoelastic properties of passive eye muscle in primates. i: static forces and step responses. *PLoS One*, 4(4):e4850.

Quaia, C., Ying, H. S., and Optican, L. M. (2009b). The viscoelastic properties of passive eye muscle in primates. ii: testing the quasi-linear theory. *PLoS One*, 4(8):e6480.

Quinet, J. and Goffart, L. (2005). Saccade dysmetria in head-unrestrained gaze shifts after muscimol inactivation of the caudal fastigial nucleus in the monkey. *J Neurophysiol*, 93(4):2343–2349.

Quinet, J. and Goffart, L. (2007). Head-unrestrained gaze shifts after muscimol injection in the caudal fastigial nucleus of the monkey. *J Neurophysiol*, 98(6):3269–3283.

Quinet, J. and Goffart, L. (2009). Electrical microstimulation of the fastigial oculomotor region in the head-unrestrained monkey. *J Neurophysiol*, 102(1):320–336.

Ramat, S., Leigh, R. J., Zee, D. S., and Optican, L. M. (2007). What clinical disorders tell us about the neural control of saccadic eye movements. *Brain*, 130(Pt 1):10–35.

Rambold, H., Churchland, A., Selig, Y., Jasmin, L., and Lisberger, S. G. (2002). Partial ablations of the flocculus and ventral paraflocculus in monkeys cause linked deficits in smooth pursuit eye movements and adaptive modification of the vor. *J Neurophysiol*, 87(2):912–924.

Rashbass, C. (1961). The relationship between saccadic and smooth tracking eye movements. *J Physiol (Lond)*, 159:326–338.

Raybourn, M. S. and Keller, E. L. (1977). Colliculoreticular organization in primate oculomotor system. *J Neurophysiol*, 40(4):861–878.

Richmond, F., Vidal, P., and Winters, J. (1988). *Control of Head movement*, chapter The motor system: joints and muscles of the neck, pages 1–21. Oxford university press.

Ritchie, L. (1976). Effects of cerebellar lesions on saccadic eye movements. *J Neurophysiol*, 39(6):1246–1256.
Robinson, D. (1973). Models of the saccadic eye movement control system. *Kybernetik*, 14:71–83.
Robinson, D. (1975). Oculomotor control signals. *Basic mechanisms of ocular motility and their clinical implications*, pages 337–374.
Robinson, D. (1981). Models of the mechanics of eye movements. *Models of oculomotor behavior and control*, pages 21–41.
Robinson, D. A. (1965). The mechanics of human smooth pursuit eye movement. *J Physiol*, 180(3):569–91.
Robinson, D. A. (1972). Eye movements evoked by collicular stimulation in the alert monkey. *Vision Res*, 12(11):1795–1808.
Robinson, D. A. (1976). Adaptive gain control of vestibuloocular reflex by the cerebellum. *J Neurophysiol*, 39(5):954–969.
Robinson, D. A., Gordon, J. L., and Gordon, S. E. (1986). A model of the smooth pursuit eye movement system. *Biol Cybern*, 55(1):43–57.
Robinson, F. R., Phillips, J. O., and Fuchs, A. F. (1994). Coordination of gaze shifts in primates: brainstem inputs to neck and extraocular motoneuron pools. *J Comp Neurol*, 346(1):43–62.
Robinson, F. R., Straube, A., and Fuchs, A. F. (1993). Role of the caudal fastigial nucleus in saccade generation. ii. effects of muscimol inactivation. *J Neurophysiol*, 70(5):1741–1758.
Ron, S. and Robinson, D. A. (1973). Eye movements evoked by cerebellar stimulation in the alert monkey. *J Neurophysiol*, 36(6):1004–1022.
Rottach, K. G., Zivotofsky, A. Z., Das, V. E., Averbuch-Heller, L., Discenna, A. O., Poonyathalang, A., and Leigh, R. J. (1996). Comparison of horizontal, vertical and diagonal smooth pursuit eye movements in normal human subjects. *Vision Res*, 36(14):2189–2195.
Roucoux, A., Guitton, D., and Crommelinck, M. (1980). Stimulation of the superior colliculus in the alert cat. II. eye and head movements evoked when the head is unrestrained. *Exp Brain Res*, 39(1):75–85.
Roy, J. E. and Cullen, K. E. (2002). Vestibuloocular reflex signal modulation during voluntary and passive head movements. *J Neurophysiol*, 87(5):2337–2357.
Roy, J. E. and Cullen, K. E. (2004). Dissociating self-generated from passively applied head motion: neural mechanisms in the vestibular nuclei. *J Neurosci*, 24(9):2102–2111.
Sasaki, S., Isa, T., and Naito, K. (1999). Effects of lesion of pontomedullary reticular formation on visually triggered vertical and oblique head orienting movements in alert cats. *Neurosci Lett*, 265(1):13–16.
Sasaki, S. and Iwamoto, Y. (1999). Axonal trajectories of the nucleus reticularis gigantocellularis neurons in the c2-c3 segments in cats. *Neurosci Lett*, 264(1-3):137–140.
Schall, J. D. (2002). The neural selection and control of saccades by the frontal eye field. *Philos Trans R Soc Lond B Biol Sci*, 357(1424):1073–1082.

Schlack, A., Hoffmann, K.-P., and Bremmer, F. (2003). Selectivity of macaque ventral intraparietal area (area vip) for smooth pursuit eye movements. *J Physiol*, 551(Pt 2):551–561.

Schlag, J. and Schlag-Rey, M. (1985). Unit activity related to spontaneous saccades in frontal dorsomedial cortex of monkey. *Exp Brain Res*, 58(1):208–211.

Schlag, J. and Schlag-Rey, M. (1987). Evidence for a supplementary eye field. *J Neurophysiol*, 57(1):179–200.

Schlag, J., Schlag-Rey, M., and Dassonville, P. (1990). Saccades can be aimed at the spatial location of targets flashed during pursuit. *J Neurophysiol*, 64(2):575–581.

Schmid, R., Buizza, A., and Zambarbieri, D. (1980). A non-linear model for visual-vestibular interaction during body rotation in man. *Biol Cybern*, 36(3):143–151.

Schmid, R., Stefanelli, M., and Mira, E. (1971). Mathematical modelling. a contribution to clinical vestibular analysis. *Acta Otolaryngol*, 72(4):292–302.

Schmid-Priscoveanu, A., Straumann, D., and Kori, A. A. (2000). Torsional vestibulo-ocular reflex during whole-body oscillation in the upright and the supine position. i. responses in healthy human subjects. *Exp Brain Res*, 134(2):212–219.

Schmolesky, M. T., Wang, Y., Hanes, D. P., Thompson, K. G., Leutgeb, S., Schall, J. D., and Leventhal, A. G. (1998). Signal timing across the macaque visual system. *J Neurophysiol*, 79(6):3272–3278.

Schnapf, J. L., Nunn, B. J., Meister, M., and Baylor, D. A. (1990). Visual transduction in cones of the monkey macaca fascicularis. *J Physiol*, 427:681–713.

Scudder, C. A., Moschovakis, A. K., Karabelas, A. B., and Highstein, S. M. (1996). Anatomy and physiology of saccadic long-lead burst neurons recorded in the alert squirrel monkey. i. descending projections from the mesencephalon. *J Neurophysiol*, 76(1):332–352.

Shibutani, H., Sakata, H., and Hyvrinen, J. (1984). Saccade and blinking evoked by microstimulation of the posterior parietal association cortex of the monkey. *Exp Brain Res*, 55(1):1–8.

Shimizu, N., Mizuno, M., Naito, M., and Yoshida, M. (1981a). The interaction between accuracy of gaze with and without head movements in patients with cerebellar ataxia. *Ann N Y Acad Sci*, 374:579–589.

Shimizu, N., Naito, M., and Yoshida, M. (1981b). Eye-head co-ordination in patients with parkinsonism and cerebellar ataxia. *J Neurol Neurosurg Psychiatry*, 44(6):509–515.

Shinoda, Y., Kakei, S., and Muto, N. (1996). Morphology of single axons of tectospinal and reticulospinal neurons in the upper cervical spinal cord. *Prog Brain Res*, 112:71–84.

Shook, B. L., Schlag-Rey, M., and Schlag, J. (1991). Primate supplementary eye field. ii. comparative aspects of connections with the thalamus, corpus striatum, and related forebrain nuclei. *J Comp Neurol*, 307(4):562–583.

Smith, O. J. (1959). A controller to overcome dead time. *ISA J.*, 6(2):28–33.

Snider, R. S. and Stowell, A. (1944). Receiving areas of the tactile, auditory, and visual systems in the cerebellum. *J Neurophysiol*, 7(6):331–357.
Sparks, D. L. and Travis, R. P. (1971). Firing patterns of reticular formation neurons during horizontal eye movements. *Brain Res*, 33(2):477–481.
Stahl, J. (1999). Amplitude of human head movements associated with horizontal saccades. *Experimental Brain Research*, 126:41–54.
Stanton, G. B., Goldberg, M. E., and Bruce, C. J. (1988). Frontal eye field efferents in the macaque monkey: Ii. topography of terminal fields in midbrain and pons. *J Comp Neurol*, 271(4):493–506.
Stark, L., Vossius, G., and Young, L. R. (1962). Predictive control of eye tracking movements. *IRE Transactions on Human Factors in Electronics*, HFE-3(2):52–57.
Steinbach, M. J. (1976). Pursuing the perceptual rather than the retinal stimulus. *Vision Res*, 16(12):1371–1376.
Stone, L. S. and Lisberger, S. G. (1990). Visual responses of purkinje cells in the cerebellar flocculus during smooth-pursuit eye movements in monkeys. i. simple spikes. *J Neurophysiol*, 63(5):1241–1261.
Stryker, M. P. and Schiller, P. H. (1975). Eye and head movements evoked by electrical stimulation of monkey superior colliculus. *Exp Brain Res*, 23(1):103–112.
Suzuki, D. A. and Keller, E. L. (1984). Visual signals in the dorsolateral pontine nucleus of the alert monkey: their relationship to smooth-pursuit eye movements. *Exp Brain Res*, 53(2):473–478.
Suzuki, D. A. and Keller, E. L. (1988a). The role of the posterior vermis of monkey cerebellum in smooth-pursuit eye movement control. i. eye and head movement-related activity. *J Neurophysiol*, 59(1):1–18.
Suzuki, D. A. and Keller, E. L. (1988b). The role of the posterior vermis of monkey cerebellum in smooth-pursuit eye movement control. ii. target velocity-related purkinje cell activity. *J Neurophysiol*, 59(1):19–40.
Suzuki, D. A., Noda, H., and Kase, M. (1981). Visual and pursuit eye movement-related activity in posterior vermis of monkey cerebellum. *J Neurophysiol*, 46(5):1120–1139.
Suzuki, Y., Bttner-Ennever, J. A., Straumann, D., Hepp, K., Hess, B. J., and Henn, V. (1995). Deficits in torsional and vertical rapid eye movements and shift of listing's plane after uni- and bilateral lesions of the rostral interstitial nucleus of the medial longitudinal fasciculus. *Exp Brain Res*, 106(2):215–232.
Szentagothai, J. (1950). The elementary vestibulo-ocular reflex arc. *J Neurophysiol*, 13(6):395–407.
Tabak, S. and Collewijn, H. (1994). Human vestibulo-ocular responses to rapid, helmet-driven head movements. *Exp Brain Res*, 102(2):367–378.
Takagi, M., Zee, D. S., and Tamargo, R. J. (2000). Effects of lesions of the oculomotor cerebellar vermis on eye movements in primate: smooth pursuit. *J Neurophysiol*, 83(4):2047–2062.
Tanaka, M. and Lisberger, S. G. (2002). Enhancement of multiple components of pursuit eye movement by microstimulation in the arcuate frontal pursuit area in monkeys. *J Neurophysiol*, 87(2):802–818.

Thier, P. and Erickson, R. G. (1992). Vestibular input to visual-tracking neurons in area mst of awake rhesus monkeys. *Ann N Y Acad Sci*, 656:960–963.

Thier, P., Koehler, W., and Buettner, U. W. (1988). Neuronal activity in the dorsolateral pontine nucleus of the alert monkey modulated by visual stimuli and eye movements. *Exp Brain Res*, 70(3):496–512.

Thomson, D. B., Loeb, G. E., and Richmond, F. J. (1994). Effect of neck posture on the activation of feline neck muscles during voluntary head turns. *J Neurophysiol*, 72(4):2004–2014.

Thomson, D. B., Loeb, G. E., and Richmond, F. J. (1996). Effect of neck posture on patterns of activation of feline neck muscles during horizontal rotation. *Exp Brain Res*, 110(3):392–400.

Tian, J. R. and Lynch, J. C. (1996a). Corticocortical input to the smooth and saccadic eye movement subregions of the frontal eye field in cebus monkeys. *J Neurophysiol*, 76(4):2754–2771.

Tian, J. R. and Lynch, J. C. (1996b). Functionally defined smooth and saccadic eye movement subregions in the frontal eye field of cebus monkeys. *J Neurophysiol*, 76(4):2740–2753.

Tomlinson, R. D. and Bahra, P. S. (1986). Combined eye-head gaze shifts in the primate. ii. interactions between saccades and the vestibuloocular reflex. *J Neurophysiol*, 56(6):1558–1570.

Tu, T. A. and Keating, E. G. (2000). Electrical stimulation of the frontal eye field in a monkey produces combined eye and head movements. *J Neurophysiol*, 84(2):1103–1106.

Viirre, E., Tweed, D., Milner, K., and Vilis, T. (1986). A reexamination of the gain of the vestibuloocular reflex. *J Neurophysiol*, 56(2):439–450.

Vilis, T., Hepp, K., Schwarz, U., and Henn, V. (1989). On the generation of vertical and torsional rapid eye movements in the monkey. *Exp Brain Res*, 77(1):1–11.

Vilis, T. and Hore, J. (1981). Characteristics of saccadic dysmetria in monkeys during reversible lesions of medial cerebellar nuclei. *J Neurophysiol*, 46(4):828–838.

Waespe, W. and Baumgartner, R. (1992). Enduring dysmetria and impaired gain adaptivity of saccadic eye movements in wallenberg's lateral medullary syndrome. *Brain*, 115 (Pt 4):1123–1146.

Wallace, M. T., Meredith, M. A., and Stein, B. E. (1998). Multisensory integration in the superior colliculus of the alert cat. *J Neurophysiol*, 80(2):1006–1010.

Wellenius, G. A. and Cullen, K. E. (2000). A comparison of head-unrestrained and head-restrained pursuit: influence of eye position and target velocity on latency. *Exp Brain Res*, 133(2):139–155.

Westheimer, G. (1954). Eye movement responses to a horizontally moving visual stimulus. *AMA Arch Ophthalmol*, 52(6):932–941.

Westheimer, G. and Blair, S. M. (1973). Oculomotor defects in cerebellectomized monkeys. *Invest Ophthalmol*, 12(8):618–621.

Whittington, D. A., Lestienne, F., and Bizzi, E. (1984). Behavior of preoculomotor burst neurons during eye-head coordination. *Exp Brain Res*, 55(2):215–222.

Wickelgren, B. G. (1971). Superior colliculus: some receptive field properties of bimodally responsive cells. *Science*, 173(991):69–72.

Wikler, K. C., Williams, R. W., and Rakic, P. (1990). Photoreceptor mosaic: number and distribution of rods and cones in the rhesus monkey retina. *J Comp Neurol*, 297(4):499–508.

Winters, J. (1988). *Control of Head movement*, chapter Biomechanical modeling of the human head and neck, pages 22–36. Oxford university press.

Wurtz, R. H. and Goldberg, M. E. (1971). Superior colliculus cell responses related to eye movements in awake monkeys. *Science*, 171(966):82–84.

Yoshida, M. and Precht, W. (1971). Monosynaptic inhibition of neurons of the substantia nigra by caudato-nigral fibers. *Brain Res*, 32(1):225–228.

Zangemeister, W., Lehman, S., and Stark, L. (1981). Simulation of head movement trajectories: Model to fit the main sequence. *Biological cybernertics*, 41:19–32.

Zee, D. S., Optican, L. M., Cook, J. D., Robinson, D. A., and Engel, W. K. (1976). Slow saccades in spinocerebellar degeneration. *Arch Neurol*, 33(4):243–251.

Zee, D. S., Yamazaki, A., Butler, P. H., and Gcer, G. (1981). Effects of ablation of flocculus and paraflocculus of eye movements in primate. *J Neurophysiol*, 46(4):878–899.

Zeki, S. M. (1978). Functional specialisation in the visual cortex of the rhesus monkey. *Nature*, 274(5670):423–428.

Part II

Behavioral study: Spatial constancy in head-unrestrained condition

J Neurophysiol 103: 543–556, 2010.
First published November 18, 2009; doi:10.1152/jn.00656.2009.

Saccadic Compensation for Smooth Eye and Head Movements During Head-Unrestrained Two-Dimensional Tracking

P. M. Daye,[1,2] G. Blohm,[3] and P. Lefèvre[1,2]
[1]*Center for Systems Engineering and Applied Mechanics, Université catholique de Louvain, Louvain-la-Neuve;* [2]*Laboratory of Neurophysiology, Université catholique de Louvain, Brussels, Belgium; and* [3]*Centre for Neurosciences Studies, Queen's University, Kingston, Ontario, Canada*

Submitted 27 July 2009; accepted in final form 14 November 2009

Summary

Spatial updating is the ability to keep track of the position of world-fixed objects while we move. In the case of vision, this phenomenon is called spatial constancy and has been studied in head-restraint conditions. During head-restrained smooth pursuit, it has been shown that the saccadic system has access to extra-retinal information from the pursuit system to update the objects' position in the surrounding environment. However, during head-unrestrained smooth pursuit, the saccadic system needs to keep track of three different motor commands, i.e. the ocular smooth pursuit command, the vestibulo-ocular reflex (VOR) and the head movement command. The question then arises whether saccades compensate for these movements. To address this question, we briefly presented a target during sinusoidal head-unrestrained smooth pursuit in darkness. Subjects were instructed to look at the flash as soon as they saw it. We observed that subjects were able to orient their gaze to the memorized (and spatially updated) position of the flashed target generally using one to three successive saccades. Similar to the behavior in the head-restrained condition, we found that the longer the gaze saccade latency, the better the compensation for intervening smooth gaze displacements; after $\sim$400[ms], 62% of the smooth gaze displacement had been compensated for. This compensation depended on two independent parameters, the latency of the saccade and the eye contribution to the gaze displacement during this latency period. Separating gaze into eye and head contributions, we show that the larger the eye contribution to the gaze displacement, the better the overall compensation. Finally, we found that the compensation was a function of the head oscillation frequency and we suggest that this relationship is linked to the modulation of VOR gain. We conclude that the general mechanisms of compensation for smooth gaze displacements are similar to the ones observed in the head-restrained condition.

1

Introduction

To experience a stable world in spite of self-motion, we have to take the movements of our eyes and head into account. This is known as spatial constancy and has been extensively investigated during saccadic eye movements (Hallett and Lightstone, 1976b,a), for head-restrained smooth pursuit (Schlag and Schlag-Rey, 2002), and during whole-body rotations (Blouin et al., 1995, 1998; Klier et al., 2005, 2006) and translations (Berthoz et al., 1995; Israël et al., 1997; Klier and Angelaki, 2008). Most of these previous studies have considered how spatial constancy is achieved across movements generated by a single motor system. More recently, the mechanisms involved in maintaining a spatially stable internal representation of the world have been examined during combined saccadic and pursuit eye movements (Blohm et al., 2003, 2005a,b, 2006). However, the latter studies were performed with the head restrained (except for (Herter and Guitton, 1998)). In the present study, we sought to consider the saccadic compensation for smooth eye movements in a more natural behavioral condition where the head was free to move. When the head is restrained, it has been shown that saccades can compensate for smooth pursuit eye movements if the saccadic system is given sufficient time (Blohm et al., 2003, 2005a,b). As a result, short latency saccades typically do not compensate for smooth eye displacements in darkness (Blohm et al., 2005b), while long latency saccades almost fully compensate (Blohm et al., 2005b). For medium latency saccades, there is a partial compensation of the smooth eye displacement. These findings could be explained by a delayed integration of the smooth pursuit command by the saccadic system (Blohm et al., 2003, 2006). Not much is known about this mechanism in head-unrestrained conditions. It has been shown that saccades can compensate for head rotations (Medendorp et al., 2002b,a) while maintaining fixation. Herter and Guitton (1998) have also shown that saccades to targets memorized before visually driven head-unrestrained pursuit are accurate. It remains unknown how spatial constancy is achieved for targets presented during ongoing head-unrestrained smooth pursuit eye movements. This is not a trivial extension of previous work on spatial constancy during smooth pursuit (Blohm et al., 2003, 2005a,b, 2006; Herter and Guitton, 1998; McKenzie and Lisberger, 1986; Schlag et al., 1990) because adding the head motor system also introduces interactions with the vestibulo-ocular reflex (VOR)

(Angelaki and Cullen, 2008; Barnes, 1993). As a consequence, several questions arise. First, it remains unknown to what extent the displacements of the head during the saccadic latency period are taken into account in the compensation for head-unrestrained pursuit. Second, what is the time course of this compensation during head-unrestrained pursuit and which factors might it depend on? Third, what is the influence of the VOR on this process? The VOR acts as a stabilization system for vision during the perturbations induced by head movements. During head-unrestrained eye movements, this is a counterproductive mechanism that needs to be suppressed or cancelled out by an additional ocular-motor command (Barnes, 1993). VOR cancellation is present during eye-head tracking (see for example (Lanman et al., 1978)). Lefèvre et al. (1992) showed that the VOR is suppressed as soon as the gaze saccade starts and that the VOR gain increases progressively before the end of the saccade. Using electrophysiological recordings of the vestibular nuclei, Roy and Cullen (2002, 2004) showed that the firing rate of vestibular nuclei neurons is attenuated when the discharge of neck proprioceptors matches the expected effect of the neck command during active head movements. Therefore we expect a reduction of the apparent VOR gain during head-free smooth pursuit; however, how large this reduction might be and how it might depend on the head movement frequency remains unknown. To investigate how the saccadic system keeps track of head-unrestrained smooth eye displacements in darkness, we designed a head-unrestrained version of our previous two-dimensional tracking experiment (Blohm et al., 2003, 2005b). By briefly presenting a visual target during ongoing eye and head pursuit and asking subjects to orient toward the memorized location of this target, we were able to address how spatial constancy was obtained across movements of both effectors. We here show how the compensation for eye and head movements depends on the relative contribution of the eyes and head to the overall smooth gaze displacement during the saccadic latency period. In addition, we estimate an interval for plausible values of the VOR gain dependence on the head movement frequency during the orientation process in darkness.

2

Methods

Eight human subjects (4 male, 4 female, aged 22-32 years) without any known oculomotor abnormalities participated in this experiment after giving informed consent. Three subjects (EM, LA and GA) were completely na ive to oculomotor research, three subjects (CO, GL and SC) were knowledgeable about general oculomotor studies and two subjects (DP and GB) were knowledgeable about the purpose of the study. All procedures were approved by the Universit catholique de Louvain ethics committee, in compliance with the Declaration of Helsinki.

1 Experimental setup

Subjects sat 1 [m] in front of a translucent tangent screen in a completely dark room. The screen spanned ± 40 [deg] of their horizontal and vertical visual field. A green and a red laser spot (0.2 [deg] diameter) were back-projected onto the screen. Target position was controlled by mirror-galvanometers (GSI Lumonics, Billerica, LA) at 1 [kHz] via an embedded real-time computer (PXI-8186 RT, National Instruments, Austin, Texas) running LabView (National Instruments, Austin, Texas). Horizontal and vertical eye movements were recorded at 200 [Hz] by a Chronos head-mounted video eye-tracker (Chronos Vision GmbH, Berlin, Germany). To keep a good accuracy during the video recording of the eye position, it is important to reduce any relative movement between the position of the eye and the Chronos helmet. To that goal, a bite bar was mounted onto the Chronos frame to prevent any slippage of the helmet during head movements. The subject's head was free to move. Head position was computed from the position of a set of six infrared light-emitting diodes (IREDs) mounted onto the Chronos helmet. IRED position was sampled at 200 [Hz] by two 3D optical infrared cameras (Codamotion system, Charnwood Dynamics, Leicestershire, United Kingdom).

2 Paradigm

A recording session was composed of eight blocks of twenty-five trials. Each trial started with a fixation of a red target at the center of the screen for 500 [ms]. Then the target performed movements along a randomly oriented straight line with a sinusoidal velocity at a random frequency ([0.6...1.2] [Hz]) and random amplitude ([20...25] [deg]) over a random duration ([3000...3750] [ms])[88]. For all randomizations, we sampled in a continuous fashion (uniform distribution) between the specified boundaries. Around the end of the red target motion, a green target was briefly presented (duration: 10 [ms]) and will henceforth be referred to as the "flash". The flashed target was located inside a virtual annular surface and could appear at a random radius ([15...30] [deg]) and at a random orientation ([0...360] [deg]) with respect to the pursuit target. The flash could be presented either at the same time, before or after the extinction of the pursuit target. The probability of occurrence of these three conditions was equal. The duration between flash presentation and pursuit extinction was randomly selected from the following list of possible values: [200,175,150,125,100,75,50,25,0,-100,-200,-300,-400,-500,-600,-700,-800] [ms]. This resulted in a gap condition (Fig. II-1, panel A), a no gap no overlap (NGNO) condition (Fig. II-1, panel B) and an overlap condition (Fig. II-1, panel C). We used these different conditions to increase both the range of observed gaze saccade latencies and head movement amplitudes during the saccade latency period following the presentation of the flash (see below).

During the pursuit part of the protocol, subjects were asked to track the red target actively with both their eyes and head. They were asked to reorient their gaze to the memorized position of the flash as soon as they saw the flash and to maintain gaze on this memorized location until a second end-of-trial target appeared for 500 [ms] at the center of the screen. The orientation period after the flash presentation lasted for at least 1 [s] so that the overall duration of all trials was 6 [s].

3 Data calibration

We performed three calibration blocks during an experimental session, one at the start of the experiment, one mid-way through the session and one after the last experimental block of trials. Calibration was necessary to reconstruct gaze (i.e., eye orientation relative to an inertial reference frame) from eye-in-head orientation measurements taken by the Chronos eye tracker and head-in-space orientation obtained through the IRED positions. Each calibration was composed of five series of five successive fixation targets (each fixation lasted 2 seconds). Subjects were asked to maintain their head position during a fixation series and to move it to a new position between two series. This calibration sequence allowed determination of the IRED positions for the primary upright

[88] The target made between 1.8 and 4.5 cycles of motion with the range of duration and frequency used in the protocol.

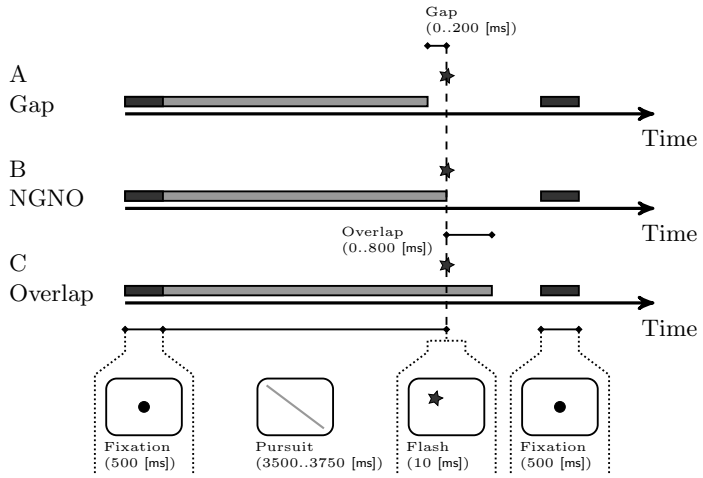

Fig. II-1: **Experimental protocol.** The trial starts with a 500 [ms] fixation at the center of the screen. Then a red pursuit target with a random sinusoidal velocity along a randomly oriented ramp with random amplitude is presented for a random duration. Afterwards, a green target is flashed (duration: 10 [ms]) at a random position. A: Gap. The pursuit target is off before the flash presentation for a random duration up to 200 [ms]. B: No Gap No Overlap (NGNO). The pursuit target is off when the flash is presented. C: Overlap. The pursuit target is still on for a duration up to 800 [ms] after the flash presentation. Trial ends with a center fixation for 500 [ms].

straight-ahead head position. All head movements were computed as the angular difference from this primary orientation. Next, we reconstructed gaze from the eye tracker and head orientation data using a previously described method (Ronsse et al., 2007). Briefly, this method computes the exact relationship between eye-centered, head-centered and inertial reference frames to estimate a three-dimensional gaze orientation vector from eye-in-head and head-in-space positions and orientations. This method also required determining the relative position of the eyes with respect to the head markers, which we measured by holding an IRED in front of the closed eyeball prior to the calibration. Finally we transformed eye-in-head, head-in-space and gaze-in-space orientations into the target reference frame (as if all centers of rotation align), which resulted in gaze being the sum of eye and head orientations.

4 Data analysis

The IRED and eye positions were stored on a computer hard-drive for off-line analysis. Matlab® (The MathWorks, Natick, Massachusetts) was used to implement analysis algorithms. Recorded data was low-pass filtered (cut-off frequency: 50 [Hz]) using a zero-phase digital filter (autoregressive, forward-backward filter). Velocity and acceleration were derived from position using a

central difference algorithm on a ± 10 [ms] window. Data were rotated with respect to pursuit target direction sampled either at flash time for NGNO and overlap conditions, or at pursuit target disappearance for the gap condition. This rotation induced a new coordinate system; the movement was decomposed into direction parallel to pursuit (X axis in text and figures) and direction orthogonal to pursuit (Y axis in text and figures). Gaze saccade detection[89] was based on a Kalman filter (Sauter et al., 1991) combined with a generalized likelihood ratio (GLR) fault detection algorithm (Basseville and Nikiforov, 1993). Onset and offset of a detected gaze saccade were computed with a traditional acceleration threshold (750 [deg/s^2]) on the eye-in-head signal (de Brouwer et al., 2002a,b). Every trial was visually inspected; the acceleration threshold was decreased to 500 [deg/s^2] if a saccade was not automatically detected. All trials were aligned to flash presentation. As part of our analyses, we computed the absolute and relative latency of every saccade within a trial. Absolute latency of a saccade was defined as the time between the flash presentation and gaze saccade onset. Relative saccade latency was defined as the time between onsets of two successive saccades. To estimate the latency distribution, we used a LATER model (Carpenter and Williams, 1995). The LATER model assumes both a linear rate of rise of a decision signal to a threshold value and that the rate of rise has a Gaussian distribution. To obtain the parameters of the LATER model, we fitted a recinormal (inverse-Gaussian) distribution on our latencies dataset (Lat):

$$f(Lat, \mu, \gamma) = \sqrt{\frac{\gamma}{2\pi Lat^3}} e^{\frac{-\gamma(Lat-\mu)^2}{2Lat\mu^2}} \tag{1}$$

The distribution of (1) is characterized by a mean μ, and a standard deviation $\sigma = \sqrt{\frac{\mu^3}{\gamma}}$.

We also define the smooth gaze displacement (SGD) as the gaze movement after removing gaze saccades. To remove a gaze saccade, the velocity from 20 [ms] before a gaze saccade onset up to 20 [ms] after the gaze saccade offset was replaced by a linear interpolation (For a detailed procedure see (de Brouwer et al., 2001)). Through this procedure of saccade removal, we assume that the gaze displacement is the sum of saccadic and smooth tracking commands, as this has been shown during head-restrained smooth pursuit (de Brouwer et al., 2001, 2002a). Smooth head displacement (SHD) was defined as the head displacement during the experiment. Then we defined smooth eye displacement (SED) as:

$$SED = SGD - SHD \tag{2}$$

We computed head contribution (HC) to the gaze displacement as:

$$HC = \frac{SHD}{SGD} \tag{3}$$

Equivalently, eye-in-head contribution (EC) to the gaze displacement was computed as:

[89] A complete description of the detection algorithm is presented in appendix 2

$$EC = \frac{SED}{SGD} \tag{4}$$

Straightforward computations lead to EC =1-HC. An EC equal to zero means that SGD was entirely realized by head displacement. In contrast, an EC equal to one indicates that SGD was completely comprised of eye displacement (it can be seen as a head-restrained situation). An EC of less than zero or greater than one, respectively, means that the head was moving faster than the gaze or in the opposite direction of the gaze (the same kind of reasoning applies to HC). To characterize the head movement during the pursuit part of the paradigm, we evaluated the frequency of head movement. First, we selected the head movement preceding flash presentation for a duration equivalent to 1.2 periods of target oscillation. We then determined the head movement frequency as the maximum of the frequency spectrum after fast Fourier transformation (FFT)[90]. Thus, we assume that the head oscillation frequency was stable during this elapsed time. To test this assumption, we divided the selected head movement into two subparts and computed for each part the head oscillation frequency. We then performed a two-tailed t-test and found that the two distributions had an equivalent mean (two-tailed t-test, t(2780,2780)=0.1999, p=0.842). Those results validated our hypothesis of constant head oscillation frequency.

5 Compensation

To quantify the effect of SGD on the final orientation error, we computed a compensation index CI describing how much of the smooth gaze displacement occurring after the flash was accounted for by the saccadic system at the end of the orientation process. To do so, we defined PE as the remaining position error at the end of an orienting gaze saccade and SGD as the smooth gaze displacement between flash presentation and the onset of the considered orientation saccade. The normalization of the data resulted in SGD mainly in the X direction (direction parallel to pursuit); therefore we assume that the SGD along the Y direction was negligible compared to SGD along X direction. Thus we only analyzed the X component. We measured SGD at the saccade onset as we were interested in how much a given saccade would compensate for SGD that had occurred before the execution of the saccade. Assuming that all pure position error at the moment of the flash is perfectly accounted for by the saccadic system (de Brouwer et al., 2002a), one can then write the position error as:

$$PE = SGD - CI * SGD \tag{5}$$

[90] Due to the small number of cycles used for the analysis, a FFT method is probably not the best choice (for a discussion on the leakage phenomenon for discrete fast-fourrier transform, see (Bracewell, 2000)). Nevertheless, it was successful for the purpose of this analysis: check if the frequency of the head movement was stable during the last 1.2 periods of motion.

Solving (5) for the compensation index (CI) then results in:

$$CI = \frac{SGD - PE}{SGD} \tag{6}$$

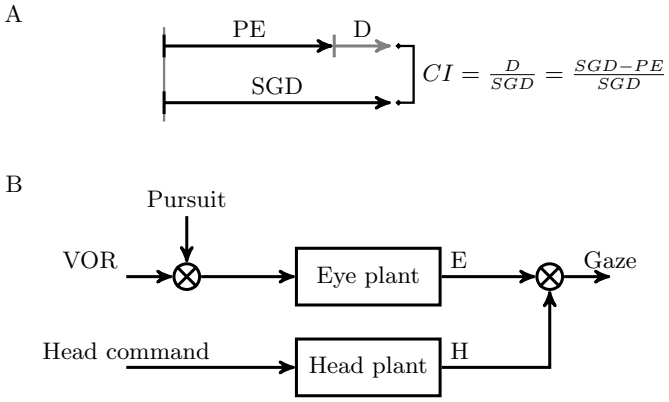

Fig. II-2: **Panel A: Representation of the parameters involved in the computation of the global compensation index.** PE corresponds to the position error. SGD represents the smooth gaze displacement. D is the difference between SGD and PE. **Panel B: Hypothetical model of the compensation process during gaze shift latency.** VOR corresponds to the integrated vestibulo-ocular signal coming from the semi-circular canals, proportional to head displacement. Pursuit corresponds to eye command signal. E corresponds to the measured eye-in-head displacement during the latency. H corresponds to the measured head displacement during the latency. Hence, the gaze is a sum of the pursuit, the VOR and the head displacement.

When PE is equal (both the sign and the magnitude) to SGD, the saccade did not compensate for SGD and CI =0. When PE =0, the compensation is perfect, i.e. CI =1. An overcompensation of the saccade would result in PE having the opposite sign as SGD and CI >1. Fig. II-2, panel A shows a graphical representation of the parameters involved in the computation of the global compensation index.

However, equations (5) and (6) only describe the overall compensation for gaze displacement but do not allow inferring the individual compensation indices for smooth eye (SED) and head (SHD) displacements. Using (2), we can now write:

$$SGD = SED + SHD \tag{7}$$

$$PE = SGD - CI^{\mathrm{E}} * SED - CI^{\mathrm{H}} * SHD \tag{8}$$

With (3), (4) and HC =1-EC, expression (8) can be modified to explicitly include the eye and head compensation index as follows:

$$\frac{SGD - PE}{SGD} = CI = CI^{\mathrm{E}} * EC + CI^{\mathrm{H}} * (1 - EC) \tag{9}$$

Furthermore, we can separate the smooth eye displacement (SED) into a vestibulo-ocular reflex (VOR) component and a smooth pursuit displacement (SPD):

$$SED = SPD + VOR \tag{10}$$

This is shown in Fig. II-2, panel B. At the level of the oculomotor neurons, the command sent to the eye plant is composed of the VOR and SPD while the head plant receives a single input, the SHD. We can also implement the finding that the VOR depends on head movement:

$$VOR = -g(f_H) * SHD \tag{11}$$

In (11), g(f_H) is the VOR gain depending on the head movement frequency f_H. It is well known that the VOR gain varies as a function of a number of parameters (for a review see (Barnes, 1993)). Nevertheless, for the sake of this paper, we considered that the VOR gain can be approximated by an average value over the first saccade latency period. This mean value depends on the head oscillation frequency of individual trials (see figure 10 of (Barnes, 1993)). Using these considerations and equations (8), we can now write:

$$\begin{aligned} PE = SGD - CI^{\mathrm{P}} * EC * SGD - \\ ((CI^{\mathrm{V}} - CP^{P}) * g(f_H) + CI^{\mathrm{H}}) * (1 - EC) * SGD \end{aligned} \tag{12}$$

$$\begin{aligned} CI = \left[CI^{\mathrm{P}} - (CI^{\mathrm{P}} - CI^{\mathrm{V}}) * g(f_H) - CI^{\mathrm{H}}\right] * EC + \\ \left[(CI^{\mathrm{P}} - CI^{\mathrm{V}}) * g(f_H) + CI^{\mathrm{H}}\right] \end{aligned} \tag{13}$$

Equation (13) gives a more detailed expression of the evolution of the overall compensation index as a function of the different components (pursuit, VOR and head) of the SGD. The complete mathematical developments to obtain equation (13) are given in appendix 2.

6 Collected data set

We collected a total of 6533 trials, out of which 2783 were valid (around 42.6%). Trials were removed from the analysis if a saccade occurred during an interval of [-50. . . 50] [ms] around the flash presentation (39.6% trials removed). We also removed trials for which the final gaze position error had a magnitude either larger than 16 [deg] or larger than the error at flash time (13.4% trials removed). Those cases corresponded to situations in which flash localization was erroneous or ambiguous. Finally, we removed "catch-up trials", where the first saccade after the presentation of the flash was directed towards the pursuit target (4.4% trials removed) instead of the flash. Every trial was visually inspected and removed if it did not comply with the above validity criteria. Among valid trials, 1137 were gap trials (around 41%), 910 were No Gap No Overlap (NGNO) trials (around 33%) and 736 were overlap trials (around 26%).

3

Results

The aim of this study was to investigate how the saccadic system compensated for smooth gaze displacements in a head-unrestrained condition, and if this compensation differed between the smooth pursuit, head and VOR components of the smooth gaze displacement. Therefore, we will first show typical trials and analyze orienting saccade latencies. We also showed how the compensation for smooth eye and head displacements depends on saccade latency and the relative contribution of the eye movement to the total smooth gaze displacement. Finally, we estimated an upper limit for the rate of change of the VOR gain with different head movement frequencies during the orientation process.

1 Typical trials

Figure II-3 shows a short latency gap trial (gap duration: 200 [ms]) where the first orienting saccade had a latency of 100[ms]. Fig. II-3, panel A shows a X-Y plot of target and gaze trajectories in space, starting 400[ms] before the flash presentation (the star represents the location of the 10[ms] flash while the dot represents gaze position at the moment of flash presentation) until 800[ms] after the occurrence of the flash. Gaze (thin dark gray line) pursued the oscillating target (0.7 [Hz], 29[deg] amplitude, light gray line) to the right in Fig. II-3, panel A, and two orienting gaze saccades towards the memorized location of the flash were generated (bold gray lines). Fig. II-3, panel B shows the individual components of gaze, eye and head position as a function of time for the same trial. Fig. II-3, panel C shows a detailed view of the gaze displacement after the flash. As can be seen, gaze continued to track the now invisible red target during the gap (gray boxes) and continued moving for about 100[ms] after the flash presentation. During the latency of the first gaze saccade, smooth gaze displacement (SGD) along the direction normal to pursuit was negligible (-0.84 [deg]) compared to SGD parallel to pursuit (8.55 [deg], SGD label on Fig. II-3, panel C), and the eye only contributed minimally (EC: 8.7%). As can be observed in Fig. II-3, panel A, the direction of the first orienting gaze saccade was approximately parallel to the position error at flash presentation.

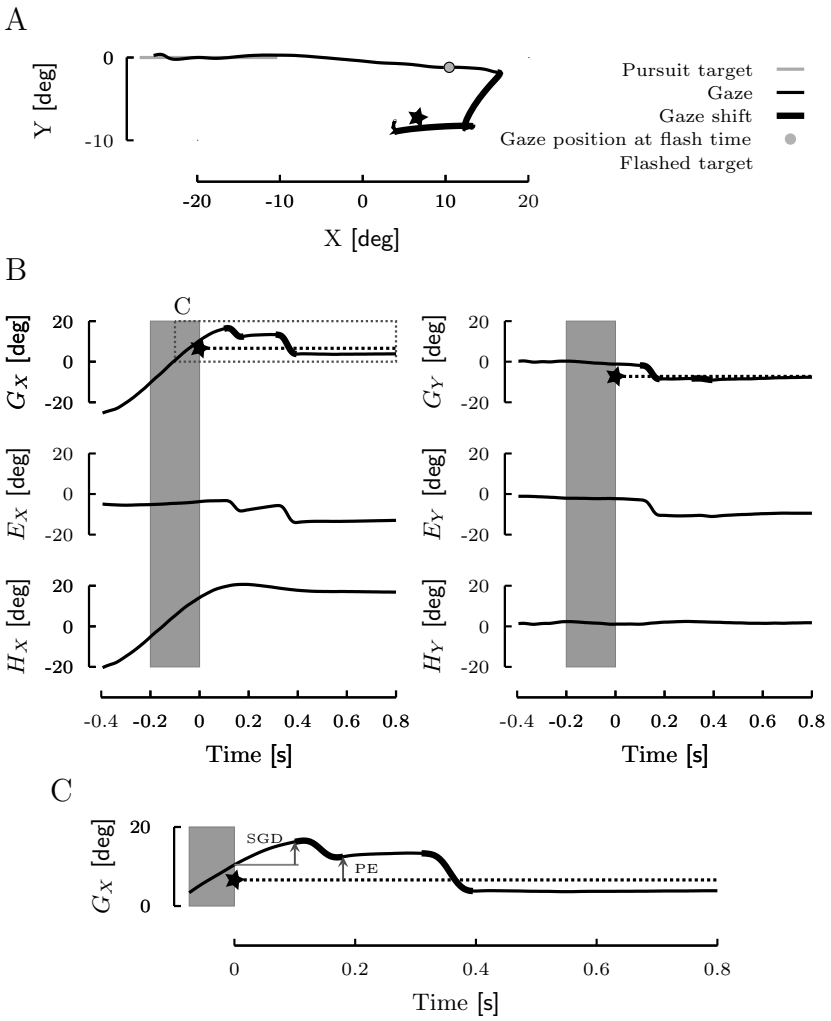

Fig. II-3: **Typical normalized short latency trial.** X corresponds to the direction parallel to pursuit, Y represents the direction normal to pursuit. Panel A: Spatial representation of the normalized gaze and target position. Panel B: Left column represents X evolution as a function of time for either gaze, eye in head or head (depending on rows) while right column represents Y evolution for the same signals. Time origin is set at the flash appearance. The dashed line in the gaze row represents the flash position. Shaded boxes represent gap period (duration: 200 [ms]). Panel C: Detailed representation of X evolution as a function of time. Relevant gaze shifts are represented with bold lines on panels A, B and C.

Because this saccade obviously did not account for smooth gaze displacement during the latency period, the position error was still large (PE =6.01[deg], PE label on Fig. II-3, panel C) at the end of the first gaze saccade. Therefore, the system executed a second corrective gaze saccade (with a latency of 310[ms]) towards the remembered flash position, resulting in a final orientation error of PE =-3.32[deg]. Importantly, this corrective saccade could not rely on visual information about the smooth gaze displacement due to darkness, and thus had to result from some mechanism that internally monitored the smooth gaze displacement. A different behavior was observed in our second typical example, as is shown in Figure 4 (same conventions as Figure 3 apply). This NGNO trial shows a long latency (385[ms]) response to a flash presented after gaze pursuit (amplitude = 21[deg], frequency = 0.64[Hz]), where SGD before the first saccade was 16.6[deg] (EC =14.9%). This saccade resulted in a position error of 1.03[deg] and a second, corrective saccade (with a latency of 590 [ms]) brought the gaze to a final position error of -2.53[deg]. Compared to the short latency trial in Figure 3, the first saccade of this trial immediately corrected for the smooth gaze displacements that occurred during the latency period, and the saccade was therefore quite accurate (Compare PE amplitudes between figures 3 and 4).

As explained in the method section, the smooth gaze displacement along a direction orthogonal to the pursuit target direction is negligible compared to the component along the pursuit target direction (mean SGD_X=7.75 [deg], mean SGD_Y=0.83 [deg]).

2 Latency distribution

As can be readily observed from the typical trials, and in agreement with previous findings (Blohm et al., 2005a, 2003), the saccadic latency has an important role in determining the accuracy of the gaze position. Therefore, we first set out to characterize saccade latencies. Figure II-5, panel A shows the distribution of absolute latencies (time between flash appearance and gaze saccade onset) of the three first gaze saccades for all subjects and all conditions pooled together (1st saccade: , 2nd saccade: , 3rd saccade:). The relative latency (with respect to flash presentation for first saccade and with respect to the previous saccade onset for successive saccades) is shown in Fig. II-5, panel B. To further characterize the relative latency distribution, we fitted a LATER model (see Methods) on each distribution. The means (± 95% confidence intervals) of these distributions for the first, second and third saccades are 254± 7ms (CI: 101± 1ms), 298± 10ms (CI: 125± 1ms) and 298± 21ms (CI: 145± 2ms), respectively. Table II-1 shows these parameters for each subject individually (note, that we did not fit a LATER model on data-sets with less than 40 samples). Statistical analysis showed that relative saccade latencies differed between the first and second saccades (two-sided Kolmogorov-Smirnov, $p<0.001$) but not between the second and third saccades (two-sided Kolmogorov-Smirnov, $p=0.085$).

To evaluate differences in latency distribution due to variations in flash presentation conditions, we evaluated LATER models for the latency distributions of the first gaze saccades separately for the gap condition (mean=205±

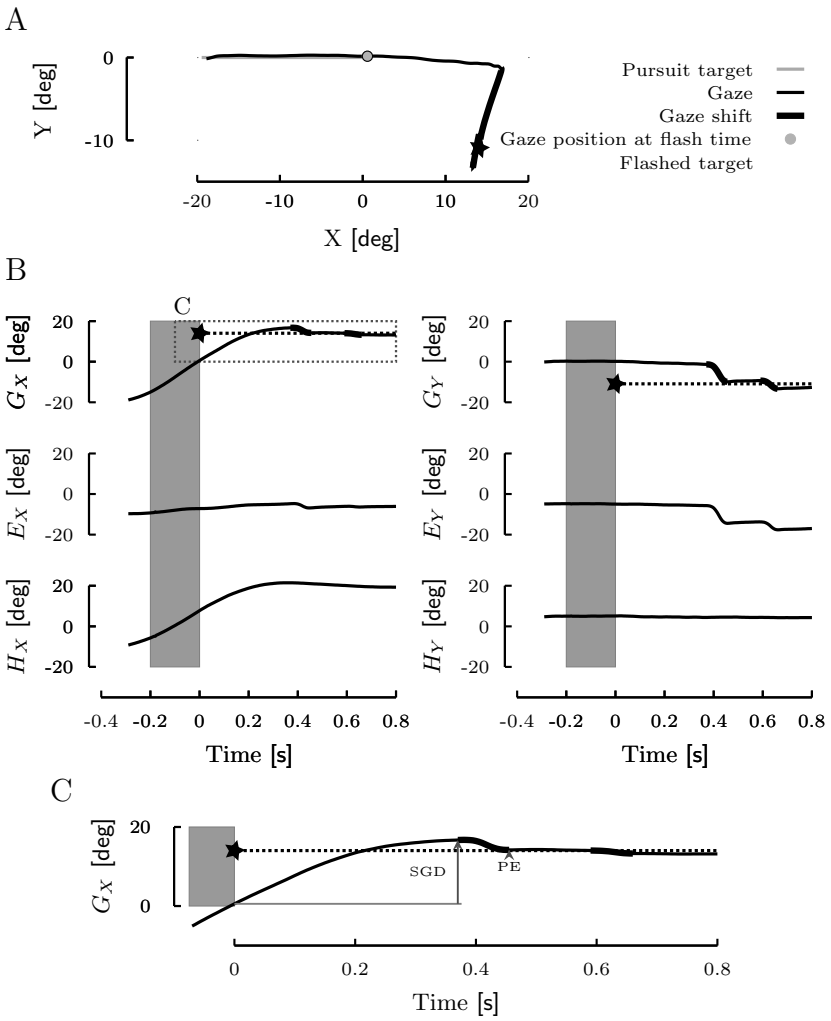

Fig. II-4: **Long latency trial.** Same conventions as figure II-3. Panel A: Spatial representation. Panel B: Left column represents X evolution as a function of time for gaze, eye-in-head or head. Right column represents Y evolution as a function of time for the same signals. Panel C: Detailed representation of X evolution as a function of time.

7ms SD=76± 1ms), the NGNO condition (mean=263± 8ms, SD=83± 3ms) and the overlap condition (mean=299± 13ms, SD=95± 4ms). These results showed that the three flash presentation conditions had an influence on the observed latency of the first gaze saccade. There was a significant increase in latency between the gap and the NGNO conditions (two-sided Kolmogorov-Smirnov, $p<0.001$) and between the NGNO and the overlap conditions (two-sided Kolmogorov-Smirnov, $p<0.001$), results which are in agreement with head-restrained findings obtained by Krauzlis and Miles (1996). The goal of

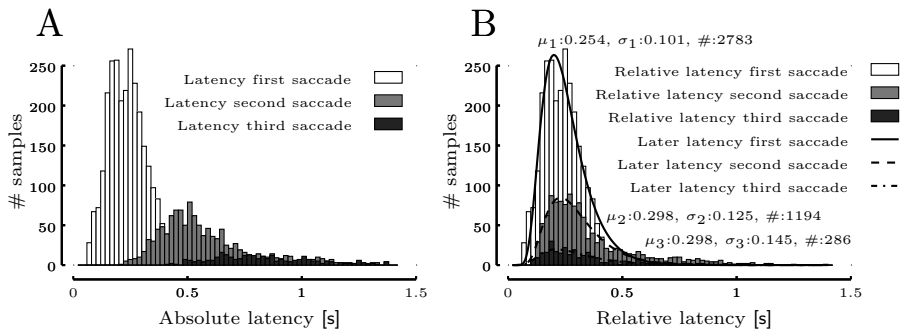

Fig. II-5: **Latency distribution.** A: absolute saccade latency distribution for the 3 first saccades. First saccade distribution includes first saccades for trials with 1, 2, or 3 saccades; second saccade distribution includes second saccades for trials with 2 or 3 saccades; and third saccade distribution includes third saccades for trials with 3 saccades. B: relative saccade latency distribution, with the same color convention and for the same trials as A. LATER models were fitted on relative latency distributions. Maximums of recinormal vary from 254 to 298 [ms].

our experimental paradigm, to obtain a large range for first saccade latencies, was thus achieved.

Table II-1: LATER model parameters on gaze saccade relative latency for every subject

	First Gaze Saccade			Second Gaze Saccade			Third Gaze Saccade		
Subject	#Trials	Mean [ms]	SD [ms]	# Trials	Mean [ms]	SD [ms]	# Trials	Mean [ms]	SD [ms]
CO	378	178 ± 4	51 ± 2	146	339 ± 43	190 ± 11	15	-	-
DP	398	265 ± 8	58 ± 5	195	381 ± 32	157 ± 4	65	252 ± 20	83 ± 8
EM	410	318 ± 12	110 ± 3	186	263 ± 13	94 ± 3	27	-	-
GA	294	274 ± 7	82 ± 3	69	283 ± 13	81 ± 6	9	-	-
GB	245	242 ± 8	64 ± 4	192	229 ± 9	65 ± 4	89	254 ± 26	125 ± 2
GL	350	270 ± 11	87 ± 4	205	284 ± 15	115 ± 1	41	347 ± 65	183 ± 10
LA	437	213 ± 7	62 ± 3	96	296 ± 25	141 ± 1	11	-	-
SC	263	253 ± 27	142 ± 7	105	323 ± 15	81 ± 8	29	-	-
All	2783	254 ± 7	101 ± 1	1194	298 ± 10	125 ± 1	286	298 ± 21	145 ± 2

Values are means ± confidence interval at 95%.
We did not fit a LATER model on data sets with < 40 trials

3 Eye contribution distribution

Besides saccade latency, another important factor that might influence the compensation for smooth gaze displacements is the eye contribution (EC). EC has been chosen as a parameter because, as it will be showed later, it is an independent parameter with respect to the latency (which is not the case for SED and SHD). Therefore, we analyzed to what extent the eyes and head

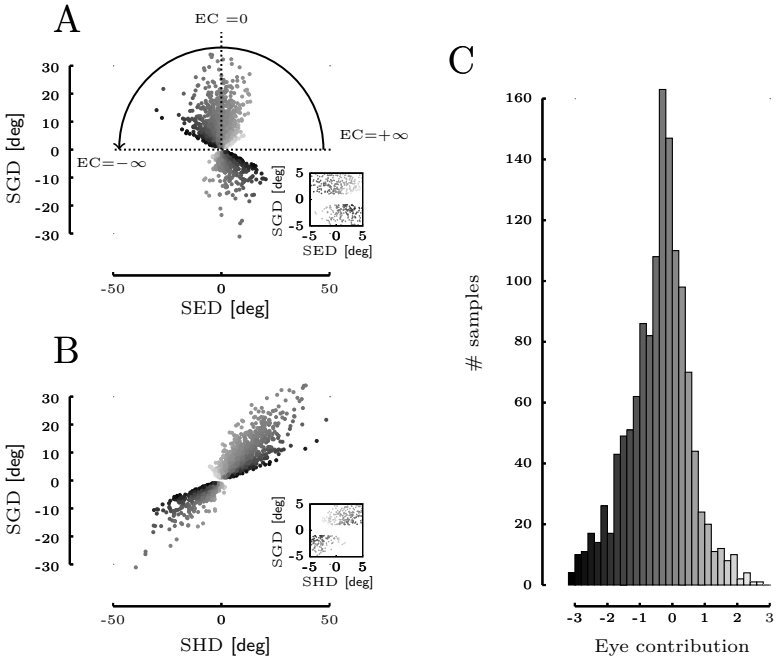

Fig. II-6: **Eye contribution distribution.** Panel A: Smooth gaze displacement (SGD) as a function of smooth eye displacement (SED) for single saccade trials. Panel B: SGD as a function of smooth head displacement (SHD) for single saccade trials. Inserts on panel A and B represent a zoomed portion of their corresponding panels. Those inserts show that we removed trials with absolute SGD amplitude lower than 1 degree. Panel C: Eye contribution (EC =SED/SGD) distribution for single saccade trials. We represented data with , which included 94% of the single-saccade trials. On each panel, when EC is small, the data representation is darker and when EC is large, the data representation is lighter. The arrow on panel A represents EC evolution from -∞ to +∞ (from dark to light).

contributed to the gaze displacement during the latency period of the saccades. Figure II-6 shows SGD as a function of SED (Fig. II-6, panel A) and SHD (Fig. II-6, panel B) for trials containing a single saccade. EC is color-coded in Fig. II-6. Given a certain SED (SHD), the range of associated SGD values can be determined from these graphs. The variability of associated SGD values in this data is important because it allows us to analyze compensation for smooth eye and head displacements separately, despite their obvious correlation. This can be observed from the arrows in Fig. II-6, panel A, which represent the evolution of EC. Because EC =SED/SGD, when SGD approaches zero, eye contribution approaches ± infinity. To avoid this issue, we removed trials with $\|SGD\|_2$ <1[deg] (see inserts in panels A and B), leaving 82% (1305 trials) of first-saccade trials. That the contribution of the eye to a given SGD is not stereotypical is also apparent in Fig. II-6, panel C, where we present a histogram

of ECs. This observation was crucial to allowing for the separate analyses of compensation for smooth eye and head movements during the latency period (see below).

4 Compensation as a function of latency

Our typical trials depicted in Fig. II-3-II-4 clearly show that the compensation for smooth gaze displacements depends on saccade latency, as has previously been shown for head-restrained pursuit (Blohm et al., 2003, 2005b). To quantify the overall behavior for combined eye-head gaze displacements in our head-unrestrained data, we calculated a compensation index for SGD (see Methods section) and for up to three orientation saccades. We then separately plotted in Fig. II-7 the mean compensation index as a function of absolute saccade latency (i.e. flash presentation time; grouped in 50[ms] bins) for each saccade individually (Fig. II-7, panel A) and for the last orientation saccade of the trial only (Fig. II-7, panel B). Figure II-7, panel A shows that for the first gaze

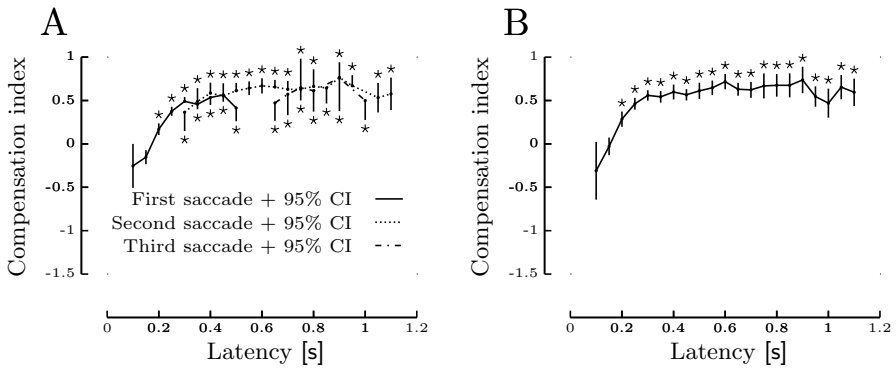

Fig. II-7: **Compensation as a function of absolute latency.** Panel A: Evolution of the compensation index (CI =1-PE/SGD) as a function of absolute latency for the three first saccades of a trial. First saccade curve includes trials with one, two or three saccades. Second saccade curve includes trials with two or three saccades and third saccade curve includes trials with three saccades. Error bars represents 95% confidence intervals. Stars upon error bars represent bins with a compensation index significantly larger than zero (p-value<0.05). Panel B: Evolution of the final compensation index (compensation index for the last saccade of a trial) as a function of absolute latency. Stars upon error bars represent bins with a compensation index significantly bigger than zero (p-value<0.05).

saccade, the compensation increased with latency. For latencies up to around 200[ms], the compensation was not statistically greater than zero (upper tail t-test, t(166)=-1.9746, p=0.975 at 100 [ms]; t(506)=-3.73, p>0.999 at 150 [ms]), while the compensation index reached significance for latencies ≥200[ms] (mean

CI values for all first saccade latencies ≥200ms = 0.39± 0.03; upper tail t-test; t(1725)=25.76, p<0.001). Because after the first gaze saccade the spatial error generally remained large, we often observed a second (∼43% of the trials) or even third (∼10% of the trials) corrective saccade. Across the latencies of the second saccade, we continued to observe an increase in CI (CI =0.36± 0.22 at 300 [ms], CI =0.58± 0.12 at 400 [ms]). At this point, CI reached a plateau value (mean CI = 0.64± 0.05 for second saccade with latency >400ms, mean CI = 0.57± 0.15 for third saccade), and we did not observe any further statistically significant change of CI with saccade latency (two-tailed t-test, t(615)=29.67, p<0.001). Note that the transition between the CI evolution curves for the three saccades is surprisingly smooth, which suggests that it is not the number of saccades that determine the amount of SGD compensation but rather when the saccade was triggered relative to flash presentation.

FigureII-7, panel A represents the intermediate stages of the compensatory mechanism for all saccades individually. To study the global orientation process, we computed CI for the last saccade of a trial ("final compensation") and plotted it as function of saccade latency in Fig. II-7, panel B, similarly to Fig. II-7, panel A. As can be observed, the shape of this curve is very similar to the CI of the individual saccades. As in Fig. II-7, panel A, the compensation in Fig. II-7, panel B only starts to be significantly greater than 0 for latencies longer than 150 [ms] (CI =0.28± 0.09 at 200 [ms]; upper tail t-test, t(324)=6.4, p<0.001). With an increase in latency, we observed a significant increase in CI, up to latencies equals to 300 [ms] (CI =0.28± 0.09 at 200 [ms], CI =0.56± 0.06 at 300 [ms]; t(324,297)=-5.016, p<0.001). At this point, the global compensation reaches a plateau and we did not observe any further significant changes (mean CI = 0.62± 0.02, two tailed t-test, t(1330)=50.53, p<0.001).

To evaluate the individual performances of our subject, we computed the mean value of the final compensation index for absolute latencies longer than 400 [ms] for every subject. The corresponding values are presented in table 2. To summarize, we have qualitatively reproduced previous findings from head-restrained situations (Blohm et al., 2003, 2005b, 2006) and generalized them to head-unrestrained smooth pursuit. FigureFig. II-7 also shows that there is a continuous transition between two extreme behaviors in our typical trials (Figs II-3-II-4), apparently implementing the speed-accuracy tradeoff and the existence of a continuous compensatory mechanism that have previously been suggested (Blohm et al., 2005b). After this necessary verification, we next analyzed the compensatory mechanism for the eye and head-related components of the smooth gaze displacement separately (see following section).

Table II-2: Mean final contribution for latencies longer than 400 [ms] for each subject

	Subjects								
	CO	DP	EM	GA	GB	GL	LA	SC	All
CI final, %	75.9± 11	68± 5.8	53.3± 12.4	53.3± 2	37.4± 3	77.7± 11.6	17.6± 3	41.9± 6	62± 2

5 Eye and head compensation

Up to this point, we have shown that the global gaze compensation mechanism is similar during head-unrestrained pursuit and head-restrained pursuit, as previously reported (Blohm et al., 2003, 2005b). In this section, we will decompose the smooth gaze displacement into its respective eye and head movement components to investigate potential differences in compensation for smooth eye displacements (SED) and smooth head displacements (SHD).

To analyze the potential differences between compensation for smooth eye and head displacements, we represented the compensation index as a function of eye contribution (EC, see Methods for definition) on figure 8A for the same subset of trials as in figure 6 (single saccade trial, $\|SGD\|_2$ <1[deg]). The rationale behind this analysis is that if smooth eye and head displacements are equally accounted for, then the correlation between CI and EC should be zero. In contrast, any non-zero correlation means that there are differences in the compensation for SED and SHD. A linear regression analysis provided the following result:

$$CI = (0.25 \pm 0.03) * EC + (0.53 \pm 0.03)\,,\ vaf = 0.42,\ pval < 0.001 \qquad (14)$$

The strong relationship between CI and EC clearly points towards a difference in the mechanisms compensating for SED and SHD. When analyzing subjects individually, we found that the slope of the regression varies in a range between 0.1229 and 0.48. To ensure that this observation was not due to a side effect of the saccade latency (i.e., the longer the latency, the smaller EC), we performed several control analyses. First, we subdivided our data into several EC bins and drew the evolution of CI with saccade latency (Fig. II-8, panel B). FigureII-8, panels B1-B3 show representative plots of this relationship for EC =-1.4 (B1), EC =0 (B2) and EC =0.6 (B3). FigureII-8, panel B shows that for each EC bin, CI evolves similarly to what we have observed in Fig. II-7 (the longer the latency, the bigger the compensation). Nevertheless, the mean value of compensation is less important for smaller values of EC (B1: CI =-0.02± 0.25) than for larger values of EC (B3: CI =0.78± 0.18).

Next, we tested the independence between EC and latency. To do so, we used a method proposed by Diks and Manzan (2002). This method uses a bootstrap procedure on the mutual information between EC and latency to test the null hypothesis that the two samples are independent. The test did not confirm the independence hypothesis (p>0.73), pointing towards latency having no effect on EC. We further tested whether the saccade latency distribution might change across bins of EC, and thus induce a correlation between EC and CI. We therefore compared the latency distributions for each EC bin in Fig. II-8, panel A, but did not find any difference between latency distributions across the EC bins (two dimensional Kolmogorov-Smirnov test, p>0.05), except for in one comparison (p=0.0085). Using the same method, we compared the global latency distribution with the latency distributions corresponding to each EC bin and did not find any differences (p>0.05). Consequentially, we made sure that for each EC bin there was an equivalent range of saccade latencies. Taken together, these results suggest that there was an increase of CI with EC independent of saccade latency.

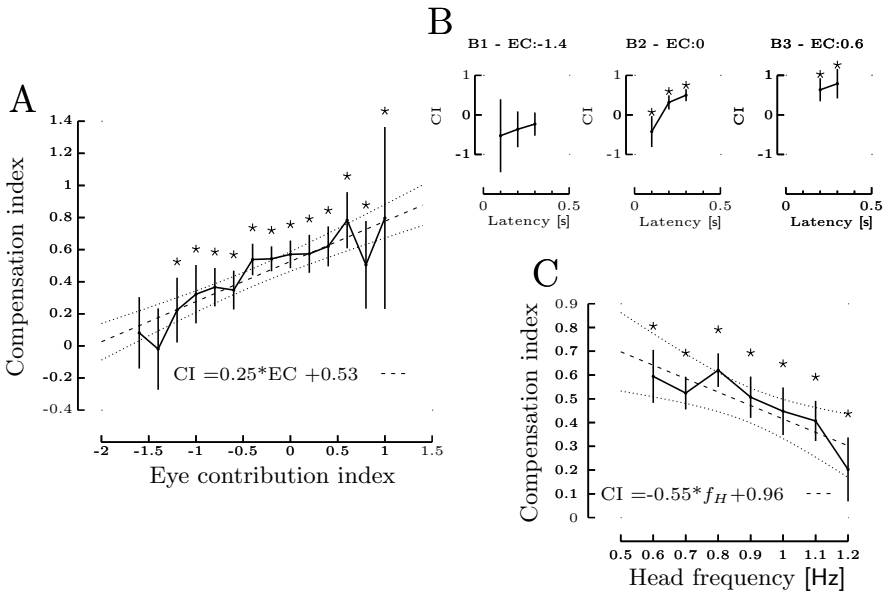

Fig. II-8: **Compensation as a function of eye contribution (EC) and head oscillation frequency (f_H).** Panel A: Evolution of the compensation index (CI) as a function of EC. The dotted line represents a linear fit between CI and EC and dashed lines represent 95% confidence intervals of the fit. Stars upon error bars represent bins with CI significantly bigger than zero (p-value<0.05). Panel B: Evolution of CI as a function of absolute latency for trials within an EC bin. B1 corresponds to trials with -1.5<EC<-1.3, B2 corresponds to trials with -0.1<EC<0.1 and B3 to trials with 0.5<EC<0.7. Stars upon error bars represent bins with CI significantly bigger than zero (p-value<0.05). Panel C: CI evolution as a function of head oscillation frequency (f_H). The dotted line represents a linear fit between CI and fhead and dashed lines represent 95% confidence intervals of the fit.

Once this independent effect of EC on CI was established, we could use (8) to compute individual compensation indices for smooth eye and head movements from the parameters identified in (14). This resulted in $CI^{\mathrm{E}} = 0.78 \pm 0.03$ and $CI^{\mathrm{H}} = 0.53 \pm 0.03$. Therefore, on average 78% of smooth eye movements and 53% of smooth head movements that occurred during the latency period of the saccade were compensated for by the saccadic system. As a result of the different CI values for eye and head, we can explain the linear relationship between CI and EC in Figure8 by the large range of different combinations of SED and SHD (and thus EC) in our data set.

A supplementary step to test the importance of EC in the evolution of CI was to test whether the addition of a supplementary parameter in a multiple regression analysis improved the quality of the fit. As can be observed in Fig. II-7, the compensation index saturated for longer latencies. Conversely, Fig. II-8, panel B showed that the trend between EC and CI is well explained by a

linear regression. Therefore, we used a linear regression to describe the effect of EC on CI and added a non-linear term to express the saturating effect of the latency on the compensation index. We then compared the regression with one parameter (saccade latency, equation (15)) with the regression with two parameters (equation (16)).

$$CI = -e^{\left(-\frac{1}{0.059} * Lat + 1.93\right)} + 0.48,\ vaf = 0.46 \tag{15}$$

$$CI = -e^{\left(-\frac{1}{0.067} * Lat + 1.76\right)} + 0.32 * EC + 0.67,\ vaf = 0.75 \tag{16}$$

Comparing the variance accounted for (vaf) of the fit equations (15) and (16) shows that the addition of supplementary parameters to the regression increased the quality of the fit. We performed an f-test and showed that the addition of a new parameter significantly increased the fit (one-sided f-test, f(1384,1384)=0.90, p-val<0.05). This is additional evidence that the eye contribution was an important parameter to explain the evolution of the compensation index.

As a final step, we attempted to further refine our analysis and divide SED into components resulting from an active smooth pursuit command and the vestibulo-ocular reflex (VOR). This is formalized in Eq.(13) and now includes aside from the three CIs relative to head, pursuit and VOR a head-movement frequency-dependent VOR gain term ($g(f_H)$) (Barnes, 1993). Unfortunately, we do not know the contribution of the VOR to SED and thus cannot directly evaluate the compensation for VOR. However, this is not the case for the pursuit compensation index. This can be directly seen when rewriting Eq. (13) in the following form:

$$\begin{aligned} CI &= A * EC + B \\ A &= \left[CI^{\mathrm{P}} - \left(CI^{\mathrm{P}} - CI^{\mathrm{V}}\right) * g(f_H) - CI^{\mathrm{H}}\right] \\ B &= \left[\left(CI^{\mathrm{P}} - CI^{\mathrm{V}}\right) * g(f_H) + CI^{\mathrm{H}}\right] \end{aligned} \tag{17}$$

Using Eq.(17), we could now directly evaluate the pursuit compensation index as CI^{P} =A+B using the parameters A and B from the regression in Eq.(15). This resulted in a value of CI^{P} =0.78± 0.03. Although we could not evaluate the VOR compensation index in a similar fashion, the following discussion will attempt to provide a clearer understanding about the influence of the VOR gain on the compensation for the VOR-related portion of SED. To understand the influence of the VOR gain ($g(f_H)$) on CI, we computed the sensitivity of CI (the derivative of Eq.(13)) to a variation in the VOR gain as follows:

$$\frac{\partial CI}{\partial g(f_H)} = \left(CI^{\mathrm{P}} - CI^{\mathrm{V}}\right) * (1 - EC) \tag{18}$$

Equation(18) shows that (for EC <1), the sensitivity of CI to a variation in the VOR gain increases with EC. This can be explained more intuitively; the smaller the EC, the larger the contribution of the head to the smooth gaze displacement and therefore the larger the VOR component of SED. EC =1 corresponds to a head-restrained condition and therefore Eq.(18) shows that CI is insensitive to a change in the VOR gain. When EC >1, the relationship

between a change in the VOR gain and CI is inverted compared to when EC <1. Unfortunately, as things are, this equation is insufficient as we do not know the VOR gain and can only measure the frequency of head movement. Therefore we evaluated the sensitivity of CI to head movement frequency as follows:

$$\frac{\partial CI}{\partial f_H} = \frac{\partial CI}{\partial g(f_H)} * \frac{\partial g(f_H)}{\partial f_H} \tag{19}$$

Using Eq.(18), this results in an interpretable description of the head frequency-dependent compensation index:

$$\frac{\partial CI}{\partial f_H} = \left(CI^{\mathrm{P}} - CI^{\mathrm{V}}\right) * (1 - EC) * \frac{\partial g(f_H)}{\partial f_H} \tag{20}$$

Interestingly, Eq.(20) now suggests that we should find a relationship between the overall compensation index and the head movement frequency. This is represented in Fig. II-8, panel C and shows that, indeed, the compensation index decreased with head movement frequency. Linear regression resulted in the following equation:

$$CI = (-0.55 \pm 0.11) * f_H + (0.96 \pm 0.12)\,,\ vaf = 0.44,\ pval = 0.007 \tag{21}$$

Analyzing subjects' individual performance, the slope of the regression varies in a range between 0.21 and -1.23. For all subjects, the slope was either not significantly different from zero (n=2) or negative (n=6). Comparing Eq. (20) to Eq.(21), the correlation clearly could only result from the change of the VOR gain with head movement frequency. These sorts of changes have previously been reported (Barnes, 1993), such that with increasing head oscillation frequency, the VOR gain decreases.

The regression results from Eq.(21) allowed us to further evaluate the sensitivity of the VOR gain to changes in head movement frequency. If we take Eq.(20), we now have only two unknown entities left: CI^{V} and $\frac{\partial g(f_H)}{\partial f_H}$. We know CI^{P} from Eq.(17) (see above), EC can be evaluated from our data (i.e., the mean measured EC in our data set) and $\frac{\partial CI}{\partial f_H} = -0.55$ (from Eq.(20) and (21)). Figure II-9 represents the relationship between CI^{V} and the VOR gain sensitivity to head movement frequency. The confidence intervals take the variability of all parameters into account and thus present the worst-case scenario. Since only CI^{V} values between 0 and 1 make sense behaviorally, this graph allowed us to obtain an estimate of the VOR gain sensitivity to head movement frequency. For those values of CI^{V}, we found an upper limit on the value of $\frac{\partial CI}{\partial f_H}$ equal to -0.365± 0.099 (mean ± 95% confidence interval). This means that the VOR gain changed linearly with a slope smaller than -0.365 in our range of head oscillation frequencies (0.6-1.2 [Hz]). An approximately linear relationship between the VOR cancellation[91] gain and head movement frequency has

[91] Assuming that there is no modulation of the output gain of the VOR (VOR suppression mechanism), the sensitivity to the modulation of the cancellation gain to a modification of the head movement frequency is similar to the sensitivity of the VOR gain to the same parameter.

previously been reported for this range of frequencies (Barnes, 1993), but the estimated slope was shallower, i.e., around -0.1. Using the data from Barnes, one can predict that CI^V should lie on the vertical dashed line represented in Fig. II-9. Therefore, our analysis suggests that the VOR gain was more sensitive to the head oscillation frequency during actively generated head movements as opposed to passive head rotations (Barnes, 1993). We conducted additional

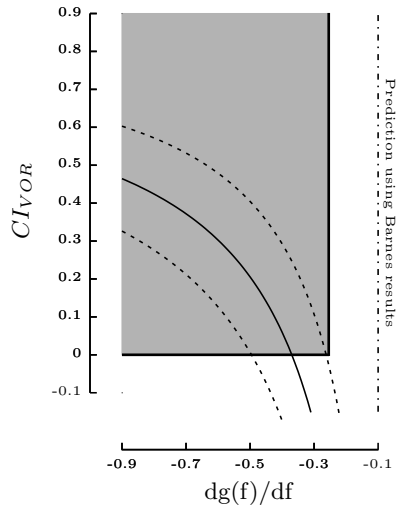

Fig. II-9: **VOR compensation index as a function of VOR gain sensitivity to a variation of head frequency.** X axis represents the sensitivity of the gain of the VOR with respect to the head oscillation frequency. Y axis corresponds to the value of the compensation index for the VOR component of the eye command (see Fig. II-2, panel B). The gray box corresponds to the feasible domain for CI^V values. The right boundary of the gray box corresponds to the limit for which CI^V is bigger than 0 (sensitivity<-0.365). The dashed lines correspond to the 95% confidence intervals on the compensation index of the VOR component of the eye command. The vertical dashed line corresponds to the prediction that we can make if we use the data from (Barnes, 1993).

analyses to test whether the eye-in-head position, the head-in-space position or the relative position of the flash with respect to the direction of the ongoing movement could significantly influence the compensation index. We found no statistically significant influence of those parameters on the compensation index.

4

Discussion

In this study, we examined how visual constancy is maintained during head-unrestrained smooth pursuit. We found that during head-unrestrained pursuit, similar mechanisms are in play to those during head-restrained conditions. However, our data revealed a difference in the compensation gain for smooth eye displacements and head movements. Dividing the smooth eye displacements into smooth pursuit commands and VOR-related components, we estimated an interval for the rate of change of the VOR gain with respect to head movement frequency.

1 Compensation for smooth gaze displacements

We found that when subjects were asked to look at a briefly flashed target presented during head-unrestrained smooth pursuit, the brain was able to compensate for the smooth gaze movements that occurred during the saccadic latency period. Our analyses suggest that the general mechanisms of compensation for smooth eye displacements are similar to those observed in head-restrained conditions (Blohm et al., 2003, 2005b, 2006); hence, short latency gaze saccades were better correlated with retinal error at the flash presentation whereas long latency gaze saccades were better correlated with the spatial error at saccade onset (see figure 7, panels A and B). We found that the compensatory mechanism reached a plateau of $\sim$62% of smooth gaze displacement compensation after about 400 [ms]. This was comparable to results previously reported during head-restrained pursuit (Blohm et al., 2005b). Those results indicated that the brain needs time to integrate eye and head displacements during the latency period. This finding has also been interpreted in the past as evidence for a speed-accuracy tradeoff (Blohm et al., 2005b).

Comparing the degree of compensation for smooth gaze displacements between head-restrained and head-unrestrained conditions, we observed very similar changes in the compensation index as a function of latency. However, a more detailed analysis revealed that on average the brain compensated for different percentages of smooth eye and head displacements, resulting in overall compensation values that largely depended on the contribution of the eye to the overall

smooth gaze displacement. We showed that the eye contribution is independent with respect to the latency and that for each bin of eye contribution, the relationship between latency and compensation remains valid (figure 8B1-3, the longer the latency, the bigger the compensation). It appears clearly that the latency is the predominant parameter that influences the compensation. We can only speculate as to why the compensation gain for head displacements during the latency period was smaller than the gain for smooth eye displacements. One possibility involves the fact that to maintain spatial constancy, the brain has to take into account both eye and head displacements (or compute their absolute position). Wang et al. (2007) showed that there is a proprioceptive representation of the eye-in-head position in area 3a of the somatosensory cortex. They concluded that there are two ways for the central nervous system to assess eye position: a rapid (but more sensitive to noise) corollary discharge and a slower (but more accurate) proprioceptive eye-in-head position in the somatosensory cortex. They proposed that the proprioceptive inputs may be used to calibrate the corollary discharge. As for head position, Blouin et al. (1995, 1998) used passive head rotation to show that the central nervous system has difficulty integrating vestibular signals to maintain spatial constancy. The authors of these studies argued that the CNS is not able to process the vestibular signals while fixating on a target in a head-fixed condition. It seems that, as is the case for eye position, there are two ways for the brain to have access to information about the head position: a fast one (which is noisier (Blouin et al., 1998)) from the semicircular canals, and a slow one using the proprioceptive neck inputs to compute head position. We propose that the brain has two choices linked to this speed-accuracy tradeoff; either it can directly integrate the eye-velocity efference copy and the vestibular signal from the head to plan a gaze saccade, or it can wait until an update of position comes from the proprioceptive inputs. This model could explain the observed speed-accuracy tradeoff. It may seem strange that when the VOR gain is equal to one, any head movement is perfectly compensated by an eye movement while, conversely, the same head velocity signal is not well-integrated during spatial updating. However, we believe that the processing of vestibular information coming from the semi-circular canals is totally different (in that it lasts longer and it is more sensitive to noise) than that of the proprioceptive inputs in the computation of head position (displacement) driving eye movement during the VOR. This could explain why the central nervous system would rely more heavily on the less noisy eye information than on head information to keep spatial constancy, and why we observed a relationship between compensation and eye contribution. However, our data show that, with enough time to accurately compute the head displacement, the effect of EC on the compensation becomes less important. It is important to emphasize that authors have previously shown that vestibular signals are important in maintaining spatial constancy in monkeys (Wei et al., 2006). However, these authors used stationary targets, so the subject has no need of a speed-accuracy tradeoff in order to decrease the influence of an intervening perturbing movement. Therefore, it is difficult to distinguish the relative influence of the proprioceptive and vestibular inputs on the spatial constancy in this case.

Only a few studies have investigated spatial constancy in head-unrestrained conditions. It has been shown (Medendorp and Crawford, 2002; Medendorp et al., 2002a) that humans can (at least in part) update memorized targets across translational head movements between stationary targets. In another study (Medendorp et al., 2002b), subjects were presented with a flashed target after making a torsional rotation of the head while fixating on a central target. The subjects then had to null the head torsion and look at the memorized (and updated) flash position when the fixation target was extinguished. The mean elapsed duration between flash presentation and fixation extinction was around 2 seconds. The authors demonstrated that subjects perfectly compensated for the head torsion. It is difficult to compare the results from these studies to our results for a major reason: in (Medendorp et al., 2002b), subjects had plenty of time to process signals coming from the semi-circular canals and the proprioceptive inputs of the neck. There was no need for subjects to execute the movement quickly because there was no intervening movement acting as a perturbation during the planning of the gaze saccade.

In another study, Vliegen et al. (2005) studied head-unrestrained gaze saccade programming with a dynamic double-step paradigm. However, they only addressed how the saccadic system keeps track of its own movements, whereas we studied its interaction with the smooth pursuit system. Both their and our studies provide converging evidence that the brain uses dynamic retinal and extra-retinal signals to keep track of self-motion.

In this study, we did not account for the 3D retinal geometry when performing our analysis of spatial constancy. Eye rotations can theoretically be executed around any rotational axis. Practically, the torsional component of the eye movement is defined by Listing's law (Tweed et al., 1990). Because of Listing's law, there is a rotational misalignment of retinal and spatial axes for oblique eye-in-head positions (Blohm and Crawford, 2007; Crawford and Guitton, 1997; Tweed et al., 1990). This rotation can yield a supplementary source of error if it is not taken into account by the updating mechanism during the programming of the gaze saccade. To test for a possible influence of the 3D retinal projection geometry on our results, we computed the amount of rotational misalignment for our dataset, its mean (μ=-0.037 [deg]) and its variance (σ^2=0.39 [deg^2]) using a previously described algorithm (Crawford and Guitton, 1997). These values show that in our experiment the effects of 3D projection geometry was negligible compared to the magnitude of SGD. A more specific paradigm that allows the experimenter to obtain a larger range of angular misalignment would be necessary to precisely address the influence of the 3D retinal geometry on the spatial constancy mechanism. Because in our experiment subjects usually oriented their head with respect to the pursuit target using a roll rotation (data not shown), the updating mechanism of the flash position on the retina needs to take into account the torsional part of the eye movement (ocular counter-roll) linked to the rotation of the head along the naso-occipital axis. It has been shown that passive (Klier et al., 2006) and active (Medendorp et al., 2002b) head roll rotations (and the accompanying ocular counter-roll) are taken into account during spatial updating of memorized targets. Based on these findings, we postulate that the torsional component of the

eye movement shares the same properties for the integration as the horizontal and vertical components; the longer the latency, the bigger the compensation.

In a study involving head-unrestrained tracking and gaze saccades, Herter and Guitton (1998) used a one-dimensional paradigm in which they first presented a flashed target while the subject was fixating on another target. Then subjects tracked a moving target with a combined eye-head movement. When the pursuit target extinguished, they had to look at the memorized (and updated) position of the flash. The authors of this study showed that subjects were able to accurately integrate smooth gaze displacements and update the memorized flash position to produce spatially accurate behavior.

2 VOR gain consideration

With a more detailed expression of the compensation index, we were able to make some predictions about the sensitivity of the VOR gain to the active head oscillation frequency. Our results suggest that the VOR gain is more sensitive to the head oscillation frequency during active head movement than during passive head rotations (Barnes, 1993). Our predictions present supplementary evidence that there are major differences between an active and a passive head movement on the modulation of the VOR gain.

To stabilize gaze, the central nervous system needs to evaluate the head velocity and must dissociate an active head movement (during which the VOR must be negated and thus not be counterproductive) and a passive head movement (during which the VOR must be active to stabilize the gaze). The inputs used to evaluate head velocity are different in the present paper than in (Barnes, 1993). During the chair rotations employed in the previous study (Barnes, 1993), only the semi-circular canals relay information about the head velocity. In contrast, during our head-unrestrained active movements, at least two sources are available to evaluate the head velocity; the output of the semicircular canals (proportional to the head-in-space velocity) and the proprioceptive discharge of the neck muscles (proportional to the head-on-trunk velocity). The difference in evaluation of the head velocity between the two cases may be an explanation of the important sensitivity of the gain of the VOR to the active head oscillation frequency.

In a series of experiments, (Roy and Cullen, 2004) showed the importance of dissociating active and passive components of head movement in understanding how the discharge of neurons in the vestibular nuclei is modulated. These authors proposed an expression that integrates the head-on-trunk and the head-in-space velocity to account for the discharge of vestibular neurons.

Making a parallel with the observations of (Roy and Cullen, 2004), we propose a mechanism to explain the differences between (Barnes, 1993) and our predictions. The sensitivity of the gain of the VOR to head oscillation frequency observed here may correspond to the active component of the firing rate modulation expression proposed by Roy and Cullen (2004). In contrast, (Barnes, 1993) observed the sensitivity of the gain to only the passive component of the expression.

Our result indicating that the gain of the VOR is less sensitive to passive head velocity than to active head velocity seems to be reasonable. Generally, a passive head movement acts as a perturbation for the gaze and must be negated to keep the gaze stable. Thus, it appears that the VOR gain must not be overly sensitive to variations in the passive head oscillation frequency. Conversely, an active head movement is usually not a perturbation during a gaze movement and therefore should not be negated systematically. During large head-unrestrained saccades, (Cullen et al., 2004; Lefèvre et al., 1992; Tomlinson and Bahra, 1986) showed that the gain of the VOR quickly decreases at the onset of a gaze saccade and rapidly increases before the end of the movement; therefore the VOR is not counterproductive during head-unrestrained saccade. The important sensitivity of the VOR gain during active head movements seems to be related to the modulation of the gain of the VOR during head-unrestrained gaze shifts.

Additional experiments will be required to clarify how the VOR component is taken into account by the compensatory mechanism and to validate the proposed difference between active and passive head movements. Those experiments should include a more specific control of the gain of the VOR. This could be done by comparing, for example, the amount of compensation when subjects look at the same targets either on a rotating chair (passive head movement) or while making active head movements like the ones observed in this study.

3 Conclusion

In conclusion, we propose that there is a compensatory mechanism in head-unrestrained 2-D tracking that takes into account the smooth gaze displacement occurring during the latency of a gaze saccade, similar to that of a head-restrained condition. In both conditions, the central nervous system needs some time to integrate the displacement. This integration time produces two different strategies; either the movement is realized as quickly as possible and only relies on retinal error at flash presentation (thus giving rise to an inaccurate gaze saccade), or the central nervous system takes the time to integrate the displacement realized during the latency and execute a more accurate gaze saccade. If the first saccade was inaccurate, we generally observed a second (or even a third) gaze saccade which reduced the error. We also observed a relation between compensation and eye contribution; the larger the eye contribution, the greater the compensation. To explain this relationship, we proposed a simple model (see Fig. II-2, panel B) and showed that the gain of the VOR must change as a function of head oscillation frequency (see Equation (20)). From this link between head oscillation frequency and eye contribution, we deduced a relationship between head oscillation frequency and compensation of the smooth gaze displacement.

References

Angelaki, D. E. and Cullen, K. E. (2008). Vestibular system: the many facets of a multimodal sense. *Annu Rev Neurosci*, 31:125–150.

Barnes, G. R. (1993). Visual-vestibular interaction in the control of head and eye movement: the role of visual feedback and predictive mechanisms. *Prog Neurobiol*, 41(4):435–472.

Basseville, M. and Nikiforov, I. V. (1993). *Detection of abrupt changes: theory and application*. Prentice-Hall, Inc., Upper Saddle River, NJ, USA.

Berthoz, A., Israël, I., Georges-Franois, P., Grasso, R., and Tsuzuku, T. (1995). Spatial memory of body linear displacement: what is being stored? *Science*, 269(5220):95–98.

Blohm, G. and Crawford, J. D. (2007). Computations for geometrically accurate visually guided reaching in 3-d space. *J Vis*, 7(5):4.1–422.

Blohm, G., Missal, M., and Lefèvre, P. (2003). Interaction between smooth anticipation and saccades during ocular orientation in darkness. *J Neurophysiol*, 89(3):1423–1433.

Blohm, G., Missal, M., and Lefèvre, P. (2005a). Direct evidence for a position input to the smooth pursuit system. *J Neurophysiol*, 94(1):712–721.

Blohm, G., Missal, M., and Lefèvre, P. (2005b). Processing of retinal and extraretinal signals for memory-guided saccades during smooth pursuit. *J Neurophysiol*, 93(3):1510–1522.

Blohm, G., Optican, L. M., and Lefèvre, P. (2006). A model that integrates eye velocity commands to keep track of smooth eye displacements. *J Comput Neurosci*, 21(1):51–70.

Blouin, J., Gauthier, G. M., van Donkelaar, P., and Vercher, J. L. (1995). Encoding the position of a flashed visual target after passive body rotations. *Neuroreport*, 6(8):1165–1168.

Blouin, J., Labrousse, L., Simoneau, M., Vercher, J. L., and Gauthier, G. M. (1998). Updating visual space during passive and voluntary head-in-space movements. *Exp Brain Res*, 122(1):93–100.

Bracewell, R. (2000). *The fourier transform & its applications 3rd Ed.*

Carpenter, R. H. and Williams, M. L. (1995). Neural computation of log likelihood in control of saccadic eye movements. *Nature*, 377(6544):59–62.

Crawford, J. D. and Guitton, D. (1997). Visual-motor transformations required for accurate and kinematically correct saccades. *J Neurophysiol*, 78(3):1447–1467.

Cullen, K. E., Huterer, M., Braidwood, D. A., and Sylvestre, P. A. (2004). Time course of vestibuloocular reflex suppression during gaze shifts. *J Neurophysiol*, 92(6):3408–3422.

de Brouwer, S., Demet, Y., Blohm, G., Missal, M., and Lefèvre, P. (2002a). What triggers catch-up saccades during visual tracking ? *Journal of Neurophysiology*, 87:1646–1650.

de Brouwer, S., Missal, M., Barnes, G., and Lefèvre, P. (2002b). Quantative analysis of catch-up saccades during sustained pursuit. *Journal of Neurophysiology*, 87:1772–1780.

de Brouwer, S., Missal, M., and Lefèvre, P. (2001). Role of retinal slip in the prediction of target motion during smooth and saccadic pursuit. *J Neurophysiol*, 86(2):550–558.

Diks, C. and Manzan, S. (2002). Tests for serial independence and linearity based on correlation integrals. Stud Nonlinear Dynam Economet 6: Article 2.

Hallett, P. E. and Lightstone, A. D. (1976a). Saccadic eye movements to flashed targets. *Vision Res*, 16(1):107–114.

Hallett, P. E. and Lightstone, A. D. (1976b). Saccadic eye movements towards stimuli triggered by prior saccades. *Vision Res*, 16(1):99–106.

Herter, T. M. and Guitton, D. (1998). Human head-free gaze saccades to targets flashed before gaze-pursuit are spatially accurate. *J Neurophysiol*, 80(5):2785–2789.

Israël, I., Grasso, R., Georges-Francois, P., Tsuzuku, T., and Berthoz, A. (1997). Spatial memory and path integration studied by self-driven passive linear displacement. i. basic properties. *J Neurophysiol*, 77(6):3180–3192.

Klier, E. M. and Angelaki, D. E. (2008). Spatial updating and the maintenance of visual constancy. *Neuroscience*.

Klier, E. M., Angelaki, D. E., and Hess, B. J. M. (2005). Roles of gravitational cues and efference copy signals in the rotational updating of memory saccades. *J Neurophysiol*, 94(1):468–478.

Klier, E. M., Hess, B. J. M., and Angelaki, D. E. (2006). Differences in the accuracy of human visuospatial memory after yaw and roll rotations. *J Neurophysiol*, 95(4):2692–2697.

Krauzlis, R. J. and Miles, F. A. (1996). Decreases in the latency of smooth pursuit and saccadic eye movements produced by the "gap paradigm" in the monkey. *Vision Res*, 36(13):1973–1985.

Lanman, J., Bizzi, E., and allum, J. (1978). The coordination of eye and head movement during smooth pursuit. *Progress in Brain Research*, 153:39–53.

Lefèvre, P., Bottemanne, I., and Roucoux, A. (1992). Experimental study and modeling of vestibulo-ocular reflex modulation during large shifts of gaze in humans. *Exp Brain Res*, 91(3):496–508.

McKenzie, A. and Lisberger, S. G. (1986). Properties of signals that determine the amplitude and direction of saccadic eye movements in monkeys. *J Neurophysiol*, 56(1):196–207.

Medendorp, W., Vin Gisbergen, J., and Gielen, C. (2002a). Human gaze stabilization during active head translations. *Journal Of Neurophysiology*, 87:295–304.

Medendorp, W. P. and Crawford, J. D. (2002). Visuospatial updating of reaching targets in near and far space. *Neuroreport*, 13(5):633–636.

Medendorp, W. P., Smith, M. A., Tweed, D. B., and Crawford, J. D. (2002b). Rotational remapping in human spatial memory during eye and head motion. *J Neurosci*, 22(1):RC196.

Ronsse, R., White, O., and Lefèvre, P. (2007). Computation of gaze orientation under unrestrained head movements. *Journal of Neuroscience Methods*, 159:158–169.

Roy, J. E. and Cullen, K. E. (2002). Vestibuloocular reflex signal modulation during voluntary and passive head movements. *J Neurophysiol*, 87(5):2337–2357.

Roy, J. E. and Cullen, K. E. (2004). Dissociating self-generated from passively applied head motion: neural mechanisms in the vestibular nuclei. *J Neurosci*, 24(9):2102–2111.

Sauter, D., Martin, B. J., Renzo, N. D., and Vomscheid, C. (1991). Analysis of eye tracking movements using innovations generated by a kalman filter. *Med Biol Eng Comput*, 29(1):63–69.

Schlag, J. and Schlag-Rey, M. (2002). Through the eye, slowly: delays and localization errors in the visual system. *Nat Rev Neurosci*, 3(3):191–215.

Schlag, J., Schlag-Rey, M., and Dassonville, P. (1990). Saccades can be aimed at the spatial location of targets flashed during pursuit. *J Neurophysiol*, 64(2):575–581.

Tomlinson, R. D. and Bahra, P. S. (1986). Combined eye-head gaze shifts in the primate. ii. interactions between saccades and the vestibuloocular reflex. *J Neurophysiol*, 56(6):1558–1570.

Tweed, D., Cadera, W., and Vilis, T. (1990). Computing three-dimensional eye position quaternions and eye velocity from search coil signals. *Vision research*, 30(1):97–110.

Vliegen, J., Grootel, T. J. V., and Opstal, A. J. V. (2005). Gaze orienting in dynamic visual double steps. *J Neurophysiol*, 94(6):4300–4313.

Wang, X., Zhang, M., Cohen, I. S., and Goldberg, M. E. (2007). The proprioceptive representation of eye position in monkey primary somatosensory cortex. *Nat Neurosci*, 10(5):640–646.

Wei, M., Li, N., Newlands, S. D., Dickman, J. D., and Angelaki, D. E. (2006). Deficits and recovery in visuospatial memory during head motion after bilateral labyrinthine lesion. *J Neurophysiol*, 96(3):1676–1682.

Part III

Behavioral study: Head-unrestrained tracking of two-dimensional periodic target

Summary

To track an object during everyday life activities, humans use coordinated eye and head movements. In this study, we examined subjects' behavior when they tracked periodic two-dimensional oscillating targets with the head free to move. Our analyses revealed that the gaze tracking gain was modulated by both the target oscillation frequency and the target orientation. With an increase of the target frequency, the pursuit gain decreased and the gaze lag increased with respect to the target. As for a pursuit movement in head-restrained condition, our results showed that the gain of the pursuit was also modulated by the orientation of the target: the vertical pursuit being less accurate than the horizontal pursuit. If the sensitivity to target frequency and orientation was clear for the gaze, the head behavior was less modulated by a change of target frequency than by a change of target orientation. Our results also showed that subjects had two main strategies to move their head: they promoted either horizontal or vertical head rotations, but they rarely used combined rotations.

In the second part of the study, we analyzed the initiation of head-unrestrained pursuit. The gaze had a latency of 100 [ms] and the head started to move 50 [ms] later. Remarkably, the head kinematics during the first 200 [ms] following head movement onset was insensitive to the target parameters (frequency, amplitude, velocity). The majority of the saccades were triggered with a large retinal slip and a small position error. The importance of the retinal slip in our protocol is also demonstrated by the higher variability explained by a regression linking saccades amplitude and retinal slip at the saccade onset than by a regression linking saccades amplitude and position error at the saccade onset.

1

Introduction

During everyday life, human beings track moving targets with combined eye-head movements (called gaze movements, gaze = eye-in-space = eye-in-head + head-in-space) to keep the object of interest on the highest resolution zone of the retina: the fovea. Two categories of movements are used to ensure clear vision while tracking an object: pursuit and saccadic movements. The main purpose of pursuit is to compensate for any gaze-target velocity mismatch. Saccades cancel any position error between the moving object and the gaze. With the head fixed, both saccadic (e.g. (Dodge, 1903; Bahill et al., 1975; Becker and Jürgens, 1990)) and pursuit systems (e.g. (Dodge, 1903; Kettner et al., 1996; Rottach et al., 1996; Leung and Kettner, 1997)) have been initially studied as two separate systems acting independently.

This simplistic view of two distinct controllers, one solely influenced by target position and the other only influenced by target velocity has been proven to be wrong later. By stabilizing the target on the retina during an ongoing pursuit movement, Pola and Wyatt (1980) were the first to demonstrate the influence of the retinal position error on the pursuit behavior in head-restrained condition. Those results were confirmed later either with the same technique (Morris and Lisberger, 1987) or by looking at the open-loop part of the pursuit movement, during the first 100 [ms] of pursuit initiation (Carl and Gellman, 1987). Finally, to demonstrate the existence of a direct position input to the pursuit system in head-restrained condition, Blohm et al. (2005a) used a 2-D paradigm that allowed them to separate velocity and position information during a sustained pursuit movement. In their protocol, a second target was flashed while subjects pursued a first target. Approximately 85 [ms] after the flash presentation, a smooth eye movement occurred perpendicularly to the trajectory of the moving target (Blohm et al., 2005a). The velocity of this smooth eye movement was proportional to the position of the flash on the retina (Blohm et al., 2005a).

Because the pursuit gain (ratio between eye velocity and target velocity) is usually inferior to one (90% for target velocity up to 80 [deg/s] (Meyer et al., 1985)), the eye would lag behind the target if no correcting movements occurred. To that goal, saccades (called "catch-up saccades") are triggered by the central nervous system. Those saccades cancel the increasing eye position

error during pursuit when the pursuit gain is smaller than one. If the saccadic system only takes into account the retinal error to program catch-up saccades' amplitude, they would not be accurate because of the target displacement during saccades' execution. de Brouwer et al. (2001, 2002b,a) showed that the saccadic system has an eye velocity input to correct saccades' amplitude, and to include the displacement of the target during the programming of the saccadic movements. As a result, the eye movement ends close to the target at the end of the saccade. Therefore, as for the position input to the pursuit system, the saccadic system also incorporates velocity information to program and control accurately saccades' amplitude. A complete review of the saccades-pursuit interactions in head-restrained condition can be found in (Orban de Xivry and Lefèvre, 2007).

All the above studies were conducted in head-restrained condition. If authors studied saccades (e.g. (Tomlinson and Bahra, 1986a,b; Guitton et al., 1990; Freedman and Sparks, 1997; Goossens and Van Opstal, 1997)) and pursuit (e.g. (Lanman et al., 1978; Collins and Barnes, 1999)) with the head free to move, most of the studies did not account for the saccades-pursuit interactions (except (Herter and Guitton, 1998; Daye et al., 2010)). Extending the head-restrained observations of Blohm et al. (2003b,a, 2005b) to head-unrestrained condition, Daye et al. (2010) showed that the saccadic system corrects saccades' amplitude to include the eyes and head movements. Therefore, subjects could accurately reach a target flashed during an ongoing head-unrestrained pursuit movement. This experiment demonstrated that the saccadic system combines eye and head velocities to build an estimate of the gaze velocity. This estimate is used to correct saccades' amplitude hereby ensuring gaze shifts accuracy, as is the case in head-restrained condition.

In parallel, only few studies addressed the problem of eye-head coordination in two dimensions (Goossens and Van Opstal, 1997; Daye et al., 2010), the vast majority used one-dimensional paradigms. Head-unrestrained 2-D paradigms raise difficult issues concerning the coordination of eye and head movements to ensure an appropriate gaze displacement. If usually gaze and head act jointly, it has been shown that they can also have different trajectories while achieving an accurate gaze movement, either during 2-D saccades (Goossens and Van Opstal, 1997) or during 1-D pursuit (Collins and Barnes, 1999). Two-dimensional paradigms allow special combinations of eye and head trajectories that shed light on specific characteristics of the interactions between those segments that could not be extracted from 1-D experiments. Even when the head is fixed, differences have been reported between horizontal and vertical movements. For example, Rottach et al. (1996) compared the pursuit of periodic targets moving either vertically, horizontally or diagonally. They reported a smaller gain for the vertical pursuit than for the horizontal pursuit. Similarly, using 2-D target trajectories generated from Lissajou's curves; Kettner et al. (1996) and Leung and Kettner (1997) showed that the gain of the vertical component of a pursuit movement was smaller than the gain of the horizontal component.

The pursuit system had only been studied in 1-D when the head is free to move (Lanman et al., 1978; Barnes and Grealy, 1992; Collins and Barnes, 1999; Wellenius and Cullen, 2000; Dubrovski and Cullen, 2002). Lanman et al.

(1978) compared the behavior of labyrinthectomized and healthy monkeys when a brake was suddenly applied to the head during head-free tracking. With this procedure, they demonstrated the importance of the vestibular system during head-unrestrained tracking. As for the pursuit in head-restrained condition, Barnes and Grealy (1992) demonstrated that predictive mechanisms are key players during head-unrestrained pursuit of periodic target to ensure an accurate tracking. As mentioned before, if gaze and head movements usually have similar trajectories, they can also be controlled independently. This observation points out a possible separate control for gaze and for head movements (Collins and Barnes, 1999). In the same study, Collins and Barnes (1999) also reported that the pursuit movement was sensitive to target oscillation frequency: the higher the frequency, the lower the pursuit gain and the more the gaze lagged behind the target.

Finally, to our knowledge only two studies looked at the initiation of pursuit in head-unrestrained condition. Those studies used non-periodic target trajectory (Wellenius and Cullen, 2000; Dubrovski and Cullen, 2002). No difference in pursuit latency was found between the head-restrained and the head-unrestrained situations if the initial eye position was held constant (Wellenius and Cullen, 2000). Additionally, the gaze latency was insensitive to the target velocity (Wellenius and Cullen, 2000). However, in both conditions, pursuit latency increased when the initial eye-in-head position was located toward the ipsilateral side of the target. Wellenius and Cullen (2000) also reported that the movement of the head started always 50 [ms] after the initiation of the gaze. Later, Dubrovski and Cullen (2002) compared the kinematics of pursuit movements in head-restrained and head-unrestrained condition. They did not find a significant difference between the behavior if the head was free to move or not.

The present study investigates how the central nervous system coordinates eye and head movements while tracking a periodic target. We also compared the behavior we observed in head-unrestrained condition and the behavior reported with the head fixed. To that goal, we designed a 2-D paradigm in which subjects had to pursue a target moving along a randomly oriented straight trajectory with a sinusoidal velocity. First, the observations of Collins and Barnes (1999) about the head and gaze gains' sensitivity to target frequency will be extended to our 2-D protocol. Then, this study will generalize the head-restrained observations of (Rottach et al., 1996; Kettner et al., 1996; Leung and Kettner, 1997) on the performances of gaze tracking in 2-D to head-unrestrained condition. After we will demonstrate that if the orientation of the gaze trajectory followed precisely the target orientation, the head trajectory was tilted around the roll axis to promote one of two preferred behaviors: horizontal head rotations or vertical head rotations. In a following part of the study, we analyzed the initiation of the pursuit. As reported by Wellenius and Cullen (2000), we will show that the head always lagged behind the gaze at the initiation of the movement and that neither the frequency, the velocity nor the amplitude of the target movement influenced the onset of the gaze. We will demonstrate that the head trajectory during the firsts 200 [ms] of head movement was insensitive to either the frequency or the amplitude of the target. In a last part of the study, we will

show that saccades were mostly triggered when the target velocity was large and when its trajectory was highly linear. Finally, we will show that saccades' amplitude in our paradigm was better correlated with the retinal slip than with the retinal position error, oppositely to the common beliefs that saccades are mainly triggered to cancel the retinal position error.

2

Methods

1 Experimental setup

Human subjects sat 1 [m] in front of a translucent tangent screen in a completely dark room after giving informed consent. None of the eight subjects (4 male, 4 female, aged 22-32 years) had any known oculomotor abnormalities. Three subjects (EM, LA and GA) were completely naïve about oculomotor research and five subjects (GB, DP, CO, GL and SC) were knowledgeable about general oculomotor studies. All procedures were approved by the Université catholique de Louvain ethics committee, in compliance with the Declaration of Helsinki.

The screen spanned ± 40 [deg] of the horizontal and vertical visual field. Two laser spots (0.2 [deg] diameter, red and green) were back-projected onto the screen. A dedicated real-time computer (PXI-8186 RT, National Instruments, Austin, Texas) running LabView (National Instruments, Austin, Texas) controlled the position of the targets (sampled at 1 [kHz]) via mirror-galvanometers (GSI Lumonics, Billerica, LA). Horizontal and vertical eye movements were recorded at 200 [Hz] by a Chronos head-mounted video eye-tracker (Chronos Vision GmbH, Berlin, Germany). Any relative movement between the eye and the Chronos helmet leads to a loss of accuracy of the eye movement recordings and must be avoided. To that goal, a bite bar was mounted onto the Chronos frame to prevent any slippage of the helmet during head movements. Two 3-D optical infrared cameras (Codamotion system, Charnwood Dynamics, Leicestershire, United Kingdom) measured (200 [Hz]) the position of a set of six infrared light-emitting diodes (IREDs) mounted onto the Chronos helmet. The position and the orientation of the head were computed offline from the position of the IREDs.

2 Paradigm

A recording session was composed of eight blocks of twenty-five trials. The paradigm used in this study corresponds to the first part of the paradigm described in (Daye et al., 2010). Briefly; after a 500 [ms] fixation at the center of the screen, the red laser started to move along a randomly oriented straight

line with a sinusoidal velocity at a random frequency ([0.6...1.2] [Hz]) and random amplitude ([20...25] [deg]) for a random duration ([3000...3750] [ms]). Randomizations were sampled in a continuous fashion (uniform distribution) between the specified boundaries. Around the end of the red target motion, a second green target was briefly presented (duration: 10 [ms]) at a random position inside a virtual annulus with an inner radius of 15 [deg] and an outer radius of 30 [deg]. The trial ended with a fixation at the center of the screen for 500 [ms].

Subjects were instructed to track the red target with a combined eye-head movement during the pursuit part of the protocol. As soon as they saw the flash, they had to look at its position. Finally, subjects must maintain the gaze on this position until the appearance of the end-of-trial fixation at the center of the screen. Whereas Daye et al. (2010) analyzed the behavior of the subjects to the presentation of the flash, this study focused on the combined eye-head movements during the tracking of the red oscillating target.

3 Calibration

The calibration procedure has been described in detail in (Daye et al., 2010). In summary, three calibration blocks were performed during a recording session: one at the start of the experiment, one mid-way through the session and one after the last experimental block of trials. The calibration procedure allowed the reconstruction of the gaze (i.e., gaze = eye orientation with respect to a space-fixed reference frame) from the IREDs position and the eye-in-head orientation measured by the Chronos. Gaze and head orientations were computed as described in (Daye et al., 2010).

4 Data analysis

Eye and IREDs positions were stored on a computer hard drive for off-line analysis. All the analysis algorithms were implemented in Matlab (The MathWorks, Natick, MA). Position signals were low-pass filtered (cutoff frequency: 50 [Hz]) by a zero-phase digital filter. Velocity and acceleration were derived using a central difference algorithm on a $\pm$ 10 [ms] window. Data were rotated with respect to target direction at the onset of the movement of the pursuit target (red laser spot). Therefore, each target moved horizontally and started its movement to the right. This normalization induced a new coordinate system; the movement was decomposed into the direction parallel to the pursuit (X-axis in text and figures) and the direction perpendicular to the pursuit (Y-axis in text and figures).

Gaze saccades were detected using a generalized likelihood ratio (GLR) algorithm as in (Daye et al., 2010). Every trial was visually inspected; a manual correction of the detection parameters was applied if a saccade was not detected. All the trials were aligned with respect to the onset of the pursuit target movement. The same data set as the one used in (Daye et al., 2010) was

used for the analyses. However, the present study focused on eye-head coordination during head-unrestrained tracking in 2-D. Therefore, we analyzed the data up to the flash presentation when the pursuit target was still visible at the onset of the flash. Otherwise, we analyzed the data until the extinction of the pursuit target.

We defined the smooth gaze velocity (SGV) as the gaze velocity without saccades. To remove a saccade, a linear interpolation replaced the velocity from 20 [ms] before the gaze saccade onset up to 20 [ms] after the offset of the gaze saccade using a previously described procedure (de Brouwer et al., 2001). This can be done because we assume that the gaze displacement is the sum of saccadic and smooth tracking commands as it has been shown in head-restrained condition (de Brouwer et al., 2001, 2002a).

5 Pursuit parameters

To analyze how subjects combined eye and head movements during head-unrestrained pursuit, we estimated the gain, the frequency (f_{SGV}) and the phase shift between SGV and target velocity. To compute those parameters, we first fitted a sine function on SGV. The fit was computed on the last 1.5 period of the pursuit target to ensure that subjects were not anymore in the initiation phase of pursuit.

$$SGV = A_{SGV}\, sin(2\pi\, f_{SGV}\, t + \varphi_{SGV}) \tag{22}$$

In Eq. (22), A_{SGV} is the estimate of amplitude of the gaze velocity, f_{SGV} is the mean oscillation frequency of the gaze movement and φ_{SGV} is the phase of the velocity fit. A similar fit was computed on target velocity to obtain the amplitude (A_{TV}) and the frequency (f_{TV}) of the target velocity. Then we computed the pursuit gain as:

$$g_p = \frac{A_{SGV}}{A_{TV}} \tag{23}$$

A second interesting parameter to evaluate the pursuit performances is the phase difference (or phase shift) between the target and the gaze. This is not a simple task because the target and gaze frequencies are not strictly equivalent, there is no constant time delay (and therefore no constant phase angle) between the target and the gaze displacements. Therefore, we computed the mean elapsed time between extrema of the target velocity and the corresponding extrema of gaze fit of Eq. (22) for the last 1.5 period of every trial (as a result, we had three extrema). Using this definition, a positive phase corresponds to a lead of the gaze with respect to the target while a negative phase corresponds to a lag of the gaze with respect to the target.

An identical procedure was used on head velocity and head position to compute the equivalent parameters (gain, frequency and phase shift) for the head component of the gaze displacement.

6 Head rotation strategies

Figure III-1, panel A represents four theoretical configurations of head rotation for different target orientations (represented by the red lines in Fig. III-1). In those configurations, subjects align the plane of one of their semicircular canals (SCC) according to the target orientation. In situations 1 and 2, subjects slightly inclined their head around the roll axis. After they tracked the target with a rotation that kept the orientation of the horizontal semicircular canal plane constant. Those configurations optimize the discharge of this canal (head movement represented by the double side arrow on the top of the schematic head for situations 1 and 2 in Fig. III-1). In situations 3 and 4, subjects rotated their head around the interaural axis after a roll of the head to track the target (head movement represented by the double side arrow on the side of the schematic head for situations 3 and 4 in Fig. III-1). This strategy maximizes the discharge of the posterior and the anterior canals. The roll angle is similar in situations 1 and 4 ($H_{Roll,1} = H_{Roll,4}$ in Fig. III-1) and in situations 2 and 3 ($H_{Roll,2} = H_{Roll,3}$ in Fig. III-1). As a result, the difference between situations 1 (2) and 4 (3) is the direction of the head movement. Thus, studying the amplitude of the head roll could not discriminate between the two strategies.

The following procedure was applied to all the trials to determine which strategies subjects used to track the moving target with their head as a function of the target orientation. At each instant, we computed the head velocity vector, $\vec{\dot{H}}(t)$ (represented by the double-sided black arrows in Fig. III-1). We also computed the vector that linked the two ocular globes ($\vec{E}(t)$). Then we computed the absolute value of the cross product between the two vectors and called it δ, the strategy index:

$$\delta(t) = abs \left| \frac{\vec{E}(t) \times \vec{\dot{H}}(t)}{\|\vec{E}(t)\| \, \|\vec{\dot{H}}(t)\|} \right| \tag{24}$$

Finally, to evaluate the strategy used by the subject during the pursuit maintenance, we computed the mean value of $\delta(t)$ during the last period of tracking ($\bar{\delta}$). In situations 1 and 2 of Fig. III-1, panel A, the relative distance between the two lines is minimum (ideally $\bar{\delta}$ =0) while in situations 3 and 4 the distance is larger and close to the maximum (ideally $\bar{\delta}$ =1). Panels B1-B2 in figure III-1 represent the value of the strategy index as a function of the head roll for vertical (panel B1) and horizontal (panel B2) head rotations. It appears clearly that for the same head roll, there are different values of the strategy index as a function of the orientation of the head rotations.

7 Relative onset time

Because in our paradigm the pursuit target frequency varied on a trial basis, it was impossible to use the saccade latency with respect to the initiation of the pursuit to study the strategies used by the subjects to trigger a saccade. Thus we computed the relative onset of every saccade by normalizing the latency of

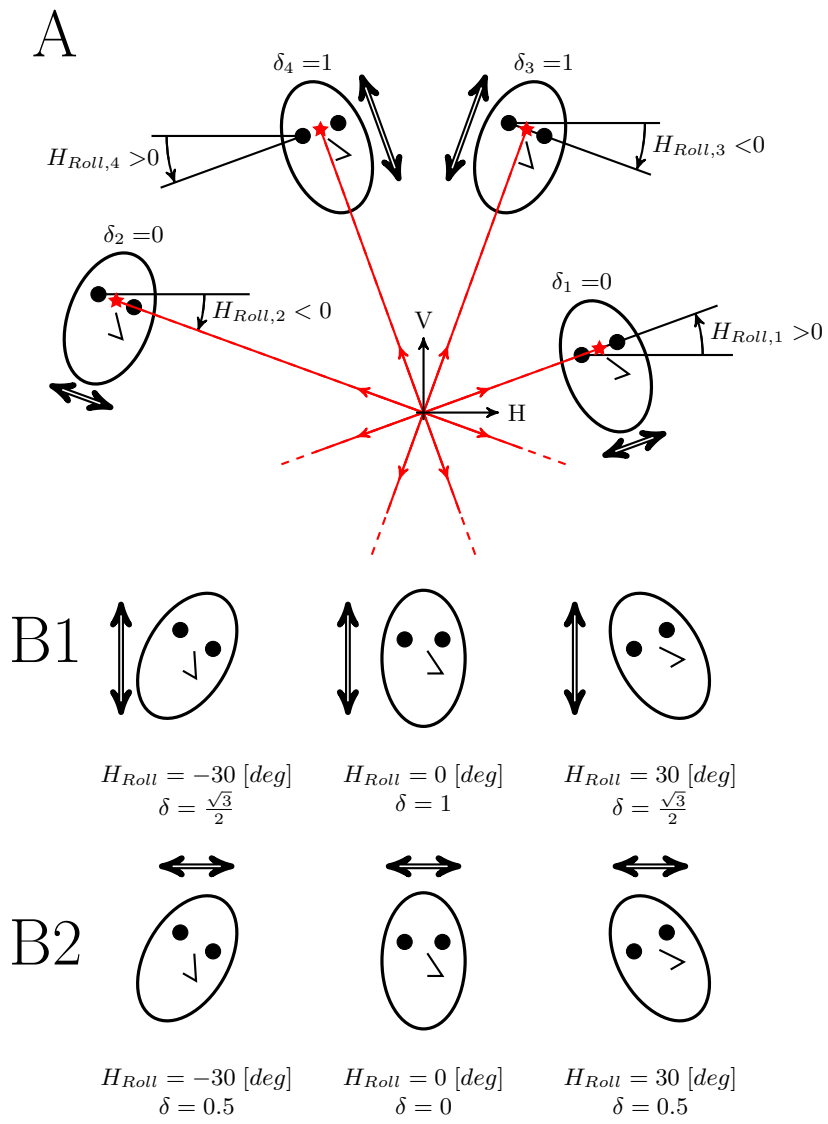

Fig. III-1: **Head configurations during head-unrestrained tracking.** This figure represents four theoretical situations linked to the strategy of head rotations used by the subjects. The head roll is similar in situations 1 and 4 and in situations 2 and 3. Red lines represent the orientation of the target movement. The double side black arrows represent the direction of the head movement. δ_i correspond to the strategy index. Panel B1 represents the evolution of the strategy index as a function of the head roll for vertical head rotations. Panel B2 represents the same evolution but for horizontal head rotations. See text for more details.

the saccade (L_{ON}) by the frequency of the pursuit target (f_T). Additionally, because the stimulus was periodic, we used the modulo operator (mod in Eq. (25)) to ensure that each saccade had a relative onset time inside a $[0 \ldots 1]$ range.

$$L_{ON,\,REL} = L_{ON}\, f_T \; (mod\; 1) \tag{25}$$

8 Additional saccade parameters

As in the studies of de Brouwer et al. (2001, 2002a,b), we computed for each gaze saccade the position error (PE_{ON}) and the retinal slip (RS_{ON}) at the saccade onset. Usually, position error (retinal slip) is computed using the difference between target position (velocity) and gaze position (velocity). Therefore, a positive error corresponds to a gaze lagging behind the target and a negative error corresponds to a gaze in advance with respect to the target. Because in our paradigm the target movement was periodic, the interpretation of the sign of position error (retinal slip) is different depending on the velocity of the target. A positive PE could correspond to either a lag (with target velocity$>$0) or an advance of the gaze with respect to the target (with target velocity$<$0). The same kind of reasoning can be applied for the interpretation of retinal slips. Therefore to have a consistent interpretation, the sign of PE_{ON} and RS_{ON} were corrected using:

$$PE_{ON,\,CORR} = PE_{ON}\, sign(\dot{T}_{ON}) \tag{26}$$

$$RS_{ON,\,CORR} = RS_{ON}\, sign(\dot{T}_{ON}) \tag{27}$$

9 Collected data set

We collected 6533 trials out of which 5748 were valid trials (88%). We removed trials from analysis if during the pursuit movement IREDs were out of sight for a camera (2%) or if the subject used only saccades or did not track the target (10%). Every trial was visually inspected. 40373 saccades were detected by the GLR algorithm and analyzed in this article.

3

Results

This study had two goals: the first one was to analyze the strategies used by human subjects to track a periodic 2-D target with combined eye-head movements. The second goal was to understand how saccadic and pursuit systems interacted to ensure an accurate tracking of the target.

We will first present two typical trials, and then analyze how the parameters of the moving target (frequency, amplitude) influenced both the tracking performances and the coordination of eye and head during the maintenance of the pursuit. Then we will show that the target orientation influenced the pursuit performances. We will demonstrate that the initiation of the pursuit was stereotyped: the gaze onset latency was not modulated by the amplitude or the frequency of the target and the head movement always started to move after the gaze. Additionally, the analysis of the first 200 [ms] of the head trajectory revealed that the initiation of the head movement was insensitive to a modification of the target parameters. In a final part, we will show that the saccades were mainly triggered when the target velocity was the highest and therefore when the target trajectory was the most linear. Finally, we will show that saccade amplitude was better correlated with the retinal slip than with the position error, demonstrating the importance of the interactions between the pursuit and the saccadic systems.

1 Typical trials

Figure III-2 shows the tracking behavior of a subject (GA) when a target oscillating at a low-frequency (target pursuit frequency = 0.66 [Hz]) and with an amplitude of 20.41 [deg] was presented. Figure III-2, panel A shows the time course of target (red lines), gaze (thin black lines), eye-in-head (green lines) and head (grey lines) positions along the direction parallel to the pursuit (X, first row) and the direction perpendicular to the pursuit (Y, second row). Figure III-2, panel A represents the evolution of target, gaze, head and eye-in-head velocities as a function of time (same color convention as in Fig. III-2, panel A) along a direction parallel to the pursuit ($\dot{X}$, Fig. III-2, panel B). Because the main displacement occurred along a direction parallel to the pursuit direction

(compare first and second rows of Fig. III-2, panel A), we only represented the velocity along this direction in Fig. III-2, panel B. Bold lines in Fig. III-2

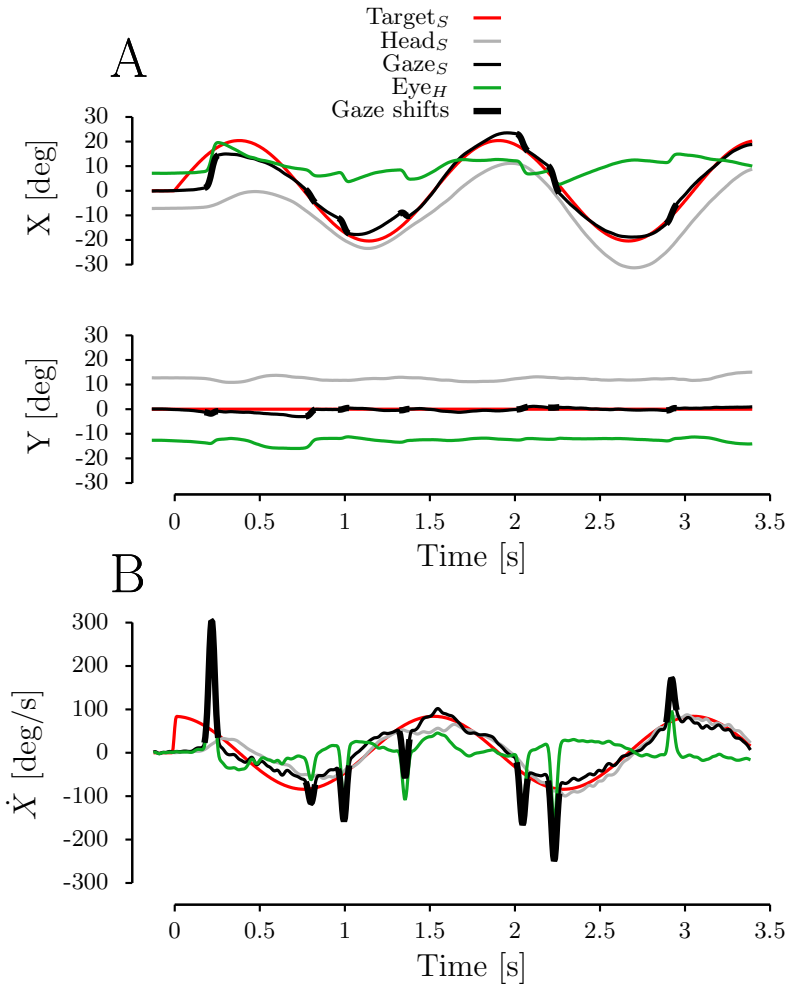

Fig. III-2: **Typical low frequency trial.** Panel A represents the time course of target (red line), gaze (thin black lines), eye-in-head (green line) and head (gray line) position. X represents the direction parallel to the pursuit. Y represents the direction perpendicular to the pursuit. Panel B represents the evolution of target, gaze, eye-in-head and head horizontal velocity ($\dot{X}$) as a function of time. Same color convention as in panel A. Thick black lines represent gaze shifts. Time origin set to the initiation of the target movement.

represent gaze saccades. As shown in Fig. III-2, the subject initially looked at the fixation target with the head oriented up to the left. The gaze movement started with a saccade (latency with respect to initiation of target motion = 180

[ms]) followed by the beginning of the gaze tracking. After the first saccade, the gaze velocity quickly matched the target velocity (approximately after a half-period, 750 [ms]). From this moment until the end of the trial, a gaze saccade was triggered if the gaze velocity was either too low (e.g., third saccade) or too high (e.g., fourth saccade). A mismatch between the gaze and the target velocity created a gaze position error that must be corrected to have an accurate gaze displacement. During the gaze pursuit initiation, the eye made the main part of the gaze displacement while the head, slower than the eye, started its movement with at first a phase difference with respect to the target. After a first target cycle (around 1.5 [s]), head and target velocities had similar amplitudes with a phase lag of (31.2± 7.5) [ms]. As expected, when the head was not on the target, the gaze trajectory was corrected by an eye movement, either through a change of the eye-in-head velocity (e.g., see eye-in-head acceleration around 1.5 [s] after the fourth saccade) or with a saccade. Additionally, as Fig. III-2, panel B shows, the majority of the saccades were triggered around the velocity extrema.

The second trial, represented in Fig. III-3, shows the tracking behavior of another subject (DP) when a high frequency oscillating target (target frequency = 1.12 [Hz]) with a 27.2 [deg] amplitude was presented (same color convention as in Fig. III-2). Panel A represents the evolution as a function of time of target, gaze, eye-in-head and head positions along a direction parallel to the pursuit direction (X, first row) and along a direction perpendicular to the pursuit direction (Y, second row). Panel B represents the time course of the target, gaze, eye-in-head and head velocities along a direction parallel to the pursuit direction ($\dot{X}$, Fig. III-3, panel B). In this trial, the subject initially looked at the fixation target with the head slightly rotated leftward. As the first trial, the gaze movement started with a saccade toward the pursuit target (latency with respect to initiation of target movement = 157 [ms]). The initial saccade ended close to the target, but the gaze velocity did not match the target velocity yet. Thus, a second saccade was triggered to cancel the remaining position error. Even after the initiation phase (approximately after one cycle of target motion = 1 [s]), the movement was in steady-state phase. Nevertheless, oppositely to the first trial in Fig. III-2, the gaze velocity in Fig. III-3 remained smaller than the velocity of the target for the rest of the trial. As a result, several saccades were triggered to compensate for the position error induced by the slower pursuit component of the gaze. As for the trial of Fig. III-2, the saccades were triggered around the velocity extrema. It can also be observed in Fig. III-3 that the head started its movement slowly compared to the target velocity. After a cycle of the target motion (around 1 [s]), the head movement was in a stationary phase. As for the preceding trial, the head velocity was close to the target velocity, and the head lagged behind the target by (25.9± 3.1) [ms]. Comparing the first typical trial (Fig. III-2) and the second one (Fig. III-3), it appears that the mean gaze velocity was smaller than the head velocity for the second trial and fairly similar to the head velocity for the first one.

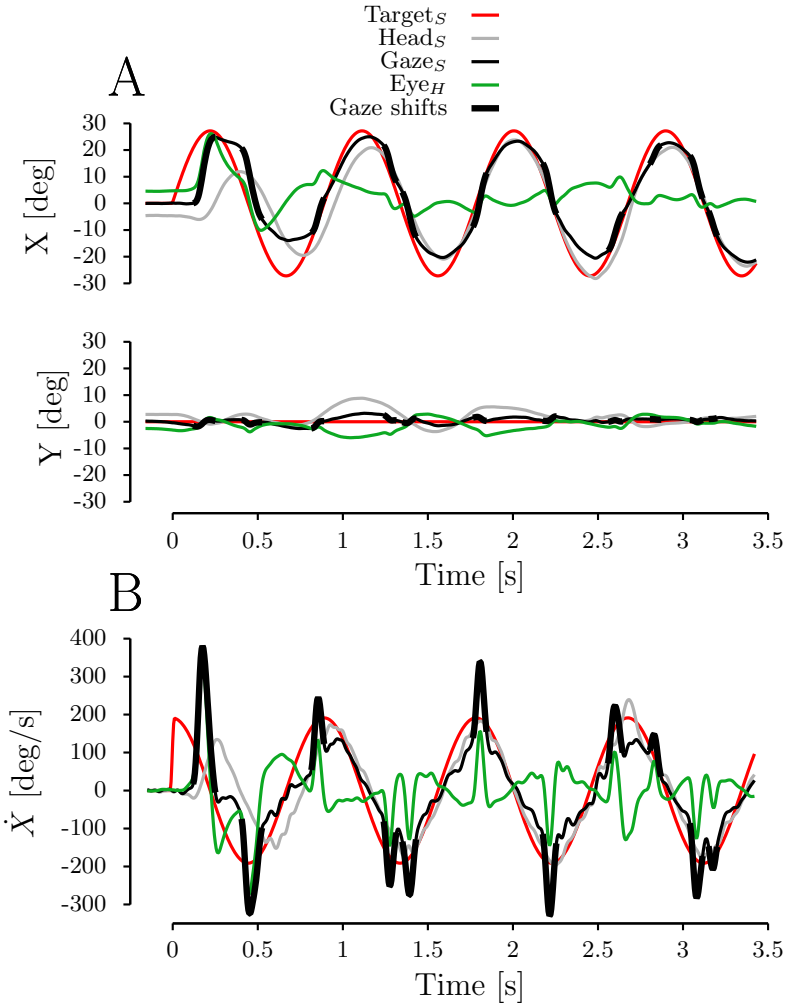

Fig. III-3: **Typical high frequency trial.** Same conventions as in Fig. III-3. Panel A, upper row: X evolution as a function of time for target, gaze, eye-in-head and head. Panel A, lower row: Y evolution as a function for the same signals. Panel B: X velocity as a function of time for the same signals as panel A.

2 Head and gaze tracking performances

As shown by the typical trials, target frequency appears to play an important role on the performances of the gaze tracking and have apparently less impact on the head trajectory. To quantify this observation, we first studied the evolution of pursuit parameters (amplitude, frequency and phase shift) as a function of the target oscillation frequency for gaze and head trajectories.

Figure III-4, panel A represents the gaze tracking gain (g_G, left column) and the head tracking gain (g_H, right column) as a function of the target oscillation frequency (f_T) for all the valid trials. Those gains were computed, as explained in the methods, as the ratio between the amplitudes of the gaze (head) velocity fit and the target velocity. Figure III-4, panel A clearly shows that, with an increase of the target oscillation frequency, there is a large decrease of the gaze tracking gain. However, as observed in the typical trials, the target frequency appears to have less influence on the gain of the head movement. Linear regressions provided the following results:

$$g_G = (-0.73 \pm 0.02)\ f_T + (1.27 \pm 0.01)\,,\ \ vaf = 0.404,\ P < 0.001 \quad (28)$$

$$g_H = (-0.13 \pm 0.02)\ f_T + (0.85 \pm 0.02)\,,\ \ vaf = 0.011,\ P < 0.001 \quad (29)$$

As expected from the observations of the typical trials and shown by regressions (28) and (29), there was a strong influence of the target frequency on the gaze tracking gain and a small effect on the gain of the head movement (compare vaf of both regressions). A t-test confirmed statistically the steeper slope of the gaze regression (thus the bigger effect of the target frequency) compared to the slope of the head regression (one-tailed t-test, t(5746)=29.37, P<0.001).

The sensitivity of the gaze pursuit gain to the target frequency (slope of regression (28)) was consistent across subjects as shown by the first column of table III-1. The second column of table III-1 shows the mean value of the gaze pursuit gain at 0.6 [Hz]. The sensitivity of the head pursuit gain to the target frequency for each subject is shown in column 3 of table III-1. Finally, the mean head tracking gain at 0.6 [Hz] is given for each subject in column 4 of table III-1. Most of the subjects showed a consistent influence of the target frequency on the head pursuit gain. Only DP and EM did not show a statistically significant influence of the target frequency on the head pursuit gain (P>0.03). GL showed a small positive sensitivity of the target frequency on the head pursuit gain close to the significance level (P=0.053). In parallel, the mean gaze pursuit gain at 0.6 [Hz] was fairly similar between subjects while variations were observed in head tracking gain. This reflects the general disparity between typical head movements, as previously reported (Fuller, 1992).

Fig. III-4 *(following page)*: **Head and gaze pursuit parameters.** Panel A, left (right) column represents the change of the gaze (head) pursuit gain as a function of the target frequency. Panel B, left (right) column represents the change of the gaze (head) frequency as a function of the target frequency. Panel C, left (right) column represents the change of the gaze (head) pursuit phase shift as a function of the target frequency. A positive phase shift corresponds to movements that led the target while negative values correspond to movements that lagged behind the target. Solid black lines represent the change of the mean of the different parameters (gain, frequency and phase shift) for 0.02 [Hz] target frequency bins. The dashed lines represent the change around the mean of the standard deviation for the same target frequency bins. Red lines represent linear fits on the different parameters.

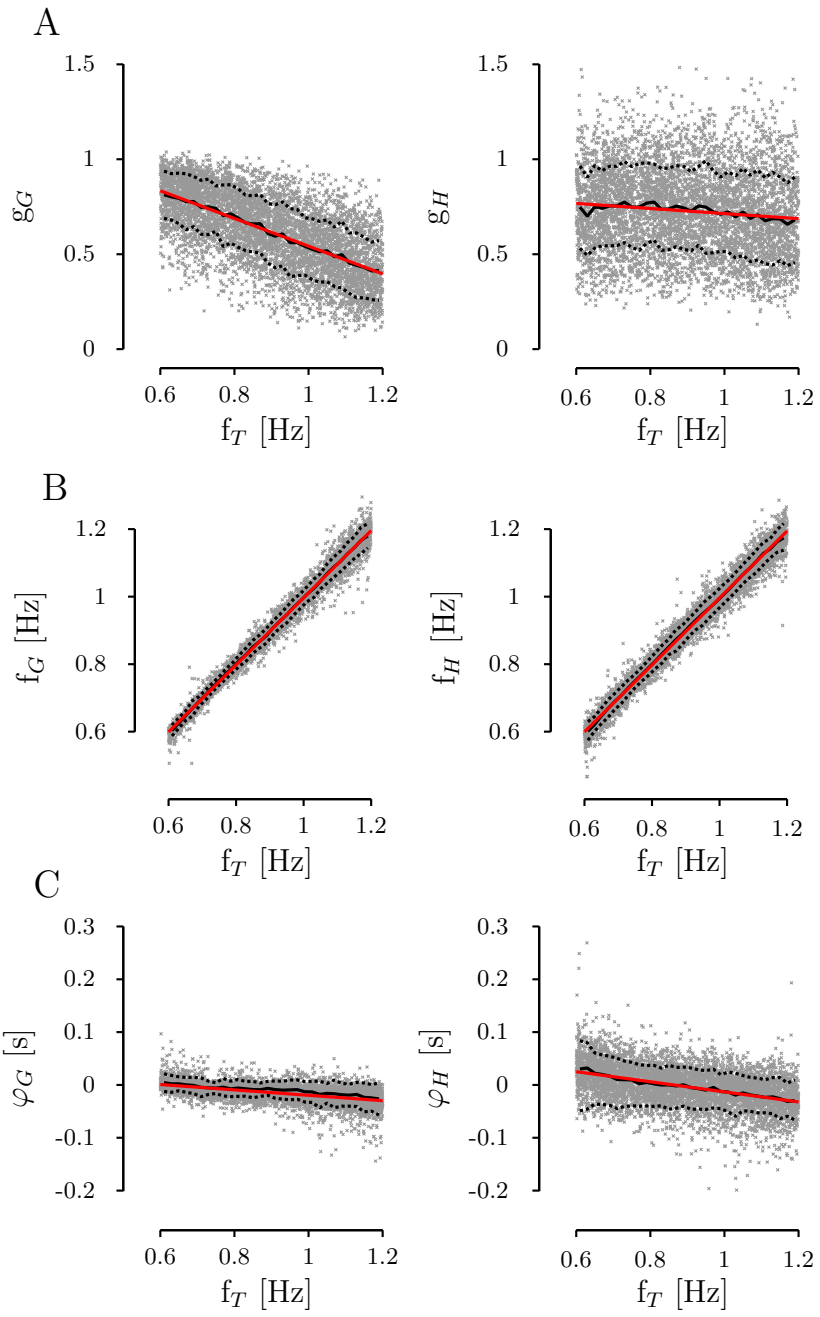
A
1.5
1
0.5
0
g_G
0.6
0.8
1
1.2
f_T [Hz]
g_H
B
1.2
1
0.8
0.6
f_G [Hz]
f_H [Hz]
C
0.3
0.2
0.1
0
-0.1
-0.2
φ_G [s]
φ_H [s]

Table III-1: Gaze and head pursuit gain sensitivity to target frequency ($\frac{\partial g_G}{\partial f_T}$, $\frac{\partial g_H}{\partial f_T}$) and mean gaze and head pursuit gain at 0.6 [Hz] for each subject

Subject	$\frac{\partial g_G}{\partial f_T}$	g_G(0.6 [Hz])	$\frac{\partial g_H}{\partial f_T}$	g_H(0.6 [Hz])
BL	(-0.85± 0.02)	(0.85± 0.08)	(-0.16± 0.03)	(0.71± 0.15)
CO	(-0.76± 0.03)	(0.86± 0.07)	(-0.10± 0.02)	(0.47± 0.14)
DP	(-0.60± 0.02)	(0.93± 0.08)	(-0.03± 0.03)	(0.93± 0.13)
EM	(-0.58± 0.03)	(0.70± 0.12)	(-0.02± 0.03)	(0.68± 0.13)
GA	(-0.77± 0.02)	(0.76± 0.09)	(-0.30± 0.03)	(0.78± 0.14)
GL	(-0.76± 0.03)	(0.83± 0.11)	(0.07± 0.04)	(0.84± 0.20)
LA	(-0.79± 0.03)	(0.73± 0.11)	(-0.17± 0.03)	(0.59± 0.11)
SC	(-0.64± 0.05)	(0.78± 0.04)	(-0.28± 0.05)	(1.04± 0.20)
Mean	(-0.73± 0.02)	(0.81± 0.12)	(-0.13± 0.02)	(0.75± 0.22)

Values are means ± confidence interval at 95%.

A second critical parameter of the movement is the frequency of the gaze and the head movement. A difference in frequency between the target and the gaze quickly led to large tracking errors. Concurrently, a frequency difference between the target and the head movements led to an increase of eye movements to ensure an accurate gaze tracking. Thus we studied the evolution of gaze and head oscillation frequency as a function of the target oscillation frequency. Figure III-4B represents the evolution of the gaze movement oscillation frequency (f_G, left column) and the head movement oscillation frequency (f_H, right column) as a function of the frequency of the oscillating target. As it can be directly observed in Fig. III-4, panel B, the frequency of both the gaze and the head movements were highly correlated with the frequency of the periodic target. Linear regressions gave the following equations:

$$f_G = (0.994 \pm 0.001)\ f_T + (0.003 \pm 0.002)\,, \quad vaf = 0.984,\ P < 0.001 \quad (30)$$

$$f_H = (0.991 \pm 0.002)\ f_T + (0.005 \pm 0.002)\,, \quad vaf = 0.975,\ P < 0.001 \quad (31)$$

Equations (30) and (31) confirm the very strong relationship qualitatively observed in Fig. III-4, panel B between gaze (head) and target oscillation frequencies. A t-test did not show a statistical difference between the two regression slopes (two-tailed t-test, t(5746)=1.153, P=0.164). When comparing the amplitude of the standard error at small frequencies to the amplitude of the standard error at high frequencies, this value increased for the gaze and remained mostly constant for the head (compare the distance between the dashed lines and the red lines Fig. III-4, panel B). To quantify this observation, we computed the standard error of the difference between the target frequency and either the gaze ($f_T - f_G$) or the head ($f_T - f_H$) frequency for bins of target oscillation frequency. Regressions between the target oscillation frequency and the computed standard error:

$$\sigma^2_{(f_T - f_G)} = (0.037 \pm 0.003)\ f_T - (0.012 \pm 0.003)\,, \quad vaf = 0.813,\ P < 0.001 \quad (32)$$

$$\sigma^2_{(f_T - f_H)} = (0.022 \pm 0.003)\ f_T + (0.007 \pm 0.003)\,, \quad vaf = 0.614,\ P < 0.001 \quad (33)$$

A t-test showed that the slope of regression (32) was statistically more significant than the slope of regression (33) (t(28)=3.25, P=0.0015). This confirmed

the observation that the variability of the gaze pursuit frequency with respect to the target oscillation frequency increases more for the gaze than for the head.

First and third columns of table III-2 represent the evolution of the sensitivity of the gaze and the head pursuit frequency to the target frequency for each subject. Second and fourth columns of table III-2 represent the evolution of the gaze and the head pursuit frequency at 0.6 [Hz] for each subject. Every subject showed a high sensitivity of gaze and head frequencies with respect to the target frequency, consistent with the mean behavior of all subjects.

Table III-2: Sensitivity of the gaze and head pursuit frequency to target frequency ($\frac{\partial f_G}{\partial f_T}$, $\frac{\partial f_H}{\partial f_T}$) and mean gaze and head pursuit frequency at 0.6 [Hz] for each subject

Subject	$\frac{\partial f_G}{\partial f_T}$	f_G(0.6 [Hz])	$\frac{\partial f_H}{\partial f_T}$	f_H(0.6 [Hz])
BL	(0.99± 0.004)	(0.61± 0.009)	(1.00± 0.005)	(0.60± 0.022)
CO	(1.00± 0.004)	(0.60± 0.013)	(0.99± 0.005)	(0.61± 0.021)
DP	(0.99± 0.004)	(0.61± 0.008)	(0.98± 0.004)	(0.61± 0.015)
EM	(0.98± 0.006)	(0.58± 0.026)	(1.01± 0.008)	(0.58± 0.052)
GA	(1.01± 0.004)	(0.60± 0.013)	(0.98± 0.006)	(0.61± 0.020)
GL	(1.00± 0.004)	(0.60± 0.013)	(0.98± 0.006)	(0.60± 0.017)
LA	(1.00± 0.005)	(0.61± 0.011)	(1.00± 0.005)	(0.61± 0.013)
SC	(0.97± 0.008)	(0.61± 0.011)	(1.00± 0.009)	(0.60± 0.036)
Mean	(0.99± 0.002)	(0.60± 0.016)	(0.99± 0.002)	(0.60± 0.029)

Values are means ± confidence interval at 95%.

The last parameter we used to quantify the global performances of the tracking system was the phase difference between the gaze and the target movements (φ_G) and between the head and the target movements (φ_H). The phase represents the mean lag (negative phase) or lead (positive phase) of the gaze (head) with respect to the target. The computation of the phase difference is described in the methods. Figure III-4C represents the evolution of the phase of the gaze (left column) and the phase of the head (right column) as a function of the target oscillation frequency. As shown in Fig. III-4, panel C, with an increase of the target oscillation frequency, gaze and head lagged the target more causing a decrease of the phase of both gaze and head with respect to the target. Linear regressions resulted in:

$$\varphi_G = (-0.051 \pm 0.001)\ f_T + (0.031 \pm 0.002)\,,\ \ vaf = 0.248,\ P < 0.001 \quad (34)$$

$$\varphi_H = (-0.096 \pm 0.003)\ f_T + (0.082 \pm 0.002)\,,\ \ vaf = 0.181,\ P < 0.001 \quad (35)$$

Contrary to the more important effect of the target frequency on the gaze tracking gain than on the head gain (see Fig. III-4, panel A), the head phase appears to be more sensitive to the target frequency than the gaze phase. A t-test shows that the slope for the gaze phase was shallower than the slope for the head phase (one-tailed t-test, t(5746)=15.22, P<0.001) pointing toward a bigger effect of the frequency on the head phase than on the gaze phase. Additionally, eq. (34) shows that the gaze is in phase or lags behind the target

in the range of frequencies used in the protocol. A different behavior is observed for the head and reported by eq. (35). For low frequencies, the head leads the target while for high frequencies (f_t >0.854 [Hz]) it lags behind the target. This observation could be evidence that the head and the gaze, even if they track the same target, could be driven separately. This is consistent with the assumption that a common drive, correlated with the gaze displacement, is sent to both eye and head but that the head receives, in addition, an independent drive that is related to an independent goal.

First and third columns in table III-3 represent the sensitivity of the head and the gaze phase shift to the target oscillation frequency for each subject. As shown by the individual regression results, the head phase shift was more sensitive to the head frequency than the gaze phase shift. The effect of the target frequency on gaze and head phase shift was fairly similar across subjects. Only EM appeared to be more sensitive compared to the other subjects to the target oscillation frequency for both head and gaze phases.

Table III-3: Sensitivity to target frequency of the gaze and the head phase shift ($\frac{\partial \varphi_G}{f_T}$, $\frac{\partial \varphi_H}{f_T}$) and mean gaze and head pursuit phase shift at 0.6 [Hz] for each subject

Subject	$\frac{\partial f_G}{f_T}$	f_G(0.6 [Hz])	$\frac{\partial f_H}{f_T}$	f_H(0.6 [Hz])
BL	(-0.013± 0.002)	(0.0040± 0.008)	(-0.120± 0.006)	(0.054± 0.028)
CO	(-0.059± 0.003)	(0.0004± 0.008)	(-0.097± 0.006)	(0.039± 0.041)
DP	(-0.033± 0.002)	(0.0006± 0.009)	(-0.092± 0.005)	(0.029± 0.030)
EM	(-0.120± 0.006)	(0.0160± 0.033)	(-0.170± 0.011)	(0.061± 0.110)
GA	(-0.047± 0.003)	(0.0080± 0.013)	(-0.120± 0.007)	(0.023± 0.034)
GL	(-0.010± 0.003)	(0.0020± 0.009)	(-0.049± 0.006)	(0.027± 0.026)
LA	(-0.031± 0.005)	(0.0005± 0.020)	(-0.031± 0.006)	(-0.011± 0.027)
SC	(-0.035± 0.005)	(0.0024± 0.007)	(-0.076± 0.007)	(0.003± 0.03)
Mean	(-0.051± 0.001)	(0.0044± 0.017)	(-0.096± 0.003)	(0.030± 0.053)

Values are means ± confidence interval at 95%.

We also analyzed the pursuit behavior with respect to the maximum velocity of the target. No significant differences were found between the regressions if we used either the frequency or the maximum velocity of the target (two sided f-test. $F(g_G = f(f_T), g_G = f(\dot{T}_M))$, P=0.640; $F(g_H = f(f_T), g_H = f(\dot{T}_M))$, P=0.473; $F(\varphi_G = f(f_T), \varphi_G = f(\dot{T}_M))$, P=0.874; $F(\varphi_H = f(f_T), \varphi_H = f(\dot{T}_M))$, P=0.704). Due to the periodical nature of our paradigm, we chose to keep the frequency of the target as the independent variable for the analyses.

At this stage, we have shown that the frequency of an oscillating target is a critical parameter that determines the tracking performances of a 2-D periodic moving target in head-unrestrained condition. This observation has already been made by others either in head-restrained condition with one-dimensional paradigms (Buizza and Schmid, 1989) or with two-dimensional paradigms (Rottach et al., 1996; Kettner et al., 1996; Leung and Kettner, 1997). In head-unrestrained condition, Collins and Barnes (1999) observed the same behavior

for one-dimensional periodic targets. The analyses generalized their observations to two-dimensional paradigms. However, the variability of the gains as a function of the target oscillation frequency appeared to be larger compared to one-dimensional observations. Therefore, we investigated if the orientation of the moving target had an influence on the head and the gaze pursuit gain. Figure III-5 represents the evolution of the gain of gaze pursuit (upper row) and the gain of head pursuit (lower row) as a function of the orientation of the pursuit target. Because of the symmetry of the pursuit target orientation

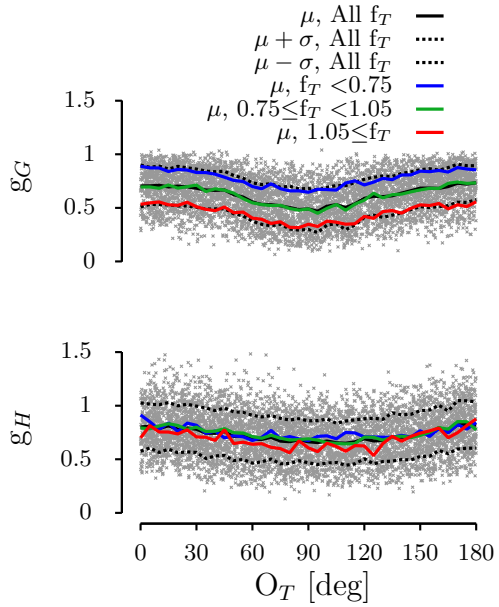

Fig. III-5: **Head and gaze gain as a function of target orientation.** The upper (lower) row represents the evolution of the pursuit gaze (head) gain as a function of the orientation of the moving target. Solid black lines represent the evolution of the mean gaze (head) pursuit gain for 5 [deg] target orientation bins. Dashed black line represents the evolution of the standard deviation around the mean of the gaze (head) pursuit gain for 5 [deg] target orientation bins. Solid blue lines represents the evolution of the gaze (head) pursuit gain as a function of the target oscillation frequency for trials with a target frequency inferior to 0.75 [Hz]. Solid green lines represents the evolution of the mean gaze (head) pursuit gain as a function of the target orientation for trials with a target oscillation frequency comprised between 0.75 and 1.05 [Hz]. Red solid lines represents the evolution of the mean gaze (head) pursuit gain as a function of the target oscillation frequency for trials with target frequency superior to 1.05 [Hz]

around the horizontal axis, we pooled together trials with target orientation between 180 and 360 [deg] with trials with targets' orientation between 0 and 180 [deg]. Solid black line in Fig. III-5, upper row (lower row) represents the

mean of the gaze (the head) pursuit gain for 5 [deg] target orientation bins. Dashed black lines in Fig. III-5, upper row (lower row) represent the evolution of the standard deviation of the gaze (the head) pursuit gain for 5 [deg] target orientation bins around the mean. A modulation of both the gaze and the head pursuit gains appeared when the orientation of the target was modified, even if the sensitivity of the head gain appeared smaller. To quantify this observation, we computed a non-linear fit between the orientation of the targets and the gaze and head gains. As shown by the evolution of the mean in Fig. III-5, a cosine function seemed a good candidate for the function fits. Non-linear regressions resulted in:

$$g_G = (0.113 \pm 0.007)\ cos\left(2\pi\,(0.0055 \pm 0.0001)\ O_T\right) + (0.617 \pm 0.005)\,, \quad vaf = 0.164,\ P < 0.001 \tag{36}$$

$$g_H = (0.078 \pm 0.008)\ cos\left(2\pi\,(0.0052 \pm 0.0002)\ O_T\right) + (0.732 \pm 0.006)\,, \quad vaf = 0.060,\ P < 0.001 \tag{37}$$

Regressions (36) and (37) confirmed the intuition made above: the gain of the head movement is less sensitive to a change of the orientation than the gain of gaze movement (compare both the amplitude of the cosine regressions and the vafs of eq. (36) and (37)).

Finally, to test if the frequency had an impact on the gains modulation with respect to the target orientation, we divided the data into three frequency bins (f_T <0.75 [Hz], 0.65≤ f_T <1.05 [Hz] and f_T ≥1.05 [Hz]). For each frequency bin, we computed the evolution of the mean gaze and head pursuit gains for target orientation bins of 5 [deg]. Lower row of Fig. III-5 demonstrates that the head pursuit gain modulation as a function of the target orientation was insensitive to the target oscillation frequency. Contrarily, Upper row of Fig. III-5 shows that both target orientation and target oscillation frequency influenced the gain of the gaze tracking system. To test this assumption, we computed two multiple non-linear regressions for the head and the gaze pursuit gain with target oscillation frequency and target orientation as independent variables. Regressions resulted in:

$$g_G = (0.110 \pm 0.005)\ cos\left(2\pi\,(0.0056 \pm 0.0001)\ O_T\right) - (0.722 \pm 0.020)\ f_T + (1.263 \pm 0.018)\,, \quad vaf = 0.560,\ P < 0.001 \tag{38}$$

$$g_H = (0.078 \pm 0.008)\ cos\left(2\pi\,(0.0052 \pm 0.0002)\ O_T\right) - (0.128 \pm 0.031)\ f_T + (0.847 \pm 0.029)\,, \quad vaf = 0.070,\ P < 0.001 \tag{39}$$

F-test confirmed that the multiple non-linear regression (38) statistically increased the quality of the fit compared to the non-linear regression (36) (two-tailed f-test, f(5747,5747)=1.899, P<0.001). Finally, a second f-test showed that the multiple non-linear regression (39) did not statistically increase the quality of the fit compared to the non-linear regression (37) (two-tailed f-test, f(5747,5747)=1.011, P=0.675). This analysis confirmed our hypothesis that the head movement was less sensitive to the orientation of the target and to the frequency of the target than the gaze.

3 Head tracking strategies

After this important evaluation of the tracking performances, we will show how the orientation of the target also influenced the strategy used to control the head and gaze movements. Figure III-6, panels A-C show a spatial representation (horizontal-vertical, not normalized) of the target (red lines), the head (gray lines) and the gaze (black lines) trajectory for three different orientations of the pursuit target. To study the stationary phase of the movement, the last 1.5 periods of the movements were represented in Fig. III-6, panel A-C. Figure III-6A shows an oscillating target with a large horizontal component compared to the vertical component (horizontal target amplitude = 22.42 [deg], vertical target amplitude = 5.38 [deg]). The gaze trajectory orientation was very similar to the orientation of the moving target. As it is shown in Fig. III-6, panel A, head displacement was slightly tilted horizontally compared to target trajectory. Figure III-6B1 shows a trial in which horizontal and vertical components of the pursuit target had equivalent amplitudes (horizontal target amplitude = 16.65 [deg], vertical target amplitude = 16.13 [deg]). As for the trial in Fig. III-6, panel A, the gaze trajectory had a very similar orientation compared to the target orientation. However, head trajectory, even if its orientation was tilted more vertically than in Fig. III-6, panel A, remained less steep than the orientation of the target. Figure III-6B1 shows another trial in which horizontal and vertical components of the pursuit target had similar amplitudes (horizontal target amplitude = 18.55 [deg], vertical target amplitude = 18.87 [deg]). In contrast to the head trajectory in Fig. III-6, panel B1, the head trajectory of Fig. III-6, panel B2 was tilted more vertically compared to the orientation of the target. Finally, Fig. III-6, panel C shows a trial with a larger vertical component than the horizontal component (horizontal target amplitude = 6.00 [deg], vertical target amplitude = 20.80 [deg]). As for the three preceding examples, gaze and head trajectories had very similar orientations. However, the head movement was titled more vertically than in the three other situations with almost no horizontal displacement.

From the examples of Fig. III-6, panel A-C, it appears that the mean orientation of the head trajectory was influenced by the orientation of the target. However, the mean gaze orientation appeared to be uninfluenced by target orientation. To quantify the effect of target orientation on gaze and head orientations, we computed the angle between the target orientation and the mean orientation of gaze and head. We found a similar pattern for each quadrant ([0...90] [deg], [90...180] [deg], [180...270] [deg] and [270...360] [deg]). Therefore, we pooled the data of the four quadrants together and plotted the evolution of the difference between the target and the head orientation (O_T-O_H) as a function of the orientation of the target in Fig. III-7. Then, we computed the mean of the difference between target and head orientations for 2.5 [deg] bins and represented it with the black solid line. Finally, we computed the standard deviation for each bin and represented its evolution around the mean value with black dashed lines.

Figure III-7, panel A shows a clear influence of the target orientation on the difference between target and head orientation. When the orientation of the target was smaller than 30 [deg], the more the target was tilted vertically,

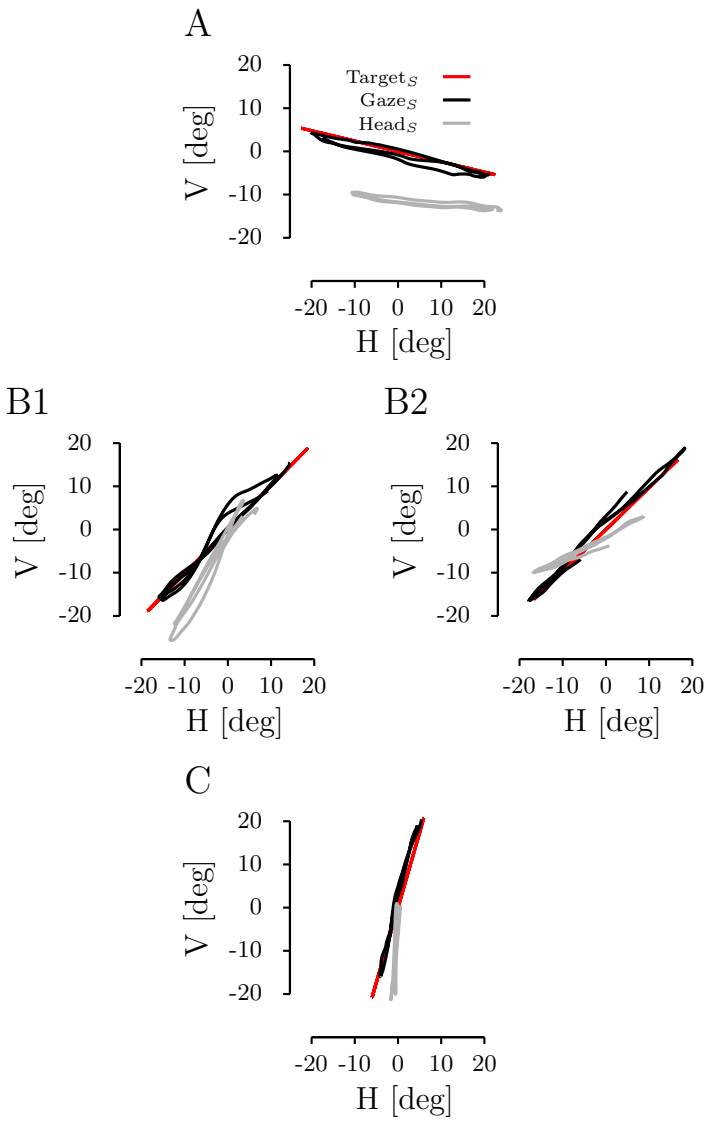

Fig. III-6: **Typical head and gaze spatial trajectories for different target orientations.** Panels A-C represents the spatial representation (horizontal-vertical, not normalized) of the target (red lines), the gaze (black lines) and the head (gray lines) for the last 1.5 period of target motion. Panel A represents a target with a larger horizontal component than the vertical one. Panels B1-B2 represent two trials with similar vertical and horizontal target components. Panel C represents a trial with a larger vertical than horizontal component of the target motion.

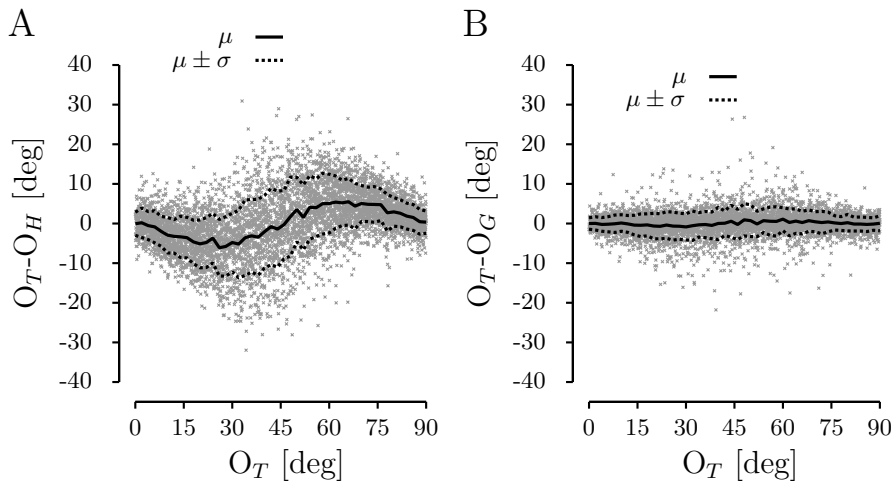

Fig. III-7: **Head and gaze movements as a function of the target orientation.** Panel A represents the evolution of the mean relative head orientation ($O_T - O_H$) as a function of the target orientation (O_T). Panel B represents the evolution of the relative gaze orientation (panel B, $O_T - O_G$) as a function of the target orientation. Solid lines correspond to the evolution of the mean values as a function of the target orientation for the relative head orientation (panel A) and the relative gaze orientation (panel B). Dashed lines represent the evolution of the standard deviation around the mean for the same data.

the larger the difference between the head and the target orientation. This observation points toward a tendency to keep a head movement with a larger horizontal component than the vertical component for small target orientation. Oppositely, when the orientation of the target was larger than approximately 60 [deg], the more the target was tilted vertically, the less the difference between the head and the gaze orientations pointing toward a tendency of the head movement to have a larger vertical displacement than the horizontal displacement. Finally, a transition between those two situations appeared when the target orientation was between 30 and 60 [deg]. To summarize, two behaviors emerged from Fig. III-7, panel A. When the target moved with an orientation inferior to approximately 30 [deg], the head moved preferentially horizontally while when the target orientation was superior to 60 [deg], the head moved preferentially vertically.

The same analysis was conducted on the gaze trajectory. We plotted in Fig. III-7, panel B the evolution of the difference between gaze and target orientations. We computed the mean and the standard deviation for bins of 2.5 [deg]. The mean value is represented using solid black lines while dashed black lines represent the mean plus and minus the standard deviation. Comparing Fig. III-7, panels A and B, one can see that the orientation of the gaze was less sensitive to the orientation of the target movement than the orientation of the head; even if more variability was present when the target orientation was comprised between 30 and 60 [deg].

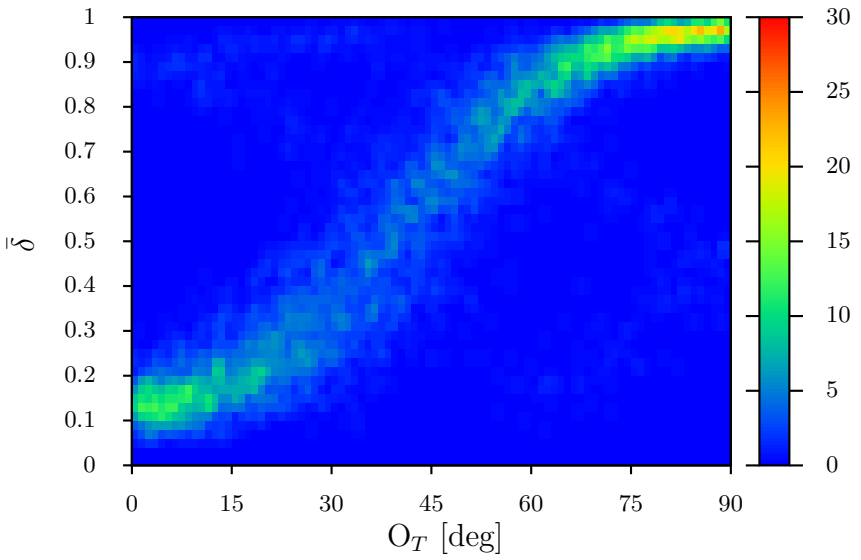

Fig. III-8: **Head rotation strategies.** This figure represents the distribution of the strategy index $\bar{\delta}$ as a function of the target orientation (O_T).

As explained in the methods, the head roll cannot be used to dissociate vertical and horizontal head movement strategy. Thus, to understand the origin of the different head tracking behaviors when the target orientation changes, we computed the strategy index $\bar{\delta}$ for every trial as described in section 6. Small values of $\bar{\delta}$ correspond to head rotations around an axis normal to the horizontal semicircular canal plane. Large (up to 1) values of $\bar{\delta}$ correspond to head rotations around an axis parallel to the interaural axis (vertical head rotations optimizing the discharge of the anterior and the posterior semicircular canals). Theoretically, if subjects switched abruptly from a horizontal to a vertical head rotation strategy, the evolution of $\bar{\delta}$ with respect to the orientation of the target should represent a staircase function. The head strategy index will be equal to zero for target orientations smaller than a threshold angle and will be equal to one for target orientations larger than the threshold.

The distribution of $\bar{\delta}$ as a function of the target orientation is represented in Fig. III-8. Figure III-8 shows that two areas of high density emerged as a function of the target orientation. For target orientations inferior to 30 [deg], subjects used a head rotation strategy which promoted the horizontal rotations of the head ($median(\bar{\delta} \leq 30\ [deg])$ =0.22). For target orientations superior to 60 [deg], Fig. III-8 shows that subjects used more and more vertical head rotations ($median(\bar{\delta} \geq 60\ [deg])$ =0.90). As for the results in Fig. III-7, panel A, a transition zone was present between the horizontal and the vertical behaviors in Fig. III-8. Those areas are represented by a less dense concentration of the data in Fig. III-8, pointing toward a less defined head rotation strategy for the subjects (for a target oriented at 45 [deg], using one strategy or the other is theoretically similar).

4 Movement initiation

After the analysis of the pursuit performances in steady-state, we looked at how subjects initiated head and gaze movements when the pursuit target started to move. The purpose of the analysis was to look at normal unanticipated initiation. Therefore, we had to remove trials that did not fit into a set of criteria. We removed trials in which subjects blinked or moved their gaze during a period of 100 [ms] before to 100 [ms] after the target onset. We also removed trials in which subjects were not initially looking at the fixation target (± 5 [deg] criteria). Finally, one subject did not initiate her pursuit movement like the others. She completely ignored the first half-cycle of the movement and started to move toward the target during the second half-cycle. As it will be shown in the typical trials figures, the other subjects sometimes used this strategy (< 5%). The choice to ignore the first cycle was not correlated with either the frequency, the amplitude or the velocity of the target. Therefore, this subject was removed from the pursuit initiation analyses. Of the 5748 trials used in the first part of the study, 3440 (59.9%) were selected as valid for the analysis of pursuit initiation.

Because in the preceding analyses, we found that the pursuit performances were modulated by the frequency of the oscillating target, we pooled the trials corresponding to the same bins of target oscillation frequency. Additionally, we looked for an effect of the amplitude of the target movement to the pursuit initiation. Thus, we divided the trials in each target frequency bin into target amplitude bins of 2 [deg]. With this division, we had 42 categories. For each category, we computed the mean evolution of the target, the gaze, the eye-in-head and the head position during the first period of target movement. Figure III-9 represents trials with the smallest amplitudes (A_T < 21 [deg]) for three frequency bins: small frequencies (first row, f_T ≤0.65 [Hz]), intermediate frequencies (second row, 0.85≤ f_T <0.95 [Hz]) and high frequencies (third row, f_T >1.15 [Hz]). Figure III-10 represents trials with the largest amplitudes ($A_T \geq 29$ [deg]) for the same frequency bins. Figures III-9 and III-10 showed that the gaze movement started by a saccade, independently of the frequency or the amplitude of the target movement. After the first saccade, the gaze did not follow the target until the apex of the cycle, it remained more or less stable (look at first row, left column in Fig. III-9 and III-10). Then the behavior changed drastically as a function of the target oscillation frequency (but it remained similar as a function of the amplitude, compare identical rows in Fig. III-9 and III-10). For low frequencies, the gaze could follow the target quickly, after a half-cycle of target movement, the mean gaze trajectory was in phase with the target movement. However, the mean gaze pursuit gain was less important for the large amplitudes than for the small ones.

For high frequencies (third row in Fig. III-9 and III-10), the mean gaze position overshot the target position after the first saccade. Then a second saccade was triggered to compensate for the increasing position error. At the end of this saccade, the gaze started to follow the target. As for low frequencies, the gain of the pursuit was less important for large amplitudes than for small ones. Because of its high inertia, the head movement started more slowly

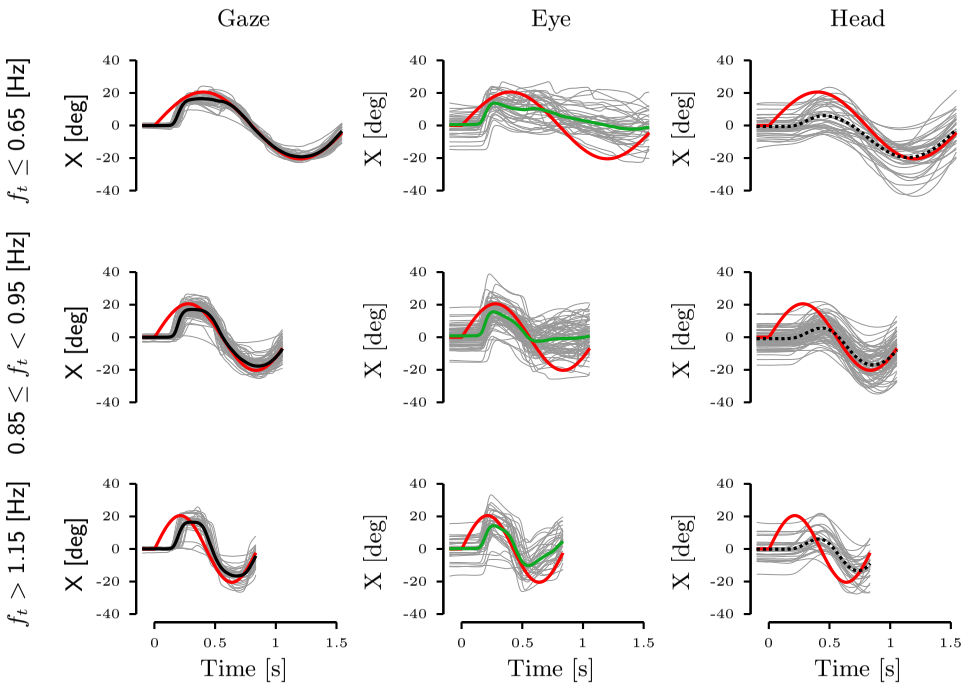

Fig. III-9: **Initiation of the pursuit for small amplitude trials ($A_T < 21$ [deg]).** Left column represents the gaze position. Second column represents the eye position. Right column represents the head position. Upper row represents low frequency trials ($f_T \leq$0.65 [Hz]). Second row represents intermediate frequency trials (0.85$\leq f_T <$0.95 [Hz]). Third row represents high frequency trials ($f_T >$1.15 [Hz]). Thin gray lines represent all the trials corresponding to a category. Thick lines represent the mean of all the individual trials. Red thick lines correspond to the mean evolution of the target for every category. Only the first period after the beginning of the target movement is represented.

Fig. III-10: **Initiation of the pursuit for large amplitude trials ($A_T \geq 29$ [deg]).** Same conventions as Fig. III-9.

than the gaze. The initial part of the head movement appeared to be fairly similar across conditions. Whatever the frequency or the amplitude of the target, head movements started simultaneously and reached its first peak position also at the same time. Therefore, the head movement lagged more behind high frequency targets than low frequency targets after the first half-cycle of target movement. During the second half-cycle of target movement, the head movement slightly led the target for low frequencies and lagged significantly the target for large frequencies.

Gaze, eye-in-head and head movement latency

The mean value of the gaze latency for the 42 bins of target amplitude and frequency was equal to (96.3± 17 [ms]). Following the qualitative observations of Fig. III-9 and III-10, no significant correlation was found between the latency of the gaze movement and the frequency (corr(L_G,f_T)=0.032, P=0.84), the maximum target velocity (corr(L_G,$max(\dot{T})$)=0.035, P=0.83)) or the amplitude (corr(L_G,A_T)=0.043, P=0.84) of the target movement. The mean latency of movement initiation observed in our results is not different from the 100 [ms] observed previously by (Wellenius and Cullen, 2000) during the initiation of pursuit when a step-ramp target was presented to monkeys.

The mean latency of the eye-in-head movement was equal to (98.1± 17 [ms]). A t-test did not reveal a significant difference between the latency of the gaze movement and the latency of the eye movement (t(82)=0.4749, P=0.636).

The mean head latency was equal to (135.5± 36 [ms]). There was a significant difference between the head and the gaze latency (40± 33 [ms], t(82)=6.45, P<0.001). Those results are in agreement with the 50 [ms] difference between gaze and head movements latency reported by (Wellenius and Cullen, 2000) during the initiation of head-unrestrained tracking of a step-ramp target.

Initial head movement kinematics

As shown in Fig. III-9 and III-10, the initial part of the head movement appeared to be insensitive to the target frequency or the target amplitude. To further test this observation, we pooled the head movements by frequency bins, and we computed the mean evolution of the head displacement, velocity and acceleration for each frequency bin.

Figure III-11 represents the evolution of head mean position (first row), head mean velocity (second row) and head mean acceleration (third row) for the first cycle of target movement for 0.1 [Hz] frequency bins. As clearly shown by the figure, during the first 200 [ms] (between 100 [ms] and 300 [ms]), there was no influence of the frequency or the amplitude of the target on the kinematics of the head movement. After 300 [ms], the mean head position, velocity and acceleration diverged, reflecting the fact that targets with different frequencies were tracked.

Those results point toward an open-loop behavior of the head control system during the initiation of the movement in response to the presentation of a predictable oscillating target. This argument will be further elaborated in the discussion (chapter 4).

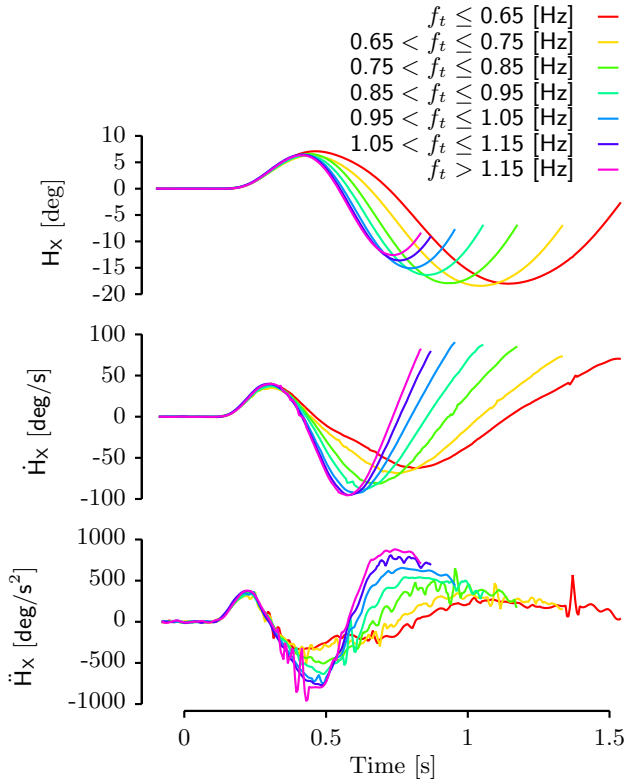

Fig. III-11: **Initiation of the head movement for different frequency bins.** First row represents the evolution of the mean head displacement as a function of time for different bins of target frequency. Second row represents the evolution of the mean head velocity as a function of time for the same bins of frequency. Third row represents the time course of the mean head acceleration.

Interestingly, if most of the curves diverged after 300 [ms], the higher the frequency, the less important the difference between the curves. This demonstrated that the head acceleration cannot continue to increase indefinitely. The jerk of the head (derivative of the head acceleration) reached a saturation approximately at 8684 [deg/s^3].

We pooled trials with similar amplitudes and we built the same figure to see the effect of target amplitude on the initiation of the head movement. There was no influence of the amplitude of the movement on the head trajectory during the first cycle of the movement. This showed that the frequency of the oscillating target is the key parameter that influenced the head kinematics during the initiation of the movement.

5 Saccades occurrence

The analysis of the gaze pursuit parameters revealed a degradation of pursuit performance with an increase of the target oscillation frequency. To compensate for the decrease of the pursuit gain, we assumed that, as shown by the typical trials of Fig. III-2 and III-3, the central nervous system had to trigger more saccades with high frequency targets than with low frequency targets. To test this assumption, we computed the proportion of time during which subjects executed a saccade and called this parameter proportion of saccadic time. We defined the proportion of saccadic time as the ratio of the sum of the duration of all saccades in a trial to the duration of the corresponding trial. With an increase of the target oscillation frequency (and a decrease of the gaze pursuit gain, see Fig. III-4, panel A), we expected to observe an increase of the proportion of saccadic time. As expected, with an increase of the target frequency, subjects increased the proportion of time during which they executed a saccade. A linear regression between target oscillation frequency and proportion of saccadic time resulted in:

$$T_{sacc,prop} = (0.255 \pm 0.006)\ f_T - (0.027 \pm 0.006)\,, \quad vaf = 231,\ P < 0.001 \tag{40}$$

Equation (40) shows that the proportion of saccadic time doubled on the range of observed frequencies (From 0.126 at 0.6 [Hz] to 0.279 at 1.2 [Hz]). Slopes of regression (40) for an individual subject varied from (0.048± 0.012) to (0.351± 0.014).

Triggering parameters of catch-up saccades

Next, we studied how subjects triggered saccades in head-unrestrained condition while tracking a periodic oscillating target. Because the frequency of the pursuit target was randomized in a [0.6...1.2] [Hz] range, we could not compare the latency of saccades with respect to the onset of target movement to extract the generic behavior of the subjects. Therefore, we computed for each saccade their relative onset time (comprised inside a [0...1] range) as described in the methods. Figure III-12 represents the distribution of the number of saccades as a function of their relative onset time. The solid black line in Fig. III-12 represents the evolution of a signal with a unitary frequency corresponding to the evolution of the relative absolute target velocity (arbitrary amplitude). The dotted lines correspond to the position of the maximum target velocity ($\|\dot{T}\|_{max}$), and thin black lines represent the position when the target velocity is equal to zero ($\|\dot{T}\|$ =0). As can be observed, the distribution of the number of saccades was modulated according to the amplitude of the target velocity. A large number of saccades were triggered when the amplitude of the target velocity was high. Contrarily, when the amplitude of the target velocity was small, fewer saccades were triggered. Moreover, the saccade distribution is not symmetric with respect to the maximum target velocity (around 0.5, 0 and 1). Figure III-12 shows that the number of saccades was the largest when the target accelerated (between 0.35 and 0.5 or between 0.85 and 1) than during the deceleration phase (between 0.5 and 0.65 or between 0 and 0.1).

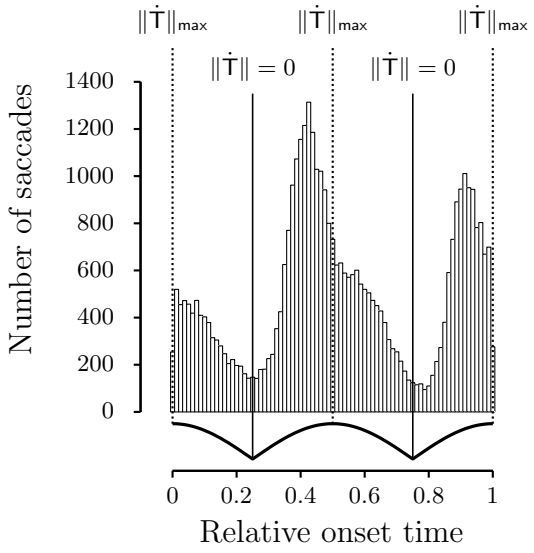

Fig. III-12: **Distribution of saccade relative onset time.** Thick black line under the distribution corresponds to the evolution of the absolute value of the target velocity as a function of the relative position in the sine function (arbitrary amplitude). Dotted lines represent the position of the maximum target velocity. Thin black lines represent the position when the target velocity is equal to zero.

To understand why subjects triggered a saccade when the target velocity was high, we first computed the corrected position error ($PE_{ON,CORR}$) and the corrected retinal slip ($RS_{ON,CORR}$) at the onset of the saccade as described in the methods. We plotted the evolution of $PE_{ON,CORR}$ and $RS_{ON,CORR}$ as a function of the relative onset position of the saccade in Fig. III-13. Solid black lines in Fig. III-13 represent a typical frequency-normalized position signal (arbitrary amplitude). Dashed black lines represent the mean over 0.025 relative position bins of either the corrected position error (upper row in Fig. III-13) or the corrected retinal slip (lower row in Fig. III-13) for all target frequencies pooled together. Color lines represent the mean over 0.025 relative position bins of either $PE_{ON,CORR}$ (upper row in Fig. III-13) or $RS_{ON,CORR}$ (lower row in Fig. III-13) for target oscillation frequency bins of 0.1 [Hz] (centered at 0.65 [Hz], 0.75 [Hz], 0.85 [Hz], 0.95 [Hz], 1.05 [Hz], 1.15 [Hz]). Finally, dashed colored lines under each plot represent the portion of time during which $PE_{ON,CORR}$ (upper row in Fig. III-13) or $RS_{ON,CORR}$ (lower row in Fig. III-13) for the two frequencies represented by the colors of the dashed lines are statistically different (t-test, $P<0.05$). We only compared two successive frequency bins (0.65 [Hz] with 0.75 [Hz], 0.75 [Hz] with 0.85 [Hz], etc.). Moreover, the horizontal black lines correspond to the time when $PE_{ON,CORR}$ or $RS_{ON,CORR}$ were significantly higher than zero (dashed black lines, one-sided t-test, $P<0.05$) or significantly smaller than zero (solid black lines, one-sided t-test, $P<0.05$).

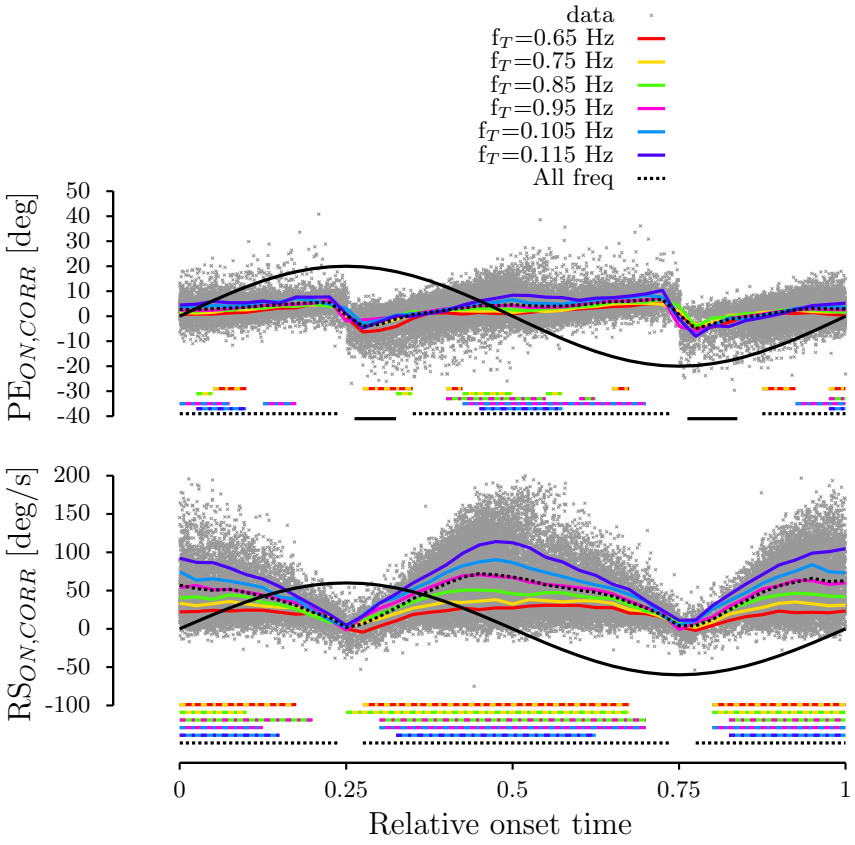

Fig. III-13: **$PE_{ON,CORR}$ and $RS_{ON,CORR}$ as a function of the relative onset position.** Upper row represents the corrected position error at saccades' onset as a function of the relative saccadic onset time. Lower row represents the corrected retinal velocity error at saccades' onset as a function of the relative saccadic onset time. Gray dots represent individual data. Thick black lines represent typical unitary frequency target position (arbitrary amplitudes). Dotted black lines represent the evolution of the mean $PE_{ON,CORR}$ (upper row) or the mean $RS_{ON,CORR}$ (lower row) as a function of the relative onset time for all the frequencies pooled together. Color lines correspond to the evolution of the mean $PE_{ON,CORR}$ (upper row) or the mean $RS_{ON,CORR}$ (lower row) as a function of the relative onset time for different bins of target frequency. Horizontal dashed color lines under the graphs correspond to the portion of time during which the two signals represented by the two colors are significantly different. Dashed (solid) horizontal black line under the graphs correspond to the period during which the mean signals are significantly larger (smaller) than 0.

As explained in the methods, a positive (negative) value of $\mathrm{PE}_{ON,CORR}$ corresponds to a gaze that lagged (led) the target and a positive (negative) value of $\mathrm{RS}_{ON,CORR}$ corresponds to a gaze that was slower (faster) than the target. The jumps observed in the upper row of Fig. III-13 appeared because of the sign change of the target velocity that influenced the computation of position error (see methods).

Upper row, Fig. III-13 shows that the gaze lagged the target during a large part of the movement. However, inside the $]0.25 \ldots 0.325]$ and $]0.75 \ldots 0.85]$ ranges, the gaze was, in mean, in phase or leading the target at saccades' onset ($\mathrm{PE}_{ON,CORR} \leq 0$). Lower row, Fig. III-13 shows that the gaze moved more slowly in mean than the target during the movement at saccades' onset, confirming the gaze pursuit gain smaller than one as represented in Fig. III-4 A, left column.

As can be observed in Fig. III-13, the position error at the onset of the saccade was not as much influenced by the target oscillation frequency as the retinal slip was. The small variations of position error with respect to the target oscillation frequency point toward a high sensitivity of the saccadic system to the position error. As soon as the position error was larger than a small threshold, a saccade was triggered. Contrarily, a large variation of the retinal slip at the onset of the saccade was observed as shown by the dashed colored lines under $\mathrm{RS}_{ON,CORR}$ plot, reflecting the saturation of the pursuit system. If the statistical difference between two frequency bins for the position error at saccades' onset is more sparsely distributed, there is a clear modulation with respect to the target position of the statistical difference between two frequency bins for the retinal slip.

To better understand the triggering mechanism, we linked $\mathrm{PE}_{ON,CORR}$ and $\mathrm{RS}_{ON,CORR}$ with the distribution of the number of saccade as a function of the relative position at saccade onset. To that goal, we represented the normalized number of saccades triggered as either a function of $\mathrm{PE}_{ON,CORR}$ (blue markers) in Fig. III-14, panel E or as a function of $\mathrm{RS}_{ON,CORR}$ (red markers) in Fig. III-14, panel D. To represent the relationships between $\mathrm{PE}_{ON,CORR}$ and $\mathrm{RS}_{ON,CORR}$ independently of the bins' width, we normalized the area under the histogram represented in Fig. III-14 to obtain the distribution represented in Fig. III-14, panel A. Then we separated the data into two pools: one grouped to the positive values of $\mathrm{PE}_{ON,CORR}$ (gaze lagged behind the target) and the corresponding $\mathrm{RS}_{ON,CORR}$ (filled markers). The second group pooled the negative values of $\mathrm{PE}_{ON,CORR}$ (gaze led the target) and the corresponding $\mathrm{RS}_{ON,CORR}$ (open markers). Finally, to build Fig. III-14, panel D, we plot the value of $\mathrm{RS}_{ON,CORR}$ at a value of the relative onset time (e.g. Y_1 in Fig. III-14, panel B) as a function of the value of the normalized distribution (e.g. X in Fig. III-14, panel A) at the same relative onset time. The same procedure was used to build Fig. III-14, panel E (e.g. using X and Y_2).

A symmetric trend of the number of saccades triggered as a function of $\mathrm{PE}_{ON,CORR}$ for the positive and the negative values of $\mathrm{PE}_{ON,CORR}$ can be observed in Fig. III-14, panel E. Concurrently, a similar trend of the number of saccades as a function of $\mathrm{RS}_{ON,CORR}$ was present for the two pools of data. With an increase of the velocity error, there was an increase of the number of saccades. Surprisingly, the increase of the retinal slip was accompanied by a

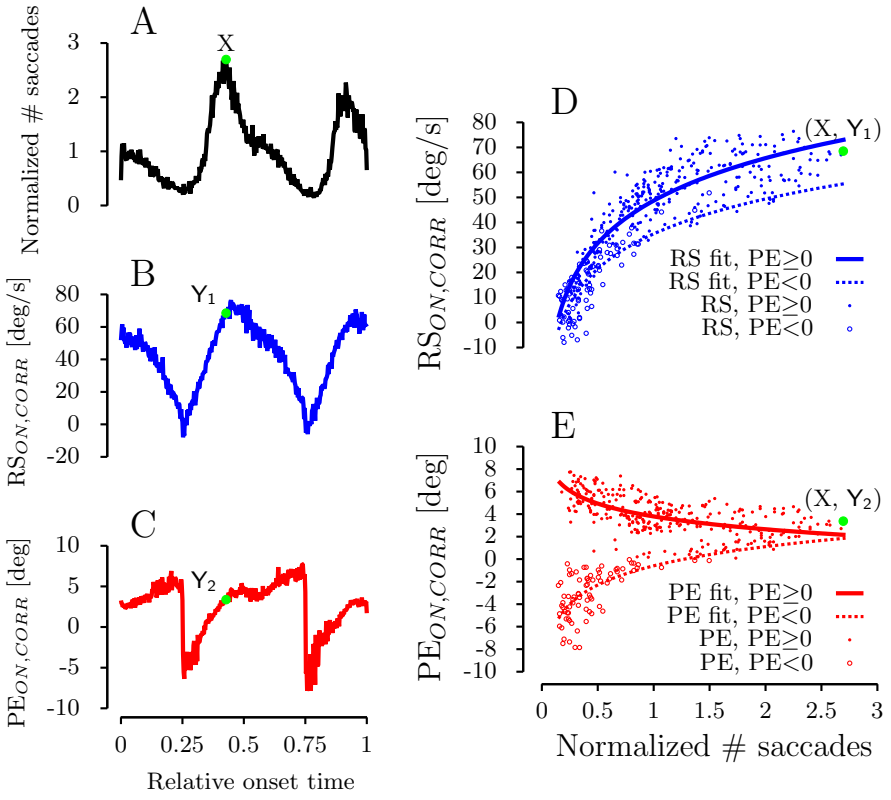

Fig. III-14: **Normalized number of saccades as a function of RS and PE.** Panel A represents the normalized distribution of the number of saccades as a function of the relative onset time. Panel B (C) represents the evolution of $\mathrm{RS}_{ON,CORR}$ ($\mathrm{PE}_{ON,CORR}$) as a function of the relative onset time. Panel D (E) represents the relationship between the relative number of saccades and $\mathrm{RS}_{ON,CORR}$ ($\mathrm{PE}_{ON,CORR}$). Open (filled) markers correspond to negative (positive) values of $\mathrm{PE}_{ON,CORR}$. Solid lines correspond to an exponential fit between $\mathrm{RS}_{ON,CORR}$ ($\mathrm{PE}_{ON,CORR}$) and the normalized number of saccades for positive values of $\mathrm{PE}_{ON,CORR}$. Dashed lines correspond to the same fits for the negative values of $\mathrm{PE}_{ON,CORR}$.

decrease of the amplitude of the position error. This showed that with a small retinal slip, the saccadic system triggered few saccades and tolerated a larger position error. On the other hand, a larger number of saccades was triggered with a smaller change in the position error when the retinal slip was large. We fitted an exponential function on $\mathrm{RS}_{ON,CORR}$ and $\mathrm{PE}_{ON,CORR}$ for the two pools of data (positive and negative values of $\mathrm{PE}_{ON,CORR}$). The four fits resulted in:

$$N^{+}_{Sacc} = exp\left(\frac{PE^{+}_{ON,Corr} - (3.80 \pm 0.07)}{(-1.66 \pm 0.12)}\right), \quad vaf = 0.374, \; P < 0.001 \qquad (41)$$

$$N^{+}_{Sacc} = exp\left(\frac{RS^{+}_{ON,Corr} - (48.68 \pm 0.45)}{(24.54 \pm 0.72)}\right), \quad vaf = 0.784, \ P < 0.001 \quad (42)$$

$$N^{-}_{Sacc} = exp\left(\frac{PE^{-}_{ON,Corr} - (0.60 \pm 0.39)}{(2.46 \pm 0.36)}\right), \quad vaf = 0.386, \ P < 0.001 \quad (43)$$

$$N^{-}_{Sacc} = exp\left(\frac{RS^{-}_{ON,Corr} - (35.41 \pm 1.89)}{(20.15 \pm 1.70)}\right), \quad vaf = 0.649, \ P < 0.001 \quad (44)$$

Dashed lines in Fig. III-14, panels D-E represent the fits (blue for $\mathrm{RS}_{ON,CORR}$ and red for $\mathrm{PE}_{ON,CORR}$) on the data corresponding to the negative values of $\mathrm{PE}_{ON,CORR}$ while solid lines represent the fits for the positive values of $\mathrm{PE}_{ON,CORR}$.

The fits quantitatively confirm the interpretation we made above: the number of triggered saccades increased with the retinal slip, even if the position error decreased. This result will be discussed in details in the discussion.

Saccades' amplitude

In the previous section, we studied which parameters triggered saccades. We showed that the triggering mechanism was highly sensitive to the amplitude of the position error. In addition, we demonstrated that when the retinal slip increased, the central nervous system decreased the threshold on the position error to trigger a saccade. In this last section, we studied which parameters influenced the amplitude of gaze saccades. de Brouwer et al. (2002b) showed that catch-up saccades' amplitude in head-restrained condition was better correlated with a multiple regression on PE and RS than with a single regression on PE. Using a multiple regression, de Brouwer et al. (2002b) showed that the amplitude of a saccade accounted for ∼86% of the position error and ∼10% of the retinal slip (see regression (1) in (de Brouwer et al., 2002b)) in head-restrained condition. This result pointed toward an influence of the retinal slip on the control of gaze saccades amplitude.

To test if such behavior was present in our paradigm, we computed first-order regressions between saccades' amplitude and $\mathrm{PE}_{ON,CORR}$ or $\mathrm{RS}_{ON,CORR}$ as independent variables. We also computed a second-order regression between saccades' amplitude and the two parameters. The linear regressions resulted in:

$$S_{A,Corr} = (0.694 \pm 0.009)\ PE_{ON,Corr} + (11.80 \pm 0.05), \quad vaf = 0.136, \ P < 0.001 \quad (45)$$

$$S_{A,Corr} = (0.157 \pm 0.001)\ RS_{ON,Corr} + (5.64 \pm 0.07), \quad vaf = 0.367, \ P < 0.001 \quad (46)$$

$$S_{A,Corr} = (0.140 \pm 0.001)\ RS_{ON,Corr} + (0.342 \pm 0.008)\ PE_{ON,Corr} + (5.64 \pm 0.07), \quad vaf = 0.396, \ P < 0.001 \quad (47)$$

F-tests between residuals of first-order regressions (45) and (46) and second-order regression (47) confirmed that the addition of a second parameter significantly increased the quality of the fit (two-tailed f-tests. PE≪≫Multi: $F(40371,40371)=0.699$ $P<0.001$; RS≪≫Multi: $F(40371,40371)=0.954$ $P<0.001$).

As for (de Brouwer et al., 2002b), our analysis showed that the amplitude of the saccades was better represented by a multiple regression using the position error and the retinal slip as independent parameters. However, the variance accounted for (vaf) of the regressions are smaller in our study than the ones observed in head-restrained condition. Those results were not surprising considering two major differences between the two studies. First, there is a large intrinsic variability of head-unrestrained saccade metrics (Freedman and Sparks, 1997) compared to head-unrestrained saccade metrics. Secondly, large position errors and retinal slips were introduced experimentally in the paradigm of (de Brouwer et al., 2002b) but not in our study.

4

Discussion

In this study, we examined how the central nervous system coordinates eye and head movements during the tracking of a 2-D periodic target. We showed a high sensitivity of gaze and head tracking performance (gain, frequency and phase) to the target oscillation frequency. Our data also revealed that the sensitivity of head performance to target oscillation frequency was less significant than the sensitivity of the gaze to the same parameter. We demonstrated that the orientation of the moving target modulated the gain of both head and gaze movements. Analyzing the relative orientation of the head and the gaze trajectories with respect to the orientation of the moving target, we showed that the control of the head followed two movement strategies: either the head used a vertical or a horizontal displacement depending on the orientation of the moving target.

In the second part of the paper, we showed that the initiation of the movement followed a stereotyped time course, independently of the target parameters: at first, a gaze shift was triggered after approximately 100 [ms] of target movement. Then the head began to move 50 [ms] later. Remarkably, our analyses showed that the kinematics of the head movement during the first 200 [ms] was insensitive to a change of the target parameters.

In the last part of the chapter, we demonstrated that subjects used more saccades to compensate for the decrease of tracking performance with the increase of target oscillation frequency. We showed that the number of saccades was modulated by the velocity of the target: more saccades were triggered when target velocity was important. Our analyses indicated that the majority of the saccades were triggered with a large retinal slip and a small position error. Finally, we showed that saccade amplitude was better explained with a multiple regression using position error and retinal slip at saccade onset as the independent variables than with simple regression with either the position error or the retinal slip.

Gaze and head tracking behavior

We found that when subjects were asked to pursue an oscillating periodic target in two-dimensions with the head free to move, the central nervous system efficiently combined gaze saccades and head-unrestrained tracking to ensure

that the target remained close to the fovea. Because the velocity of the target reached large values (188.5 [deg/s] for a target oscillating at 1.2 [Hz] with an amplitude of 25 [deg]), sometimes twice larger than the velocity saturation (around 80 [deg/s]) in head-restrained conditions described by Meyer et al. (1985), subjects had to use combined eye-head movements to increase the range of accessible velocity and thus accurately track the periodic target. In a first part of the study, we showed that the frequency and the orientation of the target modulated the performances of gaze and head movements.

Our analyses extended the observations of Collins and Barnes (1999) about the tracking of 1-D oscillating target to a two-dimensional case. We found the same relationship between gaze pursuit gain, head pursuit gain and target frequency as Collins and Barnes (1999). However, our data revealed more variability of both gaze and head pursuit gains for a given frequency bin than the variability observed by Collins and Barnes (1999). We postulated that the larger variability came from the two-dimensional nature of the paradigm. This was demonstrated by the analysis of the change of both the head and the gaze gains as a function of the target orientation. Figure III-5 clearly shows that the head and the gaze tracking gains were modulated according to the orientation of the target. As previously observed in head-restrained situations by Rottach et al. (1996); Kettner et al. (1996); Leung and Kettner (1997), the gain of the pursuit was smaller when the target moved vertically than when the target moved horizontally. Using second-order non-linear regressions, we showed that the gain of the gaze movement was sensitive to two parameters: the frequency of the oscillating target and the orientation of the moving target. Additionally, our regression analyses pointed toward a less sensitive gain of the head movement with respect to the orientation and the frequency of the target. The low variance-accounted-for of regressions (29), (36) and (38) showed that only a small part of the observed variability of the head tracking gain could be explained by a change of either the target oscillation frequency or the orientation of the target.

In parallel to the evolution of the gains as a function of the frequency, we showed that the central nervous system controlled eye-head displacement such that the frequency of gaze and head oscillating movements were very well correlated (vafs>0.97) with the frequency of the pursuit target. As previously mentioned, movement frequency is a critical parameter to ensure a general accuracy of the gaze displacement: a mismatch between either the gaze or the head movement and the target movement would increase the amplitude of the eye displacement needed. Therefore, we believe that such a large correlation for regressions (30) and (31) could be expected.

The last parameter that we computed to describe the quality of the pursuit was the phase of the movement. A negative phase corresponds to a movement that lagged behind the target while a positive phase corresponds to a movement that led the target. Our results are in agreement with the observations of Collins and Barnes (1999); their results and our observations showed that with an increase of target frequency, gaze and head movements lagged more behind the target.

Head movements strategies

To our knowledge, this paper is the first to study the strategies used by the central nervous system to control head trajectory during pursuit in 2-D. Figures III-6, III-7 and III-8 demonstrate clearly the existence of two extreme behaviors; in the first one, the head made mainly horizontal movements (small values of $\bar{\delta}$, target orientation between 0 and 30 [deg]). In the second one, the head movements were mainly vertical (large values of $\bar{\delta}$, target orientation between 60 and 90 [deg]). We believe that those two behaviors can be explained by several facts. First, horizontal and vertical head rotations are very different biomechanically. Horizontal rotations are carried out around the first cervical vertebra on the full range of motion (35-45 [deg]) while a vertical rotation implies a bending of the spine for downward rotations larger than 10-15 [deg] and for upward rotations larger than 25 [deg] (Hislop and Montgomery, 2000). Second, it is known that the central nervous system uses the head velocity information from the semicircular canals to control head trajectory. During horizontal rotations of the head, the horizontal semicircular canal is optimally aligned to maximize its sensitivity to a change of head velocity. The situation is more delicate for vertical head rotations because both the anterior and the posterior semicircular canals discharge during rotations around the interaural axis. However, it is highly probable that phylogenetically the central nervous system had learned to combine the information from both anterior and posterior canals to extract more easily the vertical head velocity. Finally, authors have shown that neck muscles in the cat can be divided into two pools: the activity of the first group do not change as a function of the head posture whereas the activity of the second pool is correlated with the head posture (Thomson et al., 1994, 1996). Therefore, it seems reasonable to modify first the head posture (through a change of head roll) by changing the activity of the second pool of muscles. Then, a similar set of muscles to the set activated for horizontal head rotations can be activated to track adequately the target with the head. As a summary, we believe that for target orientations between 0 and 30 [deg], subjects rolled their head to promote rotations around the first cervical as it was a pure horizontal rotation. For target orientations between 60 and 90 [deg], subjects rotated their head around the roll axis to promote vertical rotations. This assumption made sense physiologically because with a roll of the head, subjects also aligned optimally the semi-circular canals with the orientation of the moving target. Therefore, they had more facility to extract head velocity. Finally, a similar set of muscles could be activated to track the target independently of the target orientation because of the muscles' synergy and the initial roll of the head.

Movement initiation

As mentioned in the introduction, to our knowledge only two studies have looked at the initiation of head-unrestrained tracking movements (Wellenius and Cullen, 2000; Dubrovski and Cullen, 2002). Those studies compared the behavior of monkeys during the initiation of the pursuit movement when their head was either free to move or not. Because Wellenius and Cullen (2000);

Dubrovski and Cullen (2002) used step-ramp targets, monkeys did not trigger a saccade to initiate the movements. Therefore, it is difficult to compare our results with their observations. However, we showed that the latency of the gaze movement is similar (approximately 100 [ms]) in our study to the latency reported by Wellenius and Cullen (2000). Additionally, we also found that the initiation of head movements was delayed by 50 [ms] with respect to the gaze movement initiation, a value comparable to previous observations (Wellenius and Cullen, 2000).

The analyses of the head movement surprisingly revealed the robustness of the initial head movements to a change of target parameters. Figure III-11 clearly demonstrated that the firsts 200 [ms] of head movements were insensitive to a change of target parameters. On the opposite, Dubrovski and Cullen (2002) showed a relationship between the initial acceleration (during the first 80 [ms] of movement) of the head and the velocity of the moving target. We believe that the difference between the results of Dubrovski and Cullen (2002) and our results arises because of the predictive nature of the protocol. Because of its high inertia, it is impossible to modify quickly the head trajectory according to the target motion. Therefore, the first part of the movement could correspond to a generic response of the head controller when a periodical target was presented. Following this open-loop behavior, the head trajectory was corrected when enough information about the target motion were extracted to predict its trajectory and compute the correct muscles' commands. Interestingly, a similar result has been shown in head-restrained condition when comparing anticipatory responses between a randomized target motion[92] and a constant one[93] (Heinen et al., 2005). The authors observed that when the parameters of target motion were randomized, subjects used an average pursuit response between the extreme behaviors observed when the parameters were held constant. The initiation of the head movement in our case has some similar properties. During the first part of the movement, subjects used an average trajectory for the head movement. This strategy could correspond to an ideal trajectory that would ensure a minimization of the head tracking error during the open-loop part of the movement.

Saccades triggering

By looking at the proportion of time during which subjects were making a saccade, we saw that the position error induced by the decrease of the pursuit gain was compensated for by an increase of the proportion of saccadic time. To understand when subjects triggered their saccades, we computed the relative saccade onset time. Then we plotted the distribution of the number of saccades as a function of their relative onset time in Fig. III-12. We showed that most of the saccades were triggered when the target was accelerating and that the number of saccades was modulated according to the target velocity: the higher (lower) the velocity, the bigger (smaller) the number of saccades. We believe that this saccade triggering strategy was intuitively predictable.

[92] Either random velocity, random onset time or random direction, the two other parameters kept constant.

[93] Same velocity, same onset time and same direction.

A first order approximation of the target movement (using a Taylor development limited to the first order) represents a simple prediction of the target movement based on position and velocity of the target at saccade onset. This approximation is more accurate around the extrema of the target velocity than around the extrema of target position (or acceleration) because the movement is more linear. Thus, target movements were more predictable with a high velocity. It has been shown that catch-up saccades' amplitude in head-restrained conditions is better explained by a multiple regression with position error and retinal slip as independent variables (de Brouwer et al., 2001). This regression corresponds to a linear approximation of the target non-linear movement. The fact that subjects triggered their saccades during the most linear part of the target movement could be seen as evidence that a similar strategy is used in our situation. Additionally, by triggering a saccade with a possible underestimate of the target velocity (because the target was accelerating), subjects had less risk to overshoot the target at the end of the gaze shift than if they triggered the saccade with an overestimate of the target velocity (when the target was decelerating).

To understand what triggered catch-up saccades in our protocol; we plotted the evolution of the position error and the retinal slip at saccade onset. We showed that the amplitude of the position error at saccade onset was not influenced by the frequency of the oscillating target. On the contrary, the retinal slip at saccade onset was clearly modulated with the frequency of the pursuit target. It is worth noting that the observed modulation of the retinal slip is another representation of the limitations of the pursuit system already represented by the evolution of the pursuit gain as a function of the target frequency in Fig. III-4. If the analysis of the pursuit gain as a function of the target frequency revealed a decrease of the performances of the pursuit system with an increase of the target frequency, the modulation of the retinal slip with respect to the velocity of the target clearly demonstrated that pursuit system was saturating for high target velocities.

In the last part of this analysis, we looked at the parameters that triggered a saccade. We showed that the majority of the saccades were triggered with a large retinal slip and a small position error at saccade onset. Figure III-14 also demonstrates that with a small retinal slip, the central nervous system tolerated a more important position error. With an increase of the retinal slip, there was a decrease of the position error threshold to trigger a saccade. Another notable point was the symmetrical evolution of the position error to trigger a gaze saccade. The same modulation of the position error was observed when the gaze was leading (dashed lines in Fig. III-14) or lagging behind (solid lines in Fig. III-14) the target at the onset of the saccade. We believe that the relationship between the position error, the retinal slip and the number of saccades has an intuitive explanation. With a large retinal slip, the position error quickly increases. To ensure that the mean position error during the tracking remained low, the central nervous system had to trigger a saccade sooner than if the retinal slip was small.

As supplementary evidence of the retinal slip importance in the programming of head-unrestrained catch-up saccades, we computed the simple regres-

sions between saccades' amplitude and either the position error or the retinal slip at saccade onset revealed. A statistical test demonstrated that the amplitude of the saccades was better explained with the retinal slip as the independent variable.

In head-restrained condition, de Brouwer et al. (2002a) showed that the eye crossing time, the time at which an eye movement should cross the target, is the determining parameter that triggers a saccade. There are major differences between our protocol and the one used in (de Brouwer et al., 2002a) that makes comparison with our results difficult. First, we used a periodic target. Therefore, we enhanced the predictability of the movement. It is well admitted that gaze movements are very different if the target is predictable or not. In head-unrestrained condition, Collins and Barnes (1999) showed that the predictive behavior of the head and the gaze movements was enhanced with repeated presentations of the target. Repeated presentation of a target also induced anticipatory saccadic movements, even if, with a high pace between the presentation of targets, the behavior starts to be less anticipatory (Ross and Ross, 1987). A second difference was that our protocol used two-dimensional target movements while the protocol used by de Brouwer et al. (2002a) focused on the horizontal displacement. Additionally, de Brouwer et al. (2002a) studied head-restrained saccades-pursuit interactions. It is widely admitted that the behaviors of combined eye-head saccades or pursuit are not as stereotyped as eye-only movements, e.g. there are behavioral differences even between subjects of the same species (Fuller, 1992). Finally, the amplitudes of the position error and the retinal slip were imposed in the paradigm of (de Brouwer et al., 2002a) which is not the case in the present study.

Conclusion

In conclusion, we propose that the tracking of a head-unrestrained periodic moving target in two dimensions follows the previously described observation in head-restrained condition. We demonstrated that the performances of the gaze tracking were modulated by the orientation and the frequency of the moving target. We also demonstrated that those two parameters (frequency and orientation) of the moving target had less influence on the performances of the head movement during the experiment. We showed that two strategies were used to control head trajectory; the central nervous system controlled the head to promote either a movement mainly horizontal or mainly vertical. We observed that saccades were triggered while the target was accelerating and with a large retinal slip; the threshold on the position error to trigger a saccade was smaller. The saccade amplitude was better explained by a regression with the retinal slip than with the position error at saccade onset as the independent variable.

References

Bahill, A., Clark, M., and Stark, L. (1975). The main sequence, a tool for studying human eye movement. *Mathematical biosciences*, 24:191–204.

Barnes, G. R. and Grealy, M. A. (1992). The role of prediction in head-free pursuit and vestibuloocular reflex suppression. *Ann N Y Acad Sci*, 656:687–694.

Becker, W. and Jürgens, R. (1990). Human oblique saccades: quantitative analysis of the relation between horizontal and vertical components. *Vision Res*, 30(6):893–920.

Blohm, G., Missal, M., and Lefèvre, P. (2003a). Interaction between smooth anticipation and saccades during ocular orientation in darkness. *J Neurophysiol*, 89(3):1423–1433.

Blohm, G., Missal, M., and Lefèvre, P. (2003b). Smooth anticipatory eye movements alter the memorized position of flashed targets. *J Vis*, 3(11):761–770.

Blohm, G., Missal, M., and Lefèvre, P. (2005a). Direct evidence for a position input to the smooth pursuit system. *J Neurophysiol*, 94(1):712–721.

Blohm, G., Missal, M., and Lefèvre, P. (2005b). Processing of retinal and extraretinal signals for memory-guided saccades during smooth pursuit. *J Neurophysiol*, 93(3):1510–1522.

Buizza, A. and Schmid, R. (1989). Influence of smooth pursuit dynamics on eye tracking: a mathematical approach. *Medical and Biological Engineering and Computing*, 27(6):617–622.

Carl, J. R. and Gellman, R. S. (1987). Human smooth pursuit: stimulus-dependent responses. *J Neurophysiol*, 57(5):1446–1463.

Collins, C. J. and Barnes, G. R. (1999). Independent control of head and gaze movements during head-free pursuit in humans. *J Physiol*, 515 (Pt 1):299–314.

Daye, P. M., Blohm, G., and Lefèvre, P. (2010). Saccadic compensation for smooth eye and head movements during head-unrestrained two-dimensional tracking. *J Neurophysiol*, 103(1):543–556.

de Brouwer, S., Demet, Y., Blohm, G., Missal, M., and Lefèvre, P. (2002a). What triggers catch-up saccades during visual tracking ? *Journal of Neurophysiology*, 87:1646–1650.

de Brouwer, S., Missal, M., Barnes, G., and Lefèvre, P. (2002b). Quantative analysis of catch-up saccades during sustained pursuit. *Journal of Neurophysiology*, 87:1772–1780.

de Brouwer, S., Missal, M., and Lefèvre, P. (2001). Role of retinal slip in the prediction of target motion during smooth and saccadic pursuit. *J Neurophysiol*, 86(2):550–558.

Dodge, R. (1903). Five types of eye movement in the horizontal meridian plane of the field of vision. *Am J. Physiol.*, 8:307–329.

Dubrovski, A. and Cullen, K. (2002). Gaze-, eye-, and head-movement dynamics during closed- and open-loop gaze pursuit. *Journal Of Neurophysiology*, 87:859–875.

Freedman, E. G. and Sparks, D. L. (1997). Eye-head coordination during head-unrestrained gaze shifts in rhesus monkeys. *J Neurophysiol*, 77(5):2328–2348.

Fuller, J. H. (1992). Head movement propensity. *Exp Brain Res*, 92(1):152–164.

Goossens, H. and Van Opstal, A. (1997). Human eye-head coordination in two dimensions under different sensorimotor conditions. *Experimental Brain Research*, 114:542–560.

Guitton, D., Munoz, D., and H.L., G. (1990). Gaze control in the cats: Studies and modeling of the coupling between orienting eye and head movements in different behavioral tasks. *J Neurophysiol*, 64(2):509–531.

Heinen, S. J., Badler, J. B., and Ting, W. (2005). Timing and velocity randomization similarly affect anticipatory pursuit. *J Vis*, 5(6):493–503.

Herter, T. M. and Guitton, D. (1998). Human head-free gaze saccades to targets flashed before gaze-pursuit are spatially accurate. *J Neurophysiol*, 80(5):2785–2789.

Hislop, H. and Montgomery, J. (2000). *Le bilan musculaire de Daniels & Worthingham*, chapter 2, pages 18–38. Masson, 6 edition.

Kettner, R. E., Leung, H. C., and Peterson, B. W. (1996). Predictive smooth pursuit of complex two-dimensional trajectories in monkey: component interactions. *Exp Brain Res*, 108(2):221–235.

Lanman, J., Bizzi, E., and allum, J. (1978). The coordination of eye and head movement during smooth pursuit. *Progress in Brain Research*, 153:39–53.

Leung, H. C. and Kettner, R. E. (1997). Predictive smooth pursuit of complex two-dimensional trajectories demonstrated by perturbation responses in monkeys. *Vision Res*, 37(10):1347–1354.

Meyer, C. H., Lasker, A. G., and Robinson, D. A. (1985). The upper limit of human smooth pursuit velocity. *Vision Res*, 25(4):561–563.

Morris, E. J. and Lisberger, S. G. (1987). Different responses to small visual errors during initiation and maintenance of smooth-pursuit eye movements in monkeys. *J Neurophysiol*, 58(6):1351–1369.

Orban de Xivry, J.-J. and Lefèvre, P. (2007). Saccades and pursuit: two outcomes of a single sensorimotor process. *J Physiol*, 584(Pt 1):11–23.

Pola, J. and Wyatt, H. J. (1980). Target position and velocity: the stimuli for smooth pursuit eye movements. *Vision Res*, 20(6):523–534.

Ross, S. M. and Ross, L. E. (1987). Children's and adults' predictive saccades to square-wave targets. *Vision Res*, 27(12):2177–2180.

Rottach, K. G., Zivotofsky, A. Z., Das, V. E., Averbuch-Heller, L., Discenna, A. O., Poonyathalang, A., and Leigh, R. J. (1996). Comparison of horizontal, vertical and diagonal smooth pursuit eye movements in normal human subjects. *Vision Res*, 36(14):2189–2195.

Thomson, D. B., Loeb, G. E., and Richmond, F. J. (1994). Effect of neck posture on the activation of feline neck muscles during voluntary head turns. *J Neurophysiol*, 72(4):2004–2014.

Thomson, D. B., Loeb, G. E., and Richmond, F. J. (1996). Effect of neck posture on patterns of activation of feline neck muscles during horizontal rotation. *Exp Brain Res*, 110(3):392–400.

Tomlinson, R. D. and Bahra, P. S. (1986a). Combined eye-head gaze shifts in the primate. i. metrics. *J Neurophysiol*, 56(6):1542–1557.

Tomlinson, R. D. and Bahra, P. S. (1986b). Combined eye-head gaze shifts in the primate. ii. interactions between saccades and the vestibuloocular reflex. *J Neurophysiol*, 56(6):1558–1570.

Wellenius, G. A. and Cullen, K. E. (2000). A comparison of head-unrestrained and head-restrained pursuit: influence of eye position and target velocity on latency. *Exp Brain Res*, 133(2):139–155.

Part IV

Two-dimensional head-unrestrained gaze saccade model

Summary

Coordinating the movements of different body parts is a challenging process for the central nervous system for three main reasons: first, the segments can have different dynamics; second, segments are often hierarchically linked; and third some subparts can have different motor goals. A simple policy would be to control the overall task goal and send a common drive to every segment, hence ensuring overall task accuracy. Unfortunately, this approach can not reproduce situations where subparts have different goals. Another policy that has been previously suggested would be to independently control the different subsystems in such a way that the overall task goal is fulfilled. However, this policy is not robust to perturbations on parts of the system, which can lead to failure of achieving the goal(s).

Here, we propose a novel approach for the hierarchical control of linked systems in which the end segment is controlled by feedback and for which each lower segment can have a separately controlled sub-goal. We apply this new control policy to eye-head coordination in two-dimensional head-unrestrained saccades. Our simulations demonstrate that the proposed control structure naturally reproduces empirical behavioral data, is robust to perturbations and accurately reaches goals for gaze and head with differently oriented trajectories. We also show that the model reproduces published results during stimulation in the brainstem or recordings in the superior colliculus. We conclude by showing how our model can be easily expanded to control structures with more linked segments, such as the control of coordinated eye on head on trunk movements.

1

Introduction

Everyday activities require the coordination of several body parts that are linked to each other (e.g., the hand, arm and shoulder) where movement of the proximal parts also moves the distal parts. If an American football player wants to catch a ball, he has to orient his gaze (gaze = eye-in-space = eye-in-head + head-on-trunk + trunk-on-legs + legs-in-space) to follow the ball trajectory and change his body posture to ensure good reception of the ball while he is running. Because eyes are carried by the head, which is carried by the trunk, which is carried by the legs, the coordination of all those body segments needs to account for the dynamics of each subpart while allowing these subparts to have different goals. A theoretical policy for the control of linked systems (LS) is to divide the overall, or global, goal into subgoals for each segment and let each one be controlled independently. This approach faces several problems: perturbations on subparts can defeat the overall task goal; the timing of each command is critical for trajectory control; and separate goals for each subpart are needed. We propose a new architecture for LS, where subparts can have individual goals, but are coupled by feedback to the most distal (and usually fastest) subpart. The most distal subpart is governed by feedback of the global goal. We call this architecture hierarchical control of linked systems (HCLS), and demonstrate its performance with a prototypical linked system, the gaze control system consisting of coordinated eye-head movements.

Gaze control naturally appears as a good candidate to test HCLS for several key reasons: firstly, eye and head have different dynamics (therefore the command timing is crucial (Guitton et al., 1990)). Secondly, head and gaze movements can follow different trajectories toward a common visual target (Goossens and Van Opstal, 1997). Finally, even if head position is perturbed, the final gaze position remains accurate (Laurutis and Robinson, 1986; Tomlinson and Bahra, 1986b; Pélisson et al., 1989, 1995).

Currently, two mechanisms have been proposed to model 1-D gaze behavior but neither of them can easily be updated to 2-D nor simulate both of the above described behaviors. In the first (Fig. IV-1, panel A), a gaze feedback loop drives both eyes and head based on gaze motor error and compensates for any perturbations during saccades (Galiana and Guitton, 1992; Lefèvre and Galiana, 1992). However, this model can only generate a head movement along

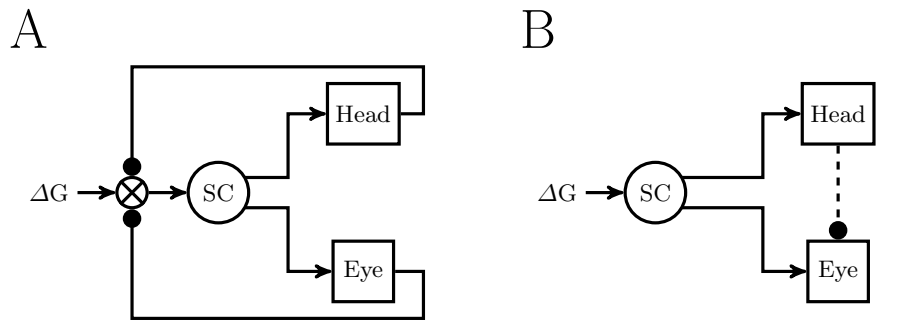

Fig. IV-1: Schematic representation of previous models of head-unrestrained gaze saccades control. Panel A schematically represents the organization of gaze feedback models. First, the desired gaze displacement (ΔG) is compared to the actual gaze displacement (Galiana and Guitton, 1992; Guitton, 1992; Lefèvre and Galiana, 1992). After, the superior colliculus (SC) sends a common motor command to the eye and the head. Panel B represents the feedforward mechanism of Freedman (2001, 2008). The desired gaze displacement is sent to the SC which sends separate commands to the eye and the head plants. An inhibition proportional to the head velocity is sent from the head controller to the eye controller (dashed line on panel B) to modulate the maximum eye velocity as a function of the head velocity. In this figure, crossed circle corresponds to a sum operator. Tip arrows correspond to an excitation (+ for a sum) and filled circles correspond to an inhibition (- for a sum).

the gaze direction. Additionally, its neural structure based on the superior colliculus can not explain how it is possible to make accurate saccades (with longer latencies and lower peak velocities) after collicular lesions (Schiller et al., 1979, 1980; Aizawa and Wurtz, 1998; Quaia et al., 1998). In the second (Fig. IV-1, panel B), a central gaze controller pre-computes separate desired eye and head displacements to execute a gaze movement (Freedman, 2001, 2008). The only interaction between eye and head pathways during gaze shifts is a modulation of the eye-in-head velocity as a function of the head velocity (represented by the dashed line with filled circle tip in Fig. IV-1, panel B). This model can generate uncorrelated head and gaze trajectories but the neck reflexes used to compensate for head perturbations cannot reproduce several published observations when the predicted eye and head trajectories are drastically changed (i.e. by braking the head for a long duration after gaze shift onset).

The current chapter presents different concepts of a new control scheme for linked systems. We chose a lumped approach instead of a distributed model to keep a fairly low number of parameters for the model. This approach stresses the general properties of the control architecture without drowning the reader in too many mathematical details. For the same reasons, we chose to use a state-space formalism instead of neural dynamics representation. Therefore, the outputs of the different subparts of the model are difficult to link to the actual discharge of the corresponding neuronal structure. Nevertheless, the main assumption is

that each subpart of the model behaves functionally like the neuronal area it represents.

We propose a unifying approach for LS and apply it to the 2-D gaze saccade control system to simulate, with the same model, both of the behavioral observations described above. HCLS is based on a hierarchical control structure in which the different subparts are driven according to their own subgoals, but the most distal part is driven by the global goal. Coupled feedback of all subparts to the most distal one ensures the accuracy of the overall task goal.

2

Methods

All the reported simulations in the present paper were performed on a personal computer running MATLAB/SIMULINK® (The Mathworks, Natick, MA, USA). In the following subsections, we will first describe the general architecture of the model. Then, we will present experimental and anatomical evidences to explain the proposed circuitry. A complete mathematical description is provided in appendix C.

1 General structure of the model

The key components of the model are given in Fig. IV-2. Our model does not include the cerebral cortex, which is assumed to select the desired gaze and head goals. The proposed circuit for the control of head-unrestrained saccades is a multi-input multi-output (MIMO) control system. It has two inputs: the desired gaze displacement (ΔG) and the desired head displacement (ΔH) and two outputs: the discharge sent to the eye muscles and the drive to the neck muscles. It includes two pathways to control gaze: one through the superior colliculus (SC) and one through the cerebellum (CB_G). In addition, the model has a second cerebellar pathway (CB_H) to control head trajectories. This novel architecture is thus based on the interactions between two separate controllers: one dedicated to the gaze trajectory and one dedicated to the head trajectory. Importantly, there is no eye controller. Because the head movement is fed back to both the gaze and the head controllers and the gaze cerebellar controller influences the head trajectory, the new architecture has a hierarchical structure. In this hierarchy, the gaze is the highest parent and the head is the child. Therefore, the gaze can modify the trajectory of the head to reach its target (through the collicular discharge). However, at the same time, the head controller tries to drive the head towards its own goal. Therefore, there is an interaction between the gaze and the head controller with the gaze having the highest priority. To control the gaze trajectory, we combined an updated lumped version of the head-restrained distributed model of Lefèvre et al. (1998) and the gaze feedback principle of (Guitton et al., 1990; Galiana and Guitton, 1992; Lefèvre and Galiana, 1992). The original head-fixed model of Lefèvre et al. (1998) includes

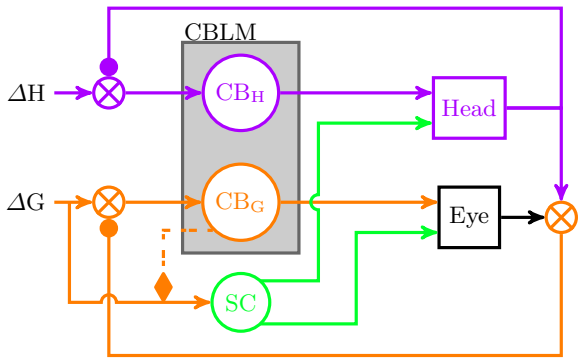

Fig. IV-2: General structure of the model. The model includes three major pathways. Two receive the desired gaze displacement (ΔG) as input: one goes through the superior colliculus (SC and green items) and projects to the eye and head plants and one goes through a first part of the cerebellum (CB_G and orange items) and projects only to the eye plant. The third pathway (CB_H and purple items) has the desired head displacement as input (ΔH); it goes through another part of the cerebellum and only projects to the head plant. SC sends a collicular drive in the direction of the desired gaze displacement to both eye and head but it does not control gaze trajectory. CB_G is the core of gaze control, it sends a drive to the eye to control gaze trajectory. It also sends a facilitation signal that mediates collicular level of activity as a function of the gaze motor error (orange diamond on SC input). CB_H controls head trajectory and sends a drive to the head. In this figure, crossed circles correspond to a sum operator. Tip arrows correspond to an excitation (+ for a sum) and filled circles correspond to an inhibition (- for a sum).

two pathways: an initial drive sent by the superior colliculus to the brainstem and a corrective drive from the cerebellum to the brainstem. In the following paragraphs, we will describe the general structure of the model and stress the differences between the head-restrained model of (Lefèvre et al., 1998; Quaia et al., 1999), the one-dimensional head-unrestrained model of (Guitton et al., 1990; Galiana and Guitton, 1992; Lefèvre and Galiana, 1992) and our new architecture. Therefore, we will refer to (Guitton et al., 1990; Galiana and Guitton, 1992; Lefèvre and Galiana, 1992; Lefèvre et al., 1998; Quaia et al., 1999) for the neural substrates already described in those studies. A complete diagram including all the modeled connections between the neural areas of the model is presented in Fig. IV-3.

2 Brainstem and spinal cord

Our model includes two premotor structures: the brainstem that sends commands to the extraocular muscles and the spinal cord that sends commands to the neck muscles. Those structures are at the interface between the neuronal discharges coming from higher areas (cortex, cerebellum, SC, etc.) and

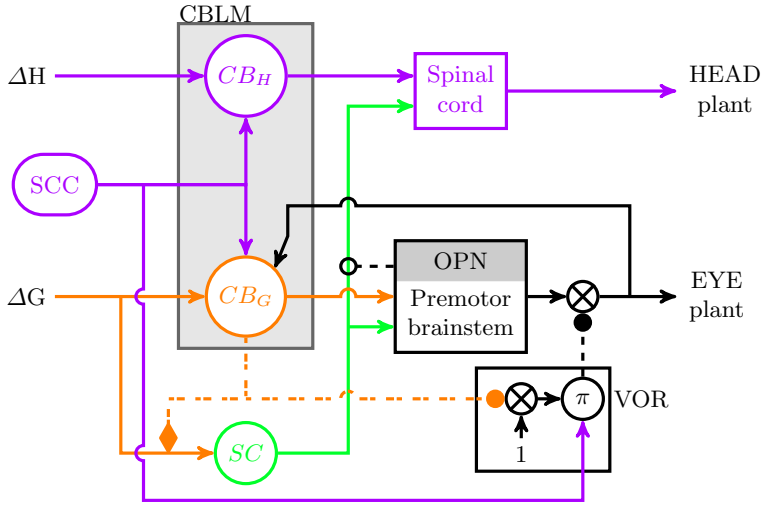

Fig. IV-3: Complete structure of the model. The complete model includes the premotor brainstem and the spinal cord. Those structures are respectively at the interface between the commands sent by higher areas and the eye and head plants. The complete model also includes the semi-circular canals (SCC) that estimate head velocity and project to the gaze cerebellar controller (CB_G), the head cerebellar controller (CB_H) and the vestibulo ocular reflex (VOR). CB_G sends a choke signal to the premotor brainstem (see a detailed representation of the brainstem circuitry in appendix C) to stop the saccade. The OPN partially inhibits the collicular activity projecting to the spinal cord. In this figure, crossed circles correspond to a sum operator and circle with a π corresponds to a multiplication operator. Arrows and solid lines correspond to excitatory signals, filled circles and dashed lines correspond to full inhibition, open circles and dashed lines correspond to partial inhibition and dotted-dashed lines and diamonds correspond to facilitation.

the muscles controlling eye and head displacements. The brainstem circuitry is modeled to sustain the inhibition on the omnipause neurons (OPN) during a gaze shift and thus allow the excitatory burst neurons (EBN) to drive the eye motoneurons (Langer and Kaneko, 1984; Fuchs et al., 1985; Scudder et al., 1996). The input of the EBN is the sum of collicular and gaze cerebellar activities (Optican and Robinson, 1980; Keller et al., 1983; Fuchs et al., 1985). As shown in Fig. IV-3, OPNs project to the collicular output to the spinal cord (Kaneko and Fuchs, 1982). Similarly, the spinal cord model conveys collicular and head cerebellar activities to the head motoneurons (Anderson et al., 1971). A complete description of brainstem and spinal cord models is present in appendix C.

The input-output relationship between the innervation of the ocular muscles and the movement of the eye is modeled as a second order transfer function with two time constants: 0.005 and 0.15 [s] as in (Robinson, 1973; Lefèvre et al., 1998; Quaia et al., 1999).

The relationship between the complex activation of the neck muscles and the resulting head movement is modeled as a second order transfer function with two identical time constants of 0.3 second as in Lefèvre and Galiana (1992).

3 The superior colliculus and the collicular pathway

The collicular pathway includes the SC (green items in Fig. IV-2 and IV-3), the brainstem, the eye plant (i.e., the eyeball, extraocular eye muscles and orbital tissues), the spinal cord and the head plant (i.e., the head, the neck muscles and tissues). This pathway has two roles: it releases the inhibition of the omnipause neurons (Langer and Kaneko, 1984; Fuchs et al., 1985; Scudder et al., 1996) to trigger the start of a head-unrestrained saccade and it provides a directional drive (in the direction of the desired gaze displacement) to the eye plant (Wurtz and Goldberg, 1972; Guitton et al., 1980) and the head plant (Anderson et al., 1971; Roucoux et al., 1980; Corneil et al., 2002a,b) respectively through the brainstem and the spinal cord. Unlike the traditional gaze feedback control models of (Guitton et al., 1990; Galiana and Guitton, 1992; Lefèvre and Galiana, 1992), the SC does not contribute to the correction of gaze trajectory but it receives a facilitation signal from the cerebellum proportional to the gaze motor error. Thus, the activity of the SC is modulated in intensity through the cerebellar facilitation (Niemi-Junkola and Westby, 2000) but the orientation of the collicular drive sent to the eye and the head does not change during a gaze saccade.

In our model, SC receives two inputs: one comes from higher cortical areas as described in (Lefèvre et al., 1998; Quaia et al., 1999) and gives the desired gaze displacement (ΔG). The second input is a facilitation signal from the cerebellum that mediates the collicular level of activity. Several studies have shown the existence of an excitatory projection from the deep cerebellar nuclei (dCN) to SC in the rat (Gonzalo-Ruiz and Leichnetz, 1987; Gayer and Faull, 1988; Niemi-Junkola and Westby, 2000) and in the grey squirrel (May and Hall, 1986) that can facilitate or disfacilitate collicular activity (Niemi-Junkola and Westby, 2000).

In the model, we divided the SC into two subparts: a rostral part that models the activity of the fixation neurons and a caudal part that models the combined activity of the burst and buildup neurons. In the rostral part of the modeled SC, there is no collicular discharge when the desired gaze displacement is smaller than a threshold value of 1 degree (output of SC in Fig. IV-2 and IV-3 is equal to zero). This zone corresponds to the rostral pole of the SC initially observed by (Munoz and Wurtz, 1993) but must be seen as a simplification of the actual SC circuitry (Hafed et al., 2009). In more caudal recordings, Wurtz and Goldberg (1972) have shown that the activity of the SC deep layers is related to a particular displacement (orientation and amplitude) of the eye in head-restrained condition. In head-unrestrained condition, using micro-stimulation (Roucoux et al., 1980) or extracellular recording (Munoz and Guitton, 1985, 1986), authors have shown that the activity of the SC deep layers is correlated with gaze displacement. Other studies have shown that there is a relationship

between the activity in the SC and the discharge of the neck motoneurons (Anderson et al., 1971) and the EMG activity of the neck muscles (Corneil et al., 2002a,b). Therefore, we modeled a projection of SC to the excitatory burst neurons (EBNs) in the brainstem (Wurtz and Goldberg, 1972) and, to account for the tecto-spinal pathway, a projection from SC to the spinal cord (Anderson et al., 1971; Guitton et al., 1980; Roucoux et al., 1980; Munoz and Guitton, 1985, 1986). The modeled collicular activity in the caudal part is proportional to the amplitude of the desired gaze displacement and is modulated by a facilitation from the cerebellum (dotted-dashed orange line with diamond tip in Fig. IV-2 and IV-3). The equations of SC activity are presented in appendix C. The second collicular output (not shown in Fig. IV-2) is a signal that releases the inhibition of the omnipause neurons (OPNs) to trigger the start of a saccade (see appendix C), as soon as there is activity in the caudal part of SC.

4 The cerebellar gaze drive

The gaze cerebellar pathway includes the cerebellum (orange items in Fig. IV-2 and IV-3), the brainstem and the eye plant. Note that in our model we do not have a projection from the cerebellar gaze pathway to the head plant (e.g., in Fig. IV-2, there is no orange line from CB_G to the spinal cord). We have not included a gaze cerebellar projection to the head because the head's inertia is so high that it would not have a significant effect on the compensation of the gaze perturbations during the short duration of a head-unrestrained saccade (around 100 [ms] for a saccade of 30 [deg], (Freedman and Sparks, 1997)). If physiological evidence of such a projection becomes compelling, adding such a projection would constitute a minor change to the model. This connection could also be useful for other species with low head inertia and a smaller oculomotor range: e.g., cat, owl, squirrel monkey, etc.

However, to account for the described effect of the cerebellum on the control of head trajectory (Goffart et al., 1998b), a second cerebellar pathway that exclusively controls head trajectory is present in the model (see below).

The cerebellum is the core of the gaze controller in the proposed model. It has three different roles; it controls the gaze trajectory to ensure that the gaze saccade ends close to the target, it modulates the level of activity of the SC and it stops the saccade by sending a choke signal to the contralateral IBNs.

The present model includes four inputs to the gaze cerebellar controller; the first is a projection from higher cortical areas through the pontine nuclei and the nucleus reticularis tegmenti pontis (NRTP) as in (Lefèvre et al., 1998; Quaia et al., 1999). This input provides the desired gaze displacement to the cerebellar controller. The second input is an estimate of the head velocity from vestibular information (Carpenter et al., 1972; Shinoda and Yoshida, 1975; Waespe et al., 1981). The third input is an efference copy of the eye velocity (Baker et al., 1972; Buchtel et al., 1972; Langer et al., 1985). The last input (not shown in Fig. IV-2) is a projection from the OPN through the NRTP to the cerebellar fastigial nucleus (Langer and Kaneko, 1983) to reset the controller when the gaze saccade is over.

To control the trajectory, the gaze cerebellar controller compares the desired gaze displacement to an estimate of the current displacement built from an efference copy of eye velocity and an estimate of head velocity. The importance of gaze feedback will become clearer in the results section and will be further elaborated in the discussion (Note that because the cerebellum receives feedback from the ongoing movement and corrects gaze trajectory, it plays the role of the resettable or bootstrap integrator in the local feedback loop of Jürgens et al. (1981)). Figure IV-4 shows the coordinate system of the 2-D controller

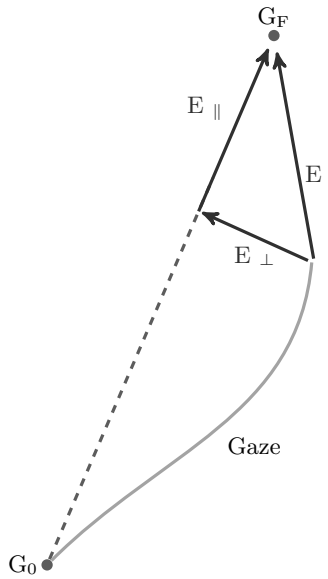

Fig. IV-4: Cerebellar-controller coordinates. G_0 corresponds to the initial gaze position. G_F is the desired final gaze position. $\mathbf{E}$ corresponds to the current gaze error. $\mathbf{E}_{\|}$ is the projection of the error along the desired initial gaze displacement (the vector from G_0 to G_F). This corresponds to the remaining gaze displacement along the desired trajectory. $\mathbf{E}_{\perp}$ corresponds to the perturbation with respect to the desired gaze trajectory. The figure represents the decomposition implemented in the Cerebellar controller. Two separate controllers are working at the same time. One nulls the error normal to the initial displacement ($\mathbf{E}_{\perp}$) and one controls the activity parallel to the initial displacement ($\mathbf{E}_{\|}$). The same architecture has been implemented for the control of the head trajectory.

implemented in the model. G_0 corresponds to the initial position of the gaze; G_F is the desired final position. $\mathbf{E}$ corresponds to the current error (the vector between the current gaze position and the target position). $\mathbf{E}_{\perp}$ is the perturbation to the desired gaze displacement (the vector from G_0 to G_F). $\mathbf{E}_{\|}$ is the remaining displacement along the desired trajectory. The key concept behind this decomposition is that when there is no deviation of the gaze trajectory with

respect to its desired trajectory, the perturbation component, $\mathbf{E}_{\perp}$, is equal to zero. Conversely, any deviation from the desired trajectory corresponds to a non-zero perturbation component that must be compensated. The gaze cerebellar drive corresponds to the sum of two drives, one for the parallel error (the remaining trajectory) and one for the perturbation component. With this error decomposition, we can control at the same time the kinematics (through the parallel drive) and the trajectory (through the perpendicular drive) of the gaze.

The proposed controller reproduces the functional properties of the cerebellum without neurophysiological realism. A more realistic distributed version could be developed similar to (Lefèvre et al., 1998; Quaia et al., 1999). In our new architecture, the controller, based on a vectorial decomposition, implicitly adjusts the commands to ensure that horizontal and vertical components of the gaze end at the same time, independently of their relative amplitudes. A complete mathematical description of the gaze controller is provided in appendix C.

As explained in the previous section, the cerebellum block also sends a facilitation signal (dotted-dashed orange line with diamond tip in Fig. IV-2 and IV-3) to the SC that modulates the intensity of the collicular drive (Niemi-Junkola and Westby, 2000). The facilitation signal is proportional to the amplitude of the gaze error ($\mathbf{E}$ in Fig. IV-4). The mathematical computation of this signal is presented in appendix C.

The third output of the cerebellum is a choke sent to the brainstem to indirectly activate the OPN and stop the saccade (dashed orange line with filled circle tip in Fig. IV-3, (Lefèvre et al., 1998; Quaia et al., 1999)). When the magnitude of the gaze error is less than a threshold value defined by a piecewise linear function, the choke is set to one. Otherwise, it is set to zero. The threshold function was adaptively tuned once before the simulations to match the observed relationship in the literature (Becker and Fuchs, 1969; Kowler and Blaser, 1995) between the amplitude of the target step and the final error of gaze position (the key values and a plot of this function are presented in appendix C). All the simulations presented in the results section had the same tuning function for the reactivation of the OPN.

5 The cerebellar head controller

The model includes a third pathway which controls the head posture (purple items in Fig. IV-2 and IV-3). This pathway permits the simulation of different trajectories for the head and the gaze displacements as previously observed (Goossens and Van Opstal, 1997). It also gives the possibility of combining different head orientations with the same final gaze position. Sprague and W. W. Chambers (1954) showed that the vermis (medial cerebellum) is inter alia implicated in the control of head movement. Wilson et al. (1978) found neurons in the rostral fastigial nucleus (rFN) that project to the upper cervical cord of the cat. Stimulations of these neurons induced monosynaptic EPSPs in neck motoneurons with a latency of 2-3 [ms]. To account for those observations, the head cerebellar controller projects only to the spinal cord (Batton et al.,

1977; Wilson et al., 1978; Isa and Sasaki, 2002) to modify the trajectory of the head, and thus acts like a perturbation to the gaze controller.

The proposed control pathway is a simplified version of the actual pathways used by the central nervous system to control the head trajectory (for a review see (Isa and Sasaki, 2002)). A more realistic control scheme would include the gigantocellular head movement region (Cowie and Robinson, 1994; Cowie et al., 1994), the interstitial nucleus of Cajal (Fukushima et al., 1978) and the Forel's field H (Isa and Sasaki, 2002). Nevertheless, the behavior of our head controller is functionally sufficient for the purpose of this model: the control of head-unrestrained gaze saccades.

The core of this pathway is the cerebellum. Compared to the gaze cerebellar controller, this controller receives only two inputs: one from cerebral cortical areas (e.g., Tu and Keating (2000) have stimulated FEF neurons that generate head-only movements) that provides the desired head displacement (ΔH) and an estimation of head velocity from the semi-circular canals (Carpenter et al., 1972; Shinoda and Yoshida, 1975; Waespe et al., 1981).

The same control principle as the one presented for the gaze cerebellar controller is used to control head trajectory. To summarize, the controller computes two terms, one along the desired head trajectory (remaining trajectory) and one perpendicular to the desired head trajectory (perturbation). The head cerebellar drive corresponds to the sum of two drives: one that controls the displacement along the desired head trajectory (linked to the movement kinematics) and one that negates the error perpendicular to the desired head trajectory (linked to the deviations from the desired head trajectory). The separation of the error in two components permits the control of the kinematics and the curvature of the head trajectory. The mathematical development of the cerebellar head controller is presented in appendix C.

As for the gaze controller, the head cerebellar controller is a functional representation of the actual control scheme used by the central nervous system. In addition, there is no current evidence that the cerebellum is explicitly involved in the control of head trajectory. Nevertheless, we believe that the general properties of the cerebellum and its known involvement in the control of limb trajectory make it a strong candidate for the head trajectory controller.

6 Vestibulo-ocular reflex

Our model includes a simplified vestibulo-ocular reflex model (box labeled VOR in Fig. IV-3) to simulate the well-known stabilization of the visual axis when the gaze is on the target (see (Leigh and Zee, 2006) for a general description of the VOR).

Several authors have shown that the VOR is suppressed during a gaze saccade (Lefèvre et al., 1992; Cullen et al., 2004). The gain of the VOR decreases at the onset of the gaze saccade (Cullen et al., 2004) and quickly increases before the end of the saccadic movement (Lefèvre et al., 1992). To simulate the suppression of the VOR, the model includes a suppression signal that inhibits the activity of the VOR. There is evidence that the VOR gain could be adapted and/or modified by the cerebellum (Gardner and Fuchs, 1975; Zee

et al., 1981). We used the same signal sent from the cerebellum to modulate SC activity (dotted-dashed line with diamond tip in Fig. IV-2 and IV-3) as the suppression signal in the model. Therefore, the VOR was computed as the product between the head velocity that goes through a first order transfer function (time constant = 10 [ms]) to simulate the semi-circular canal and a variable gain (one minus the facilitation signal form the cerebellum).

7 Desired gaze and head displacement: cortical system

In this model, we did not include a cortex that computes the correct inputs (ΔG and ΔH in Fig. 2 and 3). Instead, we directly provide the desired gaze (ΔG) and head (ΔH) displacements. Because we did not include any cortical areas, the model does not simulate any saccade-decision mechanism. We set the time origin of the simulations at saccade onset.

Additionally, we simplify the real 3-D geometry of rotations to 2-D vectors, i.e., a pair of horizontal and vertical coordinates, ignoring torsion and the non-commutativity of rotations (Quaia and Optican, 1998; Blohm and Crawford, 2007). Finally, the purpose of the model was to mimic the general behavior of primates. Therefore the set of parameters were hand-tuned once, and then kept constant during all the simulations.

3

Results

We will present simulations that emphasize the general behavior of the proposed hierarchical controller for linked systems (HCLS) as applied to gaze. To begin with, we will discuss an example that presents the general interaction between the three loops of the model. Next, different typical cases reported in the literature will be simulated to show the ability of our model to generate head-unrestrained saccades with different head and gaze trajectories toward a common visual target. Thereafter, we will present some simulations that show the influence of an artificial lesion (internal perturbation) or a brake (external perturbation) on the head during a gaze saccade. Finally, we will present the ability of the model to reproduce the observed behavioral effect of OPN stimulation during a gaze shift and the direct relationship between the collicular activity and the duration of the gaze shift. Those simulations will stress the indispensable need of feedback for gaze trajectory control. Each simulation will be compared with predictions from the two previous models. We will show that, even if some cases could be theoretically simulated by one of the two preceding models; the new model is the only one that can reproduce the behavior of previously observed experimental data without special tuning of its structure to account for a particular situation.

1 Interactions between the different pathways of the model: time course of a head-unrestrained saccade

A simulation of a head-unrestrained gaze saccade is presented in Fig. IV-5. This example will be used to explain how the different pathways of the model interact. Figure IV-5, panel A shows a spatial representation of gaze (black line), head (gray line), and eye-in-head trajectory (green line), their initial positions (filled circles), and the target (red circle). Gaze started from (0, 0) [deg] and a target step was simulated to (10, 18) [deg], in 2-D (H, V). Head started from (10, 0) [deg]; its desired final position was (10, 10) [deg] (vertical displacement of 10 [deg]). The parameters of this simulation were chosen to emphasize the general behavior of a typical simulated two-dimensional gaze saccade and were not related to a specific experimental paradigm from the

literature. The upper right panel (Fig. IV-5, panel E) shows a detailed view of the spatial representation of the head trajectory. The small arrows represent the discharge of the collicular pathway (in green) and the head cerebellar pathway (in purple) that were sent to the head plant through the spinal cord. Discharges with small amplitudes are not represented. Sizes of the arrows in Fig. IV-5, panel E are proportional to the collicular discharge and the head cerebellar discharge (arbitrary scale).

Figure IV-5, panel B represents the time course of the signals presented in Fig. IV-5, panel A (left column of Fig. IV-5, panel B represents the evolution of the horizontal position as a function of time while the right column represents the evolution of the vertical position as a function of time; the same color-code as in Fig. IV-5, panel A is used). Figure IV-5, panel C represents the time course of the gaze velocity, the eye-in-head velocity and the head velocity for the same movement as in Fig. IV-5, panel A. Figure IV-5, panel D represents the time course of the discharges of the superior colliculus (first row, SC), the gaze cerebellar pathway (second row, CB_G) and the head cerebellar pathway (third row, CB_H) along the horizontal (left column of Fig. IV-5, panel D) and the vertical (right column of Fig. IV-5, panel D) axis for the movement in Fig. IV-5, panel A. All the discharges shown in Fig. IV-5, panel D were normalized with respect to their maximum magnitude.

Open squares on the curves of Fig. IV-5 represent the value of the corresponding signal when the OPNs were reactivated at the end of the gaze saccade. The movement that preceded the open squares corresponds to the first part of the simulated head-unrestrained saccade (gaze part), i.e. the 85 [ms] between

---

Fig. IV-5 *(following page)*: Typical gaze saccade simulated by the model. Panel A: Spatial representation of eye-in-head (green lines), head (gray lines) and gaze (black lines) positions. Initial positions of gaze, eye and head are represented by filled circles on the gaze, eye and head traces. Panel B, left column: horizontal position as a function of time. Panel B, right column: vertical position as a function of time. Panel C: Horizontal (left column) and vertical (right column) velocities as a function of time. Panel D: Collicular (SC, first row), gaze cerebellar (CB_G, second row) and head cerebellar (CB_H) normalized horizontal (left column) and vertical (right column) discharges as a function of time. Panel E: Detailed view of the head trajectory with head cerebellar (purple arrows) and collicular (green arrows) relative drives. Open squares in Fig. IV-5, panels A to D indicate the value of the corresponding signal when the cerebellum released the OPN inhibition. A head-unrestrained saccade simulation can be divided into two parts. The first part is the gaze saccadic part and corresponds to eye and head movements that preceded the squares. The second part, the gaze stabilization part, corresponds to all the movements after the squares. During the first part, the eye moved quickly towards the target, so did the gaze. During the gaze stabilization part, any head movement was compensated for by a counter-rotation of the eye in the orbit through the VOR. Therefore the gaze remained stable and the head cerebellar controller corrected the head trajectory so it ended close to the desired head position.

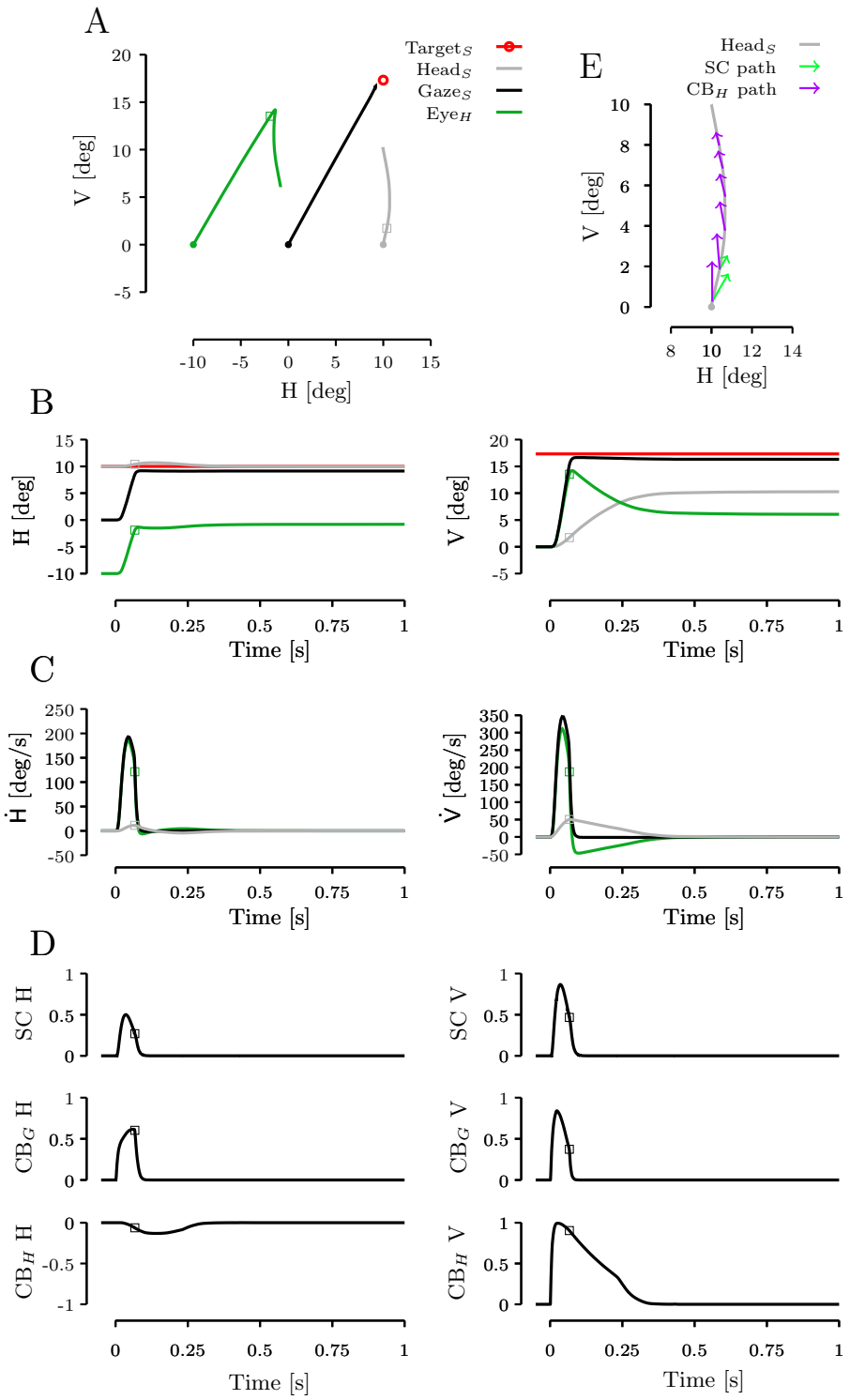
A
Target$_S$
Head$_S$
Gaze$_S$
Eye$_H$
V [deg]
H [deg]
E
Head$_S$
SC path
CB$_H$ path
V [deg]
H [deg]
B
H [deg]
V [deg]
Time [s]
C
Ḣ [deg/s]
V̇ [deg/s]
Time [s]
D
SC H
SC V
CB$_G$ H
CB$_G$ V
CB$_H$ H
CB$_H$ V
Time [s]

the onset of the gaze saccade and the reactivation of the OPN (represented by the open squares). During this period, SC and CB_G discharged to orient the gaze to its new position. CB_H discharged also but the collicular discharge was stronger at the beginning of the movement (compare the first purple and green arrows in Fig. IV-5, panel E). Therefore, the head started to move in the direction of the desired gaze displacement, even though it moved the head away from its own goal. During the first part of the movement, the VOR gain was inversely proportional to the facilitation signal that came from the cerebellum. Therefore the VOR gain decreased during the head-unrestrained gaze saccade and any perturbations of the head had to be compensated by the cerebellar gaze controller. When the OPNs were reactivated, the gain of the VOR quickly increased to one (1) and any head movement was compensated for by a counter-rotation of the eye-in-head. Therefore the gaze remained stable. This corresponds to the second part of the movement (gaze stabilization part). As shown in Fig. IV-5, panel D the collicular and the gaze cerebellar pathways ceased to discharge after the first part of the movement. Only the head cerebellar pathway continued to discharge to correct the head trajectory and moved it to its desired final position.

The interactions and the specificities of the collicular and the head cerebellar pathways appear clearly in Fig. IV-5, panel E. While the collicular drive (green arrows) remained in the same direction (direction of the desired gaze movement) with a modulation in amplitude (e.g., compare the amplitudes of the first and the second green arrow), the head cerebellar discharge (purple arrows) changed in orientation and amplitude to correct the head trajectory so the head finished its movement close to the desired final head position. Because head and gaze trajectories did not have the same orientation, the collicular head drive acted as a perturbation on the head trajectory. This can be seen in the third row, first column of Fig. IV-5, panel D as well as in Fig. IV-5, panel E. The desired head displacement did not have any horizontal component; therefore, without any collicular drive, the horizontal discharge of the head controller should be equal to zero. Because of the influence of SC on the head trajectory, the head controller tried to compensate for the collicular head drive by sending a discharge in the direction opposite to the collicular discharge. Similarly, in Fig. IV-5, panel E, the first purple arrow is oriented towards the desired head position. Once the gaze was on the target, the head cerebellar drive was updated to compensate for the accumulated head shift due to the collicular head drive.

This situation, in which gaze and head were not aligned and moved towards a common visual target, can not be solved by the traditional gaze feedback models of (Guitton et al., 1990; Galiana and Guitton, 1992; Lefèvre and Galiana, 1992). Those models predict that head and gaze trajectories moved along the same direction, driven by the gaze motor error. Conversely, the model of (Freedman, 2001, 2008) could theoretically simulate accurate gaze, eye and head movements but because it lacks online interactions between head and eye during the gaze saccade, it could not simulate the initial deviation of the head trajectory along the direction of the gaze trajectory.

2 Similar versus different orientation for desired head and gaze displacements

Using a two-dimensional paradigm, Goossens and Van Opstal (1997) showed what happens when the initial positions of the gaze and the head were not aligned. Figure IV-6 shows a simulation of two movements based on their protocol (Figure 13 of (Goossens and Van Opstal, 1997), second column, first row), one in which the desired gaze and head displacements were in the same direction (solid lines) and one in which the desired displacements had perpendicular directions (dashed lines). Same color conventions as Fig. IV-5 apply. Figure IV-6, left column of panel A, shows a spatial representation of gaze, eye-in-head and head positions in both situations. Figure IV-6, right column of panel A, shows the time course of horizontal (top row) and vertical (bottom row) positions of the gaze, eye-in-head and head in both situations. The desired final gaze and head positions were the same in the two cases. The difference in the trajectories arose from a horizontal shift of the initial position of the gaze due to a horizontal shift of the eye-in-head. Therefore, as expected, there were no big differences between the two simulations with respect to the vertical trajectories (see lower right panel in Fig. IV-6, panel A).

Figure IV-6, panel B shows a detailed view of the head trajectory with the relative discharge of the collicular (green arrows) and the cerebellar head pathways (purple arrows) that were summed and sent to the head plant through the spinal cord when head and gaze had parallel desired trajectories. Figure IV-6, panel C shows the same detailed view for perpendicular head and gaze desired displacements. The same color code was used as in Fig. IV-6, panel B.

In the parallel condition (solid lines in Fig. IV-6), the desired gaze displacement and the desired head displacements had the same orientations. Therefore, the discharge of SC had the same orientation as the head cerebellar pathway (compare the orientation of green and purple arrows in Fig. IV-6, panel B). In this situation, the collicular and the cerebellar head drives were parallel. When the gaze was on the target, the choke from the gaze cerebellar controller released the inhibition on the OPN (see methods and appendix C). From this moment (open squares on the solid lines in Fig. IV-6, panel A), the gain of the VOR quickly increased to one (not shown); thus any head movement was compensated for by a counter-rotation of the eye in the orbit and the gaze remained stable.

In the nonparallel condition (dashed lines in Fig. IV-6), the collicular activity did not have the same orientation as the head cerebellar activity (compare the direction of green and purple arrows in Fig. IV-6, panel C). Hence, as was observed in Fig. IV-5, there was a deviation of the head movement due to the collicular discharge during the first part of the gaze saccade that acted as a perturbation on the head controller. Angles between the collicular and the head discharge in Fig. IV-6, panel C are close to 90 [deg] leading to an almost vertical initial head movement. As soon as the gaze was on target (gaze stabilization part of the simulated gaze saccade), only the head pathway discharged. Therefore, collicular perturbation of the head ceased and the head cerebellar controller brought the head close to its desired final position.

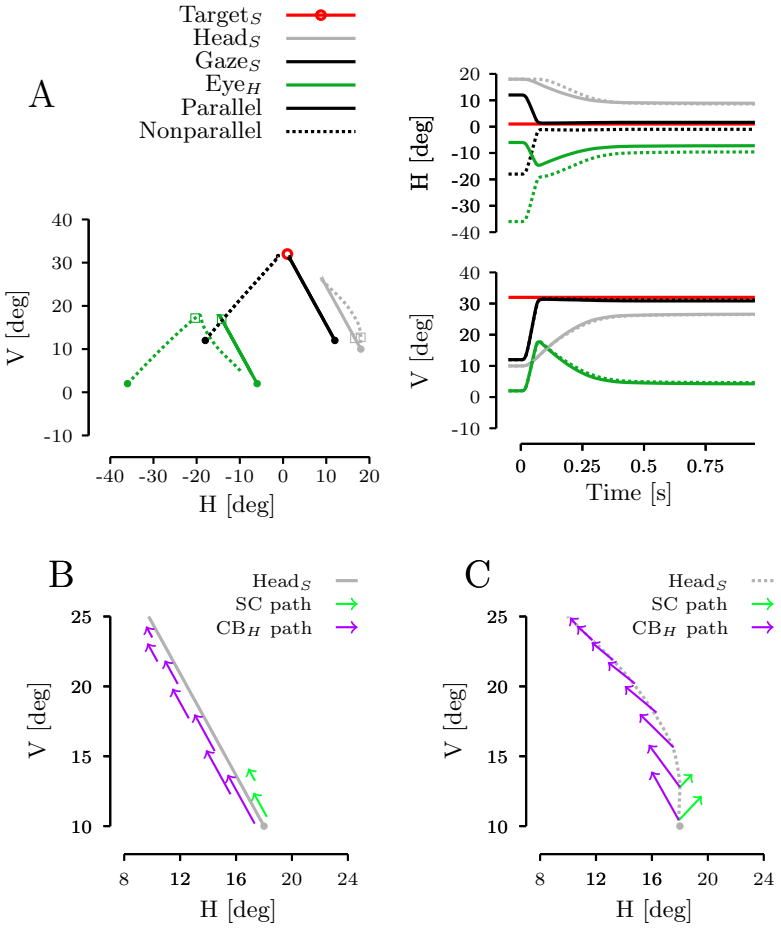

Fig. IV-6: Gaze saccades to a common final target; gaze and head with parallel displacements versus non-parallel displacements. Panel A: Gaze, eye and head displacements in the parallel condition are represented by solid lines. Gaze, eye and head displacements in the non-parallel condition are represented by dashed lines. Panel B represents a detailed view of the head movement with the collicular (green arrows) and the head cerebellar (purple arrows) drives when head and gaze desired trajectories were parallel. For the visibility of the arrows, we inserted an offset between the tails of the arrows and the head curve. Panel C represents a detailed view of the head trajectory with collicular (green arrows) and head cerebellar (purple arrows) drives when head and gaze did not have parallel desired displacements. Same color conventions as in Fig. IV-5 apply. In the parallel condition, gaze and head trajectories had the same orientation, thus collicular, gaze cerebellar and head cerebellar drives also had the same orientation (compare green and purple arrows on panel B). When gaze and head trajectories had different orientations, the collicular drive was oriented accordingly with the gaze trajectory and the head cerebellar trajectory changed its orientation and amplitude to correct the head trajectory (compare green and purple arrows on panel C).

A qualitative comparison between our simulations and the behavioral observations of Goossens and Van Opstal (1997) (Fig. 13, first row, second column) is obvious. As for their recordings, the simulated head movement in the unaligned condition is initially deviated along the gaze direction (gaze not represented in Fig. 13 of (Goossens and Van Opstal, 1997), sum of eye and head movements) but the head trajectory is corrected and ends close to the aligned situation. It is important to stress that, both in their behavioral recordings and in our simulations, the spatial position of the visual target corresponds to the goal of both head and gaze.

Neither gaze feedback models (Guitton et al., 1990; Galiana and Guitton, 1992; Lefèvre and Galiana, 1992), because of the common drive for eye and head, nor the independent control model of Freedman (2001, 2008), because its lack of eye-head interactions during the gaze saccade, can simulate gaze and head trajectories experimentally observed by Goossens and Van Opstal (1997) and simulated by the novel proposed architecture.

3 Lesion of the brainstem: compensation for internal perturbation

A practical way of testing a model is to perturb its normal behavior. Like saccade trajectories in head-restrained conditions (Erkelens and Sloot, 1995; Schreiber et al., 2006), head-unrestrained gaze saccades can exhibit a curved trajectory (e.g., (Freedman and Sparks, 1997; Goossens and Van Opstal, 1997)). Quaia and Optican (1997) showed with a model that a change in the bursters of the brainstem can create curvature in the saccade. Figure IV-7 shows a simulation in which we perturbed the commands sent to the eye by simulating a lesion on the vertical EBN gain. The gain of the vertical EBNs has been decreased by 66% while the horizontal gain remained at 100%.

Figure IV-7 represents two simulations: one with full gains for the horizontal and the vertical burst neurons (solid lines) and one with the horizontal gain remaining at 100% and the vertical gain decreased by 66% (dashed lines). The same color conventions as Fig. IV-5 and IV-6 apply. Figure IV-7A, left column, shows a spatial representation of the gaze, eye-in-head and head position in the two situations. The right column of Fig. IV-7, panel A represents the time course for horizontal (top row of Fig. IV-7, panel A) and vertical (bottom row of Fig. IV-7, panel A) positions of the gaze, the eye-in-head and the head in both simulated cases. Figure IV-7B shows a detailed view of the eye trajectory when the horizontal gain and the vertical gain of the bursters were equal. Figure IV-7C is a detailed view of the eye trajectory when the gain of the vertical bursters was decreased by 66%. Green arrows in Fig. IV-7, panel B and IV-7C represent the collicular discharge sent to the eye plant through the brainstem while orange arrows represent the gaze cerebellar drive sent to the eye plant.

In both situations shown in Fig. IV-7, the initial gaze position and the final target position remained the same. The head also had the same initial position and the same desired head displacement in the two conditions presented in Fig. IV-7. The simulated initial position of gaze and head as the position of the target were set as in Fig. 10 of (Goossens and Van Opstal, 1997).

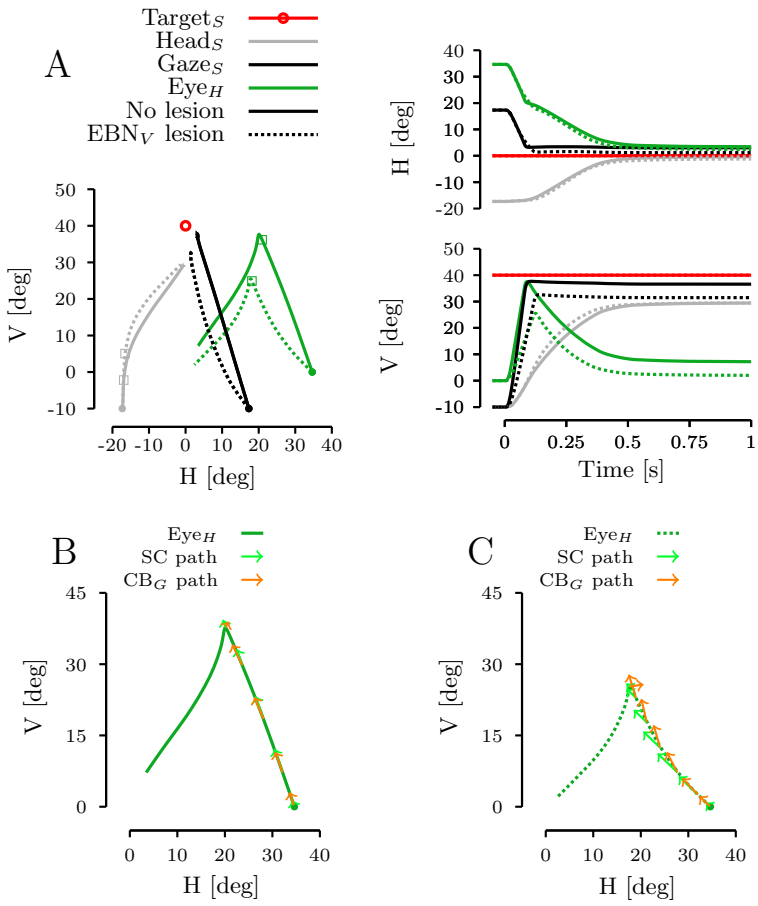

Fig. IV-7: Influence of a lesion of the vertical eye bursters (brainstem) on gaze saccade trajectory. Panel A represents positions of eye-in-head, head and gaze trajectories. Solid lines correspond to the same gain value for horizontal and vertical eye bursters. Dotted lines correspond to a normal horizontal eye bursters gain and a gain of the vertical eye bursters decreased by 66%. Same color convention as Fig. IV-5 and IV-6 apply. Panel B represents a detailed view of the eye trajectory with gaze cerebellar (orange arrows) and collicular (green arrows) relative discharges when the bursters gains were identical. Panel C represents a detailed view of the eye trajectory with collicular (red arrows) and gaze cerebellar (orange arrows) relative discharges when the vertical bursters gain was three times smaller than the horizontal bursters gain. When the gains of the two components were identical, the observed trajectories of the gaze, the eye-in-head and the head have the same properties as the trajectories of Fig. IV-5 and IV-6. Panel B shows that the collicular and the gaze cerebellar discharge were parallel. By decreasing the gain of the vertical bursters relative to the gain of the vertical ones, the collicular and the initial cerebellar discharge were not aligned with the target anymore. As shown in panel C, they were rotated towards the horizontal. However, the gaze cerebellar controller has an efference copy of the output of the bursters (see gaze feedback in Fig. IV-2 and IV-3); thus it could account for the difference in the gains and correct the trajectory of the gaze.

The influence of the lesion to the brainstem can be seen on the gaze trajectories in Fig. IV-7, panel A and on the eye trajectory in Fig. IV-7, panel B and IV-7C. By decreasing the vertical bursters' gain, the same command sent to the eye created a smaller vertical displacement than normal. This can be observed by comparing the orientation of the first pairs of green and orange arrows in Fig. IV-7, panel B and IV-7C. Therefore, the gaze saccade started with a bigger horizontal component than the vertical component. Nevertheless, because the gaze cerebellar controller used an efference copy of the discharge of the eye motoneurons to estimate the gaze displacement, it corrected the gaze trajectory to ensure that the gaze ended close to the target position.

The action of the gaze cerebellar pathway during the gaze saccade appears clearly when one compares the gaze cerebellar discharge in Fig. IV-7, panel B and IV-7C. In Figure IV-7B, the collicular and the gaze cerebellar discharges were parallel. Conversely, the orientation of the gaze cerebellar discharge changed by approximately 30 [deg] between the first and the last orange arrow in Fig. IV-7, panel C. This modification of the gaze cerebellar discharge compensated for the perturbation from the slow vertical bursters in the brainstem and thus corrected the gaze trajectory.

Because the total discharge sent to the eye was smaller than normal, the gaze movement lasted longer (compare dashed and solid black lines in Fig. IV-7, panel A, right panel). Therefore, the influence of the collicular discharge on the head trajectory lasted longer and the head was more deviated along a direction parallel to the gaze trajectory (compare dashed and solid grey lines and the position of the grey squares in Fig. IV-7, panel A) when there was a lesion compared to the normal situation.

The shorter final position when there was a lesion compared to the healthy case came from the structure of the controller; when the OPNs were reactivated, the gaze velocity was smaller in the lesioned case than in the normal situation. Therefore, the gaze stopped earlier and the final gaze position ended further from the target when there was a lesion compared to the normal situation (difference in errors amplitude: 3.6 [deg]).

Gaze feedback control models (Guitton et al., 1990; Galiana and Guitton, 1992; Lefèvre and Galiana, 1992) would predict that the final gaze error will be close in both the normal and the lesioned situations because the perturbation will be, as in our case, inside a gaze feedback loop. Nevertheless, as was the case for the previous simulations, this model could not simulate the different orientations for gaze and head trajectories because the common drive sent to both effectors is related to gaze error.

Without changing the model parameters between the two simulations, the independent model of Freedman (2001, 2008) would not simulate an accurate gaze saccade. As shown by the simulation in Fig. IV-7, panel C, the lesion decreased the amplitude of the drive at the output of the brainstem. Therefore, without any online correction of the command sent to the eye, the displacement of the gaze will be smaller with a lesion than in the unperturbed case. Because the prior decomposition mechanism of the desired gaze displacement into head and eye-in-head components as proposed by Freedman (2001, 2008) is located before the perturbation, it has no information about the effect of the lesion

on gaze trajectory. Therefore, with their model, the lesioned gaze saccade will be simulated as in the normal situation and the gaze displacement will be smaller than in the normal situation (approximately a third of the normal displacement).

4 Torque pulse on the head during a gaze shift: external perturbation rejection

Using a torque pulse on the head during a gaze saccade, Tomlinson and Bahra (1986a,b) showed that the VOR is suppressed during the gaze saccade but that the final gaze position remains accurate. Later, Lefèvre et al. (1992) and Cullen et al. (2004) reported a more detailed evolution of VOR suppression during gaze saccades. They showed that the VOR gain decreases quickly at saccade onset (Cullen et al., 2004) and increases back to one (1) before saccade offset (Lefèvre et al., 1992). The suppression of the VOR combined with the accuracy of the gaze endpoint implies a continuous feedback control of the gaze trajectory. To demonstrate the importance of a gaze feedback circuit in rejecting perturbations on gaze trajectory when the VOR gain is close to zero, we simulated a horizontal torque pulse on head trajectory that occurred shortly after the onset of a gaze saccade, when the VOR gain was minimal (g_{VOR}=0.015). The initial position of the gaze and the head and the target position were set as in the previous simulation, according to the experiments presented in (Goossens and Van Opstal, 1997).

Figure IV-8 represents two simulations: one without perturbation (solid lines) and one with a torque pulse on the head 15 [ms] after saccade onset (dotted lines). The same color conventions as in Fig. IV-5-IV-7 apply. Figure IV-8A shows a spatial representation of the gaze, eye-in-head and head position in the two situations. Figure IV-8B represents the time course for horizontal (left column) and vertical (right column) positions of the gaze, the eye-in-head and the head in both simulated cases. Figure IV-8C, left column (right column) represents the time course of the horizontal (vertical) gaze velocity, the horizontal (vertical) eye-in-head velocity and the horizontal (vertical) head velocity. Only the first 75 milliseconds near the perturbation are presented in Fig. IV-8, panel B and IV-8C but the whole trial (1 second) is shown in the spatial representation (Fig. IV-8, panel A). The simulated perturbation was applied during 15 [ms], oriented to the right and induced a perturbed peak velocity of 300 [deg/s] (perturbation delimited by the purple boxes in Fig. IV-8, panel B and IV-8C).

As presented by Tomlinson and Bahra (1986b), the influence of an external perturbation on the head can be clearly seen on head and gaze trajectories in Fig. IV-8 (compare head and gaze velocities of Fig. 2, panel B of (Tomlinson and Bahra, 1986b) and horizontal head and gaze velocities of Fig. IV-8, panel C). Figure Fig. IV-8 C shows a drastic change in horizontal head and gaze velocities due to the perturbation. As soon as the perturbation was over, the gaze and head controllers corrected the trajectories so that they ended close to the desired final positions. Thus, even with a perturbation, gaze and head trajectories ended close to the unperturbed trajectories (compare solid and dashed lines

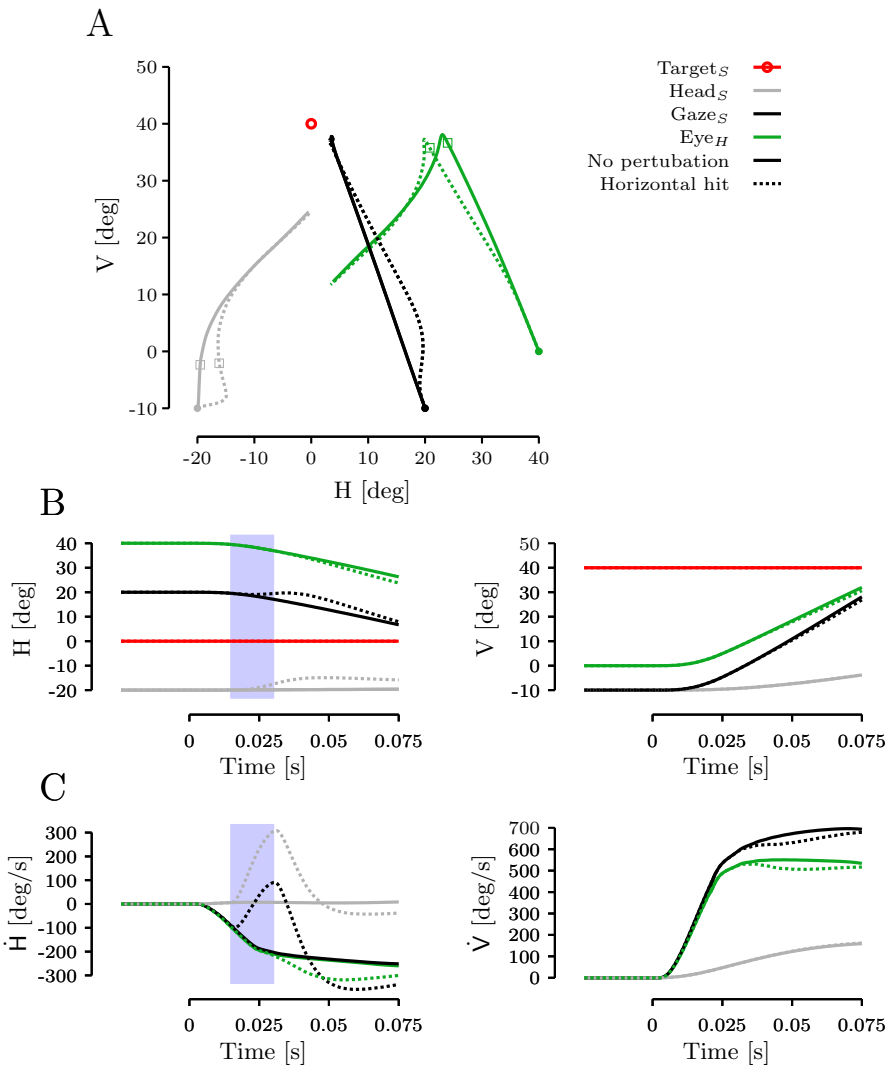

Fig. IV-8: Effect on gaze trajectory of a head perturbation during a gaze saccade. Panel A represents positions of eye-in-head, head and gaze trajectories. Solid lines correspond to a non-perturbed situation. Dotted lines correspond to the perturbed case. The simulated perturbation was applied during 15 [ms] on the head which started 15 [ms] after gaze saccade onset. Panel B, left column: horizontal position as a function of time. Panel B, right column: vertical position as a function of time. Panel C: Horizontal (left column) and vertical (right column) velocities as a function of time. Same color convention as in Fig. IV-5-IV-7 apply. Purple boxes on panels B and C correspond to the timing of the perturbation. When the perturbation was applied, the VOR gain was suppressed. Therefore head but also gaze trajectory was modified by the perturbation but the two controllers corrected the trajectories. At the end of the movement, gaze and head positions in the perturbed case were close to the unperturbed situation.

for head and gaze trajectories) as previously demonstrated by Tomlinson and Bahra (1986b). This shows the importance of the two feedback loops to control gaze and head trajectories when the VOR gain is smaller than one. Additionally, as observed by Tomlinson and Bahra (1986b), the simulated horizontal perturbation did not importantly affect the vertical gaze displacement.

As for the preceding simulation, the gaze feedback models (Guitton et al., 1990; Galiana and Guitton, 1992; Lefèvre and Galiana, 1992) would drive the gaze toward a similar final position during both the unperturbed and the torque situations because of the gaze feedback which, as in our situation, would compensate for the perturbation. However, because head and gaze are driven by a common drive, this model could not simulate distinct orientations for gaze and head trajectories.

The independent control model of Freedman (2001, 2008) could simulate head and gaze displacements in the unperturbed situation (without the initial interaction between head and gaze trajectories as previously explained). However, head position at the time of OPN reactivation is not the same in perturbed and unperturbed situations (compare the location of the open squares on the head trajectories in Fig. IV-8, panel A). This need of equivalent positions at the time of OPN reactivation is a fundamental assumption to ensure a proper compensation by the neck reflexes mechanism used in the independent model of Freedman (2001, 2008), because the eye trajectory is not modified by the perturbation. Thus, neck reflex used in the independent model of Freedman (2001, 2008) would not compensate the gaze trajectory for the torque perturbation on the head.

5 OPN stimulation during a gaze shift.

Gandhi and Sparks (2007) studied the influence of stimulation of the omnipause neurons during a gaze shift on eye and head trajectories. They showed that the stimulation of the OPNs after (before) gaze onset interrupts (delays) the gaze shift but not the head trajectory. They also observed that after the stimulation there is a re-acceleration of the head movement (Fig. 1B of (Gandhi and Sparks, 2007)). To reproduce this result, we simulated a 40 [deg] horizontal gaze saccade with gaze and head initially positioned at -20 [deg].

Figure IV-9 shows the results of two simulations: one without stimulation (solid lines) and one in which the OPNs were stimulated 25 [ms] after saccade onset for 150 [ms]. (color conventions as in Fig. IV-7). Panel A, left column shows the time course of target and gaze trajectories, whereas right column shows gaze velocity. Panel B shows the time course of head position (left column) and velocity (right column). Panel C shows the time course of eye-in-head position (left column) and velocity (right column). Gray boxes in panels A-C represent the OPN stimulation period. Open squares on the curves indicate when the OPNs were reactivated at the end of the gaze saccade.

As shown by Gandhi and Sparks (2007), the simulated gaze shift, but not the head trajectory, was interrupted when the OPNs were stimulated (see gaze velocity in Fig. IV-9, panel A, right column). Because the stimulation of the OPNs inhibits the EBNs, there was no more drive to the eye plant from either

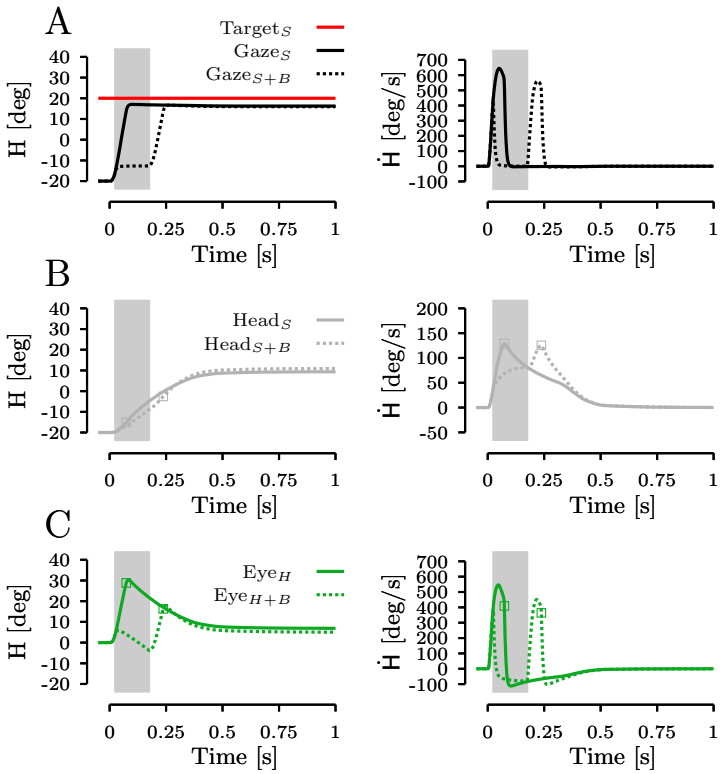

Fig. IV-9: OPN stimulation during gaze shift. Left column of panel A represents gaze and target positions as a function of time and right column of panel A represents gaze velocity as a function of time. Panel B represents head position (left column) and head velocity (right column) as a function of time. Panel C represents eye-in-head position (left column) and eye-in-head velocity (right column) as a function of time. Solid lines in panels A, B and C represent the normal situation while dashed lines represent the simulation with an OPN stimulation. Red boxes in panels A, B and C represent the 150 [ms]OPNs stimulation period which started 25 [ms] after the onset of the gaze shift. Open squares in Fig. IV-9, panel A to IV-9C) correspond to the value of the corresponding signal when the cerebellum released the OPN inhibition (gaze on target). During the OPNs stimulation period, the EBNs were inhibited and no more gaze cerebellar drive went to the eye plant. Nevertheless, the head cerebellar controller continued to drive the head towards its desired final position. Because the OPNs were discharging, the VOR gain was fully functional. So the eye counter-rolled in the head and the gaze remained stable. When the OPNs' stimulation finished, there was a slight acceleration of the head because of the reactivation of the collicular input to the spinal cord.

the gaze cerebellar controller or the superior colliculus. Moreover, because the OPNs indirectly modulate the VOR gain in the model (see computation of the suppression signal in the supplementary materials), their stimulated activation leads to a fully operational VOR. Thus, as observed by Gandhi and Sparks (2007), a counter-rotation of the eye in the orbit compensated for any head movement and gaze remained stable during the stimulation (compare head and eye-in-head positions and velocities in IV-9, panels B and C). When the stimulation was over, the collicular and the gaze cerebellar discharges were sent to the eye to drive gaze towards its final position. Because the OPNs also partially inhibited the collicular discharge to the spinal cord (see appendix C), as soon as the stimulation was over, the amplitude of the collicular discharge at the input of the spinal cord increased. Thus a re-acceleration of the head was observed (see dashed gray line in Fig. IV-9, panel B, right column) as described by Gandhi and Sparks (2007). As soon as the gaze was on the target, the gaze cerebellar controller released the inhibition on the OPNs and the gaze movement stopped.

As for the previous simulations with perturbations, traditional gaze feedback models (Guitton et al., 1990; Galiana and Guitton, 1992; Lefèvre and Galiana, 1992) would simulate an accurate final gaze position, as observed by Gandhi and Sparks (2007), because of the feedback on the gaze. Moreover, because in this model head and eye are driven by the same signal, an acceleration of the head should occur with the end of the OPN stimulation.

Because the overall displacement of the head does not change, with or without OPN stimulation, the independent control model of Freedman (2001, 2008) can simulate an accurate final gaze position (if one assumes that the eye controller is not reset by an OPN stimulation and that the VOR is gated by the OPN activity) as described by Gandhi and Sparks (2007). However the independent control model could not simulate the re-acceleration of the head when the OPN stimulation is over because there is no interaction from the eye controller to the head controller.

6 Brake on the head during a gaze shift and SC discharge

To demonstrate the importance of feedback on the gaze trajectory and the coupling between the collicular discharge and the gaze position error, Choi and Guitton (2006) developed a paradigm in which they braked the head movement during a large gaze shift and recorded the activity in the superior colliculus at the same time. Using this combination, they artificially changed the duration of the gaze shift. They found that the timing of the reactivation of the fixation neurons in the superior colliculus was correlated with the duration of the gaze shift (see Fig. 2F of (Choi and Guitton, 2006)). To compare their results with our model's prediction, we simulated the same protocol as the one used by Choi and Guitton (2006). Figure IV-10A shows the time course of the horizontal target (red line), gaze (black line), eye-in-head (green line) and head (gray line) positions for a typical simulation of a braked head movement during a 70 [deg] gaze shift. Open squares in Fig. IV-10, panel A indicate when the gaze cerebellar controller released the inhibition of the OPNs at the end of the gaze

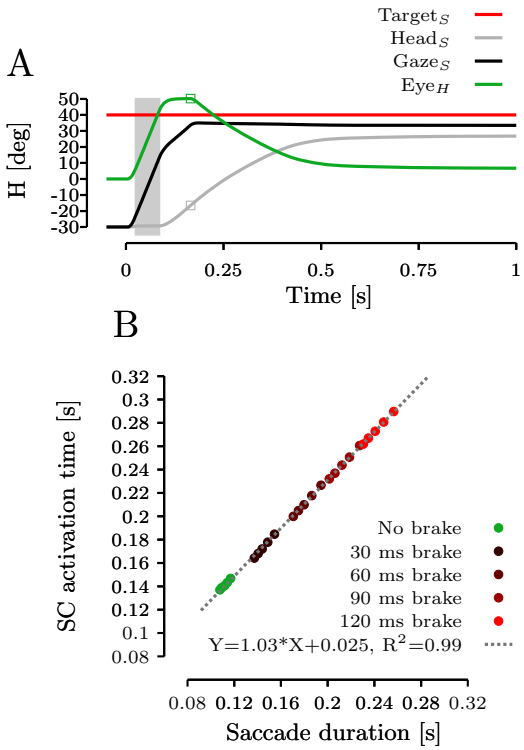

Fig. IV-10: Brake on the head during gaze shifts. Panel A represents horizontal position of target, eye-in-head, head and gaze trajectories as a function of time for a typical trial. Gray box in panels A represents a 60 [ms] braking period which started 25 [ms] after the onset of the gaze shift. Open squares in panel A correspond to the value of the corresponding signal when the cerebellum released the OPN inhibition. During the braking period, the head stopped to move but the gaze cerebellar controller continued to drive the gaze towards the target with eye movement only. As soon as the brake was released, the head accelerated and moved towards its target. When the gaze was on the target, the cerebellum released the OPNs inhibition. Therefore any head movement was compensated for by a counter-rotation of the eye in the orbit through the VOR (gaze stabilization part). Panel B represents the SC activation time as a function of the saccade duration. We simulated several brake durations and several head amplitudes during a 70 [deg] gaze shift. All the data conditions are pooled together in panel B.

shift. The gray box in Fig. IV-10, panel A represents the period during which the brake was applied. The braking period started 25 [ms] after the onset of the gaze shift and lasted for 60 [ms]. Because the model includes a functional representation of the oculomotor range (OMR) of 50 [deg] (see appendix C), as soon as the eye reached the boundary of the OMR, its velocity decreased and it remained stationary in the orbit. From this time, only the head was moving. Therefore, the gaze and the head moved at the same velocity until gaze reached its final position. As soon as the gaze reached its goal, the inhibition on the OPNs was released, thus the VOR was activated, the eye counter-rolled in the orbit and gaze remained stable.

To compare the global behavior of our model with the observations of Choi and Guitton (2006), we simulated five braking durations (No brake, 30 [ms], 60 [ms], 90 [ms] and 120 [ms]) and five desired displacements of the head (40%, 50%, 60%, 70% and 80% of the desired gaze displacement) for a single gaze shift amplitude of 70 [deg]. For each simulation, we computed the duration of the gaze shift (using a velocity criterion on the gaze velocity) and the duration of the collicular activity (using a threshold on the amplitude of the collicular activity). Figure IV-10B shows the evolution of the collicular activation time as a function of the gaze saccade duration for all the braking durations and all the head displacements pooled together. The gray dashed line in Fig. IV-10, panel B represents a linear regression between the two variables of Fig. IV-10, panel B. This regression showed a strong linear relationship (slope=1.00, R^2 =0.99, p-val<0.001) between the collicular activity and the duration of a gaze saccade as observed and described by Choi and Guitton (2006). Our simulations also reproduced the findings of Choi and Guitton (2009) in which the authors showed that the collicular activity encodes the remaining gaze position error when a brake is applied on the head (data not shown). The amplitude of the collicular discharge is multiplied by a facilitation signal from the cerebellum (see methods and appendix C). Thus, when the head is braked, the colliculus still discharges with an amplitude proportional to the remaining gaze motor error until the gaze reaches its goal as described by Choi and Guitton (2009).

Prsa and Galiana (2007) tuned the original model of (Guitton et al., 1990; Galiana and Guitton, 1992; Lefèvre and Galiana, 1992) by inserting a new threshold function for the OPN to simulate gaze and head trajectories of the experiment of Choi and Guitton (2006). However, they did not show the possibility of the gaze feedback models (Guitton et al., 1990; Galiana and Guitton, 1992; Lefèvre and Galiana, 1992) to reproduce the observed relationship between the collicular activity and the duration of a gaze saccade.

In this simulation the braking period duration is longer than the duration of the gaze shift. In the independent control model of Freedman (2001, 2008), the eye displacement will not be modified by the perturbation. Thus the eye movement will be simulated as in a normal condition and will end before the gaze will be on target. Therefore, the independent control model of Freedman (2001, 2008) will not be able to reproduce the results of Choi and Guitton (2006).

4

Discussion

In this paper we presented a new approach for the hierarchical control of linked systems (HCLS). We demonstrated the usefulness of this approach for head-unrestrained gaze saccade control, but we propose that this novel architecture also applies to the control of any system of linkages, no matter how long. The example LS developed here included three major pathways, as represented in Fig. IV-2. One pathway through SC (green items in Fig. IV-2) sends a common directional drive to both eye and head plants. This collicular drive does not change in orientation during the gaze saccade but its amplitude is modulated through a facilitation signal proportional to gaze motor error. The second pathway through one part of the cerebellum (CB_G and orange items in Fig. IV-2 and IV-3) projects to the eye. The gaze cerebellar controller compares the desired gaze displacement with a current gaze displacement estimate and uses this gaze motor error to control eye trajectory. The third pathway through another part of the cerebellum (CB_H and purple items in Fig. IV-2 and IV-3) controls head trajectory. Here, the head cerebellar controller compares the desired head displacement to a current head displacement estimate. The head cerebellar controller uses this head motor error to correct the head trajectory and ensures that the head ends close to the final desired head position. Using the concurrent action of those three pathways, we simulated with the same model a correction of the gaze trajectory through a gaze feedback loop and head-unrestrained saccadic movements with different orientations of the gaze and head.

Adding more platforms to the system, e.g., by adding trunk motion to gaze control, would simply augment this model with another cerebellar pathway for controlling the trunk, which would also feedback to the cerebellar gaze controller. Figure IV-11 shows a suggested extension of our coupled-feedback controller for a LS with trunk, head, and eyes.

We showed simulations of two-dimensional, head-unrestrained gaze saccades for which the orientations of the desired head and gaze displacements were either different or similar. The simulated trajectories were close to experimentally observed behaviors as previously reported in the literature (e.g., (Goossens and Van Opstal, 1997)). With either simulated lesions or perturbations of the head, we demonstrated the importance of gaze feedback to compensate for external

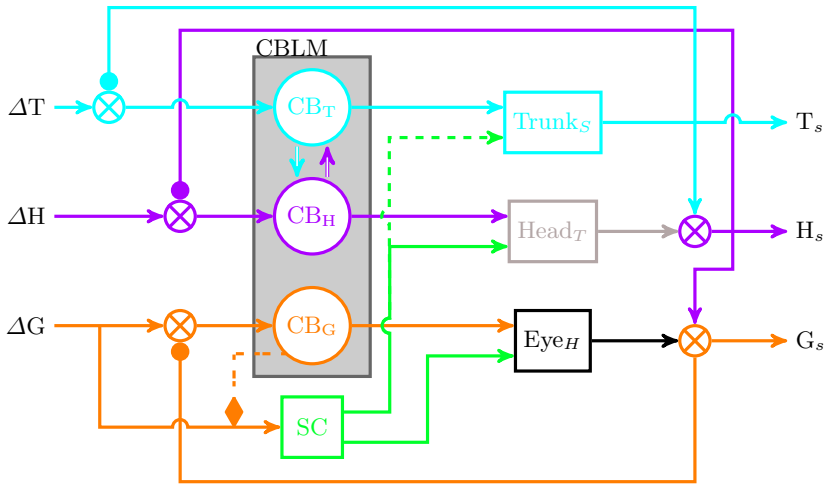

Fig. IV-11: Augmented control structure with control of trunk movements. The gaze control structure of the model is identical to Fig. IV-2. A supplementary feedback has been included to account for the control of trunk movement. A possible third projection (in dashed line) from the superior colliculus to the trunk plant has been added to account for observed body movement with SC stimulation. The head controller (CB_H) controls head position with respect to an inertial reference frame but projects to the head plant represented in a trunk-fixed reference frame ($Head_T$). A double connection between trunk and head controller inside the cerebellum is postulated. This connection influences the trunk controller for head movements outside the head motor range. In this figure, crossed circles correspond to a sum operator. Tip arrows correspond to an excitation (+ for a sum) and filled circles correspond to an inhibition (- for a sum).

or internal perturbations that occurred during gaze saccades. Finally, simulations showed that the model can reproduce experimental results either when OPNs were stimulated during the gaze shift (Gandhi and Sparks, 2007), or when recording in SC (Choi and Guitton, 2006) while perturbing the head.

With the appearance of head-unrestrained behavioral recordings (Bizzi et al., 1971), researchers proposed models of eye-head coordination during saccades. Extending the principle of internal feedback loops introduced by Robinson (1975), Laurutis and Robinson (1986) developed a head-unrestrained gaze saccade model that included an internal, or local, feedback loop of gaze position. In their model, the feedback loop controls the gaze position using a gaze motor error built from the difference between the target position and an estimate of gaze position. Moreover, only the gaze was controlled since head position was an independent input of the model. Based on the observed tight coupling between eye and head movement kinematics (especially in head-unrestrained cats (Guitton et al., 1990)), Guitton and Galiana extended the principle of Laurutis and Robinson (1986) to the control of both eye and head during gaze saccades (Guitton, 1992; Galiana and Guitton, 1992; Lefèvre and Galiana, 1992). Their

models also included a gaze feedback loop (see Fig. IV-1, panel A) to compute gaze motor error which predominantly drives both eye and head (as opposed to gaze and head in our model).

Even though strong coupling between the eye and head (and therefore between gaze and head) has been observed, there are examples where the two systems have differently oriented trajectories (Goossens and Van Opstal, 1997), are not temporally synchronized (Freedman and Sparks, 1997) or where head movement characteristics change as a function of gaze saccade amplitude (Guitton and Volle, 1987; Freedman and Sparks, 1997). From those observations, Freedman (2001, 2008) proposed a new architecture for head-unrestrained saccade control based on an a priori decomposition of the desired gaze displacement into its eye and head components (see Fig. IV-1, panel B). Those components are then sent to two separate controllers, one for the head and one for the eye movement. The only interaction between the two separate pathways is an inhibitory signal sent from the head controller to the saccade generator that modulates the maximum eye velocity proportionally to the head velocity. In the Freedman model, the eye displacement is controlled using feedback of the eye motor error as in (Robinson, 1975), but no feedback is included to control gaze trajectory. Any perturbation on the head is postulated to be rejected by neck reflexes in Freedman's model. However, this hypothesis is hard to reconcile with several observations. For instance, the experiment of Choi and Guitton (2006) (brake on the head during a large gaze shift while recording in SC) showed that gaze shifts remained accurate even when the brake on the head lasted longer than the duration of the normal eye movement. This result is simulated by our model and could not be reproduced by the neck reflex mechanism proposed by Freedman because the eye movement will not be affected by the head perturbation (see last simulation in the results). It is important to stress that without an interaction from the head to the eye movement (and therefore, a form of gaze feedback), it is impossible for any updated neck reflex mechanism to correct the gaze trajectory to negate long head perturbations.

The previous models were designed to simulate 1-D gaze trajectories. A 2-D update of those models is not a trivial task, and adding head movements to a head-fixed model requires inclusion of a vestibular system. Nonetheless, simply incorporating these changes does not get us all the way to our solution, nor does it generalize to other multi-platform controllers. The main contribution of our new model is the idea of hierarchical control where each subcontroller has its own goal, but the most distal effector has only the composite goal. Thus the 1-D to 2-D update would only produce a controller with eye and head controllers, which would not generalize to other movement controllers. In contrast, our new model has no eye controller, only gaze and head controllers, and would easily generalize to other linked platforms.

Finally, prior models cannot simulate both perturbation rejection and differently oriented gaze and head trajectories in 2-D. Our new architecture, with the parallel control of independent gaze and head trajectories, manages this in an efficient and extensible way.

As described in the methods, the new model was designed to simulate gaze saccades in two dimensions. An update to account for eye torsion and binoc-

ularity (three-dimensional structure) is not straightforward. Apart from the issue of noncommutativity, the model should include a proper balance between Listing's Law, VOR and binocularity. This has to be investigated in detail in a separate study.

The SC importance in controlling eye movements has been known since Adaműk's 1872 study (Wurtz and Goldberg, 1971, 1972; Robinson, 1972). In head-unrestrained monkeys (Stryker and Schiller, 1975; Freedman et al., 1996; Corneil et al., 2002a,b) or head-unrestrained cats (Roucoux et al., 1980; Guitton et al., 1980), authors have shown that SC electrical stimulations produce combined eye-head movements. Additionally, Corneil et al. (2002a,b) showed that SC low-current stimulations can evoke head movements without gaze displacement. Our model is compatible with those results. Their results can be simulated by turning on the SC but keeping the OPNs activated. Therefore, the VOR will be active, the gaze will remain stable and the head will move because the increased output from the SC will not be blocked by the partial OPN inhibition of the collicular output to the spinal cord (see appendix C).

In contrast to the core role of SC in classical models of gaze control, saccades appear fairly normal (albeit with increased latency and lower peak velocity) after chemical lesions of SC (Aizawa and Wurtz, 1998; Quaia et al., 1998). Additionally, when SC is ablated, Schiller et al. (1979, 1980)) showed a decrease in the frequency of saccades and in saccade maximum velocity. Those studies provided evidence that SC is not an essential structure for the execution of accurate gaze saccades. In our model, a collicular lesion does not impair the ability to simulate saccadic movements because the cerebellar pathway is sufficient for saccades. The movement will be slower (no burst of activity from SC) but the general accuracy will not vary much because the gaze cerebellar feedback compensates for the lower drive.

Concurrently with the work on SC, several studies have shown an anatomical link between the cerebellum and the extraocular muscles (Baker et al., 1972; Keller et al., 1983). Supplementary evidence for the cerebellum's importance in controlling gaze saccades comes from lesions studies. When the cerebellum is lesioned, the saccade metric is impaired in head-restrained (Ritchie, 1976; Optican and Robinson, 1980; Vilis and Hore, 1981; Goffart and Pélisson, 1998; Ohki et al., 2009) or in head-unrestrained conditions (Ritchie, 1976). Ritchie (1976) showed that saccade deficits are the same in head-restrained and head-unrestrained conditions when the cerebellum is lesioned. Later, Goffart and Pélisson (1998); Goffart et al. (1998a) showed that a lesioned contralateral fastigial nucleus does not impair the relative eye and head contributions to the gaze saccade but leads to hypermetric gaze saccades oriented towards the ipsilateral side of the lesion. Those results point toward gaze control by the cerebellum (as opposed to eye control).

We believe that the proposed mechanism could be easily extended to more complex hierarchical systems where several platforms can have different goals (cf. Fig. IV-11). In the case of the American football player presented in the introduction, he has to process several tasks concurrently. First, he has to catch the ball. Thus, he will run, change his body posture, and prepare his arms to receive the ball. A second goal for the player is to run toward the

end zone and score. In this example, two processes with different trajectories are executed concurrently: catch the ball and run to score. If the ball is sent in a different direction than the race direction, the player will initially modify his run accordingly to the trajectory of the ball to catch it. But, as soon as he catches the ball, he will correct his run toward the end zone and try to score. This example shows that, as for head-unrestrained saccades, analyses of embedded systems have to take into account the separate effect of a global goal (gaze goal) on the movement of hierarchically lower segment (head goal).

References

Aizawa, H. and Wurtz, R. H. (1998). Reversible inactivation of monkey superior colliculus. 1. curvature of saccadic trajectory. *J Neurophysiol*, 79(4):2082–2096.

Anderson, M. E., Yoshida, M., and Wilson, V. J. (1971). Influence of superior colliculus on cat neck motoneurons. *J Neurophysiol*, 34(5):898–907.

Baker, R., Precht, W., and Llinas, R. (1972). Mossy and climbing fiber projections of extraocular muscle afferents to the cerebellum. *Brain Res*, 38(2):440–445.

Batton, R. R., Jayaraman, A., Ruggiero, D., and Carpenter, M. B. (1977). Fastigial efferent projections in the monkey: an autoradiographic study. *J Comp Neurol*, 174(2):281–305.

Becker, W. and Fuchs, A. F. (1969). Further properties of the human saccadic system: eye movements and correction saccades with and without visual fixation points. *Vision Res*, 9(10):1247–1258.

Bizzi, E., Kalil, R., and Tagliasco, V. (1971). Eye-head coordination in monkeys : Evidence for centrally patterned organization. *Science*, 173:452–454.

Blohm, G. and Crawford, J. D. (2007). Computations for geometrically accurate visually guided reaching in 3-d space. *J Vis*, 7(5):4.1–422.

Buchtel, H. A., Iosif, G., Marchesi, G. F., Provini, L., and Strata, P. (1972). Analysis of the activity evoked in the cerebellar cortex by stimulation of the visual pathways. *Exp Brain Res*, 15(3):278–288.

Carpenter, M. B., Stein, B. M., and Peter, P. (1972). Primary vestibulocerebellar fibers in the monkey: distribution of fibers arising from distinctive cell groups of the vestibular ganglia. *Am J Anat*, 135(2):221–249.

Choi, W. Y. and Guitton, D. (2006). Responses of collicular fixation neurons to gaze shift perturbations in head-unrestrained monkey reveal gaze feedback control. *Neuron*, 50(3):491–505.

Choi, W. Y. and Guitton, D. (2009). Firing patterns in superior colliculus of head-unrestrained monkey during normal and perturbed gaze saccades reveal short-latency feedback and a sluggish rostral shift in activity. *J Neurosci*, 29(22):7166–7180.

Corneil, B. D., Olivier, E., and Munoz, D. P. (2002a). Neck muscle responses to stimulation of monkey superior colliculus. i. topography and manipulation of stimulation parameters. *J Neurophysiol*, 88(4):1980–1999.

Corneil, B. D., Olivier, E., and Munoz, D. P. (2002b). Neck muscle responses to stimulation of monkey superior colliculus. ii. gaze shift initiation and volitional head movements. *J Neurophysiol*, 88(4):2000–2018.

Cowie, R. J. and Robinson, D. L. (1994). Subcortical contributions to head movements in macaques. i. contrasting effects of electrical stimulation of a medial pontomedullary region and the superior colliculus. *J Neurophysiol*, 72(6):2648–2664.

Cowie, R. J., Smith, M. K., and Robinson, D. L. (1994). Subcortical contributions to head movements in macaques. ii. connections of a medial pontomedullary head-movement region. *J Neurophysiol*, 72(6):2665–2682.

Cullen, K. E., Huterer, M., Braidwood, D. A., and Sylvestre, P. A. (2004). Time course of vestibuloocular reflex suppression during gaze shifts. *J Neurophysiol*, 92(6):3408–3422.

Erkelens, A. J. and Sloot, O. B. (1995). Initial directions and landing positions of binocular saccades. *Vision Res*, 35(23-24):3297–3303.

Freedman, E. G. (2001). Interactions between eye and head control signals can account for movement kinematics. *Biol Cybern*, 84(6):453–462.

Freedman, E. G. (2008). Coordination of the eyes and head during visual orienting. *Exp Brain Res*, 190(4):369–387.

Freedman, E. G. and Sparks, D. L. (1997). Eye-head coordination during head-unrestrained gaze shifts in rhesus monkeys. *J Neurophysiol*, 77(5):2328–2348.

Freedman, E. G., Stanford, T. R., and Sparks, D. L. (1996). Combined eye-head gaze shifts produced by electrical stimulation of the superior colliculus in rhesus monkeys. *J Neurophysiol*, 76(2):927–952.

Fuchs, A. F., Kaneko, C. R., and Scudder, C. A. (1985). Brainstem control of saccadic eye movements. *Annu Rev Neurosci*, 8:307–337.

Fukushima, K., van der Hoeff-van Halen, R., and Peterson, B. W. (1978). Direct excitation of neck motoneurons by interstitiospinal fibers. *Exp Brain Res*, 33(3-4):565–581.

Galiana, H. and Guitton, D. (1992). Central organisation and modeling of eye-head coordination during orienting gaze shifts. *Annals of the New York Academy of Sciences*, 656:452–471.

Gandhi, N. J. and Sparks, D. L. (2007). Dissociation of eye and head components of gaze shifts by stimulation of the omnipause neuron region. *J Neurophysiol*, 98(1):360–373.

Gardner, E. P. and Fuchs, A. F. (1975). Single-unit responses to natural vestibular stimuli and eye movements in deep cerebellar nuclei of the alert rhesus monkey. *J Neurophysiol*, 38(3):627–649.

Gayer, N. S. and Faull, R. L. (1988). Connections of the paraflocculus of the cerebellum with the superior colliculus in the rat brain. *Brain Res*, 449(1-2):253–270.

Goffart, L., Guillaume, A., and Pélisson, D. (1998a). Compensation for gaze perturbation during inactivation of the caudal fastigial nucleus in the head-unrestrained cat. *J Neurophysiol*, 80(3):1552–1557.
Goffart, L. and Pélisson, D. (1998). Orienting gaze shifts during muscimol inactivation of caudal fastigial nucleus in the cat. 1. gaze dysmetria. *J Neurophysiol*, 79(4):1942–1958.
Goffart, L., Pélisson, D., and Guillaume, A. (1998b). Orienting gaze shifts during muscimol inactivation of caudal fastigial nucleus in the cat. ii. dynamics and eye-head coupling. *J Neurophysiol*, 79(4):1959–1976.
Gonzalo-Ruiz, A. and Leichnetz, G. R. (1987). Collateralization of cerebellar efferent projections to the paraoculomotor region, superior colliculus, and medial pontine reticular formation in the rat: a fluorescent double-labeling study. *Exp Brain Res*, 68(2):365–378.
Goossens, H. and Van Opstal, A. (1997). Human eye-head coordination in two dimensions under different sensorimotor conditions. *Experimental Brain Research*, 114:542–560.
Guitton, D. (1992). Control of eye-head coordination during orienting gaze shifts. *Trends in Neurosciences*, 15(5):174–179.
Guitton, D., Crommelinck, M., and Roucoux, A. (1980). Stimulation of the superior colliculus in the alert cat. I. eye movements and neck emg activity evoked when the head is restrained. *Exp Brain Res*, 39(1):63–73.
Guitton, D., Munoz, D., and H.L., G. (1990). Gaze control in the cats: Studies and modeling of the coupling between orienting eye and head movements in different behavioral tasks. *J Neurophysiol*, 64(2):509–531.
Guitton, D. and Volle, M. (1987). Gaze control in humans: eye-head coordination during orienting movements to targets within and beyond the oculomotor range. *J Neurophysiol*, 58(3):427–459.
Hafed, Z. M., Goffart, L., and Krauzlis, R. J. (2009). A neural mechanism for microsaccade generation in the primate superior colliculus. *Science*, 323(5916):940–943.
Isa, T. and Sasaki, S. (2002). Brainstem control of head movements during orienting; organisation of the premotor circuits. *progress in neurobiology*, 66:205–241.
Jürgens, R., Becker, W., and Rieger, P. (1981). Different effects involved in the interaction of saccades and the vestibulo-ocular reflex. *Ann N Y Acad Sci*, 374:744–754.
Kaneko, C. R. and Fuchs, A. F. (1982). Connections of cat omnipause neurons. *Brain Res*, 241(1):166–170.
Keller, E. L., Slakey, D. P., and Crandall, W. F. (1983). Microstimulation of the primate cerebellar vermis during saccadic eye movements. *Brain Res*, 288(1-2):131–143.
Kowler, E. and Blaser, E. (1995). The accuracy and precision of saccades to small and large targets. *Vision Res*, 35(12):1741–1754.
Langer, T., Fuchs, A. F., Scudder, C. A., and Chubb, M. C. (1985). Afferents to the flocculus of the cerebellum in the rhesus macaque as revealed by retrograde transport of horseradish peroxidase. *J Comp Neurol*, 235(1):1–25.

Langer, T. P. and Kaneko, C. R. (1983). Efferent projections of the cat oculomotor reticular omnipause neuron region: an autoradiographic study. *J Comp Neurol*, 217(3):288–306.

Langer, T. P. and Kaneko, C. R. (1984). Brainstem afferents to the omnipause region in the cat: a horseradish peroxidase study. *J Comp Neurol*, 230(3):444–458.

Laurutis, V. P. and Robinson, D. A. (1986). The vestibulo-ocular reflex during human saccadic eye movements. *J Physiol*, 373:209–233.

Lefèvre, P., Bottemanne, I., and Roucoux, A. (1992). Experimental study and modeling of vestibulo-ocular reflex modulation during large shifts of gaze in humans. *Exp Brain Res*, 91(3):496–508.

Lefèvre, P. and Galiana, H. L. (1992). Dynamic feedback to the superior colliculus in a neural network model of the gaze control system. *Neural Netw.*, 5(6):871–890.

Lefèvre, P., Quaia, C., and Optican, L. M. (1998). Distributed model of control of saccades by supperior colliculus and cerebellum. *Neural Networks*, 11:1175–1190.

Leigh, R. and Zee, D. (2006). *The Neurology Of Eye Movement*. Oxford University Press, 4 edition.

May, P. J. and Hall, W. C. (1986). The cerebellotectal pathway in the grey squirrel. *Exp Brain Res*, 65(1):200–212.

Munoz, D. P. and Guitton, D. (1985). Tectospinal neurons in the cat have discharges coding gaze position error. *Brain Res*, 341(1):184–188.

Munoz, D. P. and Guitton, D. (1986). Presaccadic burst discharges of tecto-reticulo-spinal neurons in the alert head-free and -fixed cat. *Brain Res*, 398(1):185–190.

Munoz, D. P. and Wurtz, R. H. (1993). Fixation cells in monkey superior colliculus. i. characteristics of cell discharge. *J Neurophysiol*, 70(2):559–575.

Niemi-Junkola, U. J. and Westby, G. W. (2000). Cerebellar output exerts spatially organized influence on neural responses in the rat superior colliculus. *Neuroscience*, 97(3):565–573.

Ohki, M., Kitazawa, H., Hiramatsu, T., Kaga, K., Kitamura, T., Yamada, J., and Nagao, S. (2009). Role of primate cerebellar hemisphere in voluntary eye movement control revealed by lesion effects. *J Neurophysiol*, 101(2):934–947.

Optican, L. M. and Robinson, D. A. (1980). Cerebellar-dependent adaptive control of primate saccadic system. *J Neurophysiol*, 44(6):1058–1076.

Pélisson, D., Guitton, D., and Goffart, L. (1995). On-line compensation of gaze shifts perturbed by micro-stimulation of the superior colliculus in the cat with unrestrained head. *Exp Brain Res*, 106(2):196–204.

Pélisson, D., Guitton, D., and Munoz, D. P. (1989). Compensatory eye and head movements generated by the cat following stimulation-induced perturbations in gaze position. *Exp Brain Res*, 78(3):654–658.

Prsa, M. and Galiana, H. L. (2007). Visual-vestibular interaction hypothesis for the control of orienting gaze shifts by brain stem omnipause neurons. *J Neurophysiol*, 97(2):1149–1162.

Quaia, C., Aizawa, H., Optican, L. M., and Wurtz, R. H. (1998). Reversible inactivation of monkey superior colliculus. ii. maps of saccadic deficits. *J Neurophysiol*, 79(4):2097–2110.

Quaia, C., Lefèvre, P., and Optican, L. (1999). Model of the control of saccades by superior colliculus and cerebellum. *Journal of Neurophysiology*, 82:999–1018.

Quaia, C. and Optican, L. M. (1997). Model with distributed vectorial premotor bursters accounts for the component stretching of oblique saccades. *J Neurophysiol*, 78(2):1120–1134.

Quaia, C. and Optican, L. M. (1998). Commutative saccadic generator is sufficient to control a 3-d ocular plant with pulleys. *J Neurophysiol*, 79(6):3197–3215.

Ritchie, L. (1976). Effects of cerebellar lesions on saccadic eye movements. *J Neurophysiol*, 39(6):1246–1256.

Robinson, D. (1973). Models of the saccadic eye movement control system. *Kybernetik*, 14:71–83.

Robinson, D. (1975). Oculomotor control signals. *Basic mechanisms of ocular motility and their clinical implications*, pages 337–374.

Robinson, D. A. (1972). Eye movements evoked by collicular stimulation in the alert monkey. *Vision Res*, 12(11):1795–1808.

Roucoux, A., Guitton, D., and Crommelinck, M. (1980). Stimulation of the superior colliculus in the alert cat. II. eye and head movements evoked when the head is unrestrained. *Exp Brain Res*, 39(1):75–85.

Schiller, P. H., True, S. D., and Conway, J. L. (1979). Effects of frontal eye field and superior colliculus ablations on eye movements. *Science*, 206(4418):590–592.

Schiller, P. H., True, S. D., and Conway, J. L. (1980). Deficits in eye movements following frontal eye-field and superior colliculus ablations. *J Neurophysiol*, 44(6):1175–1189.

Schreiber, C., Missal, M., and Lefèvre, P. (2006). Asynchrony between position and motion signals in the saccadic system. *J Neurophysiol*, 95(2):960–969.

Scudder, C. A., Moschovakis, A. K., Karabelas, A. B., and Highstein, S. M. (1996). Anatomy and physiology of saccadic long-lead burst neurons recorded in the alert squirrel monkey. i. descending projections from the mesencephalon. *J Neurophysiol*, 76(1):332–352.

Shinoda, Y. and Yoshida, K. (1975). Neural pathways from the vestibular labyrinths to the flocculus in the cat. *Exp Brain Res*, 22(2):97–111.

Sprague, J. M. and W. W. Chambers, B. R. (1954). Control of posture by reticular formation and cerebellum in the intract, anesthetized and unanesthetized and in the decerebrated cat. *Am J Physiol*, 176(1):52–64.

Stryker, M. P. and Schiller, P. H. (1975). Eye and head movements evoked by electrical stimulation of monkey superior colliculus. *Exp Brain Res*, 23(1):103–112.

Tomlinson, R. D. and Bahra, P. S. (1986a). Combined eye-head gaze shifts in the primate. i. metrics. *J Neurophysiol*, 56(6):1542–1557.

Tomlinson, R. D. and Bahra, P. S. (1986b). Combined eye-head gaze shifts in the primate. ii. interactions between saccades and the vestibuloocular reflex. *J Neurophysiol*, 56(6):1558–1570.

Tu, T. A. and Keating, E. G. (2000). Electrical stimulation of the frontal eye field in a monkey produces combined eye and head movements. *J Neurophysiol*, 84(2):1103–1106.

Vilis, T. and Hore, J. (1981). Characteristics of saccadic dysmetria in monkeys during reversible lesions of medial cerebellar nuclei. *J Neurophysiol*, 46(4):828–838.

Waespe, W., Bttner, U., and Henn, V. (1981). Visual-vestibular interaction in the flocculus of the alert monkey. i. input activity. *Exp Brain Res*, 43(3-4):337–348.

Wilson, V. J., Uchino, Y., Maunz, R. A., Susswein, A., and Fukushima, K. (1978). Properties and connections of cat fastigiospinal neurons. *Exp Brain Res*, 32(1):1–17.

Wurtz, R. H. and Goldberg, M. E. (1971). Superior colliculus cell responses related to eye movements in awake monkeys. *Science*, 171(966):82–84.

Wurtz, R. H. and Goldberg, M. E. (1972). Activity of superior colliculus in behaving monkey. 3. cells discharging before eye movements. *J Neurophysiol*, 35(4):575–586.

Zee, D. S., Yamazaki, A., Butler, P. H., and Gcer, G. (1981). Effects of ablation of flocculus and paraflocculus of eye movements in primate. *J Neurophysiol*, 46(4):878–899.

Part V

A Dual Sensor VOR model that compensates for estimated perturbations of the head.

Summary

Everyday activities generate head movements that must be compensated for by eye movements to ensure clear vision. For example, the vestibulo-ocular reflex (VOR) rotates the eyes in the orbit in the opposite direction of an unexpected head movement, ensuring that the gaze (i.e., eye-in-space = eye-in-head + head-in-space) remains stable. However, this reflex is counterproductive if gaze and head are directed in the same direction. Past studies revealed that two mechanisms modulate the VOR effect during active head movements: suppression (VOR gain, g_{VOR}, decreases at the onset of head unrestrained saccades and increases back to 1 before the end of the saccadic movement) and cancellation (g_{VOR} =1, but a command opposite to the head movement command is sent to the eyes, e.g., during head-free pursuit). This study proposes a new VOR model that integrates both suppression and cancellation modulation mechanisms. In the first stage semi-circular canal velocity and neck muscle proprioceptive information are combined with the expected head-on-body velocity to estimate the current head-on-body and body-in-space velocities and get rid of measurements and computational delays. In the second stage those estimates are used to evaluate and cancel current head perturbations. The new model was integrated with a saccade and a pursuit model. Traditional tests (on-chair rotations) of the VOR functionality were simulated and compared to previously published observations. The model was also used to generate a prediction about behavior during an untested paradigm, in which a head-fixed target made a vertical position step during an on-chair rotation. This simulation shows the ability of the model to separate active (related to the gaze) and passive (not related to the gaze) head movements. Finally, we conclude by showing a simulation that reproduces previously published results on the effect of a brake on the head during head-free tracking on healthy subjects and vestibular patients without a VOR

1

Introduction

Vision is degraded if an image slips on the retina, so stabilizing images on the retina is an essential task during everyday activities. Of the different mechanisms used to stabilize vision, the vestibulo-ocular reflex (VOR) is certainly the most important. The VOR compensates for head movements that would perturb vision by turning the eye in the orbit in the opposite direction of the head movement (Angelaki and Cullen, 2008; Barnes, 1993; Leigh and Zee, 2006). However, there are numerous situations during which compensation of the head movement would not be appropriate, e.g. if gaze and head are moving in the same direction. Researchers have found two mechanisms in the central nervous system that prevent the VOR from inappropriately compensating for head movements. The first one, called suppression, is a modulation of the gain of the VOR. Authors have shown that the gain decreases at the onset of large gaze shifts and increases to one just before the end of the movement (Cullen et al., 2004; Lefèvre et al., 1992). In the second mechanism, called VOR cancellation, the VOR gain remains unitary but an external signal, in the opposite direction of the VOR, is added to negate its action. Several evidences show that this mechanism is used during head-unrestrained tracking (Lanman et al., 1978; Koenig et al., 1986; Leigh et al., 1987). The VOR is also active when subjects are rotated in the dark without a visible target but imagine either a target fixed to the head (non-visual cancellation) or a target fixed with respect to an inertial reference frame (non-visual enhancement) (Barnes, 1993). More recently, Cullen and colleagues (Cullen and Roy, 2004; Roy and Cullen, 2002, 2004) compared active and passive head movements in a monkey while recording in the vestibular nuclei. They showed that the discharge of the neurons in the vestibular nuclei is modulated by the expectation of a head movement. They proposed that an expected head movement (generated from a command sent by the central nervous system to the neck muscles) is not compensated for by the VOR while a passive movement (not related to a command sent by the central nervous system) is negated by the VOR. Additionally, Brooks and Cullen (2009) recorded neurons in the rostral fastigial nucleus of the monkey that modulated their activity accordingly to the body-in-space motion.

Several approaches had been used to model the VOR depending on the goal of the study. A first example of VOR model is presented in (Barnes, 1993). The

author proposed a model of the mechanisms for visual-vestibular interaction that incorporates three loops to account for the visual (when a target is visible) and the non-visual (in the dark) modulation of the VOR. This model was not designed to account for the suppression mechanism observed during head-unrestrained saccades. A second type of VOR model has been developed by Galiana and Outerbridge (1984). They presented a bilateral model of the VOR that mimicked the activity of the main neural connections present in the central VOR pathway. The model reproduced the neural activity observed during semi-circular canal stimulation in the dark (vestibular nystagmus) but was not built to simulate suppression and cancellation mechanisms observed during active head movements. In a last example, the model proposed by Schmid et al. (1980) combined an optokinetic reflex (OKR) model with a VOR model. This model reproduced experiments during which subjects sat on a rotating chair (to stimulate the VOR) inside a rotating drum with vertical black and white stripes (to stimulate the OKR).

This paper proposes a new model of the vestibulo-ocular reflex that integrates both a suppression and a cancellation mechanism. The model was not designed to mimic the neural activity of all the neurons previously described to be involved in the vestibulo-ocular reflex (For a review of the major pathways, see (Leigh and Zee, 2006)). It is a unilateral model that incorporates two sensors to measure head velocity. Both sensors measure head velocity in a different spatial reference frame and are delayed with respect to the current movement. Through the combination of the sensory inputs, the model first decomposes the head velocity measurements into their active and passive components. Next, the model phase-advances those estimates into the current time reference frame using the expected amplitude of the head velocity. Finally, the model compensates for unexpected head-in-space movements. Traditional tests of the VOR will be presented to assess the general behavior of the model. A second result will present a prediction of the model linked to the separation of the active and the passive components of the head movement. Finally, we reproduce the experiment of Lanman et al. (1978) and compare our simulations with their results.

2

Methods

All the reported simulations were conducted on a personal computer running SIMULINK/MATLAB® (The Mathworks, Natick, MA, USA). The following sections will describe the structure of the different sub-models combined during the simulations. First, the saccade and pursuit models, based on the model structure presented in part IV, will be briefly described. Then the new VOR model structure will be presented.

1 Updated saccade model

Figure V-1 shows an updated version of the saccadic system proposed in part IV. As in the original model, the new version includes two pathways to control gaze position: a common gaze collicular pathway (gray items in Fig. V-1) that projects to both eye and head, and a cerebellar gaze feedback pathway (orange items in Fig. V-1) that projects only to the eye. A facilitation signal from the gaze cerebellar controller (CB_G) is used to modulate the collicular discharge (dotted-dashed orange line with a diamond tip in Fig. V-1). In parallel, a third pathway, controlling head position through a second cerebellar feedback controller (CB_H) projects only to the head (purple items in Fig. V-1). Figure V-1 also includes the VOR model (red items). The VOR, gaze cerebellar and collicular discharges all project to the vestibular nuclei (VN in Fig. V-1), which in turn projects to the eye plant. In an addition to the original structure presented in part IV, this version also includes a supplementary gaze cerebellar input (blue arrow in Fig. V-1), which corresponds to an estimate of the current target velocity to account for a target displacement during a saccade. It was previously shown by de Brouwer et al. (2001, 2002a,b) that the amplitude of a saccade triggered during an ongoing head-restrained pursuit movement is corrected to account for the displacement of the target during the saccade, ensuring an accurate saccadic displacement. The target velocity input is integrated during the saccade to adjust the desired gaze displacement (ΔG) and ensure that the saccade ends on the target.

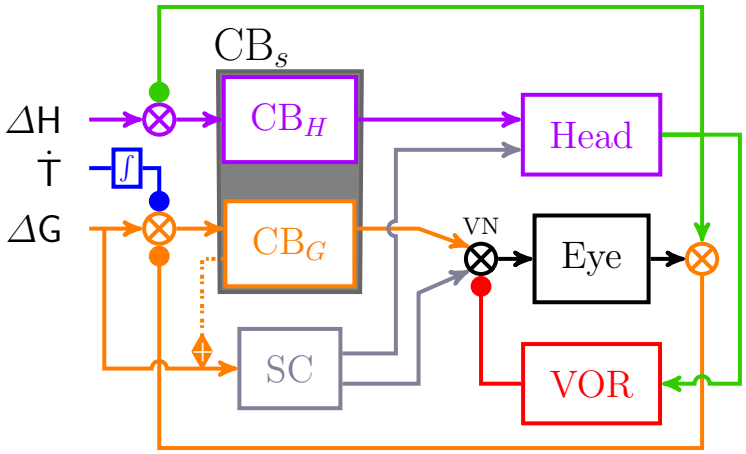

Fig. V-1: Enhanced saccadic model. The structure of the saccadic model is based on the architecture presented in part IV. The model contains three major pathways. A first pathway (CB$_H$ and purple items) received the desired head displacement (ΔH) and the current head position as inputs; it goes through a first part of the cerebellum and projects only to the head plant. The second pathway, through another part of the cerebellum (CB$_G$ and orange items), received the desired gaze displacement (ΔG), the current gaze position and the target velocity (blue arrow) as inputs. The gaze cerebellar controller is the core of the second pathway: it sent a drive to the eye through the vestibular nuclei (black sum labeled VN) to control the gaze trajectory. It also sent a facilitation signal (orange dashed line with a diamond tip) to the superior colliculus to mediate the collicular level of activity. The third pathway goes through the superior colliculus (gray items). It receives the desired gaze displacement and a facilitation signal from the gaze cerebellar controller as inputs. It sends a common drive in the direction of the gaze to both the eye (through VN) and the head. The vestibular nuclei have a third input that comes from the vestibulo-ocular reflex (VOR red box). The VOR receives the head velocity as input. An arrow tip corresponds to an excitatory signal while a filled circle corresponds the signal with a negative sign.

2 Pursuit model

Figure V-2 shows the model structure used to simulate head-unrestrained pursuit. Like the saccade model of Fig. V-1, this model includes two feedback pathways: one part of the cerebellum (B$_{Gp}$) controls gaze velocity and projects only to the eye (turquoise items) through the vestibular nuclei (VN in Fig. V-2). A second feedback pathway through another part of the cerebellum (CB$_{Hp}$) projects only to the head and controls head velocity (khaki items). Unlike the saccade model, the pursuit model does not include a common pathway that projects to both eye and head. Originally the saccade and pursuit systems were thought to have different neural architecture, however recent findings point to-

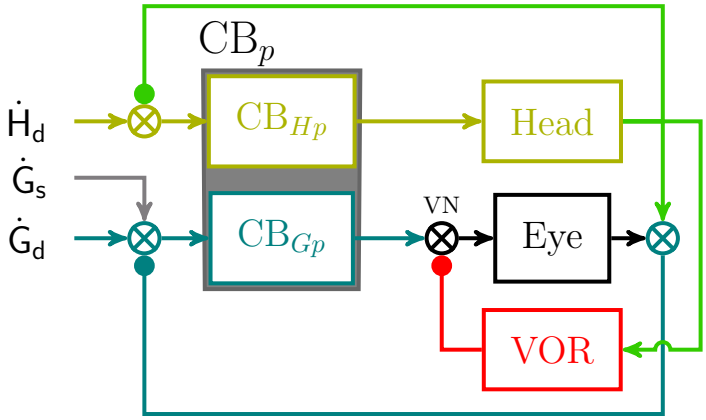

Fig. V-2: Pursuit model. The pursuit model has a similar architecture to the saccade model of Fig. V-1. It has two main pathways: one through a part of the cerebellum controls the gaze velocity (CB$_{Gp}$ and turquoise items). The gaze pursuit controller receives the desired gaze velocity ($\dot{G}_d$), the current gaze velocity and the saccadic component of the gaze velocity ($\dot{G}_s$ and gray arrow) as inputs. It sends a drive only to the eye through the vestibular nuclei (VN black sum). The second pathway, through another part of the cerebellum (CB$_{Hp}$ and khaki items) controls the head velocity. This controller receives the desired head velocity ($\dot{H}_d$) and the current head velocity as inputs. It sends a drive to the head. As for the saccade model, the VN in the pursuit model has a supplementary input that comes from the vestibulo-ocular reflex (VOR red box). The VOR model receives the head velocity as input and projects to the eye through the vestibular nuclei. An arrow tip corresponds to an excitatory signal while a filled circle corresponds to an inhibition.

ward a neural architecture for the pursuit control very similar to that of saccade control (see (Krauzlis, 2004) for a detailed review of the comparison between saccade and pursuit pathways). It must be stressed that the pursuit model of Fig. V-2 was built to reproduce the maintenance of pursuit. It does not include a series of known properties of the actual pursuit system, e.g., anticipation, prediction, etc. Therefore, the proposed control structure for pursuit does not include all known pursuit areas and pathways. This simplified circuitry was sufficient for the purpose of the current paper, which is to demonstrate the ability of our new VOR model to reproduce previously published data while getting rid of the internal delays of the sensory system. As can be observed in Fig. V-2, the central structure of our model is organized around the cerebellum. Several past studies implicated the cerebellum in the control of active gaze pursuit: Zee et al. (1981) showed that removing the flocculus and the paraflocculus created large impairments of the pursuit efficiency that did not recover. Later, Rambold et al. (2002) showed that the ventral paraflocculus was the key neural area for the control of pursuit and the adaptation of the VOR gain. The structure of the controllers used in the head and gaze cerebellar pursuit models is iden-

tical to the ones used for the saccadic model. The mathematical description of those controllers is developed in appendix C. Additionally, as observed by de Brouwer et al. (2001), the pursuit system appears to stay active during a catch-up saccade. Therefore, the model does not switch between two modes: one for the saccade and one for the pursuit movement. The pursuit controller remains functional during catch-up saccades. However, gaze velocity changes drastically during saccades. This modulation induces a large change in retinal slip. Because the gaze pursuit controller normally negates the retinal slip, we added at the input of the gaze pursuit controller a term that corresponds to gaze saccade velocity (gray arrow in Fig. V-2). Therefore, the retinal slip input of the pursuit controller does not change significantly during the saccade.

3 Saccade-pursuit interaction

As explained in the description of the pursuit model (section 2), there is no switching strategy between saccade and pursuit. The pursuit system is always active. To compute the head drive, we sum all the signals that are sent to the head from both the pursuit (the head cerebellar pursuit drive, khaki output in Fig. V-2) and the saccadic (the head cerebellar saccadic drive, purple output in Fig. V-1 and the collicular drive, gray output in Fig. V-1) systems. The same approach was used for the computation of the drive sent to the eye. We sum the cerebellar gaze pursuit drive (turquoise output in Fig. V-2) with the collicular drive (gray output in Fig. V-1) with the cerebellar saccadic drive (orange output in Fig. V-1) with the VOR (red items in Fig. V-1 and Fig. V-2). Additionally, the model does not include a cortical mechanism that triggers a saccade when a set of conditions is satisfied. Thus, to decide when a saccade must be triggered, we ran the simulation a first time using only the pursuit system. Then, we chose the time at which a saccade would be adequate. Finally, we ran the simulation a second time with the saccadic system being functional and correctly parameterized.

4 VOR model: estimating current head velocity

To build a model that was able to simulate previously described VOR behaviors, we first looked at the signals that could generate head movements. We assumed that head velocity with respect to a spatial reference frame (head-in-space) could be decomposed into several subparts. The components we used in the model are presented in Fig. V-3, panel A. We integrated two active (active = head velocity generated by a voluntary command sent from the central nervous system) head velocity signals, one to account for the portion of the velocity of the head from the gaze saccadic controller ($\dot{H}_{s,g}$ in Fig. V-3, panel A) and one to account for the portion of the head velocity from the pursuit controller ($\dot{H}_{p,g}$ in Fig. V-3, panel A). The sum of those two components gives the active head-on-trunk velocity ($\dot{H}_a$ in Fig. V-3, panel A). Because the trunk supports the head, a trunk rotation induces a movement of the head (unless compensated for

by a counter-rotation of the head). Therefore, to express head-in-space velocity ($\dot{H}_{sp}$ in Fig. V-3), we added the trunk-in-space velocity ($\dot{T}_{sp}$ in Fig. V-3) to the active component of the head movement.

It is important to point out that we assumed that the central nervous system does not have directly access to the different components of head velocity. Therefore, to control a head movement and to reject potential perturbations, it must construct an internal representation of those signals. Additionally, there is no link between this first part of the computation and the VOR. The single goal of this part of the model is to estimate the *current* head-on-trunk and trunk-in-space velocity.

Because of the different internal delays of the sub-parts of the model, the signals used (or produced) by the model are not expressed in the same time reference frame. Thus it is critical to synchronize the different signals in some time reference frame before doing any computation.

To achieve that, the estimation of the different head velocity components in the model was accomplished in two stages. First, active and passive head velocities in a delayed time reference frame (the time reference frame of the sensors) were computed and then efference signals were used to advance those estimates in the current time reference frame.

To compute the active and the passive head velocities in a delayed reference frame, we modeled two types of sensors: the semi-circular canals (SCC in Fig. V-3, panel B) and proprioceptive inputs from the neck muscles (cervical afferent pathway, CAP in Fig. V-3, panel B). Two sensors were integrated into the model to account for experiments in which both were stimulated independently (Cullen and Roy, 2004; Roy and Cullen, 2002, 2004) or to reproduce experiments in which one of the two systems was deficient (Lanman et al., 1978; Blouin et al., 1995).

If SCC measures head-in-space velocity ($\dot{H}_{sp}$ in Fig. V-3, panel A), CAP measures head-on-trunk velocity ($\dot{H}_{a}$ in Fig. V-3, panel A). Both sensors were modeled using first order transfer functions with a time constant of 10 [ms] to account for their dynamics. A measurement white noise (noise variance: SCC $= \sigma_1^2 = 0.05$ [deg^2/s^2], CAP $= \sigma_2^2 = 0.01$ [deg^2/s^2]) was added at the output of the sensors. We selected a low white noise variance for the CAP measurements. But to account for the likely higher noise of the efferent measurements, we set the white noise variance of the SCC five times bigger than for the CAP. The absolute values of those noises are not a critical factor, the important point is that cervical afference is less noisy than vestibular afference (Blouin et al., 1998). Changing the variance of the noise would not change drastically the behavior of the model. Finally, to account for the neural transmission latency and the sensor latency, we added a pure delay to each sensor ($\tau = 10$ [ms] in Fig. V-3, panel B). Therefore the outputs of the SCC ($\dot{H}^m_{SCC}(t-\tau)$ in Fig. V-3, panel B) and CAP ($\dot{H}^m_{CAP}(t-\tau)$ in Fig. V-3, panel B) are delayed compared to their inputs ($\dot{H}_{sp}(t)$ for SCC and $\dot{H}_{a}(t)$ for CAP). The internal delay and time constant of SCC were chosen according to previously published observations (Gauthier and Vercher, 1990; Johnston and Sharpe, 1994; Crane and Demer, 1999) in which authors measured the latency of the eye movement with respect

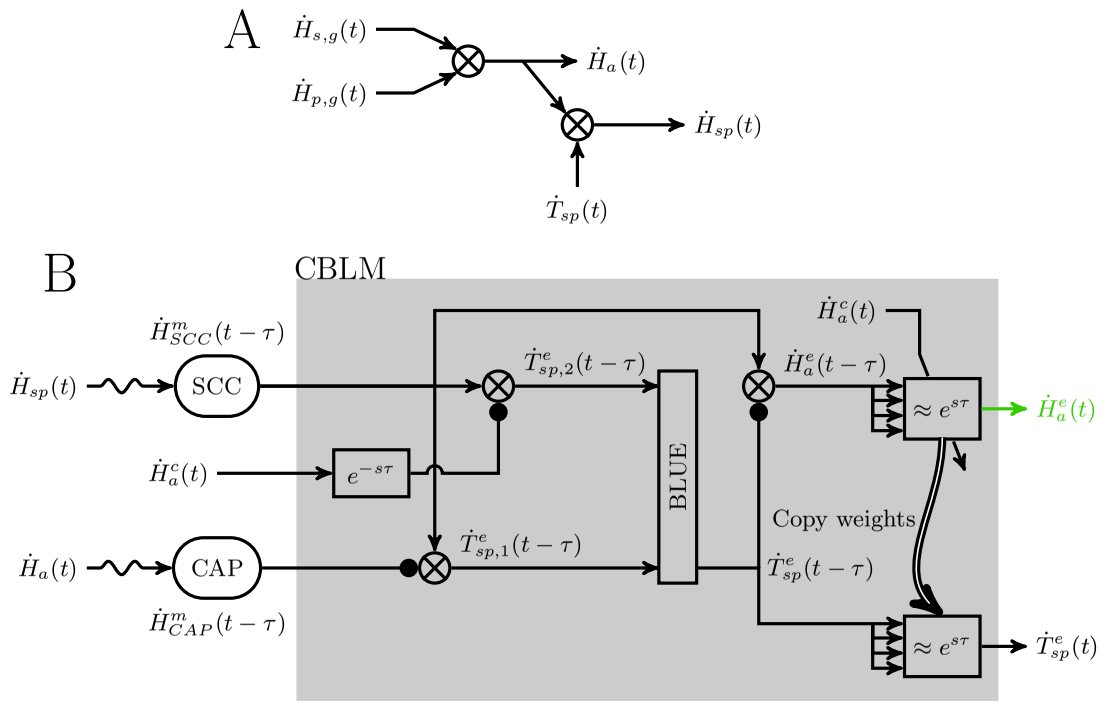

Fig. V-3: Cerebellar time synchronization model. Panel A represents the signals that composed the head-in-space velocity. $\dot{H}_{s,g}$ represents the head velocity linked to a gaze saccade. $\dot{H}_{p,g}$ represents the head velocity generated by a gaze pursuit command. The sum of those two signals corresponds to the active component of the head velocity ($\dot{H}_a$) with respect to the body. $\dot{T}_{sp}$ corresponds to the trunk-in-space velocity. An arrow tip corresponds to an excitatory signal while a filled circle corresponds to an inhibition.

Fig. V-3: Cerebellar time synchronization model. (cont.) The sum of the trunk-in-space and the active head velocity is equal to the head-in-space velocity. Panel B represents the cerebellar time synchronization model. It has two inputs: the semi-circular canals (SCC) are sensitive to head-in-space velocity ($\dot{H}_{sp}$) and the cervical afferent pathway (CAP) is sensitive to active head velocity on the body ($\dot{H}_a$). It also used an efference copy of the current active head velocity ($\dot{H}_a^c$) built from an internal model of the head. Those three signals contain noise. Both the SCC and the CAP measure the head velocity in a delayed time reference frame. First two estimates of the trunk-in-space velocity are computed by subtracting from the SCC output either the CAP measurement ($\dot{T}_{sp,1}^e(t-\tau)$) or a delayed version of the efference copy of the head velocity ($\dot{T}_{sp,2}^e(t-\tau)$). The two signals are then combined into a Best Linear Unbiased Estimator (BLUE) to compute the minimal variance estimate of the body-in-space velocity ($\dot{T}_{sp}^e(t-\tau)$). Then, the trunk-in-space velocity inhibits the SCC output to compute the active component of the head velocity. After, a phase-advance filter is used to estimate the current active head velocity (green arrow) using the computed estimate with the sensors of the active head velocity and the efference copy of the active head velocity ($\dot{H}_a^c$). Finally, the weights of the first filter are used to synchronize the estimate of the delayed trunk-in-space velocity.

to a passive rotation of the head. Estimating the time constant and the delay of the CAP from the literature was less easy. Several authors showed that a stimulation of the neck afferents generated a modulation of the vestibular neurons in the decerebrate cat after approximately 2-4 [ms] (Hikosaka and Maeda, 1973; Kasper and Thoden, 1981; Sato et al., 1997). An overlapping range of delays (but slightly faster 1.35-3.2 [ms]) has been observed for the neural transmission between the vestibular nerve and the vestibular nuclei (Baker et al., 1969). Therefore, we used the same pure delay ($\tau = 10$ [ms]) for both the SCC and the CAP sensors in the model. The issue of having different delays for the CAP and the SCC is debated in the discussion.

Now that we have measurements of head velocity from two sources, we can combine them to compute the trunk-in-space velocity and the head-on-trunk velocity. Using the definition of the head velocity components, we can write:

$$\dot{T}_{sp,1}^e(t-\tau) = \dot{H}_{SCC}^m(t-\tau) - \dot{H}_{CAP}^m(t-\tau) \tag{48}$$

A second estimate of the trunk-in-space velocity can be computed from the SCC measurements and from an efference copy representing the head-on-trunk velocity ($\dot{H}_a^c$ in Fig. V-3, panel B) delayed by the same time (τ) as the SCC. It must be pointed out that an efference copy of the head-in-space velocity could have been used instead of the head-on-trunk velocity[94]. However, the estimate of the head-on-trunk seems easier to compute because the commands sent to the neck could also be sent to an internal model of the head-neck system that

[94] This would require some trivial modifications of the architecture presented in Fig. V-3.

would estimate the head-on-trunk velocity. Therefore, using an efference copy of the head-on-trunk velocity and the SCC measurements, we can compute:

$$\dot{T}^{e}_{sp,2}(t-\tau) = \dot{H}^{m}_{SCC}(t-\tau) - \dot{H}^{c}_{a}(t)e^{-s\tau} \tag{49}$$

Because the sensory afferents contain noise, the brain can get a better estimate of the trunk-in-space velocity by combining them. We used a simple estimator to represent this process: the best linear unbiased estimator (BLUE in Fig. V-3, panel B). This estimator used a weighted sum of the inputs to estimate a signal with a minimal variance criterion. Because we know in advance the sensors noise variance, we computed the weights of the estimator offline. We assume that the efference copy of the head-in-body velocity contains less noise than the SCC, but more noise than the CAP (variance $= \sigma_3^2 = 0.02$ $[\mathsf{deg}^2/\mathsf{s}^2]$). Thus, the equation of the estimator is equal to:

$$\dot{T}^{e}_{sp}(t-\tau) = \alpha_1 \dot{T}^{e}_{sp,1}(t-\tau) + \alpha_2 \dot{T}^{e}_{sp,2}(t-\tau) \tag{50}$$

With the weights equal to:

$$\alpha_1 = \frac{\sigma_1^2 + \sigma_2^2}{2 * \sigma_1^2 + \sigma_2^2 + \sigma_3^2} \tag{51}$$

$$\alpha_2 = \frac{\sigma_1^2 + \sigma_3^2}{2 * \sigma_1^2 + \sigma_2^2 + \sigma_3^2} \tag{52}$$

As shown by equations (51) and (52), the values of α_1 and α_2 are a function of the noises in the original signals. Thus, the asymmetry of the weight equations (51) and (52) is explained by the fact that one input ($\dot{T}^{e}_{sp,2}(t-\tau)$, eq. (49)) contains the sum of SCC and efferent noise while the second input contains the sum of the noises of both sensors ($\dot{T}^{e}_{sp,1}(t-\tau)$, eq. (48)). With the chosen values for sensor noise, α_1 is equal to 0.47 and α_2 is equal to 0.53. This can be interpreted as the fact that the system relies more on the less noisy measurements that come from the combination of the semi-circular canals and cervical afferent pathway than on the combination of the efference copy of the active head velocity and the semi-circular canals. Finally, equations (51) and (52) gives the optimal combination of the inputs to generate the least noisy velocity information. Therefore, a modification of the sensors' noise would not drastically modify the behavior of the model because α_1 and α_2 could be recomputed to ensure an optimal estimation of the trunk-in-space velocity from the noisy measurements of the sensors.

Computing the head-on-trunk velocity is not easy because the SCC measurements (head-in-space) include both head-on-trunk and trunk-in-space components. The simple way to compute head-on-trunk velocity would be to only rely on the measurements given by the cervical afferent pathway. However, Blouin et al. (1995) tested a patient without proprioception of the neck and body muscles but with an intact vestibular nerve. They observed that the VOR gain of the patient was very similar to the gain of control subjects. Thus, using only the CAP output, the model would not simulate the observations of Blouin et al. (1995). Therefore, to compute the active component of the head velocity

(head-on-trunk velocity), we removed the output of the BLUE estimator (corresponding to the best approximation of the trunk-in-space velocity) from the SCC output.

At this point, the model has combined the information of the two sensors and an efference copy of the head velocity to compute the active (related to a head command) and passive (not related to a head command) head velocity components. It is well known that a pure delay inside a feedback loop generates instabilities (Smith, 1959). Thus, to be usable by the control part of the model, the estimated head-on-trunk and trunk-in-space velocities must represent the current velocities, not a delayed version of them. To synchronize the signals with the current time reference frame, we used adaptive filtering. We implemented a gradient adaptive Lattice-Laguerre filter that matched the expected head velocity that comes from an efference copy of the head velocity ($\dot{H}_a^c$ in Fig. V-3, panel B) with the head-on-trunk velocity previously computed. The complete algorithm of the filter used in the model is described in (Fejzo and Lev-Ari, 1997). In summary, to synchronize the two signals, the filter adaptively changes the weights β_0 to β_N of the model:

$$\dot{H}_a^e(t) = \sum_{k=0}^{N} \beta_k \dot{H}(t - \tau - k\zeta) \tag{53}$$

In (53), ζ represents a fixed parameterizable delay of the filter. As shown by eq. (53), the model combined several successively delayed copies of the input signal to approximate the reference signal. At the output of the advance filter, we now have an estimate of the current head-on-trunk velocity.

The same procedure could be used to synchronize the trunk-in-space velocity signal previously computed. However, this is not directly feasible because we do not have a reference signal that corresponds to the expected current value of the trunk-in-space velocity. However, because the delay is equal for both head-on-trunk and trunk-in-space velocity estimates, we used the same weights (β_0 to β_N of eq. (53)) to advance the delayed trunk-in-space velocity and therefore estimate the current trunk-in-space velocity.

At this stage, the model has computed an estimate of the current head-on-trunk and trunk-in-space velocities. The head-on-trunk velocity is used by the different controllers in Fig. V-1 and V-2 (green arrows at the output of the head box in Fig. V-1 and V-2) and by the process that computes the VOR signal compensation.

5 VOR model: compensation

Figure V-4 shows how the model combines the estimates of the current head-on-trunk and trunk-in-space velocities with an efference copy of the expected head velocity from the saccadic component ($\dot{H}_{s,g}^c$ in Fig. V-4), a projection from the omnipause neurons (OPN in Fig. V-4) and a suppression signal that comes from the cerebellum (SUP in Fig. V-4) to evaluate the VOR compensation. The VOR is computed as:

$$VOR = \left[\dot{T}^e_{sp}(t) + OPN\ \dot{H}^e_a(t) - (1 - OPN)\left(\dot{H}^c_{s,g} - \dot{H}^e_a\right)\right] SUP \qquad (54)$$

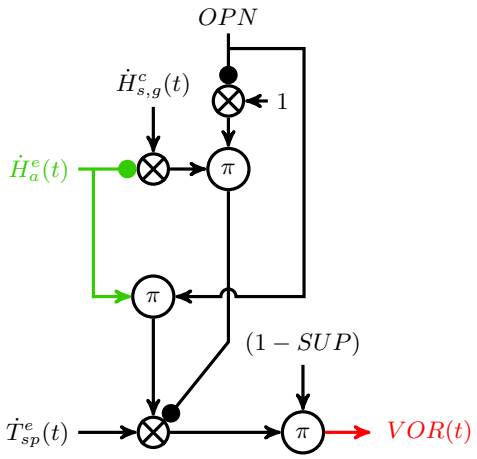

Fig. V-4: VOR mechanism model. This figure represents the combination of signals used to model the cancellation and the suppression mechanisms of the VOR. $\dot{H}^e_a$ corresponds to the estimate of the current active head velocity. $\dot{T}^e_{sp}$ corresponds to the estimate of the current trunk-in-space velocity. OPN corresponds to the omnipause neurons. $\dot{H}^c_{s,g}$ represents the head velocity linked to a gaze saccade. SUP corresponds to the suppression signal sent by the cerebellum. An arrow tip corresponds to an excitatory signal while a filled circle corresponds to an inhibition. The model computes the amount of compensation made by the VOR and sent to the vestibular nuclei. The suppression signal gates the output of the VOR. $\dot{T}^e_{sp}$ is always seen as a perturbation and therefore always canceled. When the OPN are discharging, $\dot{H}^e_a$ is seen as perturbation and compensated (if SUP = 0). During a saccade, the model compensates the difference between $\dot{H}_{s,g}$ and $\dot{H}^e_a$.

As expressed by eq. (54), the VOR activity (red arrow in Fig. V-4) is gated by the suppression signal that comes from the cerebellum (SUP in eq. (54) and in Fig. V-4). There is strong evidence that the VOR activity is suppressed during large saccades between two fixed targets (Tomlinson and Bahra, 1986a,b; Cullen et al., 2004; Lefèvre et al., 1992). Parallel to those studies, authors have also shown that the VOR is active during head-unrestrained tracking, but canceled by the pursuit signal (see results for simulations involving VOR cancellation) (Lanman et al., 1978; Leigh et al., 1987; Barnes, 1993). Nothing is known about the VOR activity during catch-up saccades (saccades triggered during an ongoing pursuit to compensate for a position error). We assumed that the VOR was not suppressed during catch-up saccades. The suppression is a copy of the facilitation signal generated by the cerebellum during gaze saccades to modulate the activity of the superior colliculus (see part IV for more details

on the computation of the facilitation signal). Additionally, to account for our assumption about the VOR activity during catch-up saccades, SUP is equal to zero if the pursuit system is active while triggering a saccade.

Three terms composed the signal modulated by the suppression signal. The trunk-in-space velocity estimate ($\dot{T}^e_{sp}$ in eq. (54) an in Fig. V-4) is always considered as a perturbation for the gaze system by the model and therefore it is always compensated (if the suppression is OFF). The second term in eq. (54) is the product between the OPN activity and the estimate of the active head-on-trunk velocity. The omnipause neurons do not discharge during saccades and start to discharge when gaze is on target at the end of the gaze saccade (see part IV for the computation of the OPN signal in the saccadic model). Therefore, during a saccade, the second term of eq. (54) is equal to zero. When gaze is on target, usually, the head movement is not finished. Therefore, to keep the gaze stable, all the remaining active head movements must be compensated. Because the OPNs discharge when gaze is on target, active head-on-trunk velocity is compensated for by the VOR model through this pathway.

However during catch-up saccades the VOR could be counterproductive if it compensates for the saccadic component of the active head-on-trunk velocity. Thus a third term has been added to eq. (54). This term removes the expected head-on-trunk velocity that comes from a gaze saccadic command ($\dot{H}^c_{s,g}$ in Fig. V-4) from the estimated active head-on-trunk velocity. This difference is weighted by a mirror activity of the OPN as shown by Fig. V-4. During a catch-up saccade, OPN and SUP are OFF, so this pathway compensated for every expected head movement not related to the gaze saccadic command. When gaze is on target, at the end of the gaze saccade, the OPNs activity goes to one and this term is equal to zero. Therefore, the pursuit component of the active head-on-trunk velocity is always compensated for by the VOR model during simulation of head-unrestrained tracking as previously reported (Lanman et al., 1978; Leigh et al., 1987; Barnes, 1993).

Figure V-4 and eq. (54) show that the VOR model integrates both the suppression mechanism observed during large gaze shifts (Tomlinson and Bahra, 1986a,b; Cullen et al., 2004; Lefèvre et al., 1992) and the cancellation mechanism observed during pursuit (Lanman et al., 1978; Leigh et al., 1987; Barnes, 1993). Additionally, it is important to stress that the VOR model computes the expected head movements that come from an active head command and compensates for all the head movements that are not predicted. This behavior has been previously reported by others (Cullen and Roy, 2004; Roy and Cullen, 2002, 2004).

3

Results

We will present simulations that emphasize the general behavior of our VOR model. First, we will present two classical tests used to quantify the VOR: on-chair rotations with either a chair-fixed target or an earth-fixed target. Then we will present a simulation in which a vertical saccade is triggered during whole-body, horizontal, on-chair rotation, a paradigm which has not be reported in the literature. This simulation is thus a prediction of the model, providing insight into the separation of active and passive components of the head movement and the compensation of the passive component. Finally, we will present the ability of the model to reproduce the well known experiment of Lanman et al. (1978) in which they compared the behavior during head-unrestrained tracking of healthy subjects and labyrinthine-deficient monkeys. Simulations will be compared to published observations to assess their general behavior.

1 On-chair rotations

Two classical tests are traditionally used to quantify VOR efficiency in normal subjects or during clinical tests on patients. Subjects (or patients) sat on a rotating chair with the head fixed with respect to the chair. During the rotation of the chair, subjects have to look either at an earth-fixed target or at a head-fixed target. While subjects look at an earth-fixed target, a passive head movement is induced by the rotation of the chair and must be compensated for by an opposite eye movement to keep the gaze stable on the target. With this procedure, researchers (or doctors) evaluate VOR performance. During a second test, subjects (or patients) have to look at a target that is fixed with respect to the chair (head-fixed target). In this situation, if the head movement is compensated for by the VOR, the eyes will counter-rotate in the head, the gaze will be stable in space, and the target will move away from the gaze axis. Therefore, the VOR must be counteracted. Indeed it has been shown that a pursuit signal is added to the eye movement command to cancel the VOR command (Koenig et al., 1986).

Figure V-5, panel A represents the time course of the target-in-space (red line), head-in-space (gray line), eye-in-head (green line) and gaze position (eye-in-space, black line) for the earth-fixed test. Figure V-5, panel B represents the

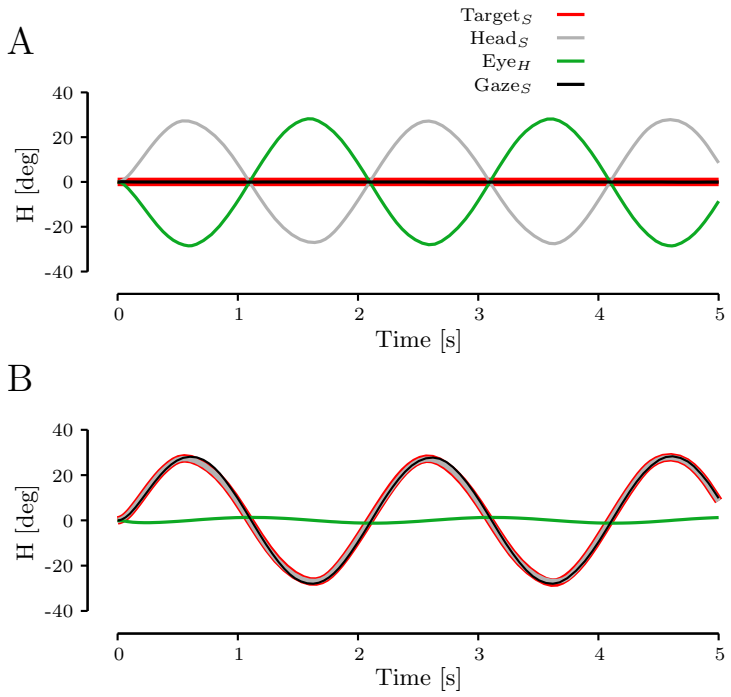

Fig. V-5: On-chair rotation simulation. Panels A and B present simulations of horizontal whole-body rotation using a chair with a sinusoidal velocity. In both simulations, the oscillation frequency was set to 0.5 [Hz] and the amplitude of the chair rotation was fixed to 30 [deg]. The sinusoidal command sent to the chair went through a first order transfer function (100 [ms] time constant). Panel A represents target (red line), gaze (black line), eye-in-head (green line) and head-in-space (gray line) horizontal position as a function of time for a simulation in which the target remained fixed with respect to an inertial reference frame. Panel B represents the same signals for a simulation in which the target remained fixed with respect to a chair-fixed reference frame. Head position also represents chair position in panels A and B. In earth-fixed condition, the gaze remained stationary on the target during the whole simulation, showing the efficiency of the VOR system. In head-fixed condition, the VOR must be canceled by the pursuit signal to accurately fixate the target. Because our pursuit model does not include a predictive mechanism, the cancellation always lagged the VOR. Therefore, a small oscillation of the eye-in-head was observed.

time course of the same signals (same color conventions) for the head-fixed test. We have not represented the chair position, because the head movement also represents the chair rotation. Both simulations used a sinusoidal chair rotation with a frequency of 0.5 [Hz] with an amplitude of 30 [deg]. To be closer to a real rotating chair, the chair position was low-pass filtered by a single pole filter with a 0.1 [s] time constant. A sine function passed through a first-order transfer function gives a pure delay approximately equal to the time constant of the transfer function when the movement is stationary. This delay can be observed in Fig. V-5 because the head movement did not cross the midline (0 [deg]) each second but it is slightly decayed by approximately 0.1 [s].

To test the quality of the VOR model, we first simulated the earth-fixed, on-chair rotation. In this situation, desired head and gaze velocities at the inputs of the pursuit model ($\dot{H}_d$ and $\dot{G}_d$ in Fig. V-2) were set equal to zero. The efficiency of the VOR model can be observed in Fig. V-5, panel A. The gaze remained stationary with respect to the target because only the VOR drove the eye-in-head in the opposite direction of the head movement. Because of the advance filters that allow the model to predict the current body-in-space velocity, both eye and head were exactly in phase opposition and the gaze remained stable. Without the predictive mechanisms there would have been a phase shift between eye and chair movements, which would have led to small movements of the gaze.

To test the cancellation mechanism, Fig. V-5, panel B shows a simulation of the head-fixed, on-chair rotation. Here two systems are evaluated at the same time: the pursuit and the VOR. The desired gaze velocity at the input of the pursuit system ($\dot{G}_d$ in Fig. V-2) was set to the velocity of the chair (because the target moved with the chair) and the head desired velocity ($\dot{H}_d$ in Fig. V-2) was set to zero. Because of the internal delays in the pursuit system, authors have previously shown that the pursuit system needs a predictive mechanism to get rid of those internal delays (Dallos and Jones, 1963) when pursuing a periodic target. The pursuit model used in this study does not include a predictive mechanism and therefore, with a periodic target movement, the gaze always lags the target by a delay that corresponds approximately to the sum of the internal delays of the pursuit system. Because the simulated movement was sinusoidal, a linear transfer function of the inputs led to a fixed delay that came from the time constants of the controllers. Therefore, to minimize this effect, we decrease those time constants by increasing the integral and proportional gains of the pursuit controller. In the head-fixed target condition, a perfect situation would be that the eyes remained fixed in the orbit during the whole simulation because the target was moving with the head. If a phase difference is present between the gaze and the target, the eye will move in the orbit to try to cancel the gaze velocity mismatch between gaze and target (but without prediction, it will never match the gaze velocity). Therefore a small oscillation of the eye-in-the orbit would be observed. Our simulation represented in Fig. V-5, panel B confirmed the theoretical assumption that we just described. The eye-in-head position was sinusoidally modulated with a phase lag of $\sim$90 [deg], a frequency of 0.5 [Hz] and an amplitude of $\sim$1.3 [deg].

2 Vertical saccade during on-chair rotation: model prediction

Figure V-6 shows a simulation that represents a prediction of the model. This simulation shows a vertical position step of the head-fixed target during an on-chair rotation. It has been shown that the discharge of vestibular neurons is modulated by a match between the expectation of a head movement and the actual head movement (Roy and Cullen, 2004; Cullen and Roy, 2004). Therefore, by mixing an active head movement (linked to the vertical gaze shift) and a passive head movement (linked to the chair rotation), the model should predict the observed behavior. The parameters of the chair rotation were identical to those used in Fig. V-5 A and V-5B. After one second, we simulated a vertical step of 15 [deg] of the target. The horizontal target position continued to follow the head. The model does not include a saccade decision mechanism, so we simply started the saccade after a delay of 100 [ms]. Because the VOR model compensates only for the passive movement, the time course of the vertical saccade should be independent of the chair rotation. Figure V-6A, left column,

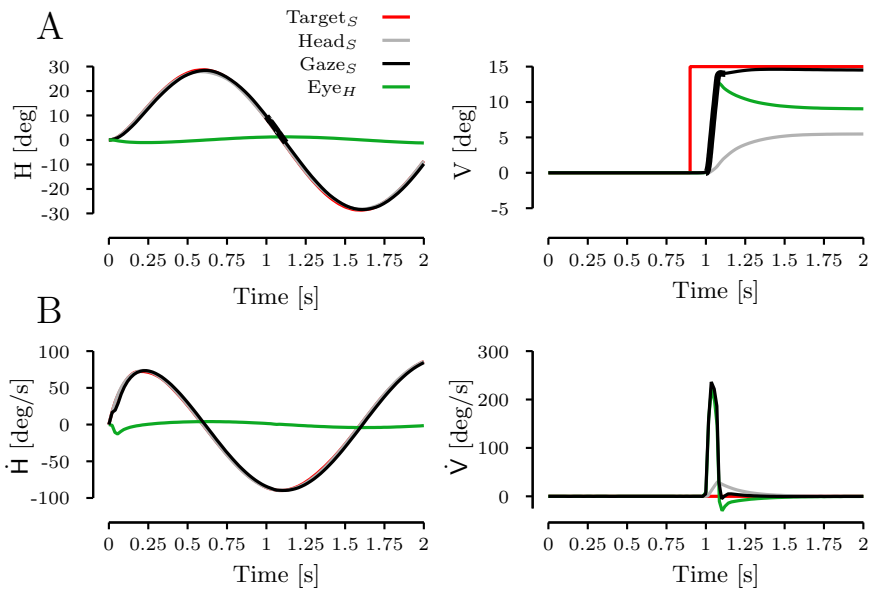

Fig. V-6: Dissociation of active and passive head movements. Simulation of a vertical step of chair-fixed target during horizontal on-chair rotation. Panel A represents target, head, eye-in-head and gaze horizontal (left column) and vertical (right column) positions as a function of time. Panel B represents the evolution of the target, head, eye-in-head and gaze horizontal (left column) and vertical (right column) velocities as a function of time. Thick black lines represent the gaze saccade. The cancellation mechanism during head-free pursuit was not influenced by the vertical saccade. Concurrently, there was no influence of the tracking mechanism on the accuracy of the saccade.

represents the time course of the eye-in-head (green line), gaze (thin black line) head (gray line) and target (red line) horizontal position while the right column represents the time course of the vertical position as a function of time for the same signals. Figure V-6B, left column, shows the evolution of the target (red line), the gaze (thin black line), the eye-in-head (green line) and the head (gray line) horizontal velocity as a function of time. Finally, the right column of Fig. V-6, panel B represents the vertical velocity of those signals as a function of time. Thick black lines in Fig. V-6 represent the time during which the system executed the saccade. Because the VOR model decoupled the active and the passive components of the head-in-space velocity, the horizontal displacement should not have an influence on the vertical saccade and the saccade should not influence the cancellation mechanism on the horizontal VOR. As expected, the horizontal time course of the gaze, the eye-in-head and the head positions and velocities during this simulation (left column in Fig. V-6) were not modified during the saccade and were similar to the classical cancellation test simulated in Fig. V-5, panel B. Concurrently, the vertical saccade evolution was similar to a saccade triggered between two fixed targets. This simulation shows the efficiency of having decomposed head-in-space velocity into its active (related to the gaze) and passive (not related to the gaze) components. At the offset of the saccade, any head movement was taken as a perturbation and the gaze velocity was higher than the target velocity (0 [deg/s]). Therefore, both the VOR and the pursuit controller were making the eye-in-head velocity decrease. Therefore, the decay of the eye-in-head velocity was faster than in the normal situation. This faster decrease induced a small drift of the gaze (1.5 [deg]) towards the target that was observed at the gaze saccade offset.

3 Tracking with a brake on the head: healthy and absent VOR comparison

To evaluate the effect of the VOR during head-unrestrained tracking, Lanman et al. (1978) compared the behavior of head-free tracking between healthy and VOR-deficient monkeys. We reproduced one of their experiments in which a brake was applied to the head during head-free tracking of a constant velocity target in the healthy condition (Fig. V-7) and with an absent VOR (Fig. V-8).

Figure V-7, upper row, shows the time course of target (red line), eye-in-head (green line), head-in-space (gray line) and gaze (thin black line) horizontal positions. Thick black lines in Fig. V-7 represent gaze saccade. Figure V-7, lower row, shows the horizontal velocity evolution as a function of time for the same signals. Target and gaze initial positions were set to -20 [deg]. The head initial position was set to -17 [deg] (thus the eye-in-head started at -3 [deg]). The simulated target moved horizontally with a velocity of 20 [deg/s]. After 500 [ms], the head movement was braked using a viscous torque on the head. We set the input of the head and the gaze velocity controllers to 20 [deg/s]. The yellow rectangles in Fig. V-7 represent the time during which a brake was applied on the head (and thus the head remained stationary). The predictive mechanism that computed the commands of the pursuit system is

less critical when tracking a target with a constant velocity than when tracking an oscillating target. Therefore, to be more realistic, we introduced a 50 [ms]

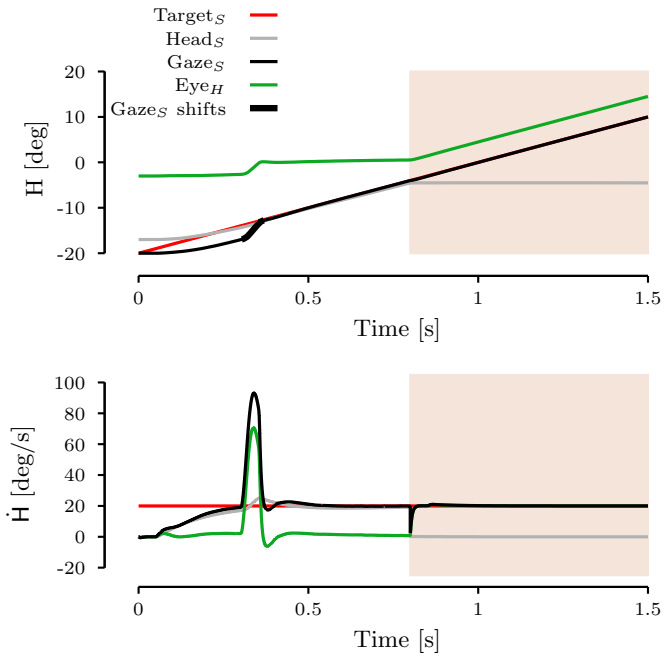

Fig. V-7: Brake on the head during head-unrestrained tracking: healthy situation. Upper row represents the time course of target, eye-in-head, head and gaze horizontal positions. Lower row represents the time course of target, eye-in-head, head and gaze horizontal velocities. Thick black line represents a gaze saccade triggered after the onset of the simulation to cancel the initial position error. After 800 [ms], a brake was applied on the head to stop its movement. The yellow rectangles represent the time during which the head brake was applied. After the first saccade, gaze and target velocities and position were close. Head velocity was close to target velocity. Therefore, eye-in-head velocity was close to zero. No transient can be observed on the gaze position trace when the brake was applied on the head as previously reported (Lanman et al., 1978). However, the model predicted that a small transient should be observed on the gaze velocity trace in order for the eye to accelerate.

delay at the input of the gaze velocity controller (this issue will be elaborated in the discussion). After 300 [ms], we triggered a first saccade to correct the position error on the gaze due to the initiation and the delay of the pursuit system. At the end of the saccade, the gaze was on the target and the velocity of the gaze was close to the velocity of the target. Moreover, the head velocity was also close to the target velocity, thus the eye-in-head remained stationary. After 800 [ms], the viscous torque was applied to stop the head. As observed by Lanman et al. (1978), directly after the head stopped, the simulated gaze

position continued to track the target without any noticeable transient on the position trace. When the head motion stopped, the eye-in-head (which was stationary during the head-free tracking) started immediately to move (this can be observed on both position and velocity traces of the eye-in-head in Fig. V-7). Lanman et al. (1978) assumed that the absence of a transient at the onset of the head brake was strong evidence that the gaze velocity controller was active but opposed by the VOR signal during the head-free tracking. Therefore, when the head movement stopped, the VOR signal also stopped, but the pursuit signal remained activated so the gaze was still pursuing the target without a significant decay of the gaze velocity. Lanman et al. (1978) only show position traces and not velocity traces. However, in our simulations we see that the model predicts a small transient on the velocity trace when the head stops, because the eye needs to accelerate in the head to reach target velocity. Because the eye was stationary in the orbit during the head-free pursuit part, it needs some time (corresponding to the time constant of the mechanical model of the eye) to start its movement. Because the uncompensated time constant of the eye is small ($\sim$5 [ms]), the effect of the velocity transient could not be observed on the position traces in Lanman's paper, but should be visible on the velocity traces in future experiments. The rapidity of the eye movement response after the onset of the brake shows only a small variation of the retinal slip. Because we inserted a delay of 50 [ms], the visible effect of the retinal slip change on the motor command is shown by the small increase of the gaze velocity trace approximately 50 [ms] after the brake. This effect was so small compared to the target velocity that it could not be observed on the position trace. Also, the observed transient oscillations in the gaze velocity at the end of the saccade and after the brake are a numerical artifact of the model.

To gain more insight into the role of the VOR, Lanman et al. (1978) did the same tests on vestibulotectomized monkeys. To simulate this second part of their experiment, we removed the VOR input from both saccadic and pursuit models (red lines in Fig. V-1 and V-2). Leigh et al. (1987) showed that the gain of the smooth pursuit in head-fixed condition was smaller for VOR-deficient human subjects than the gain when the head was free to move. Therefore, the model simulated a gaze velocity overshoot when the head was free to move because we kept the same parameter set for the pursuit system in healthy and VOR-absent situations and there was no more cancellation of the VOR signal. Figure V-8 shows the results of the simulation. The same color conventions as Fig. V-7 were used. Simulations in Fig. V-7 and Fig. V-8 both used the same initial conditions for target, gaze and head positions (-20 [deg], -20 [deg] and -17 [deg] respectively). Oppositely to the simulation in Fig. V-7, we did not trigger a first saccade to cancel the initial position error that comes from the pursuit initiation. Because the gaze velocity overshot the target velocity, the position error was canceled by the acceleration of the gaze. If we had changed the parameters of the controllers, a first saccade would have been necessary to correct the initial position error linked to the initiation of the pursuit exactly as we did for the simulation in Fig. V-7. Thus the eye-in-head remained stable during the tracking when the head was free to move. As observed experimentally by Lanman et al. (1978), no noticeable difference could be observed between

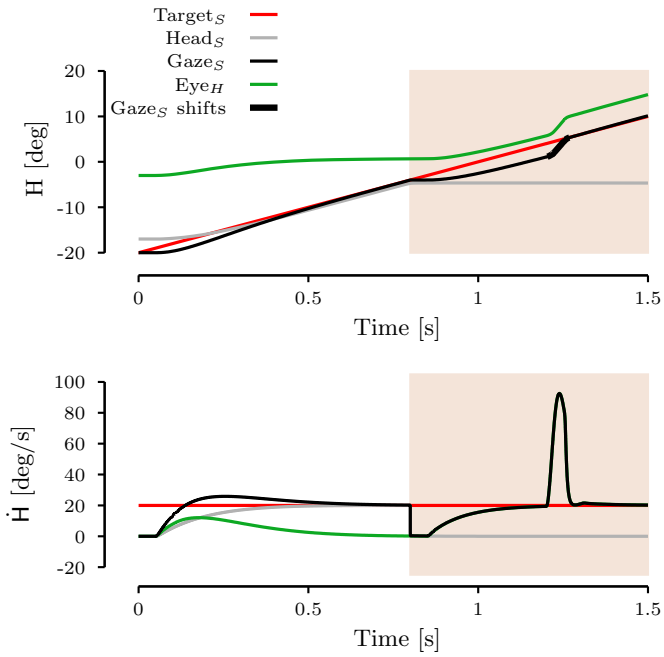

Fig. V-8: Brake on the head during head-unrestrained tracking: VOR-absent situation. Upper row represents the time course of target, eye-in-head, head and gaze horizontal positions. Lower row represents the time course of target, eye-in-head, head and gaze horizontal velocities. Thick black line represents a gaze saccade triggered after head brake to cancel the position error. After 800 [ms], a brake was applied on the head to stop its movement. The yellow rectangles represent the time during which the head brake was applied. Without the VOR, because the gains of the controllers were kept constant, the velocity of the gaze overshot the velocity of the target. After the transient of the pursuit system, gaze and target velocities and positions were close like in the healthy situation showed in Fig. V-7. After the application of the brake on the head, a strong transition was observed. The first 50 [ms] of the transient, the gaze remained stable due to the delay to process the retinal slip. Then the pursuit answer was built. Finally, to compensate for the accumulated position error, we triggered a saccade at 1.2 [s]. After the saccade, gaze and head velocities and positions were matched.

the healthy and the VOR-deficient simulations for the behavior during head-free tracking when the transient of the velocity was finished. After 800 [ms] we simulated a brake on the head to stop its movement. Compared to the simulation presented in Fig. V-7 for the healthy case, the behavior of the VOR-absent simulation shown in Fig. V-8 was totally different. The pursuit system does not need to cancel the VOR action in this simulation. Therefore, when the head is stopped, no signals are available to drive the eye. Because of the delay at the input of the pursuit controller, no eye (which is now the same as

gaze, because the head is stationary) movement occurred before 50 [ms]. The gaze velocity increased more slowly than in the healthy simulation because there was no head movement to help with the gaze movement. To cancel the position error created by initiation of the pursuit, we triggered a first saccade 300 [ms] after the onset of the brake. From this moment, the velocity of the gaze was close to the velocity of the target and therefore no more saccades were necessary to compensate for a position error.

Our simulation is in agreement with the hypotheses proposed by Lanman et al. (1978). When there is no VOR, the system needs more time to continue the tracking movement because the gaze pursuit controller does not discharge. However, because the VOR needs to be canceled in healthy situation, a signal equal to the pursuit signal is sent by the pursuit controller. Therefore, when the head is braked, a pursuit signal is already available to drive the eye and no transient can be observed on the position trace.

4

Discussion

This paper presented a new model of the vestibulo-ocular reflex (VOR). We demonstrated the ability of the model to reproduce published results of traditional VOR tests (on-chair rotations). We also presented a prediction of the model about the decomposition of the head movement into its active (related to the gaze) and passive (unrelated to the gaze) components and the ability of the model to compensate only for passive movements. Finally, to our knowledge, we are the first to simulate the experiment of Lanman et al. (1978), which compared the head-tracking behavior of healthy and VOR-deficient monkeys.

The new VOR model is also the first to integrate two sensors to measure head velocity: the semi-circular canals (SCC) measure the head velocity with respect to an inertial reference frame, and the cervical afferent pathway (CAP) measures head velocity with respect to a trunk-fixed reference frame. Those sensors measure the head velocity in a delayed time reference frame. However, combining their measurements with an efference copy of the active head velocity, the model estimates the current active and passive head velocities.

Additionally, because the model has two sensors, we could simulate previously published experiments in which researchers tested the VOR with either a stimulation of only one of the sensors or when one sensor was deficient. Lanman et al. (1978) used a brake on the head during active head-unrestrained tracking of a moving target to compare the behavior of healthy and VOR-deficient monkeys. As shown by their results and reproduced by our simulation, the tracking behavior in stationary phase when the head is free to move is very similar for healthy and labyrinthine-deficient monkeys. Because we wanted to stress the effect of the VOR during pursuit, we did not change the value of the pursuit gain to match the results reported by Leigh et al. (1987). However, our model gives a hypothesis for the reason why they observed a reduction of the pursuit gain in patients with absent-VOR. If the gain remains identical in healthy and VOR-deficient condition, the patients should overshoot the target velocity. It is well known that subjects preferentially use an undershooting strategy to look at a visual target and maybe correct the movement if needed (e.g., see (Becker and Fuchs, 1969; Kowler and Blaser, 1995) for saccades' accuracy toward fixed targets). It seems therefore logical to adapt the pursuit gain and thus ensure that the gaze velocity will not exceed the target velocity during a long period.

To that goal, a modulation of the pursuit gain must be involved to compensate for the perturbation generated by the absence of the VOR. Optican et al. (1985) showed that an adaptation process is present for patients with an ocular muscle weakness. We believe that a similar adaptation can be used to compensate for the change of the behavior linked to the deficiency of the VOR.

Blouin et al. (1995) compared the spatial constancy (spatial representation of fixed objects while moving) between healthy subjects and a subject with an intact vestibular nerve but without neck and body muscle afferents. They showed that the patient always overestimated her own movements and concluded that the afferent signals from the neck are used to calibrate the measurements from the semi-circular canals. Our results are consistent with the observations of Blouin et al. (1995). Because the CAP output acts as an inhibition (see Fig. V-3, panel B), the model will overestimate the actual trunk-in-space velocity. Adaptation of the weights of the estimator will give more importance to the SCC measurements, because of the loss of the CAP information. However, the output of the BLUE will always overestimate the real trunk-in-space velocity. Correspondingly, the active head-on-trunk velocity at the input of the phase-advance filter in Fig. V-3, panel B will be underestimated. The output of the phase-advance filter is in the feedback path of both the saccadic and the pursuit controllers. Thus, both the gaze and the head movements will overshoot their goals because of the reduced feedback gain.

Moreover, we set the CAP noise five times smaller than the noise of the SCC sensor to account for previously published observations (Blouin et al., 1998). When the CAP is not functional, the model only relies on the information from the SCC, which is noisier, and on a predicted head-on-body velocity from an efference copy to compute the body-in-space velocity, which will thus contain more noise than the estimate in the healthy situation. Therefore, the estimate to the delayed active head-on-trunk velocity will also be noisier and the whole head velocity estimation system would be mis-calibrated, leading to a second source of the loss of accuracy.

It could be surprising that we set the internal delays of both the CAP and the SCC equal (see methods). However, it is worth noting that if evidence to the contrary becomes compelling, using different delays would just require adding a supplementary computational stage at the input of the system. In that new stage the delayed efference copy of the active head-on-trunk velocity would be used to phase-advance the measurements from the CAP into the SCC time reference frame.

Roy and Cullen (2004) compared the discharge of the vestibular neurons in monkeys in several tasks that combined or isolated active and passive head movements. They found that the discharge of the vestibular neurons was correlated with the expectation of a head movement and proposed a regression that describes the discharge as a function of the head-on-trunk and head-in-space velocity. They showed that a cancellation signal is added to the vestibular neurons when the expectation of the movement matches the neck proprioceptive input. Our VOR model is consistent with that interpretation, because it only compensated for the unexpected head movements that do not result from a command sent to the head.

This study does not explain the suppression mechanism used during head-unrestrained saccades. However, authors have shown that the gain of the VOR decreases at the onset of large gaze shifts (Cullen et al., 2004) and quickly increases before the end of the saccade (Lefèvre et al., 1992). Therefore, whatever the signal used to compensate during large gaze shifts between fixed targets, the suppression mechanism will gait off the output of the VOR and no compensation signal will be sent to the eye. So the combination of both the two sensors and the phase-advance mechanism is useful during pursuit to compute the cancellation term that must be sent to the eye but not during head-unrestrained large gaze saccades. The saccadic controller was presented in detail in part IV which showed the interactions with the suppression of the VOR during large head-unrestrained gaze shifts. As previously mentioned, although the VOR behavior has been studied during head-unrestrained saccades and head-free tracking, nothing is known about the VOR modulation during catch-up saccades (saccades that correct a position error during an ongoing movement to compensate for a pursuit gain smaller than one) in head-unrestrained condition. Therefore, we assumed that the VOR gain remains unitary during catch-up saccades, but that the saccadic component of the head velocity would not be compensated for by the VOR (see methods) during the saccade (when the OPNs are not firing). Using this assumption, the model allows a prediction that the passive component of the head movement should be compensated while the active components should be uncompensated. This prediction is presented by the second simulation in which a vertical saccade was triggered during horizontal on-chair rotations while fixating a head-fixed target. The model predicts that no interaction between the saccade movement (active) and the on-chair rotation (passive) should be observed. Both movements could be analyzed independently. Additional experimental tests are needed to evaluate this prediction.

The structure of the model is simpler than the actual neural organization that mediates the VOR (see (Barnes, 1993; Leigh and Zee, 2006) for a review of the pathways involved in the VOR) and the model does not claim to be universal. As an example, showing the partial cancellation of the VOR during torsional rotation (rotation around the naso-occipital axis), Leigh et al. (1989) proved that the VOR is not only canceled by the pursuit system during head-free tracking (there is no torsional pursuit). Other experiments have proved that the modulation of the VOR is not only mediated by vision (for a review on visual-vestibular interactions, see (Barnes, 1993)). Because the model used the output of the pursuit controller to cancel the VOR during head-unrestrained tracking, it can not explain the observation of (Leigh et al., 1989). However, the purpose of this new model is to present a structure that can account for the internal delay of the sensors and estimate the current head velocity. Therefore, the novel structure gets rid of the instabilities linked to the presence of delays in the feedback loop.

Brooks and Cullen (2009) recorded neurons in the rostral fastigial nucleus that were sensitive to the body-in-space rotations. Our model mimics the observations of (Brooks and Cullen, 2009), the cerebellar part of the model has two outputs: the first one gives the current head-on-body velocity and the sec-

ond one estimates the current body-in-space velocity as described by Brooks and Cullen (2009).

As mentioned in the introduction, several authors had already proposed a model of the vestibulo-ocular reflex (Lau et al., 1978; Schmid et al., 1980; Galiana and Outerbridge, 1984; Lefèvre et al., 1992; Barnes, 1993). However, those models explained the VOR behavior either during head-unrestrained pursuit (Lau et al., 1978; Schmid et al., 1980) or during head-unrestrained saccades (Lefèvre et al., 1992). On the contrary, authors have proposed several models for the control of head-unrestrained movements (Galiana and Guitton, 1992; Guitton et al., 1990; Lefèvre and Galiana, 1992; Freedman, 2001; Chen et al., 2002) but those models included the VOR as a simple product between a gain and the head velocity without accounting for sensor delay that could create instabilities during the movement.

To summarize, we demonstrated the validity of a new VOR model structure that integrates two sensors to estimate the current active and passive head velocity components. The model reproduces the on-chair rotation tests that are used by researchers and clinicians to quantitatively evaluate VOR performance in healthy subjects and in patients. The model also predicted what should be observed during an experiment in which the active and the passive components of the head movement are not aligned. Finally, we reproduced the behavior of normal and VOR-deficient monkeys when a brake is applied on the head while they are tracking a moving target with combined eye-head movements.

In conclusion, the model allowed us to stress the importance of internal estimates of executed movements to control their trajectories. Because the sensors' outputs are delayed with respect to the actual movement, there is a need to synchronize the provided measurements realized by sensors to avoid instabilities created by pure delays in sensory feedback loops. Combining an internal estimate of the current movement with sensor outputs, the central nervous system can predict the evolution of a planned movement and compensate appropriately for the unexpected events created by a possible perturbation. Finally, because of the redundancy of the evaluation of a signal (sensors, internal estimates), when one of those information sources is missing, the whole system remains functional. Even if in such case, the accuracy of the movement is decreased, the global behavior is still acceptable. It is widely accepted that the reorganization of the central nervous system to an internal structural change is one of its most fascinating properties. That is the main reason why we believe that models should be able to explain perturbed situations, as is the case for this new VOR architecture.

References

Angelaki, D. E. and Cullen, K. E. (2008). Vestibular system: the many facets of a multimodal sense. *Annu Rev Neurosci*, 31:125–150.

Baker, R. G., Mano, N., and Shimazu, H. (1969). Postsynaptic potentials in abducens motoneurons induced by vestibular stimulation. *Brain Res*, 15(2):577–580.

Barnes, G. R. (1993). Visual-vestibular interaction in the control of head and eye movement: the role of visual feedback and predictive mechanisms. *Prog Neurobiol*, 41(4):435–472.

Becker, W. and Fuchs, A. F. (1969). Further properties of the human saccadic system: eye movements and correction saccades with and without visual fixation points. *Vision Res*, 9(10):1247–1258.

Blouin, J., Labrousse, L., Simoneau, M., Vercher, J. L., and Gauthier, G. M. (1998). Updating visual space during passive and voluntary head-in-space movements. *Exp Brain Res*, 122(1):93–100.

Blouin, J., Vercher, J. L., Gauthier, G. M., Paillard, J., Bard, C., and Lamarre, Y. (1995). Perception of passive whole-body rotations in the absence of neck and body proprioception. *J Neurophysiol*, 74(5):2216–2219.

Brooks, J. X. and Cullen, K. E. (2009). Multimodal integration in rostral fastigial nucleus provides an estimate of body movement. *J Neurosci*, 29(34):10499–10511.

Chen, K. J., Keshner, E. A., Peterson, B. W., and Hain, T. C. (2002). Modeling head tracking of visual targets. *J Vestib Res*, 12(1):25–33.

Crane, B. T. and Demer, J. L. (1999). Latency of voluntary cancellation of the human vestibulo-ocular reflex during transient yaw rotation. *Exp Brain Res*, 127(1):67–74.

Cullen, K. E., Huterer, M., Braidwood, D. A., and Sylvestre, P. A. (2004). Time course of vestibuloocular reflex suppression during gaze shifts. *J Neurophysiol*, 92(6):3408–3422.

Cullen, K. E. and Roy, J. E. (2004). Signal processing in the vestibular system during active versus passive head movements. *J Neurophysiol*, 91(5):1919–1933.

Dallos, P. and Jones, R. W. (1963). Learning behavior of the eye fixation control system. *IEEE Transactions on automatic control*, 8(3):218–227.

de Brouwer, S., Demet, Y., Blohm, G., Missal, M., and Lefèvre, P. (2002a). What triggers catch-up saccades during visual tracking ? *Journal of Neurophysiology*, 87:1646–1650.

de Brouwer, S., Missal, M., Barnes, G., and Lefèvre, P. (2002b). Quantative analysis of catch-up saccades during sustained pursuit. *Journal of Neurophysiology*, 87:1772–1780.

de Brouwer, S., Missal, M., and Lefèvre, P. (2001). Role of retinal slip in the prediction of target motion during smooth and saccadic pursuit. *J Neurophysiol*, 86(2):550–558.

Fejzo, Z. and Lev-Ari, H. (1997). Adaptive laguerre-lattice filters. *IEEE Transactions on Signal Processing*, 45(12):3006–3016.

Freedman, E. G. (2001). Interactions between eye and head control signals can account for movement kinematics. *Biol Cybern*, 84(6):453–462.

Galiana, H. and Guitton, D. (1992). Central organisation and modeling of eye-head coordination during orienting gaze shifts. *Annals of the New York Academy of Sciences*, 656:452–471.

Galiana, H. L. and Outerbridge, J. S. (1984). A bilateral model for central neural pathways in vestibuloocular reflex. *J Neurophysiol*, 51(2):210–241.

Gauthier, G. M. and Vercher, J. L. (1990). Visual vestibular interaction: vestibulo-ocular reflex suppression with head-fixed target fixation. *Exp Brain Res*, 81(1):150–160.

Guitton, D., Munoz, D., and H.L., G. (1990). Gaze control in the cats: Studies and modeling of the coupling between orienting eye and head movements in different behavioral tasks. *J Neurophysiol*, 64(2):509–531.

Hikosaka, O. and Maeda, M. (1973). Cervical effects on abducens motoneurons and their interaction with vestibulo-ocular reflex. *Exp Brain Res*, 18(5):512–530.

Johnston, J. L. and Sharpe, J. A. (1994). The initial vestibulo-ocular reflex and its visual enhancement and cancellation in humans. *Exp Brain Res*, 99(2):302–308.

Kasper, J. and Thoden, U. (1981). Effects of natural neck afferent stimulation on vestibulo-spinal neurons in the decerebrate cat. *Exp Brain Res*, 44(4):401–408.

Koenig, E., Dichgans, J., and Dengler, W. (1986). Fixation suppression of the vestibulo-ocular reflex (vor) during sinusoidal stimulation in humans as related to the performance of the pursuit system. *Acta Otolaryngol*, 102(5-6):423–431.

Kowler, E. and Blaser, E. (1995). The accuracy and precision of saccades to small and large targets. *Vision Res*, 35(12):1741–1754.

Krauzlis, R. J. (2004). Recasting the smooth pursuit eye movement system. *Journal of Neurophysiology*, 91:591–603.

Lanman, J., Bizzi, E., and allum, J. (1978). The coordination of eye and head movement during smooth pursuit. *Progress in Brain Research*, 153:39–53.

Lau, C. G., Honrubia, V., Jenkins, H. A., Baloh, R. W., and Yee, R. D. (1978). Linear model for visual-vestibular interaction. *Aviat Space Environ Med*, 49(7):880–885.

Lefèvre, P., Bottemanne, I., and Roucoux, A. (1992). Experimental study and modeling of vestibulo-ocular reflex modulation during large shifts of gaze in humans. *Exp Brain Res*, 91(3):496–508.

Lefèvre, P. and Galiana, H. L. (1992). Dynamic feedback to the superior colliculus in a neural network model of the gaze control system. *Neural Netw.*, 5(6):871–890.

Leigh, R. and Zee, D. (2006). *The Neurology Of Eye Movement*. Oxford University Press, 4 edition.

Leigh, R. J., Maas, E. F., Grossman, G. E., and Robinson, D. A. (1989). Visual cancellation of the torsional vestibulo-ocular reflex in humans. *Exp Brain Res*, 75(2):221–226.

Leigh, R. J., Sharpe, J. A., Ranalli, P. J., Thurston, S. E., and Hamid, M. A. (1987). Comparison of smooth pursuit and combined eye-head tracking in human subjects with deficient labyrinthine function. *Exp Brain Res*, 66(3):458–464.

Optican, L. M., Zee, D. S., and Chu, F. C. (1985). Adaptive response to ocular muscle weakness in human pursuit and saccadic eye movements. *J Neurophysiol*, 54(1):110–122.

Rambold, H., Churchland, A., Selig, Y., Jasmin, L., and Lisberger, S. G. (2002). Partial ablations of the flocculus and ventral paraflocculus in monkeys cause linked deficits in smooth pursuit eye movements and adaptive modification of the vor. *J Neurophysiol*, 87(2):912–924.

Roy, J. E. and Cullen, K. E. (2002). Vestibuloocular reflex signal modulation during voluntary and passive head movements. *J Neurophysiol*, 87(5):2337–2357.

Roy, J. E. and Cullen, K. E. (2004). Dissociating self-generated from passively applied head motion: neural mechanisms in the vestibular nuclei. *J Neurosci*, 24(9):2102–2111.

Sato, H., Ohkawa, T., Uchino, Y., and Wilson, V. J. (1997). Excitatory connections between neurons of the central cervical nucleus and vestibular neurons in the cat. *Exp Brain Res*, 115(3):381–386.

Schmid, R., Buizza, A., and Zambarbieri, D. (1980). A non-linear model for visual-vestibular interaction during body rotation in man. *Biol Cybern*, 36(3):143–151.

Smith, O. J. (1959). A controller to overcome dead time. *ISA J.*, 6(2):28–33.

Tomlinson, R. D. and Bahra, P. S. (1986a). Combined eye-head gaze shifts in the primate. i. metrics. *J Neurophysiol*, 56(6):1542–1557.

Tomlinson, R. D. and Bahra, P. S. (1986b). Combined eye-head gaze shifts in the primate. ii. interactions between saccades and the vestibuloocular reflex. *J Neurophysiol*, 56(6):1558–1570.

Zee, D. S., Yamazaki, A., Butler, P. H., and Gcer, G. (1981). Effects of ablation of flocculus and paraflocculus of eye movements in primate. *J Neurophysiol*, 46(4):878–899.

Part VI

General discussion and perspectives

1

Contributions of the thesis

With the head free to move, the central nervous system is confronted by several problems when a change of the visual axis is needed: e.g., coordination of the eye and the head trajectories to ensure an accurate gaze displacement, modulation of the vestibulo-ocular reflex, etc. The aim of this thesis was to understand better, through behavioral and modeling studies, how the central nervous system controls and coordinates the eye and the head trajectory during a reorientation of the gaze. The behavioral studies of this work generalized results previously reported in head-restrained condition to situations in which the head was free to move while the models proposed some generic solutions to the coordination of several body segments and the integration of delays in the control of hierarchically embedded body systems.

Building an accurate spatial representation of our surroundings is important to program adequately a sequence of movements (spatial constancy). Previous studies have shown how the central nervous system updates our visual environment when one segment (the eye) is moving (Blohm et al., 2005, 2003b,a, 2006). To get closer to more natural conditions, it would be interesting to generalize if and how spatial constancy is achieved when several body parts are moving. As a second step toward this global goal, this thesis used the eye-head system to study how the update of an internal representation of the visual space was done when two body segments (in our case, the eye and the head) are moving during the programming of a movement. Even if the generalization to a head-unrestrained situation could appear as straightforward, the integration of the head movement, the relative contribution of the eye/head movement to the gaze displacement and the interactions with the VOR are examples of the difficulties that the central nervous system must face to update accurately its internal spatial representation during head-unrestrained displacements. The results of this thesis demonstrated the ability of the central nervous system, if it is given enough time, to update its representation of the visual space when both eye and head are moving. The analyses demonstrated that two parameters are key players to guarantee the accuracy of the visual space updating: the latency of the gaze movement and the relative contribution of the eye to the gaze displacement. As in head-restrained condition, the longer the latency, the better the integration of self-movements. Additionally, the analyses showed

that eye and head displacements are not taken equally into account during the updating process: the more the eye contributed to the gaze displacement, the better the update of the visual space. Finally, these results were the first to demonstrate behaviorally a difference of the VOR gain modulation between passive and active head movements.

When a target is moving at a high velocity, smooth eye movements are not sufficient to accurately track it when the head is fixed. Thus, subjects use saccades to compensate for the decrease in pursuit performances. Because of the loss of visual perception during the execution of a saccade, an increase of the number of saccades is accompanied by a global decrease of the visual acuity. This is probably a reason why subjects start to use combined eye-head movements when they track a target in everyday life situations. Therefore, understanding how the central nervous system coordinates eye and head movements during head-unrestrained tracking is important. As described in the introduction of the second behavioral study of the thesis (part III), only a few studies looked at tracking of moving targets when the head was free to move. Additionally, to my knowledge this study was the first to address the issue of two-dimensional tracking in head-unrestrained conditions. The analyses demonstrated that two parameters influence the gaze tracking performances: the frequency and the orientation of the oscillating target. If the influence of the target frequency has been previously reported (Collins and Barnes, 1999), this study was the first to demonstrate the modulation of the pursuit gain linked to the orientation of the tracking target in head-unrestrained conditions. Our results also showed that the head movement is less influenced by the frequency than by the orientation of the target. The analyses of the head trajectory in 2-D revealed two strategies used by the subjects while tracking the target. If the target was moving mostly horizontally, subjects rolled their head to align the plane of the horizontal semicircular canal with the target orientation, and then they rotated their head as if the target was moving horizontally. If the target moved more vertically, they also rolled their head but to align the normal to the plane of the horizontal semicircular canal with the target orientation, and then they moved their head as if the target was moving vertically. Additionally, the study demonstrated the independence of the firsts 200 [ms] of head movement to a modification of the target parameters. This result pointed either toward a predefined typical head response or a saturation of the neural commands sent to neck muscles. Finally, saccades' amplitude was better explained by a simple regression with the retinal slip instead of the position error as the independent parameter, oppositely to previous observations and common beliefs.

From behavioral observations and electrophysiological recordings, researchers started to build mathematical models of the oculomotor apparatus. One of the most difficult tasks when building a model is to select the appropriate level of detail to include. With too many details, the complexity of the proposed architecture can hide its main features. At the opposite, models without enough details cannot reproduce a large set of experimental observations. A second difficulty arises when different theoretical concepts are proposed to model the same system. All models have good points and pitfalls; thus without an open discussion and the acceptance of the model limits, no consensus can be found.

In the third study presented in this thesis (part IV), a model of eye-head coordination during gaze shift was developed. This model is the first to reconcile the two proposed theoretical concepts briefly presented in the introduction of part IV. Several typical cases have been presented to show the general abilities of the model: differently oriented head and gaze trajectories, head perturbations, lesions, etc. Importantly, all the simulations were compared to previously published observations. Those comparisons demonstrated the efficiency of the proposed model. Maybe the most important aspect of the novel architecture is the generic approach proposed. The model could be easily extended to explain how the central nervous system controls and coordinates embedded systems with more layers than the two-layer eye-head system studied in this thesis (e.g. the head on the trunk on the legs). A global approach to control functionally different body parts is a strength. It could explain why brain areas involved in several functions contain similar patterns of neural connection (e.g., the cerebellum). However, in its current design, the proposed architecture also has some pitfalls (see the next chapter for a discussion on the possible ameliorations of the model) that could be corrected.

The first model presented in this thesis dealt principally with the motor control of the eye and the head during rapid reorientations of the gaze. A second important aspect to control correctly a movement is the accuracy of the sensory part of the system. In the case of vision, the vestibulo-ocular reflex (VOR) needs a correct estimation of head movements to counter-rotate adequately the eye in the head to keep the vision stable. As explained in the general introduction (part I, chapter 2, section 4), not all head movements are compensated for by the VOR to avoid inefficient effects. It has been shown that only unpredicted head movements of a neural command sent to the neck muscles are negated by the VOR (Roy and Cullen, 2004). The last part of this thesis (part III) proposed a model that estimates the active (related to the gaze) and the passive (no related to the gaze, perturbations) components of the head velocity. The novelty of the approach is the combination of three information sources for the computation of the head velocity components: the semicircular canals, the neck proprioceptive inputs and an efference copy of the neck muscles' command. The integration of three estimations of head velocity permitted to get rid of the internal delays present intrinsically in the sensors; hence giving a correct approximation of the current head velocity. Four simulations were presented that exemplified the properties of the VOR model during head-unrestrained tracking. Two simulations reproduced the classical on-chair rotation tests (head- or earth-fixed target) to demonstrate the basic properties of the model. Then, the model was used to predict the trajectory of the gaze if a subject triggered a vertical saccade during rotations on a vestibular chair with a head-fixed target. It is well known that the VOR gain decreases with large saccades. Thus, this prediction is of particular interest because it could demonstrate simply if the VOR still compensates for the passive head movement (linked to the rotation of the chair) during saccadic movement in the perpendicular direction. Finally, this model was the first to simulate the braking experiment of Lanman et al. (1978) that demonstrated the cancellation mechanism during head-unrestrained tracking. The model made some predic-

tions concerning the transient behavior at the time of the brake onset. Those were not observed in the initial measurements made by Lanman et al. (1978) because of the large noise-to-signal ratio of their study.

2

General comments, perspectives, and future experiments

In this last chapter of the thesis, I first give some general comments about head-unrestrained studies. Finally, some suggestions for future experiments and their theoretical predictions will conclude this work.

1 Head-unrestrained studies: an open-field full of traps

Since the early beginning of my PhD, I have been really excited by the "head-unrestrained" approach of my project. In this section, I tried to take a step back and to summarize what are the good points and the drawbacks of head-unrestrained studies.

Experimental apparatus

A challenging part of this work was to upgrade an experimental setup initially designed for head-restrained recordings. At first, I did not imagine that the modifications to the setup would take so much time. Now I recognize that the constraints linked to a setup are such that upgrading an experimental apparatus is **never** a simple task.

A generic setup can be divided into two parts: target presentation and movement recording. Both parts have to be perfectly synchronized to ensure that recorded data and targets are in phase for the offline analysis. This is done in the setup by a real-time computer (PXI-8186 RT, National Instruments, Austin, Texas) running LabView (National Instruments, Austin, Texas) that computes target position and triggers the recording devices. One of the major (and most frustrating) drawbacks of using a closed-source commercial solution to control the setup was the impossibility to understand some unpredictable, random responses of the system during basic tests[95]. On the other side, the graphical user interface was easy to use, and I did not have to consider several complicated aspects (e.g., the communication between the host and the real-time computer). However, I believe that the possibility to observe or to control

[95] I spent **hours** to get rid of software bugs and to find tricks to ensure the robustness of the system.

the processes at the lowest software layer is a major asset for an experimental setup. The drawback being that strong C/C++ notions are important to program or to modify the setup. Because electronic systems evolve rapidly, I think that it could be useful to upgrade the current system. In this perspective, because of the costs to upgrade the acquisition data boards, the computers (host and real-time) and the maintenance of the LabView license, I think the best solution would be to start from scratch and use an open-source real-time kernel configuration (e.g. a R.E.X. system based on a QNX Linux kernel). The current material could be easily used for simpler experimental setups or for students' laboratory experiments.

Several possibilities exist currently to record eye and head position during experiments. Traditionally, recordings during head-unrestrained experiments are done with two search coils: one fixed to the head and the other on the eye. This solution can be very practical because the recorded data represent directly the gaze and the head-in-space positions. However, the non-linearity of the magnetic field and the impossibility to detect movement translations were important drawbacks that forced us to switch to a less conventional solution. The configuration adopted combined eye-in-head recordings from a video eye tracker and recordings of infrared light emitting diodes (IREDs) position with motion caption cameras. The critical stage of this method is the reconstruction of the gaze position from the eye-in-head angular information and the head-in-space position. To that goal, we used an algorithm developed by Ronsse et al. (2007). This solution is elegant but has two drawbacks: the precision of the measurements and the computational time. During my experiments, subjects had to rotate their head at velocities up to $\sim$230 [deg/s]. Therefore, even if the helmet was firmly tightened to the subjects' head, and if we used a bite-bar, it was impossible to avoid small slippages between the helmet and the head of the subjects. This relative displacement changed the relationship computed by the calibration algorithm that linked the IREDs' position to the eye recordings. In addition to the slippage, from my point of view, the most critical factor against the video eye trackers comes from the extraction of the eye angular position from the recorded videos. This offline process takes **ages**, and it can be inaccurate, even if the system is well positioned with respect to subjects' eyes[96]. I believe that the best solution would be to combine the advantages of the search coil technique (accuracy, high frequency acquisition, etc.) and the record of the head position with the motion capture cameras. A new promising system is currently developed by Dale Roberts, Mark Shelhamer and Aaron Wong at Johns Hopkins university: a wireless search coil (Roberts et al., 2008). Subjects wear a search coil annulus without exiting wire that contains a resonant resistor-capacitance circuit. They also wear a pair of modified glasses that generate short trains of magnetic pulses. The pulses induced energy in the eye coil. When the pulses stop, the circuit on the eye coil is still oscillating with an exponentially decaying amplitude. A triplet of receivers located on the frame of the glasses record the intensity of the radiated signal. The orientation of the coil, and therefore, the orientation of the eye, is computed from the relative intensity of those sensors (Roberts et al., 2008). This recording method could

[96] The system is highly sensitive to the color of the subjects' iris.

easily replace the video eye tracker and provide online access to eye-in-head angular position[97] with more accuracy and more robustness than the video eye tracker.

Analyses

It makes me smile now when I read the first reports I made on what I thought could be interesting to study during my PhD thesis (e.g. binocular analyses of head-unrestrained gaze shifts, etc.). With a step back, I realize that analyzing head-unrestrained two-dimensional movements is not a simple task and that taking smaller bites is more cautious. The various combinations of eye and head movements and the large amount of idiosyncratic differences in the subjects' behavior to a similar target trajectory are examples of the difficulties that must be faced when eye-head movements are studied. As soon as the head is released, no more global rules[98] about the characteristics of the gaze movement can be easily extracted. Thus, the variability in each combined eye-head movement is relatively greater when the head is free to move than with eye-only movements in head-fixed condition. Therefore, the number of trials needed by a subject doing a single experiment must be much more important to extract correctly the mean behavioral characteristics of the studied head-free movement. Despite those problems, I believe that, with the development of recording techniques (see preceding section), studies on eye-head coordination are at childhood stage. A lot of new experiments[99] could be conducted to increase our knowledge on the way the central nervous system controls and coordinates eye and head movements.

2 Open questions, ameliorations, perspectives and future experiments.

In this section, I will enumerate open questions that followed the work developed in this thesis. For each problem, I will propose a solution (experiment or model), associated with some predictions, that could help to answer it. The different questions are not presented accordingly to the chapter organization of the thesis but follow a methodological order.

VOR: active versus passive head movements compensation

In the last study of the thesis (part V), we presented a prediction made by the VOR model about the compensation of the passive component of the head movement. Figure VI-1 represents a schematic drawing of a hypothetical experimental setup that could be used to test the prediction proposed in chapter 3, section 2 of part V. The experimental apparatus is composed of a rotating chair on which a screen has been fixed. Therefore, a rotation of the chair induced a similar rotation of the screen. To test the prediction made in part V, a subject

[97] Even torsional recordings!

[98] E.g. the main sequence for saccades in head-restrained condition.

[99] Several propositions linked to the topics of this thesis will be presented in the next section.

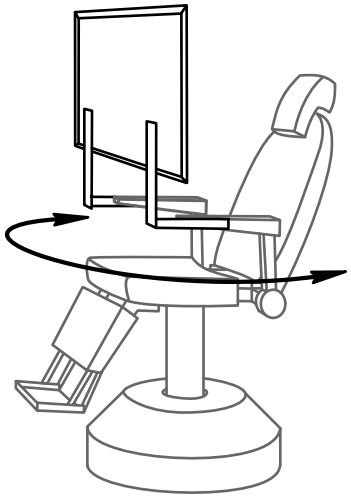

Fig. VI-1: **Rotating chair with a chair-fixed flat screen to present target.** Gray lines represent the vestibular chair while black lines represent a target presentation screen fixed to the chair. This setup could be used to test several open questions of this thesis.

would sit on the vestibular chair of Fig. VI-1.

A first series of tests would evaluate the VOR performances of the subject. As a first step, the chair would rotate the subject in a dark room with a sinusoidal velocity (at different frequencies, amplitudes) to evaluate his/her VOR gain in the dark. Then the chair would rotate at constant velocity to evaluate the time constant of the subject's VOR response. Finally, a target would be presented on the screen. The subject would be instructed to keep his/her gaze fixed on the target while the chair rotates with a sinusoidal velocity (at different frequencies, amplitudes). This procedure would serve to test his/her VOR cancellation gain.

A typical trial would start with the subject looking at a central fixation target on the screen. After a random period, the target would make a random horizontal and vertical position step in the screen reference frame. The subject would be instructed to trigger a saccade toward the target as soon as it jumps. After a fixed period of presentation, the target would jump again toward the center of the screen. Then a second trial would start. By varying the time at which the target jumps and the parameters of the rotating chair movement (frequency, amplitude) according to the prior tests on VOR performance, a large set of data would be obtained.

Finally, with the chair static, the same set of target jumps would be presented to the subject. This would serve as a final control data set.

The hypothesis proposed in part V supposed that no difference should be observed along the horizontal component between saccade-on-chair trials and typical cancellation trials. In parallel, Figure VI-2 represents the different hypotheses that the protocol could test concerning the saccades' trajectory. In

this figure, the central fixation is represented by a filled circle at the center of the screen and the position of the saccadic target is represented by a black star. If the cancellation is effective during on-chair saccades, their trajectories for a

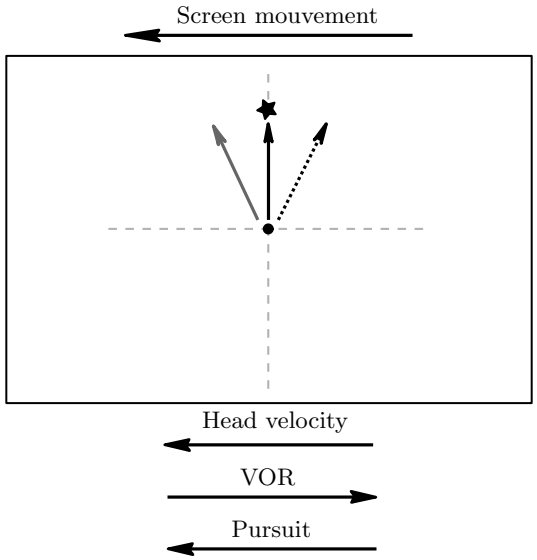

Fig. VI-2: **Passive versus active compensation and visual constancy prediction.** This figure represents schematically the screen fixated on the chair in Fig. VI-1. The black circle represents the central fixation target. The black star represents the position of the target after a jump. The three arrows (solid black, dashed black and gray) represent the theoretical possibilities for the direction of a saccadic movement.

vertical target jump should be purely vertical in the screen reference frame (Vertical black arrow in Fig. VI-2). Because the cancellation mechanism corresponds to the sum of the VOR signal and the pursuit command, if the VOR is not properly negated by the pursuit signal (e.g. at high rotation frequencies), an ideal vertical saccade should have a horizontal component in the direction of the VOR (dashed black arrow in Fig. VI-2). Finally, if the pursuit system is compensating to much, the normally vertical saccade would have a horizontal component in the direction of the head velocity (gray arrow in Fig. VI-2).

Therefore, the analysis of the horizontal position error at the end of the saccade with respect to the orientation of the target would permit to test if the cancellation mechanism of the VOR separates the active and the passive component of the head movement. Because the VOR cancellation decreases with an increase of the target oscillation frequency, a relationship should link the horizontal component of the position error and the target frequency.

Finally, this protocol mixes the two mechanisms for the VOR modulation in the same experiment. The cancellation is traditionally studied with head-fixed target fixation during on-chair rotations. On the contrary, VOR suppression is

used during head-unrestrained saccades. With purely vertical saccades, the two mechanisms of modulation will act along perpendicular directions. Therefore, this test can be used to study if the suppression mechanism acts independently of the cancellation mechanism.

Visual/Spatial constancy and VOR

At the end of the first study (part II, chapter 3, section 5), a range of sensitivities of the VOR gain to the target oscillation frequency was defined using feasible values of CI^V. Surprisingly, the VOR gain was much more sensitive to target frequency in our protocol than in previously reported results. In the discussion of the paper, we postulated that this difference arose because subjects used active head movements during the task.

The experimental setup showed in Fig. VI-1 could also be used to test this assumption. As for the previous proposed experiment, this one would start with several trials to evaluate the VOR performances of the subjects (VOR in the dark, cancellation gain, etc.). Then the protocol used during the experiment would change a little. While the subject looks at the central fixation target, a second target would be flashed (the first one remaining ON). With the extinction of the central fixation target, the subject would be instructed to trigger a saccade toward the remembered position of the flash target in the screen reference frame. I called this condition "visual constancy" because the subject would have to update his visual representation to reach accurately the target. In a second experiment, the subject would be instructed to look at the spatially fixed location of the flashed target. This condition is called "spatial constancy" because the subject would have to update the spatial location of the flashed target to reach it accurately.

Figure VI-2 represents the prediction for the visual constancy condition. Solid black arrow represents a perfect integration of the passive head rotation during the programming of the saccade trajectory. Dashed black arrow represents an under-compensated head rotation. Finally, the solid gray arrow represents an over-compensation of the passive head rotation. Figure VI-3 represents the same kind of prediction for the spatial constancy condition (perfect compensation for solid black arrow, under-compensation for dashed black arrow and over-compensation for gray arrow).

As for the preceding proposed experiment, the analysis of the horizontal component of the horizontal position error at the end of the first saccade would indicate the level of compensation realized by subjects in each condition.

Improvements of the head-unrestrained gaze saccades model

The model presented in this thesis has been developed to demonstrate a new control structure based on two main feedback loops: one that controls the gaze through eye movements and the second that controls the head trajectory. Different upgrades to the model could be made to include more experiments that could be reproduced. The following paragraphs will present the possible upgrades sorted by increasing difficulty of integration.

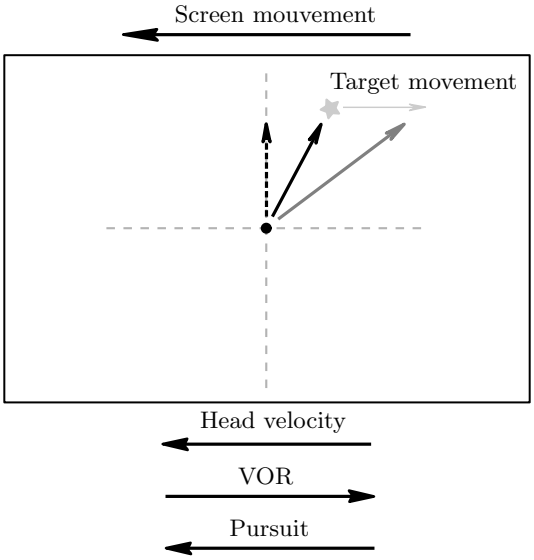

Fig. VI-3: **Spatial constancy prediction.** This figure represents schematically the screen fixated on the chair in Fig. VI-1. The black circle represents the central fixation target. The gray star represents the spatially fixed position of the flashed target after a jump. The three arrows (solid black, dashed black and gray) represent the theoretical directions of a saccadic movement depending on the amount of compensation done by the subjects.

The model was not originally designed to simulate large amplitude saccades. We integrated a functional oculomotor range (OMR) that does not have a physiological meaning. The OMR function saturates the eye-in-the-orbit position when it is bigger than a threshold. Several possibilities have been previously proposed by others (e.g. a positive feedback loop (Lefèvre and Galiana, 1992)) and must be investigated to assess their physiological likelihood. The most likely solution must be integrated in the model. Additionally, Paré and Guitton (1998) demonstrated that the OPNs are reactivated during large gaze shifts when the eye reaches the OMR boundaries during a certain amount of time. Our model cannot reproduce the results of Paré and Guitton (1998), because there is no interaction between the OPNs and the OMR. An elegant solution to this problem has been proposed by Prsa and Galiana (2007). The authors proposed to tune the OPNs activity according to a threshold that varies as a function of three parameters: the gaze motor error, the head velocity and the eye-in-head velocity. This solution could be included in our model to simulate the behavior of large gaze shifts.

As explained in the model description, the head control part of the model is a highly simplified version of the current pathways involved in the control of the head trajectory. The general introduction stresses the importance of two key areas for the control of the head movement: the nucleus reticularis gigantocellularis (NRG) and the nucleus reticularis pontis caudallis (NRPC). Two possibilities exist to include those areas in the general model scheme presented

in Fig. IV-3. A first solution would be to add a direct pathway from the head desired amplitude to the spinal cord[100]. Interactions would only occur between NRG, NRPC and SC. As for the first proposition, the second solution also integrates the direct pathway from NRG and NRPC to the spinal cord. However no connection from the head areas would project directly to the superior colliculus but NRG and NRPC would receive collicular projections. The second solution would also include the nucleus reticularis tegmenti pontis (NRTP). This area will be the relay between the gaze command from the superior colliculus and the cerebellum input. Additionally, it would receive (as in the anatomy) a projection from the gigantocellular head movement region. With this solution, the model could reproduce the results of Freedman and Quessy (2004) about the effect of NRG stimulations on gaze trajectory. Freedman and Quessy (2004) observed that NRG stimulations modified the accuracy of gaze saccades. This is one of the main evidence against a gaze feedback control. In the second solution that I proposed, the stimulation of NRG can change the gaze goal sent to the cerebellum through the NRPC/NRG $\Rightarrow$NRTP $\Rightarrow\mathsf{CB_G}$ pathway; hence influencing the gaze saccade accuracy.

The most complicated (and therefore, the nicest) update would be to upgrade our lumped model to a distributed version. The signals carried by the different boxes in Fig. IV-3 have no physiological meaning, they correspond to the mean response of a neuronal population. This is because we wanted to present theoretical concepts of parallel loops for the control of hierarchical systems. To be more physiologically plausible, each area represented in Fig. IV-3 should use an artificial neural network that mimics the neuronal architecture observed anatomically. The amount of work to switch from a lumped to a distributed version of the model is enormous. If the computations done in some areas are better known (e.g. the superior colliculus), no consensus has been found yet on how information is processed in others for which the anatomy is perfectly understood (e.g. the cerebellum). In my opinion, extending the model to a distributed version with artificial neural networks not even close to the anatomy is pointless. Like usually, a trade-off has to be found between the level of details represented by the model and the purpose of the study. As final argument attesting the difficulty of building distributed models, the increasing mathematical complexity can quickly become "unbearable" for a large majority of the neuroscience scientific community. Therefore, I think it is totally foolish to believe that a distributed version of our head-unrestrained gaze saccades model would be easily published. However, with a supplementary layer of "if" to the present text, I think that a distributed version of some parts of the model would be of particular interest. With a distributed architecture of some parts of the model, we could simulate the effect of a lesion on the behavior. This could help the clinicians to diagnose patients and therefore, to prescribe them the correct drug. Since the early stages of my PhD[101], I found that the cerebellum was an amazing neural area. As explained in the general introduction, it counts half of the total number of neural cells in only 10% of the central nervous system volume. Thereby, including a model of the cerebellum that con-

[100] Exactly like the direct gaze pathway from the superior colliculus to the brainstem.
[101] And even during my undergrad studies.

tains a learning process[102] would be an amazing achievement for the scientific community. I think the road to reach this goal remains long but each journey starts with a first step!

[102] To simulate saccades amplitude adaptation, VOR modulation, etc.

References

Blohm, G., Missal, M., and Lefèvre, P. (2003a). Interaction between smooth anticipation and saccades during ocular orientation in darkness. *J Neurophysiol*, 89(3):1423–1433.

Blohm, G., Missal, M., and Lefèvre, P. (2003b). Smooth anticipatory eye movements alter the memorized position of flashed targets. *J Vis*, 3(11):761–770.

Blohm, G., Missal, M., and Lefèvre, P. (2005). Processing of retinal and extraretinal signals for memory-guided saccades during smooth pursuit. *J Neurophysiol*, 93(3):1510–1522.

Blohm, G., Optican, L. M., and Lefèvre, P. (2006). A model that integrates eye velocity commands to keep track of smooth eye displacements. *J Comput Neurosci*, 21(1):51–70.

Collins, C. J. and Barnes, G. R. (1999). Independent control of head and gaze movements during head-free pursuit in humans. *J Physiol*, 515 (Pt 1):299–314.

Freedman, E. G. and Quessy, S. (2004). Electrical stimulation of rhesus monkey nucleus reticularis gigantocellularis. ii. effects on metrics and kinematics of ongoing gaze shifts to visual targets. *Exp Brain Res*, 156(3):357–376.

Lanman, J., Bizzi, E., and allum, J. (1978). The coordination of eye and head movement during smooth pursuit. *Progress in Brain Research*, 153:39–53.

Lefèvre, P. and Galiana, H. L. (1992). Dynamic feedback to the superior colliculus in a neural network model of the gaze control system. *Neural Netw.*, 5(6):871–890.

Paré, M. and Guitton, D. (1998). Brain stem omnipause neurons and the control of combined eye-head gaze saccades in the alert cat. *J Neurophysiol*, 79(6):3060–3076.

Prsa, M. and Galiana, H. L. (2007). Visual-vestibular interaction hypothesis for the control of orienting gaze shifts by brain stem omnipause neurons. *J Neurophysiol*, 97(2):1149–1162.

Roberts, D., Shelhamer, M., and Wong, A. (2008). A new "wireless" search-coil system. In *ETRA '08: Proceedings of the 2008 symposium on Eye tracking research; applications*, pages 197–204, New York, NY, USA. ACM.

Ronsse, R., White, O., and Lefèvre, P. (2007). Computation of gaze orientation under unrestrained head movements. *Journal of Neuroscience Methods*, 159:158–169.

Roy, J. E. and Cullen, K. E. (2004). Dissociating self-generated from passively applied head motion: neural mechanisms in the vestibular nuclei. *J Neurosci*, 24(9):2102–2111.

Appendices

A Algorithm for saccade detection: Mathematical developments

This appendix presents the saccade detection algorithm used throughout the present document.

The algorithm is based on a fault detection theory widely used in automatics and engineering called generalized likelihood ratio (GLR) (Basseville and Nikiforov, 1993; Willsky and Jones, 1974, 1976). It uses a likelihood ratio to compare two models and decides which one best represents the actual data. One model represents the "normal" situation (no saccade) and one model represents an augmented model with a fault added to the normal behavior (saccade detected).

In parallel to the description of the general equations of the GLR as presented in (Willsky and Jones, 1974, 1976), the particular models used throughout the document will be presented.

The model

Willsky and Jones (1974, 1976) proposed a stochastic discrete-time dynamical linear model:

$$x(k+1) = \phi(k+1,k) * x(k) + \Gamma(k) * \omega(k) + \delta_{\theta,k+1} * \nu \tag{.1}$$

$$z(k+1) = H(k+1) * x(k+1) + \upsilon(k+1) \tag{.2}$$

In which $x \in \Re^n$ is the state and $z(k) \in \Re^p$ is the observation (the data). The state x has an initial condition $x(0)$ with a mean $\hat{x}_0$ and a covariance P_0. $\omega(k)$ and $\upsilon(k)$ are independent gaussian zero mean white sequences with $E[\omega(k)\omega(k)'] = Q(k)$ and $E[\upsilon(k)\upsilon(k)'] = R(k)$. $P(k)$ and $R(k)$ are positive definite matrices. $\delta_{\theta,k+1}\nu$ represents a possible jump of one or more of the state variables at time $k+1$. δ corresponds to the Kronecker delta:

$$\delta_{i,j} = \begin{cases} 0 \; if \;\; i \neq j \\ 1 \; if \;\; i = j \end{cases} \tag{.3}$$

θ is a possitive integer equal to $+\infty$ if there is no jump. If there is a jump, θ is equal to a positive finite value (value corresponding to the time of the jump). Finally, ν corresponds to the unknown size of the state jump.

In the case of saccade detection, we try to detect an abrupt change of velocity in eye-in-head velocity on the horizontal and the vertical components concurrently.

Therefore, the state x corresponds to the eye velocity and the observations z are the measurements:

$$z = \begin{bmatrix} \dot{E}_h(0) & \dot{E}_V(0) \\ \dot{E}_h(1) & \dot{E}_v(1) \\ \vdots & \vdots \\ \dot{E}_h(k) & \dot{E}_v(k) \end{bmatrix} \tag{.4}$$

Additionally, we assumed that $x(k+1) \cong x(k)$. Thus the difference between two time indices comes either from measurement noise or from a "jump" (occurence of a saccade). Then, the matrices $\phi(k+1,k)$ and $H(k+1)$ of equations (.1) and (.2) are defined as:

$$\phi(k+1,k) = \begin{bmatrix} 1 & 0 \\ 0 & 1 \end{bmatrix} \tag{.5}$$

$$H(k+1) = \begin{bmatrix} 1 & 0 \\ 0 & 1 \end{bmatrix} \tag{.6}$$

Filter design: Kalman filter

As previously mentioned, the basis of the detection algorithm is the comparison between two hypotheses: one with a jump (θ is a positive finite integer) and one without jump ($\theta = +\infty$). First a Kalman filter is implemented with the assumption that there is no jump ($\theta = +\infty$) to estimate the value of the state x at time $k+1$:

$$\hat{x}(k+1|k) = \phi(k+1,k) * \hat{x}(k|k) \tag{.7}$$

$$\hat{x}(k|k) = \hat{x}(k|k-1) + K(k) * \gamma(k) \tag{.8}$$

Here the Kalman filter is used as a one-step ahead predictor (.7) using the knowledge of the current state ($\hat{x}(k|k-1)$ in (.8)) corrected by an optimal gain ($K(k)$ in (.8)) times the residual ($\gamma(k)$ in (.8)).

The residual is defined as:

$$\gamma(k) = z(k) - H(k) * \hat{x}(k|k-1) \tag{.9}$$

The Kalman gain is computed using:

$$K(k) = P(k|k-1) * H'(k) * V^{-1}(k) \tag{.10}$$

In (.10), $P(k|k-1)$ is the current error covariance updated using:

$$P(k+1|k) = \phi(k+1,k) * P(k|k) * \phi'(k+1,k)$$

$$+\Gamma(k) * Q(k) * \Gamma'(k) \tag{.11}$$
$$P(k|k) = [I - K(k) * H(k)] * P(k|k-1) \tag{.12}$$

Finally, $V(k)$ in (.10) represents the innovation covariance and is updated accordingly to:

$$V(k) = H(k) * P(k|k-1) * H'(k) + R(k) \tag{.13}$$

Two partitions of the state: a normal case and a perturbed one

The next step is to divide the state $x(k)$, the observations $z(k)$, the state estimate $\hat{x}(k)$ and the innovation $\gamma(k)$ into two components: one corresponding to the unperturbed case (no saccade, $\delta_{\theta,k+1} = 0$) and one that corresponds only to the perturbation.

$$x(k) = x_1(k) + x_2(k) \tag{.14}$$
$$z(k) = z_1(k) + z_2(k) \tag{.15}$$
$$\hat{x}(k|k) = \hat{x}_1(k|k) + \hat{x}_2(k|k) \tag{.16}$$
$$\gamma(k) = \gamma_1(k) + \gamma_2(k) \tag{.17}$$

In the following two subsections, we developed the "straightforward computations" that lead to the definitions of $x_2(k)$, $z_2(k)$, $\hat{x}_2(k|k)$ and $\gamma_2(k)$ presented in (Willsky and Jones, 1974).

$x_2(k)$ and $z_2(k)$

If a fault is detected at time step $k = \theta$, we can write equation (.1) recursively from $k = \theta - 1$ to $k = \theta + 1$:

$$x(\theta) = \phi(\theta, \theta-1) * x(\theta-1) + \Gamma(\theta-1) * \omega(\theta-1) + \nu \tag{.18}$$
$$= x_1(\theta) + x_2(\theta) \tag{.19}$$
$$x(\theta+1) = \phi(\theta+1, \theta) * x(\theta) + \Gamma(\theta) * \omega(\theta) \tag{.20}$$
$$\begin{aligned} &= \phi(\theta+1, \theta) * \phi(\theta, \theta-1) * x(\theta-1) \\ &\quad + \phi(\theta+1, \theta) * \Gamma(\theta-1) * \omega(\theta-1) + \Gamma(\theta) * \omega(\theta) \\ &\quad + \phi(\theta+1, \theta) * \nu \end{aligned} \tag{.21}$$
$$x(\theta+2) = \phi(\theta+2, \theta+1) * x(\theta+1) + \Gamma(\theta+1) * \omega(\theta+1) \tag{.22}$$

$\phi(k, \theta)$ has the following properties:

$$\phi(k, \theta) = 0 \ \ \forall \ \ k < \theta \tag{.23}$$
$$\phi(\theta, \theta) = I \tag{.24}$$

Using (.18)-(.24), we can generalize the expression of $\phi(k, \theta)$:

$$\phi(k+1, \theta) = \phi(k+1, k) * \phi(k, \theta) \tag{.25}$$

From the definition of $x_2(k)$:

$$x_2(k) = 0 \ \ \forall \ \ k < \theta \tag{.26}$$

In equation (.21), the term that corresponds to the jump can be written as:

$$x_2(\theta + 1) = \phi(\theta + 1, \theta) * \nu \tag{.27}$$

Using (.23), (.24) and (.25), we can generalize:

$$x_2(k) = \phi(k, \theta) * \nu \tag{.28}$$

Then, using (.28) we find $z_2(k)$:

$$z_2(k) = H(k) * \phi(k, \theta) * \nu \tag{.29}$$

$\hat{x}_2(k|k)$ and $\gamma_2(k)$

The same reasoning can be applied to find $\hat{x}_2(k|k)$:

$$\hat{x}(k+1|k+1) = \hat{x}(k+1|k) + K(k+1) * \gamma(k+1) \tag{.30}$$

Injecting (.9) in (.30):

$$\begin{aligned} \hat{x}(k+1|k+1) &= \hat{x}(k+1|k) + K(k+1) * z(k+1) \\ &\quad -K(k+1) * H(k+1) * \hat{x}(k+1|k) \qquad (.31) \\ \hat{x}(k+1|k+1) &= [I - K(k+1) * H(k+1)] * \hat{x}(k+1|k) \\ &\quad +K(k+1) * z(k+1) \qquad (.32) \end{aligned}$$

Combining (.32) and (.7):

$$\begin{aligned} \hat{x}(k+1|k+1) &= [I - K(k+1) * H(k+1)] * \phi(k+1, k) * \hat{x}(k|k) \\ &\quad +K(k+1) * z(k+1) \qquad (.33) \end{aligned}$$

Using (.15) and (.16), equation (.33) can be divided in a term corresponding to an estimate of the state during normal behavior (Eq. (.34)) and a term corresponding to a state estimate during a possible jump (Eq. (.35)):

$$\begin{aligned} \hat{x}_1(k+1|k+1) &= [I - K(k+1) * H(k+1)] * \phi(k+1, k) * \hat{x}_1(k|k) \\ &\quad +K(k+1) * z_1(k+1) \qquad (.34) \\ \hat{x}_2(k+1|k+1) &= [I - K(k+1) * H(k+1)] * \phi(k+1, k) * \hat{x}_2(k|k) \\ &\quad +K(k+1) * z_2(k+1) \qquad (.35) \end{aligned}$$

Injecting (.29) in (.35):

$$\begin{aligned} \hat{x}_2(k+1|k+1) &= [I - K(k+1) * H(k+1)] * \phi(k+1, k) * \hat{x}_2(k|k) \\ &\quad +K(k+1) * H(k+1) * \phi(k+1, \theta) * \nu \qquad (.36) \end{aligned}$$

Equation (.36) can be written as:

$$\hat{x}_2(k+1|k+1) = a(k+1,k) * \hat{x}_2(k|k) + b(k+1,\theta) * \nu \tag{.37}$$

With:

$$a(k+1,k) = [I - K(k+1) * H(k+1)] * \phi(k+1,k) \tag{.38}$$
$$b(k+1,\theta) = K(k+1) * H(k+1) * \phi(k+1,\theta) \tag{.39}$$

Recursively:

$$\begin{aligned}\hat{x}_2(k+2|k+2) &= a(k+2,k+1) * \hat{x}_2(k+1|k+1) + b(k+2,\theta) * \nu && (.40)\\ &= a(k+2,k+1) * [a(k+1,k) * \hat{x}_2(k|k) + b(k+1,\theta) * \nu] \\ &\quad + b(k+2,\theta) * \nu && (.41)\\ &= a(k+2,k+1) * a(k+1,k) * \hat{x}_2(k|k) \\ &\quad + a(k+2,k+1) * b(k+1,\theta) * \nu + b(k+2,\theta) * \nu && (.42)\end{aligned}$$

From (.42), we generalize:

$$\begin{aligned}\Psi(k,\theta) &= \prod_{r=\theta}^{k-1} a(r+1,r) && (.43)\\ &= a(k,k-1) * \Psi(k-1,\theta) && (.44)\\ \Psi(\theta,\theta) &= I && (.45)\\ \Psi(k,\theta) &= 0 \qquad \forall\, k < \theta && (.46)\end{aligned}$$

Using (.44), we define $\Upsilon(k,\theta)$:

$$\begin{aligned}\Upsilon(k,\theta) &= \sum_{j=\theta}^{k} \Psi(k,j) * b(j,\theta) && (.47)\\ \Upsilon(k,\theta) &= 0 \qquad \forall\, k < \theta && (.48)\end{aligned}$$

Recalling that

$$\begin{aligned}\hat{x}_2(k|k) &= 0 \qquad \forall\, k < \theta && (.49)\\ \hat{x}_2(\theta|\theta) &= K(\theta) * H(\theta) * \nu && (.50)\end{aligned}$$

The solution of (.40) can be written as:

$$\hat{x}_2(k|k) = \Upsilon(k,\theta) * \nu \tag{.51}$$

With:

$$\Psi(k,\theta) = \overbrace{[I - K(k) * H(k)] * \phi(k,k-1)}^{a(k,k-1)} * \Psi(k-1,\theta) \tag{.52}$$

$$\Upsilon(k,\theta) = \sum_{j=\theta}^{k} \Psi(k,j) * \underbrace{K(j) * H(j) * \phi(j,\theta)}_{b(j,\theta)} \tag{.53}$$

Using equations (.8), (.9), (.17) and (.29), we can write $\gamma_2(k)$:

$$\gamma(k) = z(k) - H(k) * \hat{x}(k|k-1) \tag{.54}$$
$$\hat{x}(k|k-1) = \phi(k,k-1) * \hat{x}(k-1|k-1) \tag{.55}$$
$$\gamma_2(k) = z_2(k) - H(k) * \phi(k,k-1) * \hat{x}_2(k-1|k-1) \tag{.56}$$
$$= H(k) * \phi(k,\theta) * \nu$$
$$-H(k) * \phi(k,k-1) * \Upsilon(k-1,\theta) * \nu \tag{.57}$$
$$= H(k) * [\phi(k,\theta) - \phi(k,k-1) * \Upsilon(k-1,\theta)] * \nu \tag{.58}$$

Finally:

$$\gamma_2(k) = G(k,\theta) * \nu \tag{.59}$$

With:

$$G(k,\theta) = H(k) * [\phi(k,\theta) - \phi(k,k-1) * \Upsilon(k-1,\theta)] \tag{.60}$$

Generalized likelihood ratio

The partition of the state in two parts, a part that corresponds to the normal situation and a part that represents an abrupt state(s) jump permit the definition, as expressed in (Willsky and Jones, 1974), of two hypothesis:

$$H_0 : \quad \gamma(k) = \gamma_1(k) \tag{.61}$$
$$H_1 : \quad \gamma(k) = \gamma_1(k) + G(k,\theta) * \nu \tag{.62}$$

To express how the generalized likelihood ratio is computed, I developed the equations as presented in (Trees, 1968).

The generalized likelihood ratio test is based on a bayes criterion. It combines the likelihood ratio test and the maximum likelihood estimates. The next subsection demonstrates the likelihood ratio test. Then the maximum likelihood estimates is presented to finally lead to the generalized likelihood ratio test (GLR).

Likelihood ratio test

The test compares the "a priori probabilities" of the two hypotheses H_0 and H_1. To evaluate which hypothesis is more likely, the following cost function is computed:

$$\begin{aligned} J = {} & C_{0,0} * P_0 * Prob(H_0|H_0\ is\ true) \\ & + C_{1,0} * P_0 * Prob(H_0|H_1\ is\ true) \\ & + C_{0,1} * P_1 * Prob(H_1|H_0\ is\ true) \\ & + C_{1,1} * P_1 * Prob(H_1|H_1\ is\ true) \end{aligned} \tag{.63}$$

To compute the different probabilities of equation (.63), the observation space partition defined by equations (.15) is used. When an observation corresponds

to a perturbed situation, it belongs to Z_2, otherwise it belongs to Z_1. If D is the current observed state, equation (.63) can be written as:

$$\begin{aligned} J = C_{0,0} * P_0 * \int_{Z_1} p_{d|H_0}(D|H_0)\, dD \\ + C_{1,0} * P_0 * \int_{Z_2} p_{d|H_0}(D|H_0)\, dD \\ + C_{0,1} * P_1 * \int_{Z_1} p_{d|H_1}(D|H_1)\, dD \\ + C_{1,1} * P_1 * \int_{Z_2} p_{d|H_1}(D|H_1)\, dD \end{aligned} \tag{.64}$$

As a supplementary assumption, the cost of a correct decision is postulated to be smaller than the cost of a wrong decision:

$$C_{0,0} < C_{1,0} \tag{.65}$$

$$C_{1,1} < C_{0,1} \tag{.66}$$

Because $Z = Z_1 + Z_2$, equation (.64) can be written as:

$$\begin{aligned} J = C_{0,0} * P_0 * \int_{Z_1} p_{d|H_0}(D|H_0)\, dD \\ + C_{1,0} * P_0 * \int_{Z - Z_1} p_{d|H_0}(D|H_0)\, dD \\ + C_{0,1} * P_1 * \int_{Z_1} p_{d|H_1}(D|H_1)\, dD \\ + C_{1,1} * P_1 * \int_{Z - Z_1} p_{d|H_1}(D|H_1)\, dD \end{aligned} \tag{.67}$$

Because the current observation D is a part of the observations space:

$$\int_Z p_{d|H_0}(D|H_0)\, dD = \int_Z p_{d|H_1}(D|H_1)\, dD = 1 \tag{.68}$$

Using (.68), equation (.67) can be simplified:

$$\begin{aligned} J &= C_{1,0} * P_0 + C_{1,1} * P_1 \\ &\quad + (C_{0,0} - C_{1,0}) * P_0 * \int_{Z_1} p_{d|H_0}(D|H_0)\, dD \\ &\quad + (C_{0,1} - C_{1,1}) * P_1 * \int_{Z_1} p_{d|H_1}(D|H_1)\, dD \end{aligned} \tag{.69}$$

$$\begin{aligned} &= C_{1,0} * P_0 + C_{1,1} * P_1 \\ &\quad + \int_{Z_1} [(C_{0,1} - C_{1,1}) * P_1 * p_{d|H_1}(D|H_1) \\ &\quad - (C_{1,0} - C_{0,0}) * P_0 * p_{d|H_0}(D|H_0)]\, dD \end{aligned} \tag{.70}$$

Equation (.70) has three terms: the two first ones correspond to the fixed cost. The third term represents the cost controlled by the current observation D

if we assigned it to Z_1. Because we assume that a wrong decision costs more than a right one (see equations (.65) and (.66)), the integral of equation (.70) is the difference between two positive terms. Thus, if the second term is bigger (smaller) than the first one, the current observation is more likely included in Z_1 (Z_2). With those properties, we can define the boundaries of the two regions with the following statement:

If:

$$(C_{0,1} - C_{1,1}) * P_1 * p_{d|H_1}(D|H_1) \leq (C_{1,0} - C_{0,0}) * P_0 * p_{d|H_0}(D|H_0) \quad (.71)$$

Assign the current observation to the space partition Z_1 (H_0 is true, no jump), otherwise assign it to Z_2 (H_1 is true, occurence of a jump). Finally, equation (.71) can be written as a ratio:

$$\frac{(C_{1,0} - C_{0,0}) * P_0}{(C_{0,1} - C_{1,1}) * P_1} \underset{H_1}{\overset{H_0}{\gtrless}} \frac{p_{d|H_1}(D|H_1)}{p_{d|H_0}(D|H_0)} \quad (.72)$$

The right part of equation (.72) is called the likelihood ratio:

$$\Lambda(D) \equiv \frac{p_{d|H_1}(D|H_1)}{p_{d|H_0}(D|H_0)} \quad (.73)$$

It is the ratio of two random variables and therefore it is a random variable. The left member of equation (.72) is the threshold of the test:

$$\eta \equiv \frac{(C_{1,0} - C_{0,0}) * P_0}{(C_{0,1} - C_{1,1}) * P_1} \quad (.74)$$

Using a Bayes criterion, we define the likelihood ratio test as:

$$\Lambda(D) \underset{H_1}{\overset{H_0}{\lessgtr}} \eta \quad (.75)$$

Maximum likelihood estimates and generalized likelihood ratio

An important assumption of the likelihood ratio test is the prior knowledge of the probability distribution of the two hypotheses H_0 and H_1 that allows the computation of $p_{d|H_1}(D|H_1)$ and $p_{d|H_0}(D|H_0)$.

Practically, we do not know in advance the amplitude of the jump (in our case, the amplitude of the saccade). To eliminate this problem, (Trees, 1968) proposed to used the maximum likelihood estimates of the jump. As previously mentioned (equation (.72)), $p_{d|H_1}(D|H_1)$ (and $p_{d|H_0}(D|H_0)$) gives the likelihood that a jump occured (did not occur) at the evaluated instant k. Assuming that H_1 is true, we can define the maximum likelihood estimates as:

$$\hat{\theta}(k);\, \hat{\gamma}(k) = arg\, max_{\tilde{\theta},\, \tilde{\nu}}\, p_{\gamma|H_1}(\Gamma|H_1,\, \theta = \tilde{\theta},\, \nu = \tilde{\nu}) \quad (.76)$$

In (.76), Γ represents the span of all the γ for the instants between $(1 \ldots k)$. Thus, (.76) can be written using a simplified notation:

$$\hat{\theta}(k);\, \hat{\gamma}(k) = arg\, max_{\tilde{\theta},\, \tilde{\nu}}\, p(\gamma(1), \ldots, \gamma(k)|H_1,\, \theta = \tilde{\theta},\, \nu = \tilde{\nu}) \tag{.77}$$

Once $\hat{\theta}(k)$ and $\hat{\gamma}(k)$ are computed, we can inject them into the likelihood ratio of equation (.73). Using the simplified notations of (.77), the generalized likelihood ratio (GLR) is written as:

$$\Lambda(k) = \frac{p(\gamma(1), \ldots, \gamma(k)|H_1,\, \theta = \hat{\theta}(k),\, \nu = \hat{\nu}(k))}{p(\gamma(1), \ldots, \gamma(k)|H_0)} \tag{.78}$$

By comparing the result of (.78) to a threshold value, we can decide which hypothesis (H_0 or H_1) is more likely. This test is called the generalized likelihood ratio test:

$$\Lambda(D) \underset{H_1}{\overset{H_0}{\lessgtr}} \eta \tag{.79}$$

From the Kalman filter equations, we know that the innovation γ is a white noise sequence with a covariance $V(k)$ defined in equation (.13). Therefore, the probability distribution of the innovations at instant k can be written as:

$$p(\gamma(k)|H_1) = \frac{1}{2\pi * V(k)^{0.5}} * e^{-\frac{1}{2}\gamma^T(k) * V(k)^{-1} * \gamma(k)} \tag{.80}$$

$$p(\gamma(k)|H_0) = \frac{1}{2\pi * V(k)^{0.5}} * e^{-\frac{1}{2}(\gamma(k) - G(k,\hat{\theta}) * \hat{\nu}(k))^T * V(k)^{-1} * (\gamma(k) - G(k,\hat{\theta}) * \hat{\nu}(k))} \tag{.81}$$

Injecting (.80) and (.81) into (.78) and taking its logarithm, the GLR can be written as:

$$\begin{aligned} 2 * ln(\Lambda(k)) = & \sum_{j=1}^{j=k} \gamma^T(j) * V(j)^{-1} * \gamma(j) \\ & - \sum_{j=1}^{j=k} P^T(j) * V(j)^{-1} * P(j) \end{aligned} \tag{.82}$$

$$P(j, \hat{\theta}, \hat{\nu}) = (\gamma(j) - G(j, \hat{\theta}) * \hat{\nu}(k)) \tag{.83}$$

Developing (.82):

$$\begin{aligned} 2 * ln(\Lambda(k)) = & \sum_{j=1}^{j=k} \gamma^T(j) * V(j)^{-1} * \gamma(j) \\ & - \sum_{j=1}^{j=k} \gamma^T(j) * V(j)^{-1} * \gamma(j) \\ & + \sum_{j=1}^{j=k} \gamma^T(j) * V(j)^{-1} * [G(j, \hat{\theta}) * \hat{\nu}(k)] \end{aligned}$$

$$
\begin{aligned}
&+\sum_{j=1}^{j=k}[G(j,\hat{\theta})*\hat{\nu}(k)]^T*V(j)^{-1}*\gamma(j)\\
&-\sum_{j=1}^{j=k}[G(j,\hat{\theta})*\hat{\nu}(k)]^T*V(j)^{-1}*[G(j,\hat{\theta})*\hat{\nu}(k)] \qquad (.84)\\
=&\sum_{j=1}^{j=k}\gamma^T(j)*V(j)^{-1}*[G(j,\hat{\theta})*\hat{\nu}(k)]\\
&+\sum_{j=1}^{j=k}[G(j,\hat{\theta})*\hat{\nu}(k)]^T*V(j)^{-1}*\gamma(j)\\
&-\sum_{j=1}^{j=k}[G(j,\hat{\theta})*\hat{\nu}(k)]^T*V(j)^{-1}*[G(j,\hat{\theta})*\hat{\nu}(k)] \qquad (.85)
\end{aligned}
$$

Equation (.85) can be simplified because the term "$\gamma^T(j)*V(j)^{-1}[G(j,\hat{\theta})*\hat{\nu}(k)]$" is a scalar and the covariance matrix is symetric ($V^{-T}=V^{-1}$):

$$
\begin{aligned}
2*ln(\Lambda(k)) = 2*&\sum_{j=1}^{j=k}[G(j,\hat{\theta})*\hat{\nu}(k)]^T*V(j)^{-1}*\gamma(j)\\
&-\sum_{j=1}^{j=k}[G(j,\hat{\theta})*\hat{\nu}(k)]^T*V(j)^{-1}[G(j,\hat{\theta})*\hat{\nu}(k)] \qquad (.86)
\end{aligned}
$$

Using (.86), we can compute that the maximum likelihood estimate of ν, $\hat{\nu}$. To do so we first compute the partial derivative of (.86) with respect to ν. Because the derivative is a linear operator, we can simplify the notations by computing one term of the derivative at instant j:

$$
\begin{aligned}
2*\frac{\partial[ln(\Lambda(j))]}{\partial\nu(j)} &= 2*\frac{\partial[\nu(j)^T*G(j,\hat{\theta})^T*V(j)^{-1}*\gamma(j)]}{\partial\nu(j)}\\
&\quad-\frac{\partial[\nu(j)^T*G(j,\hat{\theta})^T*V(j)^{-1}*G(j,\hat{\theta})*\nu(j)]}{\partial\nu(j)} \qquad (.87)\\
&= 2*\gamma(j)^T*V(j)^{-T}*G(j,\hat{\theta})\\
&\quad-2*\nu(j)^T*G(j,\hat{\theta})^T*V(j)^{-1}*G(j,\hat{\theta}) \qquad (.88)
\end{aligned}
$$

Then we can equate (.88) to zero to find the maximum likelihood estimate of $\nu(j)$, $\hat{\nu}(j)$:

$$
\hat{\nu}(j) = \left(G(j,\hat{\theta})^T*V(j)^{-1}*G(j,\hat{\theta})\right)^{-1}\left(G(j,\hat{\theta})^T*V(j)^{-1}*\gamma(j)\right) \qquad (.89)
$$

Finally, we can write the GLR test as expressed by equation (32) in (Willsky and Jones, 1974):

$$L(k,\hat{\theta}) \underset{H_1}{\overset{H_0}{\lessgtr}} 2 * ln(\eta) \tag{.90}$$

$$L(k,\hat{\theta}) = max_{\tilde{\theta}} \left(d^T(k,\tilde{\theta}) * C^{-1}(k,\tilde{\theta}) * d(k,\tilde{\theta}) \right) \tag{.91}$$

$$d(k,\tilde{\theta}) = \sum_{j=1}^{j=k} G(j,\hat{\theta})^T * V(j)^{-1} * \gamma(j) \tag{.92}$$

$$C(k,\tilde{\theta}) = G(j,\hat{\theta})^T * V(j)^{-1} * G(j,\hat{\theta}) \tag{.93}$$

The computation of (.90) implies the storage of a growing number of parameters because all the parameters from the previous iteration have to be stored. Willsky and Jones (1974, 1976) gives a procedure to limit the computations to a window of the last M instants. I do not go into the details for this procedure since it is straightforward.

Basseville, M. and Nikiforov, I. V. (1993). *Detection of abrupt changes: theory and application*. Prentice-Hall, Inc., Upper Saddle River, NJ, USA.

Trees, H. L. V. (1968). *Detection, Estimation, and Modulation Theory, Part I, Detection, Estimation, and Linear Modulation Theory*. John Wiley and Sons, Inc.

Willsky, A. and Jones, H. (1976). A generalized likelihood ratio approach to the detection and estimation of jumps in linear systems. 21(1):108–112.

Willsky, A. S. and Jones, H. L. (1974). A generalized likelihood ratio approach to state estimation in linear systems subjects to abrupt changes. In *Proc. IEEE Conference on Decision and Control including the 13th Symposium on Adaptive Processes*, volume 13, pages 846–853.

B Compensation indexes: Mathematical developments

In this appendix, we present the complete mathematical developments underlying the computation of the compensation indexes presented in part II.

We started with the first equation of the compensation. This equation states that the position error at the end of a saccade (PE) was a function of the smooth gaze displacement that occurred during the latency (SGD) and a compensation index (CI). CI corresponds to the amount of displacement that the compensatory mechanism has taken into account during the programming of the saccade.

$$PE = SGD - CI * SGD \tag{.94}$$

From equation (.94), one can isolate the compensation index CI.

$$CI = \frac{SGD - PE}{SGD} \tag{.95}$$

The first stage was to decompose the SGD into its head (SHD) and eye (SED) components.

$$SGD = SED + SHD \tag{.96}$$

The same principle as the one proposed in equation (.94) was used here for the computation of the partial compensation for the eye displacement (CI^E) and the partial compensation for the head displacement (CI^H) during the saccade latency.

$$PE = SGD - CI^E * SED - CI^H * SHD \tag{.97}$$

The purpose of the following developments was to obtain an expression that allows the comparison of the partial compensation indexes (CI^E and CI^H) with the global one (CI).

To begin, we defined the eye contribution (EC) as

$$EC = \frac{SED}{SGD} \tag{.98}$$

And the head contribution as

$$HC = \frac{SHD}{SGD} \tag{.99}$$

From equations (.98) and (.99), we can write:

$$SED = EC * SGD \tag{.100}$$
$$SHD = HC * SGD \tag{.101}$$
$$HC = 1 - EC \tag{.102}$$
$$SHD = (1 - EC) * SGD \tag{.103}$$

Using equations (.100) and (.103) into equation (.97):

$$PE = SGD - CI^{\mathrm{E}} * EC * SGD - CI^{\mathrm{H}} * (1 - EC) * SGD \tag{.104}$$

As expected, from equation (.104), the global compensation index CI can be expressed as a function of the partial compensation index for the eye ($\mathrm{CI^E}$), the partial compensation index for the head ($\mathrm{CI^H}$) and the eye contribution (EC):

$$\frac{SGD - PE}{SGD} = CI = CI^{\mathrm{E}} * EC + CI^{\mathrm{H}} * (1 - EC) \tag{.105}$$
$$CI = (CI^{\mathrm{E}} - CI^{\mathrm{H}}) * EC + CI^{\mathrm{H}} \tag{.106}$$

In a second stage for the development of the compensation index, we divided SED into a pursuit (SPD) and a VOR component:

$$SED = SPD + VOR \tag{.107}$$

As in (.97), this division allowed us to include two new compensation indexes, one for the VOR signal ($\mathrm{CI^V}$) and one for the pursuit component ($\mathrm{CI^P}$).

$$PE = SGD - CI^{\mathrm{P}} * SPD - CI^{\mathrm{V}} * VOR - CI^{\mathrm{H}} * SHD \tag{.108}$$

Similar to the mathematical developments leading to equation (.105), the purpose of the following series of expressions was to find an expression of the global compensation index as a function of the partial compensation indexes. Using equation (.107) into equation (.108), we obtained:

$$PE{=}SGD - CI^{\mathrm{P}} * (SED - VOR) - CI^{\mathrm{V}} * VOR - CI^{\mathrm{H}} * SHD \tag{.109}$$
$$PE{=}SGD - CI^{\mathrm{P}} * SED + CI^{\mathrm{P}} * VOR - CI^{\mathrm{V}} * VOR - CI^{\mathrm{H}} * SHD \tag{.110}$$
$$PE{=}SGD - CI^{\mathrm{P}} * SED - (CI^{\mathrm{V}} - CI^{\mathrm{P}}) * VOR - CI^{\mathrm{H}} * SHD \tag{.111}$$

As explained in the main text (Method section, compensation paragraph, 105), the VOR signal was approximated by:

$$VOR = -g(f_H) * SHD \tag{.112}$$

Using equation (.112), equation (.111) can be written as:

$$PE = SGD - CI^{\mathrm{P}} * SED - (CI^{\mathrm{P}} - CI^{\mathrm{V}}) * g(f_H) * SHD - CI^{\mathrm{H}} * SHD \tag{.113}$$

Using equations (.100) and (.103) into equation (.113):

$$PE{=}SGD - CI^{\mathrm{P}} * EC * SGD - (CI^{\mathrm{P}} - CI^{\mathrm{V}}) * g(f_H) * (1 - EC) * SGD - CI^{\mathrm{H}} * (1 - EC) * SGD \tag{.114}$$

$$PE{=}SGD - \left[CI^{\mathrm{P}} - (CI^{\mathrm{P}} - CI^{\mathrm{V}}) * g(f_H) - CI^{\mathrm{H}}\right] * EC * SGD - \left[(CI^{\mathrm{P}} - CI^{\mathrm{V}}) * g(f_H) + CI^{\mathrm{H}}\right] * SGD \quad (.115)$$

From equation (.115), we isolated the global compensation index (CI) as a function of the three partial compensation index ($\mathrm{CI^V}$, $\mathrm{CI^P}$ and $\mathrm{CI^H}$), the gain of the VOR ($g(f_H)$) and the eye contribution (EC):

$$\begin{aligned} \frac{SGD - PE}{SGD} &= CI \\ &= \left[CI^{\mathrm{P}} - (CI^{\mathrm{P}} - CI^{\mathrm{V}}) * g(f_H) - CI^{\mathrm{H}}\right] * EC \\ &\quad - \left[(CI^{\mathrm{P}} - CI^{\mathrm{V}}) * g(f_H) + CI^{\mathrm{H}}\right] \end{aligned} \quad (.116)$$

Equation (.116) corresponds to equation (13) in the main text.

C Mathematical description of the gaze saccade model

Summary. This document starts with a description of the model equations. First, we define the notations used. Then, we detail the equations of each subpart of the model. After, we list the numerical values of the parameters used in the simulations. Because the justification for the connectivity used in the model is made in the main text, we focus here on a detailed description of the model equations.

Finally, in the last section, we show the effect of a temporal asynchrony between the inputs of the model (head and gaze goals) that can be one source of the experimentally observed variability of the head and the gaze trajectories with the same goals.

Notations

We used the following notations in the current document:

β	Scalar
$\mathbf{A}$	Vector
$\mathbf{A}_H$	Horizontal component of vector A
$\mathbf{A}_V$	Vertical component of vector A

The amplitude of a vector is defined by:

$$\|\mathbf{A}\|_2 = \sqrt{\mathbf{A}_H^2 + \mathbf{A}_V^2}$$

When a vector is multiplied by a scalar, each component is multiplied by the same scalar:

$$\beta * \mathbf{A} = \beta * \mathbf{A}_H + \beta * \mathbf{A}_V$$

The Laplace operator is represented by s and corresponds to the temporal derivative:

$$\mathsf{s}X = \frac{d(X)}{dt}$$

The saturation of a signal X between a lower boundary L and an upper boundary U is defined as:

$$sat\,(X)_L^U = L \quad if\ X \leq L$$
$$sat\,(X)_L^U = U \quad if\ X \geq U$$
$$sat\,(X)_L^U = X \quad if\ L < X < U$$

Mathematical description of the model

The brainstem

Panel A of figure .1 represents the simplified connectivity of the brainstem used in the model. Note that although this model is one-sided, care was taken to keep track of the different roles played by cells on the sides ipsilateral and contralateral to the movement (cf. figure 7 of (Quaia et al., 1999)). The neural circuitry includes four populations of neurons present in the brainstem: the omnipause neurons (OPNs), the ipsilateral excitatory burst neurons (EBN_i), the contralateral inhibitory burst neurons (IBN_c) and neurons in the contralateral central mesencephalic reticular formation ($cMRF_c$). In our simplified, lumped, one-sided model, each population of neurons is represented by an equivalent single cell. Moreover, the connections between those populations are highly simplified compared to the actual connections. Nevertheless, the behavior of our modeled brainstem is functionally sufficient for the purpose of this model: the control of head-unrestrained saccades.

King et al. (1980); Langer and Kaneko (1984) and Fuchs et al. (1985) have studied the afferent connections to the OPNs to understand which structures are responsible for the release of the OPNs' activity and therefore could trigger a saccade or maintain their activity low. Following their observations, our model of the OPNs includes two of the observed inhibitory inputs: one from the caudal part of the superior colliculus (SC_c) (Langer and Kaneko, 1984; Fuchs et al., 1985; Scudder et al., 1996) and one from $cMRF_c$ (Langer and Kaneko, 1984). The collicular input can initialize the inhibition of the OPNs (thus it can trigger a gaze saccade), whereas the $cMRF_c$ sustains, through the OPNs-$cMRF_c$-OPNs loop, the inhibition on the OPNs during the execution of the saccade. In the model, the OPNs project to the EBN_i, the IBN_c, the spinal cord (Kaneko and Fuchs, 1982) and the cMRF (Scudder et al., 1996; Cromer and Waitzman, 2006; Graf and Ugolini, 2006; Horn, 2006).

The modeled $cMRF_c$ has two inputs: one inhibition from the OPNs (see (Scudder et al., 1996; Cromer and Waitzman, 2006; Graf and Ugolini, 2006; Horn, 2006)) and one from the contralateral inhibitory burst neuron (IBN_c) (Fuchs et al., 1985). As previously mentioned, the $cMRF_c$ inhibits the OPNs (Langer and Kaneko, 1984).

The ipsilateral excitatory burst neurons (EBN_i) in the model receive an inhibition from the OPNs (Kaneko and Fuchs, 1982) and send the eye saccadic drive (see Fig. .1, panel A) to the ocular motoneurons through a saturation function. When the OPNs are active, the EBN_i does not discharge. The other

modeled population of medium lead burst neurons included in the model, the contralateral inhibitory burst neurons (IBN_c), have two afferent projections: an inhibition from the OPNs (Kaneko and Fuchs, 1982) and an excitation from the cerebellum (the choke signal). This excitatory signal corresponds to a scalar signal in our simplified lumped, one-sided model although it comes from a continuous spread of activity through the fastigial oculomotor region of the cerebellum as in the model of (Lefèvre et al., 1998; Quaia et al., 1999). IBN_c projects to the EBN_i (Fuchs et al., 1985; Strassman et al., 1986; Ramat et al., 2007) and to the $cMRF_c$ (Ramat et al., 2007).

When a saccade is triggered either by the SC or the cerebellum, the OPNs' activity decreases, so the EBN_i and the $cMRF_c$ discharge. During the movement, the EBN_i sends the eye saccadic input to the eye motoneurons, while the $cMRF_c$ sustains the inhibition on the OPNs. At the end of a saccade, the choke signal from the cerebellum turns on the IBN_c. The IBN_c gates off the $cMRF_c$, which thereby desinhibits the OPNs. Then, the IBN_c inhibits the EBN_i to slow down the movement. Because our simplified model of the OPN neuron discharges when there is no inhibitory inputs, there is an increase of the OPNs' activity following the opening of the OPN-$cMRF_c$-OPN loop. Thus the EBN_i stops discharging and the saccade ends.

OPNs

The model of omnipause neurons (OPNs) has three inhibitory inputs: one from the cerebellum, one from superior colliculus (SC) and one from the contralateral central mesencephalic reticular formation ($cMRF_c$). The activity of the OPN unit was modeled as:

$$\tau_{OPN}\frac{d(OPN)}{dt} = (1 - INH) - OPN \tag{.117}$$

With INH (inhibition signal) computed according to:

$$\begin{aligned} INH = 1 \ \text{ if } \ (cMRF_c == 1)\ OR\ (\|\mathbf{\Delta G}\|_2 > thr), \\ \text{otherwise } \ INH = 0 \end{aligned} \tag{.118}$$

In eq. (.118), $\mathbf{\Delta G}$ corresponds to the desired gaze displacement at the input of SC. τ_{OPN} corresponds to the time constant of the OPN and thr corresponds to the boundary of the fixation zone.

$cMRF_c$

The model of contralateral central mesencephalic reticular formation ($cMRF_c$) has two inputs: one from the OPN and one from the contralateral inhibitory burst neuron (IBN_c). Its activity was modeled as:

$$\tau_{cMRF}\frac{d(cMRF_c)}{dt} = I_{cMRF} - cMRF_c \tag{.119}$$

$$\begin{aligned} I_{cMRF} = 1 \qquad & \text{if } \ (OPN < 1)\ OR\ (IBN_c > 0), \\ & \text{otherwise } \ I_{cMRF} = 0 \end{aligned} \tag{.120}$$

τ_{cMRF} corresponds to the time constant of the neuron.

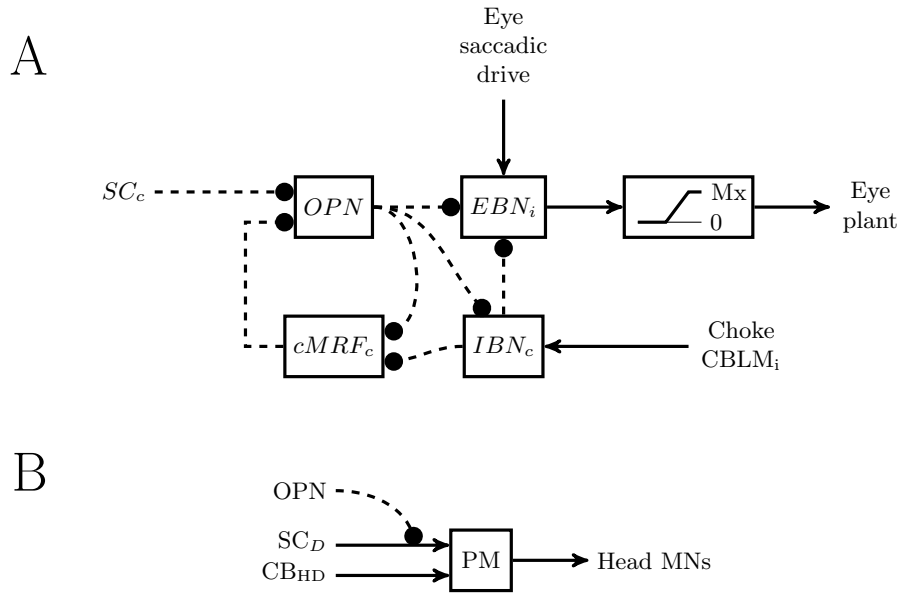

Fig. .1: Brainstem and spinal cord models. Panel A: Brainstem structure in the model. The OPN sends an inhibitory signal to the ipsilateral excitatory burst neuron (EBN_i), the contralateral central mesencephalic reticular formation ($cMRF_c$) and the contralateral inhibitory neuron (IBN_c). An onset of activity in the caudal part of the Superior Colliculus (SC_c) temporarily inhibits the OPN and hence triggers a gaze saccade. Therefore, the EBN_i is no longer suppressed and sends the eye saccadic drive to the eye plant through a saturation function. The OPN-$cMRF_c$-OPN loop ensured that during a saccade the OPN remains inactive. To end the saccade, the choke coming from the cerebellum stops the inhibition on the IBN_c. Then IBN_c inhibits the EBN activity and the $cMRF_c$, which desinhibits the OPN, which finally gates off the EBN_i. Panel B: Spinal cord structure in the model. A premotor neuron (PM) receives two inputs: one from the collicular drive (SC_D) and one from the independent-head controller (CB_{HD}). The input from the SC is gated by an inhibitory signal from the OPN in the brain stem. In this figure, arrows and solid lines correspond to excitatory signals and filled circles and dashed lines correspond to inhibitions.

IBN_c

The model of the contralateral inhibitory burst neuron (IBN_c) has two inputs: one from the OPN and a choke from the cerebellum ($CBLM_{choke}$). Its output was modeled as:

$$\tau_{IBN_c}\frac{d(IBN_c)}{dt} = (1 - OPN) * CBLM_{choke} - IBN_c \qquad (.121)$$

τ_{IBN_c} is the time constant of the IBN_c.

$\mathbf{EBN_i}$

The model of the excitatory burst neuron $\mathrm{EBN_i}$ has four inputs: one from the OPN, one from the $\mathrm{IBN_c}$, one from the collicular drive ($\mathbf{SC_D}$) and one from the gaze cerebellar drive ($\mathbf{CB_{GD}}$). Its activity was modeled as:

$$\tau_{EBN_i}\frac{d(\mathbf{EBN_i})}{dt}=(1-IBN_c)*(1-OPN)*(\alpha_{SC}*\mathbf{SC_D}+\beta_{CB_G}*\mathbf{CB_{GD}}) \\ -\mathbf{EBN_i} \qquad (.122)$$

In (.122), α_{SC} (β_{CB_G}) is the gain of the collicular (gaze cerebellar) drive at the input of the EBN and τ_{EBN_i} corresponds to the time constant of the neuron. α_{SC} and β_{CB_G} were tuned to mimic the experimental observations during head-unrestrained gaze saccades (Freedman and Sparks, 1997; Goossens and Van Opstal, 1997; Guitton et al., 1990). Therefore, we used a larger gain for the collicular discharge than for the cerebellar discharge to account for the importance of the superior colliculus at the initiation of head-unrestrained gaze saccades. Thus, as mentioned in the main text, with a collicular lesion, saccades remained accurate albeit with a lower velocity and a longer duration.

The activity of $\mathbf{EBN_i}$ passes through a dynamic saturation on the amplitude of the discharge. The lower bound of the saturation is equal to 0 while the upper bound corresponds to the maximum discharge of the neuron (defined by Mx in table 2). In the model, the gain of the eye plant is equal to 1, thus the maximum discharge Mx also corresponds to the eye maximum velocity. Therefore, we chose Mx equal to 600 spikes/s which implied a maximum eye velocity of 600 deg/s.

To simulate a functional oculomotor range of 50 deg, the output of the saturation is multiplied by an OMR gain: g_{OMR}. g_{OMR} is equal to 1 when the eye-in-head is inside the OMR. The gain linearly decreases to zero between 45 and 50 deg.

The spinal cord

Panel B of figure .1 represents the simplified connectivity of the spinal cord used in the model. PM corresponds to a premotor neuron in the spinal cord. It has three inputs: one from the OPN, one from the collicular drive ($\mathbf{SC_D}$) and one from the cerebellar head controller ($\mathbf{CB_{HD}}$). The activity of the premotor neuron was modeled as:

$$\tau_{PM}\frac{d(\mathbf{PM})}{dt}=\delta_{CB_H}*\mathbf{CB_{HD}}+(1-sat\,(OPN)_0^{\sigma_{OPN}})*\gamma_{SC}*\mathbf{SC_D} \\ -\mathbf{PM} \qquad (.123)$$

τ_{PM} corresponds to the time constant of the premotor neuron. δ_{CB_H} corresponds to the input weight of the cerebellar head drive and γ_{SC} corresponds to the input weight of the collicular drive. The OPN activity is saturated between $0 < \sigma_{OPN} < 1$. Thus, if the superior colliculus is stimulated and the OPN remains active (to create a low-current stimulation), a head movement is evoked without a gaze displacement, as observed by Corneil et al. (2002a,b). We arbitrarily set $\sigma_{OPN} = 0.8$ to let a significant drive (20% of the amplitude)

be sent to the head plant when the SC is stimulated while keeping the OPN activated. α_{SC} and β_{CB_G}, δ_{CB_H} and γ_{SC} were tuned to reproduce the observed behavior of the head during head-unrestrained gaze saccades (Freedman and Sparks, 1997; Goossens and Van Opstal, 1997; Guitton et al., 1990). Again, we used a larger gain for the collicular discharge to account for the important effect of SC during head-unrestrained gaze saccades on head trajectory.

The superior colliculus

The superior colliculus was divided in two subparts. A rostral part that corresponds to the previously called "fixation neurons" and a caudal part that corresponds to the combined effect of the burst and the buildup neurons. The superior colliculus has two inputs: one from superior cortical areas gives the desired gaze displacement ($\mathbf{\Delta G}$) and one corresponds to a facilitation signal from the cerebellum (FAC).

$$\mathbf{SC_D} = \mathbf{0} \quad if \quad \|\mathbf{\Delta G}\|_2 < thr \tag{.124}$$

$$\tau_{SC}\frac{d(\mathbf{SC_D})}{dt} = FAC * \mathbf{\Delta G} - \mathbf{SC_D} \quad if \quad \|\mathbf{\Delta G}\|_2 \geq thr \tag{.125}$$

Equation (.124) corresponds to the rostral part of SC while equation (.125) corresponds to the caudal part of SC. τ_{SC} corresponds to the time constant of the superior colliculus. As previously mentioned (see equation (.118)), thr corresponds to the boundary of the rostral zone.

The cerebellum

The description of the cerebellum model is divided in two sections. The first presents the equations of the gaze trajectory controller and the second shows the computation of the facilitation signal sent to SC and the choke sent to the IBN_c.

The gaze cerebellar controller

The gaze cerebellar controller has four inputs: the desired gaze displacement from higher cortical areas ($\mathbf{\Delta G}$), an efference copy of the eye velocity ($\dot{\mathbf{E}}^*$), an estimate of the current head velocity ($\dot{\mathbf{H}}^*$) and a projection from the OPN. The cerebellar gaze controller controls the gaze trajectory based on a vectorial computation of the gaze position error (**GPE**) evaluated from $\mathbf{\Delta G}$ and an estimate of the current gaze displacement ($\mathbf{\Delta G}^*$):

$$\mathbf{\Delta G}^* = \int \dot{\mathbf{H}}^*\, dt + \int \dot{\mathbf{E}}^*\, dt \tag{.126}$$

$$\mathbf{GPE} = \mathbf{\Delta G} - \mathbf{\Delta G}^* \tag{.127}$$

At the end of an eye-head saccade, $\mathbf{\Delta G}^*$ was reset to zero. **GPE** was then decomposed into two components: one along the direction parallel to $\mathbf{\Delta G}$ ($GPE_{\parallel}$) and one along the direction perpendicular to $\mathbf{\Delta G}$ ($GPE_{\perp}$):

$$GPE_{\parallel} = (1 - OPN) * \frac{\mathbf{GPE} \cdot \mathbf{\Delta G}}{\|\mathbf{\Delta G}\|_2} \tag{.128}$$

$$GPE_{\perp} = (1 - OPN) * \left\| \mathbf{GPE} - \left(GPE_{\parallel} * \frac{\mathbf{\Delta G}}{\|\mathbf{\Delta G}\|_2} \right) \right\|_2 \tag{.129}$$

$GPE_{\parallel}$ and $GPE_{\perp}$ were then used to compute the gaze cerebellar drive ($\mathbf{CB_{GD}}$):

$$CB_{G,\parallel} = \left(\frac{K_{I,\parallel}}{\mathsf{s} + K_F * OPN} + K_{P,\parallel} \right) * GPE_{\parallel} \tag{.130}$$

$$CB_{G,\perp} = \left(\frac{K_{I,\perp}}{\mathsf{s} + K_F * OPN} + K_{P,\perp} \right) * GPE_{\perp} \tag{.131}$$

$$\mathbf{1_{G,\perp}} = \frac{\left[\mathbf{GPE} - \left(GPE_{\parallel} * \frac{\mathbf{\Delta G}}{\|\mathbf{\Delta G}\|_2} \right) \right]}{\left\| \mathbf{GPE} - \left(GPE_{\parallel} * \frac{\mathbf{\Delta G}}{\|\mathbf{\Delta G}\|_2} \right) \right\|_2} \tag{.132}$$

$$\mathbf{CB_{GDi}} = CB_{G,\parallel} * \left(\frac{\mathbf{\Delta G}}{\|\mathbf{\Delta G}\|_2} \right) + CB_{G,\perp} * \mathbf{1_{G,\perp}} \tag{.133}$$

$$\tau_{CB_G} \frac{d(\mathbf{CB_{GD}})}{dt} = \mathbf{CB_{GDi}} - \mathbf{CB_{GD}} \tag{.134}$$

Equations (.130) and (.131) correspond to the cerebellar controller. It includes a forgetting factor (tuned by the parameter K_F). The controller is defined by two parameters: an integration gain K_I and a proportional gain K_P. Those two gains were tuned to reject the perturbations as previously observed by others (Tomlinson and Bahra, 1986a,b). When the OPN neuron discharges, the outputs of equations (.128) and (.129) were equal to zero. Therefore, $CB_{G,\parallel}$ and $CB_{G,\perp}$ decreased to zero with a time constant of K_F and the output of the gaze cerebellar drive decayed to zero at the end of a gaze saccade.

The facilitation signal and the cerebellar choke sent to IBN_i

The computations of the facilitation signal and the cerebellum choke were based on the difference (δG) between the amplitudes of the current gaze displacement and the desired gaze displacement and on the ratio between those amplitudes (εG):

$$\delta G = max\left[0\,,\ \|\mathbf{\Delta G}\|_2 - \|\mathbf{\Delta G}^*\|_2\right] \tag{.135}$$

$$\varepsilon G = sat\left(\frac{\|\mathbf{\Delta G}^*\|_2}{\|\mathbf{\Delta G}\|_2} \right)_0^1 \tag{.136}$$

$$C_1 = 1 \quad if \quad \delta G \leq \Gamma(\mathbf{\Delta G}), \quad otherwise \quad C_1 = 0 \tag{.137}$$

$$C_2 = 1 \quad if \quad \varepsilon G \geq thr_{REL}, \quad otherwise \quad C_2 = 0 \tag{.138}$$

$$C_3 = 1 \quad if \quad OPN \leq thr_{OPN}, \quad otherwise \quad C_3 = 0 \tag{.139}$$

Γ is a piecewise defined function of $\mathbf{\Delta G}$ used to tune the saccade accuracy by specifying when the OPN neuron must be reactivated as a function of the current error on the gaze displacement. The values in Γ were tuned once before the simulations and kept constant for all the simulations (typical values of the function are presented in table 2). To tune the value of Γ, we simulated a range

of amplitudes (see first column of table 2) and we adaptively tuned the values of Γ to obtain a magnitude of the error smaller than 0.01 deg for the amplitudes smaller than 10 deg and an error smaller than 10% of the saccade amplitude for the amplitudes bigger than 10 deg. The evolution of Γ as a function of the saccade amplitude ΔG is represented in Fig. .2. The three boolean relations (.137), (.138) and (.139) were used to compute the input of the facilitation (fac_{IN}) and the input of cerebellum choke (ch_{IN}):

$$ch_{IN}=1 \quad if \quad C_1 = 1 \;\; AND \;\; C_2 = 1 \;\; AND \;\; C_3 = 1, \quad otherwise \quad ch_{IN} = 0 \tag{.140}$$

$$fac_{IN}=1 - \varepsilon G \quad if \quad C_3 = 1, \quad otherwise \quad fac_{IN} = 0 \tag{.141}$$

$$\tau_{ch}\frac{d(CBLM_{choke})}{dt}=ch_{IN} - CBLM_{choke} \tag{.142}$$

$$\tau_{fac}\frac{d(FAC)}{dt}=fac_{IN} - FAC \tag{.143}$$

τ_{ch} corresponds to the time constant of the choke signal. τ_{fac} corresponds to the time constant of the facilitation signal.

The head cerebellar controller

The head cerebellar controller has two inputs: the desired head displacement from higher cortical areas ($\mathbf{\Delta H}$) and an estimate of the current head velocity ($\dot{\mathbf{H}}^*$). The cerebellar head controller controls the head trajectory based on a vectorial computation of the head position error (**HPE**) evaluated from $\mathbf{\Delta H}$ and an estimate of the current head displacement ($\mathbf{\Delta H}^*$).

$$\mathbf{\Delta H}^* = \int \dot{\mathbf{H}}^* \, dt \tag{.144}$$

$$\mathbf{HPE} = \mathbf{\Delta H} - \mathbf{\Delta H}^* \tag{.145}$$

At the end of a eye-head saccade, $\mathbf{\Delta H}^*$ was reset to zero. **HPE** was then decomposed in two components: one along the direction parallel to $\mathbf{\Delta H}$ ($HPE_{\parallel}$) and one along the direction perpendicular to $\mathbf{\Delta H}$ ($HPE_{\perp}$). Those two components were then multiplied by C_H. C_H was used to suppress the output of the controller when the amplitude of εH was smaller than a threshold value (thr_H). The computation of C_H was similar to the computation of the facilitation signal (eq. (.143)).

$$\varepsilon H = sat\left(\frac{\|\mathbf{\Delta H}^*\|_2}{\|\mathbf{\Delta H}\|_2}\right)_0^1 \tag{.146}$$

$$IN_{C_H} = 1 \quad if \quad \varepsilon H \geq thr_H, \quad otherwise \quad IN_{C_H} = 0 \tag{.147}$$

$$\tau_{C_H}\frac{d(C_H)}{dt} = IN_{C_H} - C_H \tag{.148}$$

$$HPE_{\parallel} = (1 - C_H) * \frac{\mathbf{HPE} \cdot \mathbf{\Delta H}}{\|\mathbf{\Delta H}\|_2} \tag{.149}$$

$$HPE_{\perp} = (1 - C_H) * \left\| \mathbf{HPE} - \left(HPE_{\parallel} * \frac{\mathbf{\Delta H}}{\|\mathbf{\Delta H}\|_2} \right) \right\|_2 \tag{.150}$$

$HPE_{\parallel}$ and $HPE_{\perp}$ were then used to compute the head cerebellar drive ($\mathbf{CB_{HD}}$):

$$CB_{H,\parallel} = \left(\frac{K_{IH,\parallel}}{\mathsf{s} + K_{FH} * C_H} + K_{PH,\parallel} \right) * HPE_{\parallel} \tag{.151}$$

$$CB_{H,\perp} = \left(\frac{K_{IH,\perp}}{\mathsf{s} + K_{FH} * C_H} + K_{PH,\perp} \right) * HPE_{\perp} \tag{.152}$$

$$\mathbf{1_{H,\perp}} = \frac{\left[\mathbf{HPE} - \left(HPE_{\parallel} * \frac{\mathbf{\Delta H}}{\|\mathbf{\Delta H}\|_2} \right) \right]}{\left\| \mathbf{HPE} - \left(HPE_{\parallel} * \frac{\mathbf{\Delta H}}{\|\mathbf{\Delta H}\|_2} \right) \right\|_2} \tag{.153}$$

$$\mathbf{CB_{HDi}} = CB_{H,\parallel} * \left(\frac{\mathbf{\Delta H}}{\|\mathbf{\Delta H}\|_2} \right) + CB_{H,\perp} * \mathbf{1_{H,\perp}} \tag{.154}$$

$$\tau_{CB_H} \frac{d(\mathbf{CB_{HD}})}{dt} = \mathbf{CB_{HDi}} - \mathbf{CB_{HD}} \tag{.155}$$

Equations (.151) and (.152) correspond to the head cerebellar controller. It includes a forgetting factor (tuned by the parameter K_{FH}). Like for the gaze cerbellar controller, this controller is defined by two parameters: an integration gain K_{IH} and a proportional gain K_{PH}. Those two parameters were tuned to reproduce the behavioral observations of (Tomlinson and Bahra, 1986a,b). When the relative head displacement was bigger than thr_H, the outputs of equations (.149) and (.150) were equal to zero. Therefore, $CB_{H,\parallel}$ and $CB_{H,\perp}$ decreased to zero with a time constant of K_{FH} and the output of the head cerebellar drive went to zero and the head movement stopped.

Model parameters

This section presents the numerical value of all the parameters that were used for the simulations presented in the main text. The first table presents all the time constants of the model. The time constants were chosen as in (Lefèvre et al., 1998; Quaia et al., 1999). The second table gives all the remaining parameters of the model. As explained in the main text, those parameters were tuned to reproduce the observed behavior of head-unrestrained saccades (Freedman and Sparks, 1997; Goossens and Van Opstal, 1997; Guitton et al., 1990; Tomlinson and Bahra, 1986a,b). The last table presents the parameters of the piecewise linear function Γ.

Table .1: Time constants of the model

Time constant	Value in the model
τ_{OPN}	1 ms
τ_{cMRF}	1 ms
τ_{IBN_c}	1 ms
τ_{EBN_i}	1 ms
τ_{PM}	1 ms
τ_{SC}	7.5 ms
τ_{CB_G}	5 ms
τ_{C_H}	5 ms
τ_{CB_H}	5 ms
τ_{ch}	5 ms
τ_{fac}	5 ms

Table .2: Parameters of the model

Parameter	Value in the model
thr	1 deg
α_{SC}	8
β_{CB_G}	1
τ_{OMR}	1 deg
Mx	600 spikes/s
δ_{CB_H}	4
γ_{SC}	20
$K_{I,\parallel}$	100
$K_{P,\parallel}$	5
$K_{I,\perp}$	300
$K_{P,\perp}$	30
K_F	200
thr_{rel}	0.1
thr_{OPN}	0.99
thr_H	0.8
$K_{IH,\parallel}$	2
$K_{PH,\parallel}$	7
$K_{IH,\perp}$	10
$K_{PH,\perp}$	5
K_FH	50
σ_{OPN}	0.8

Table .3: Control points of function $\Gamma(\mathbf{\Delta G})$, intermediate points are linearly interpolated between control points

ΔG [deg]	Output
0	0
1	0.2796
2	0.3390
3	0.5182
4	0.6677
5	0.8358
6	1.0038
7	1.1585
8	1.3576
9	1.5533
10	2.0167
12	3.6505
15	4.4290
18	5.4993
20	6.0022
25	7.7433
30	9.0260
35	10.2579
40	10.6480
50	12.8841
55	13.2513
60	14.4946

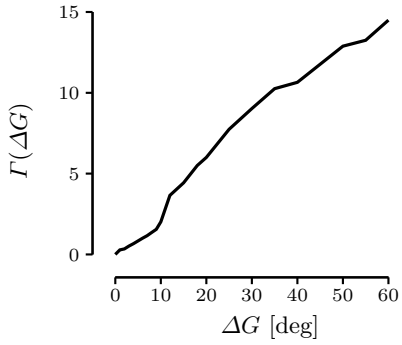

Fig. .2: Plot of $\Gamma(\Delta G)$. This figure represents the output of Γ as a function of the saccade amplitude (ΔG).

Additional simulation: influence of a theoretical delay between the desired gaze and head inputs

This section presents an intrinsic property of the model linked to its two separate inputs. If one assumed that the head input (ΔH) could be delayed or advanced by the cortical decision process with respect to the gaze input (ΔG), different behaviors of the head and gaze trajectories would be observed.

Figure .3A represents the effect of a delayed head input with respect to the gaze input and Fig. .3B presents the effect of a delay on the gaze input with respect to the head input. Solid lines in Fig. .3 represent a case where the head and the gaze inputs were sent simultaneously. Dashed lines in Fig. .3A represent a head input sent 70ms later than the gaze input. Finally, dotted-dashed lines in Fig. .3B correspond to a gaze input delayed by 70 ms with respect to the head command. Only the first 500 milliseconds are presented in the right column of Fig. .3A and .3B but the whole trial (1 second) is shown in the spatial representation (left column of Fig. .3A and .3B).

The interaction between the three pathways is emphasized by comparing the head trajectory traces in Fig. .3A and .3B. When the head input was delayed by 70ms (dotted lines in Fig. .3A), the head started its movement in a direction parallel to the gaze displacement because of the collicular discharge (the initial orientation of the head is represented by the black arrow in Fig. .3A, which has a direction parallel to the gaze trajectory). After 70ms, the head input was sent to the cerebellar independent head controller, and the trajectory of the head was corrected to go towards the desired final head position. In this situation, the gaze went straight to the final gaze target because there was no indirect perturbation (through a head movement) on the gaze trajectory during the first 70 milliseconds of the movement. In a situation where the head and the gaze command were sent at the same time (solid lines in Fig. .3), the head trajectory was influenced by the collicular pathway (in the gaze direction) and the cerebellar head pathway (in the direction of the desired head displacement). Therefore, the head trajectory started more vertically in Fig. .3A than when the gaze input was sent earlier. The initial orientation of the head movement is represented by the grey arrow in Fig. .3A-B. During the gaze part of the saccade, the gaze was influenced by the head controller and its trajectory was deviated compared to the first case. Finally, when the gaze was delayed by 70ms (dotted-dashed lines in Fig. .3B), the head started to move first because no input was sent through the gaze pathway to the eyes. During the first 70 milliseconds, the gain of the VOR was equal to one and the eye was counter-rolling in the orbit to keep gaze stationary. Since no discharge came from the collicular pathway, the head started to move in a direction parallel to the desired head displacement. The initial orientation of the head movement is represented by the blue arrow in Fig. .3B. When the gaze input was sent after 70ms, the collicular pathway discharged and modified the head trajectory.

Fig. .3 *(following page)*: Influence of the timing of the input commands. Panel A: Head delayed input with respect to the gaze input. Solid lines correspond to a simultaneous head and gaze command. Dashed lines correspond to a head command delayed by 70 ms with respect to the gaze command. Same color convention as in Fig. 5 apply. Only the first 500 ms are represented in the right column. The spatial representation includes the whole simulation (duration: 1 second). When the head command was delayed (dashed lines), the initial movement of the head (black arrow) was parallel to the gaze movement because there was no discharge from the head controller. When the head and the gaze commands were sent simultaneously (solid lines), there was an interaction between the collicular and the independent head pathways. Therefore, the initial head trajectory (grey arrow) had an orientation corresponding to a combination of the two drives. Panel B: Gaze delayed command with respect to the head command. Dotted-dashed lines correspond to a gaze command delayed by 70 ms with respect to the head command. As on panel A, solid lines represent a case in which the head and the gaze commands were sent simultaneously. When the gaze was delayed (dotted-dashed), the head started in a direction parallel to the desired head displacement (represented by the blue arrow). Seventy milliseconds later, the collicular discharge acted as a perturbation on the head and modified the initial orientation of the head displacement. However, the head cerebellar pathway corrected the trajectory and the head movement ended close to the desired final head position.

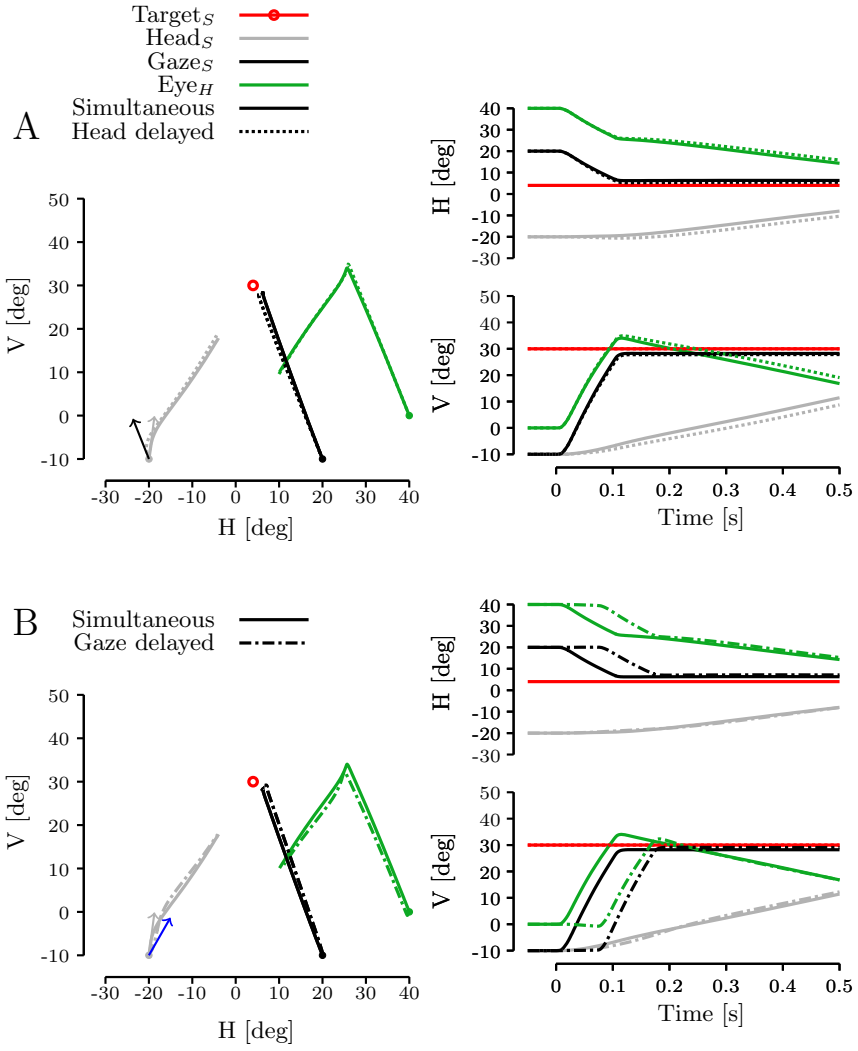
A
Target$_S$
Head$_S$
Gaze$_S$
Eye$_H$
Simultaneous
Head delayed
V [deg]
H [deg]
H [deg]
V [deg]
Time [s]
B
Simultaneous
Gaze delayed
V [deg]
H [deg]
H [deg]
V [deg]
Time [s]

Corneil, B. D., Olivier, E., and Munoz, D. P. (2002a). Neck muscle responses to stimulation of monkey superior colliculus. i. topography and manipulation of stimulation parameters. *J Neurophysiol*, 88(4):1980–1999.
Corneil, B. D., Olivier, E., and Munoz, D. P. (2002b). Neck muscle responses to stimulation of monkey superior colliculus. ii. gaze shift initiation and volitional head movements. *J Neurophysiol*, 88(4):2000–2018.
Cromer, J. A. and Waitzman, D. M. (2006). Neurones associated with saccade metrics in the monkey central mesencephalic reticular formation. *J Physiol*, 570(Pt 3):507–523.
Freedman, E. G. and Sparks, D. L. (1997). Eye-head coordination during head-unrestrained gaze shifts in rhesus monkeys. *J Neurophysiol*, 77(5):2328–2348.
Fuchs, A. F., Kaneko, C. R., and Scudder, C. A. (1985). Brainstem control of saccadic eye movements. *Annu Rev Neurosci*, 8:307–337.
Goossens, H. and Van Opstal, A. (1997). Human eye-head coordination in two dimensions under different sensorimotor conditions. *Experimental Brain Research*, 114:542–560.
Graf, W. M. and Ugolini, G. (2006). The central mesencephalic reticular formation: its role in space-time coordinated saccadic eye movements. *J Physiol*, 570(Pt 3):433–434.
Guitton, D., Munoz, D., and H.L., G. (1990). Gaze control in the cats: Studies and modeling of the coupling between orienting eye and head movements in different behavioral tasks. *J Neurophysiol*, 64(2):509–531.
Horn, A. K. E. (2006). The reticular formation. *Prog Brain Res*, 151:127–155.
Kaneko, C. R. and Fuchs, A. F. (1982). Connections of cat omnipause neurons. *Brain Res*, 241(1):166–170.
King, W. M., Precht, W., and Dieringer, N. (1980). Afferent and efferent connections of cat omnipause neurons. *Exp Brain Res*, 38(4):395–403.
Langer, T. P. and Kaneko, C. R. (1984). Brainstem afferents to the omnipause region in the cat: a horseradish peroxidase study. *J Comp Neurol*, 230(3):444–458.
Lefèvre, P., Quaia, C., and Optican, L. M. (1998). Distributed model of control of saccades by supperior colliculus and cerebellum. *Neural Networks*, 11:1175–1190.
Quaia, C., Lefèvre, P., and Optican, L. (1999). Model of the control of saccades by superior colliculus and cerebellum. *Journal of Neurophysiology*, 82:999–1018.
Ramat, S., Leigh, R. J., Zee, D. S., and Optican, L. M. (2007). What clinical disorders tell us about the neural control of saccadic eye movements. *Brain*, 130(Pt 1):10–35.
Scudder, C. A., Moschovakis, A. K., Karabelas, A. B., and Highstein, S. M. (1996). Anatomy and physiology of saccadic long-lead burst neurons recorded in the alert squirrel monkey. i. descending projections from the mesencephalon. *J Neurophysiol*, 76(1):332–352.
Strassman, A., Highstein, S. M., and McCrea, R. A. (1986). Anatomy and physiology of saccadic burst neurons in the alert squirrel monkey. ii. inhibitory burst neurons. *J Comp Neurol*, 249(3):358–380.

Tomlinson, R. D. and Bahra, P. S. (1986a). Combined eye-head gaze shifts in the primate. i. metrics. *J Neurophysiol*, 56(6):1542–1557.
Tomlinson, R. D. and Bahra, P. S. (1986b). Combined eye-head gaze shifts in the primate. ii. interactions between saccades and the vestibuloocular reflex. *J Neurophysiol*, 56(6):1558–1570.

Glossary

ABD	Abducens nucleus (VI nucleus), 32, 67, 68
Abduction	Horizontal rotation of the eye away from the nose, 12, 15
Adduction	Horizontal rotation of the eye toward the nose, 12, 15
BLUE	Best linear unbiased estimator, 243, 244
CAP	Cervical afferent pathway, 241, 243, 244, 259, 260
CBLM	Cerebellum, 37
cFN	Caudal part of the fastigial nucleus, 30, 31
CI	Compensation index, 105–107, 115–120, 299, 300
CI^E	Partial compensation index for the eye, 106, 117, 299, 300
CI^H	Partial compensation index for the head, 106, 107, 117, 119, 299, 300
CI^P	Partial compensation index for the pursuit component of the eye displacement, 107, 119, 120, 300
CI^V	Partial compensation index for the VOR component of the eye displacement, 107, 119, 120, 278, 300
CMA	Cingulate motor area, 39
cMRF	Central mesencephalic reticular formation, 32, 33, 36, 304, 305
CN	Caudate nucleus, 21, 23
dCN	Deep cerebellar nuclei, 24, 26, 28, 196
Depression	Vertical downward rotation of the eye, 12
DLPN	Dorsolateral pontine nuclei, 63, 71

EBN	Excitatory burst neurons, 32, 33, 38, 40, 194, 196, 209, 214, 304–307
EC	Eye contribution: proportion of eye-in-head movement during a gaze displacement, 104–107, 109, 113, 117–120, 123, 299, 300
Elevation	Vertical upward rotation of the eye, 12
EOR	Eye-only Range, 5
Extorsion	Outward rotation of the eye, 12
FEF	Frontal eye field, 4, 21, 23, 24, 39, 58, 61, 62, 71
FEF_{sacc}	Saccade part of the Frontal eye field, 62, 71
FEF_{sem}	Smooth eye movement part of the Frontal eye field, 62, 63, 71
FFH	Forel's field of H, 37, 40
GLR	Generalized likelihood ratio: falut detection algorithm used to detect saccade, 142, 146, 287, 292, 294–296
GPi	Internal segment of the globus pallidus, 23
HC	Head contribution: proportion of head movement during a gaze displacement, 104–106, 299
HCLS	Hierarchical control for linked systems, 189, 191, 203, 219
IBN	Inhibitory burst neurons, 32, 33, 35, 36, 38, 197, 304–306
III	Third nucleus, 32, 67
IN	Interneurons, 32
INC	Interstitial nucleus of Cajal, 34, 38
Intorsion	Inward rotation of the eye, 12
IRED	Infrared light-emitting diode, 101, 141, 142, 146, 274
LGN	Lateral geniculate nucleus, 21, 24, 58
LIP	Lateral intraparietal area, 21, 24, 58, 61–63
LS	Linked systems, 189, 191, 219
MAE	Motion after effect, 46
MIMO	Multi-input multi-output system, 193
MLF	Medial longitudinal fasciculus, 66
MN	Motoneurons, 32
MST	Medial superior temporal area, 4, 58, 60–63, 71
MT	Middle temporal area, 4, 58, 60–63, 71
MV	Medial vestibular nucleus, 67
NAcc	Nucleus accumbens, 23

NRG Nucleus reticularis gigantocellularis, 37–41, 279
NRPC Nucleus reticularis pontis caudalis, 37–41, 279
NRTP Nucleus reticularis tegmenti pontis, 197, 279

OKR OptoKinetic reflex, 235
OMR Ocular motor range, 5, 216, 278, 307
OPN Omnipause neurons, 32–35, 194, 196, 197, 199, 203, 204, 207, 211, 214, 216, 218, 219, 222, 245, 247, 260, 278, 304–309

P-cells Purkinje cells, 63, 64
PE Position error: difference in position between the target and the gaze, 105–107, 109, 115, 146, 172, 299, 300
PE_{ON} Position error at saccade onset, 146
$PE_{ON,CORR}$ Position error at saccade onset corrected by the sign of the target velocity, 167, 168, 170, 172
PMd dorsal premotor area, 39
PMv ventral premotor area, 39
PON Visuomotor nuclei in the pontine nuclei, 58, 61, 63
PPRF Paramedian pontine reticular formation, 26, 31, 32, 34, 35
PUT Putamen, 23
PVC Primary visual cortex (V1 ⇒ V4), 21, 58
Pyr Pyramidal tract, 39

rFN Rostral part of the fastigial nucleus, 30, 199
riMLF rostral interstitial nuclei of the medial longitudinal fasciculus, 34
RIP Nucleus raphe interpositus, 26
rMRF Rostral mesencephalic reticular formation, 31
RS Retinal slip: difference between target and gaze velocity, 46, 50, 53, 60, 172
RSN Reticulospinal neuron, 37, 39
RS_{ON} Retinal slip at saccade onset, 146
$RS_{ON,CORR}$ Retinal slip at saccade onset corrected by the sign of the target velocity, 167, 168, 170, 172

SC Superior colliculus, 21, 23–26, 31, 33, 36, 37, 42, 189, 193, 194, 196, 197, 199, 200, 203, 204, 206, 207, 216, 219, 221, 222, 279, 304, 305, 307, 308
SCC Semicircular canal, 13, 66, 67, 69, 143, 241, 243, 244, 259, 260
SED Smooth eye displacement: difference between SGD and SHD, 104, 106, 107, 113, 116, 117, 119, 299, 300

SEF	Supplementary eye field, 21, 23, 58, 61, 62
SGD	Smooth gaze displacement: gaze displacement without saccade, 104–107, 109, 111, 113, 115, 117, 125, 299, 300
SGV	Smooth gaze velocity: gaze velocity without saccade (removed using a linear interpolation), 143
SHD	Smooth head displacement, 104, 106, 107, 113, 116, 117, 299
SMA	Supplementary motor area, 39
SNr	Substantia nigra pars reticulata, 21, 23, 24, 37, 39
SPD	Smooth pursuit displacement, 107, 300
STR	Striatum: input stage of the basal ganglia, 23
VERM	Cerebellar vermis, 21, 58
VIP	Ventral intraparietal area, 58, 61
VN	Vestibular nuclei, 68, 237, 238
VOR	Vestibulo-ocular reflex, 5–8, 18, 43–45, 50–56, 61–64, 66–70, 97, 99, 106, 107, 119, 120, 123, 126, 127, 200, 203, 204, 207, 212, 214, 216, 221, 222, 233, 235–238, 240, 241, 244–247, 249, 251, 253, 255, 257, 259–262, 269, 271, 275–278, 280, 300
VPF	Ventral paraflocculus, 58